May 2023
Report No. 23-041

Maura Healey
Governor
Kim Driscoll
Lieutenant Governor
Gina Fiandaca
MassDOT Secretary & CEO

Massachusetts Depth to Bedrock Project

Principal Investigator (s)
Dr. Stephen Mabee
University of Massachusetts Amherst

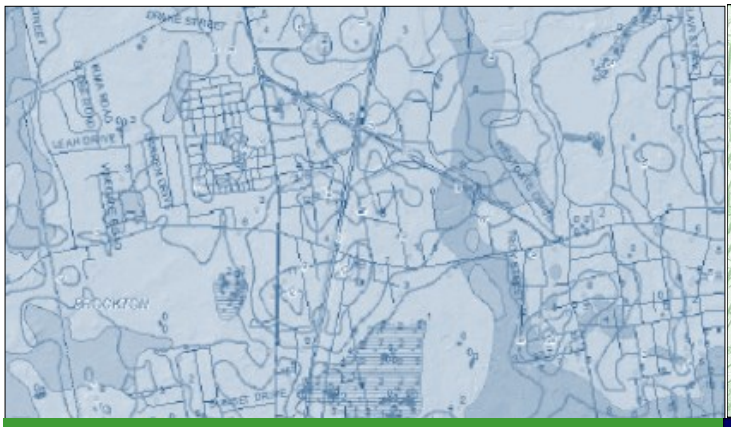

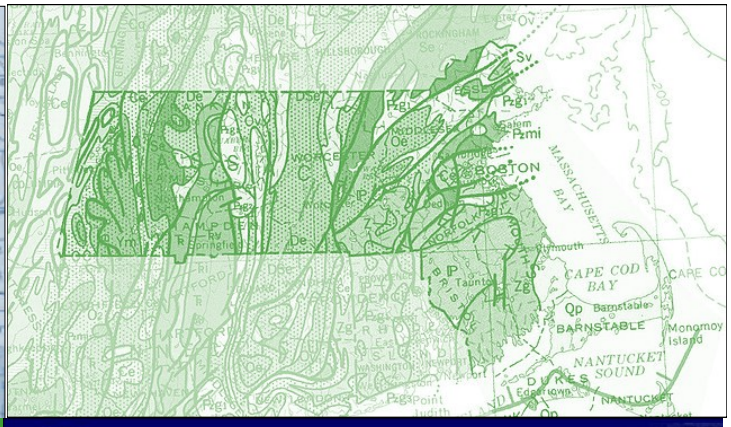

Research and Technology Transfer Section
MassDOT Office of Transportation Planning

U.S. Department of Transportation
Federal Highway Administration

Massachusetts Depth To Bedrock Project

Prepared by

Stephen B. Mabee
Christopher C. Duncan
William P. Clement
Marshall Pontrelli

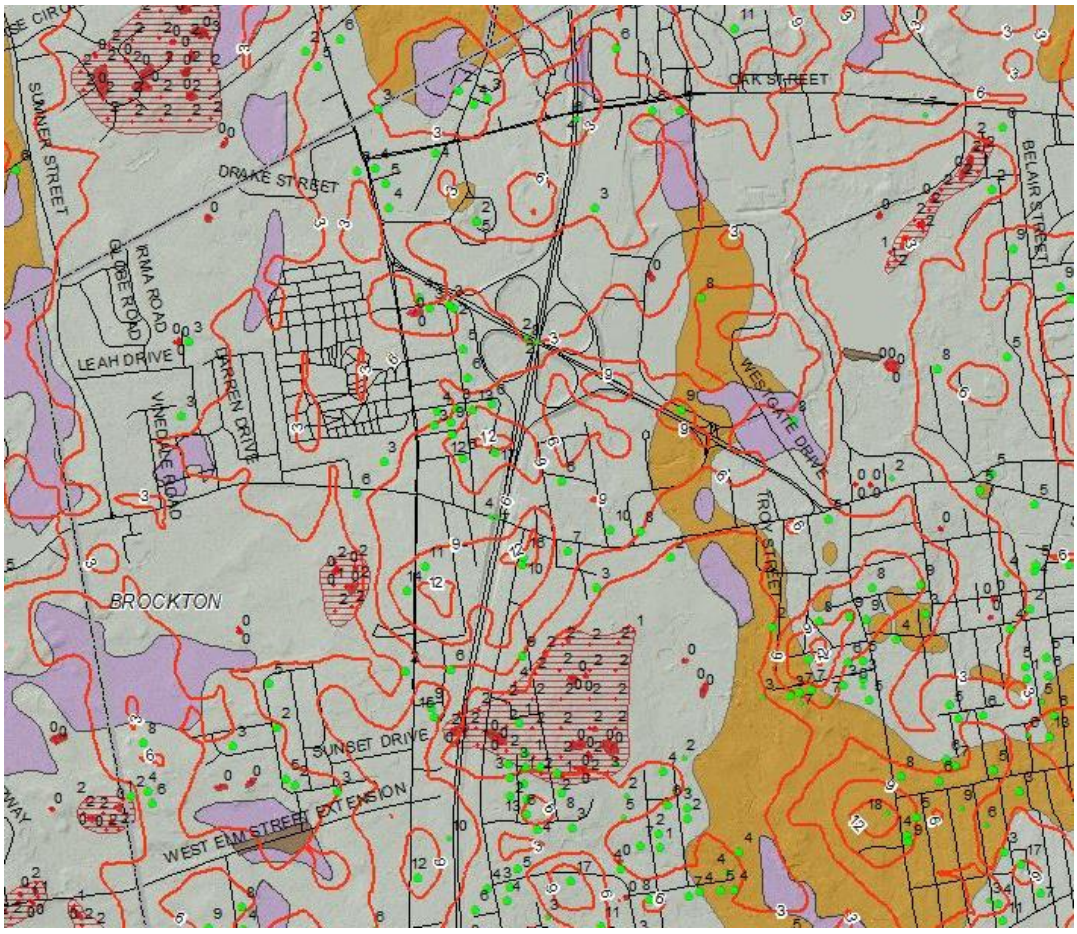

Prepared for:

Massachusetts Department of Transportation
Office of Transportation Planning
Ten Park Plaza, Suite 4150
Boston, MA 02116

May 2023

This page left blank intentionally

Technical Report Document Page

1. Report No. 23-041	2. Government Accession No.	3. Recipient's Catalog No.
4. Title and Subtitle Massachusetts Depth to Bedrock Project		5. Report Date May 2023
		6. Performing Organization Code 23-041
7. Author(s) Stephen B. Mabee, Christopher C. Duncan, William P. Clement and Marshall Pontrelli		8. Performing Organization Report No.
9. Performing Organization Name and Address Massachusetts Geological Survey, Department of Earth, Geographic and Climate Science, University of Massachusetts, 627 North Pleasant Street, Amherst, MA 01003		10. Work Unit No. (TRAIS) 11. Contract or Grant No.
12. Sponsoring Agency Name and Address Massachusetts Department of Transportation Office of Transportation Planning Ten Park Plaza, Suite 4150, Boston, MA 02116		13. Type of Report and Period Covered Final Report - May 2023 (March 2021 to May 2023) 14. Sponsoring Agency Code n/a
15. Supplementary Notes Project Champion- Jennifer Rauch, MassDOT		

16. Abstract

The depth to bedrock is perhaps one of the most important surfaces that is fundamental to many practical engineering and geological problems. Yet it is not well understood everywhere. Knowing the depth to bedrock for transportation projects not only influences cost but may also affect selection of the appropriate foundation system for a particular structure. Furthermore, estimates of the bedrock depth, along with the type of overburden (e.g., glacial till, varved clay, sand and gravel) help determine the most appropriate subsurface investigation method to use during project planning, and reduces construction delays and claims brought forward by contractors. Accordingly, there is some level of uncertainty in planning subsurface investigations for any transportation project when depth to bedrock information is lacking. This project is an attempt to reduce the uncertainty in highway project planning by providing interpolated statewide data layers of the depth to bedrock and bedrock altitude at 100-meter resolution based on currently available subsurface data. In addition, maps depicting the level of confidence in the estimate of the bedrock altitude and depth are also provided. The confidence is based on both the interpolated prediction standard error as well as the measurement uncertainties associated with the input data.

17. Key Word bedrock, depth, subsurface, data layers, geological, transportation	18. Distribution Statement		
19. Security Classif. (of this report) unclassified	20. Security Classif. (of this page) unclassified	21. No. of Pages 170	22. Price n/a

Form DOT F 1700.7 (8-72) Reproduction of completed page authorized

This page left blank intentionally.

Massachusetts Depth To Bedrock Project

Final Report

Prepared By:

Stephen B. Mabee
Principal Investigator

Christopher C. Duncan
Contractor

William P. Clement
Co-Principal Investigator

Marshall Pontrelli
Contributor

Massachusetts Geological Survey
Department of Earth, Geographic and Climate Sciences
University of Massachusetts
627 North Pleasant Street
Amherst, MA 01003

Prepared For:

Massachusetts Department of Transportation
Office of Transportation Planning
Ten Park Plaza, Suite 4150
Boston, MA 02116

May 2023

This page left blank intentionally.

Acknowledgements

Prepared in cooperation with the Massachusetts Department of Transportation, Office of Transportation Planning, and the United States Department of Transportation, Federal Highway Administration under award number INTF00X02021A0113776.

The Project Team would like to acknowledge the efforts of those who provided data and assistance to the project: Dr. Laurie Baise, Tufts University, Peter Grace from MassGIS, Byron Stone, Janet Stone, John Mullaney, and Greg Walsh from the USGS and students Patrick Scordato, Maya Pope, Keegan Moynahan, Ryan Miller, Hannah Davis and Alex Low. Reviews provided by Laura Medalie and Mary DiGiacomo-Cohen of the USGS are much appreciated.

Disclaimer

This page left blank intentionally.

Executive Summary

This study of the Massachusetts Depth to Bedrock was undertaken as part of the Massachusetts Department of Transportation (MassDOT) Research Program. This program is funded with Federal Highway Administration (FHWA) State Planning and Research (SPR) funds. Through this program, applied research is conducted on topics of importance to the Commonwealth of Massachusetts transportation agencies.

The bedrock surface is important in many geological and engineering disciplines, but its depth is poorly known because it is obscured by a thick cover of glacial sediment overburden. Yet having a reasonable estimate of the depth to bedrock is fundamental to any transportation and engineering activity. Bedrock depth not only influences cost, such as design, construction, claims, and unexpected conditions costs, but may also affect selection of the appropriate foundation system for a particular structure. Furthermore, estimates of the bedrock depth, along with the type of overburden (e.g., glacial till, varved clay, sand and gravel) help determine the most appropriate subsurface investigation method to use during project planning, pre-design, and design and reduces construction delays and claims brought forward by contractors. Accordingly, without adequate bedrock depth information there is some uncertainty in planning subsurface investigations that trend towards an ad hoc approach for any transportation project.

The purpose of this project is to compile subsurface data from a variety of sources and use this information to build a high resolution data layer of the depth to bedrock across the entire state. The overall goal is to help reduce the uncertainty in highway projects by providing a rational approach to clarifying bedrock depth during project planning and design development.

For this project a total of 107,702 drill hole and geophysical data were collected from 28 different sources consisting of 61,531 records with depth to bedrock information and 41,171 records that are considered overburden points that terminate within the overburden. These data sources included MassDOT bridge and highway borings and seismic refraction surveys, Massachusetts Water Resources Authority (MWRA) project borings through 2014, data downloads from the USGS National Water Information System (NWIS) and Ground Water Site Inventory (GWSI) databases, USGS Hydrologic Data Reports, borings shown on 1:24,000 scale surficial geologic quadrangle maps, some limited seismic survey data collected by Hager Geoscience, various USGS Scientific Investigation Reports, Water Resources Investigation Reports and Open-File Reports, the Well Driller's Well Completion Report database maintained by the Massachusetts Department of Environmental Protection (MADEP), published and unpublished Horizontal to Vertical Spectral Ratio (HVSR) survey data and, offshore analog seismic survey data collected by the USGS. All data were subjected to a series of validation steps to identify duplicate Site IDs and locations. All data were projected to the NAD 83 Mass State Plane coordinate system and elevation data converted to the NAVD 88 datum. In addition, each record in the data set was assigned a measurement uncertainty based on the method of data collection (geophysical data vs boring) and whether or not a geologist or engineer was on site during drilling operations.

In addition, 401 Horizontal to Vertical Spectral Ratio (HVSR) data points were collected across the state to provide additional depth to bedrock information in areas where well data were sparse. HVSR is a relatively new geophysical tool that allows estimation of the depth to bedrock through the use of a calibration curve relating fundamental frequency (site response to seismic waves) and bedrock depth. As part of this project, a calibration curve for Massachusetts was developed that can now be used with HVSR survey equipment to estimate bedrock depth in areas where it is not known. The equation relating fundamental frequency to bedrock depth is:

$$Z = 102.07 * f_0^{-1.24}$$

where Z is the depth to bedrock in meters and f_0 is the fundamental frequency (Hertz) measured with a 3-component seismometer. All of this data, the drill hole, geophysical and HVSR data are compiled in a Master Spreadsheet that is downloadable and ready for use.

Data processing of the drill hole and geophysical data involved the following steps: 1) determining the best presentation format for output data (raster vs. triangular irregular network, raster was ultimately selected); 2) selecting a raster resolution; a 100-meter resolution was selected because it optimizes the usefulness of the available data without compromising processing efficiency or creating unmanageable data volumes; 3) incorporating bedrock outcrops and shallow to bedock areas as points, split into the 100-meter grid, each with a depth to bedrock and bedrock altitude, providing 603,615 additional data points for a total of 711,317 points to use as input in the models; 4) conducting dozens of tests to determine the best interpolation method to create the bedrock altitude and depth to bedrock data layers; empicial Bayesian kriging and co-kriging, respectively, were found to be the best performing interpolators; 5) modeling bedrock altitude and constraining that surface by using overburden wells whose depths extended below the initial interpolated bedrock surface; this is the altitude based model; 6) modeling depth to bedrock and then subtracting the resulting surface from topography to create an alternative bedrock altitude surface, this is the depth-based altitude model; 7) blending the altitude-based and depth-based models to remove issues that occur in the altitude-based model where bedrock rises unrealistically above the land surface; this blending guarantees the bedrock is at or below the land surface everywhere; 8) reviewing the models and correcting any kriging artifacts using an inverse distance weighting script to “fill” the holes and making any adjustments manually to the bedrock elevation contours and blending the adjusted contours into the model; 9) creating corresponding kriging prediction standard error, measurement uncertainty and combined prediction error and uncertainty maps to accompany the modeled data layers to give the user some understanding of the confidence and spatial variability in the modeled bedrock altitude and bedrock depth estimates; 10) generating final bedrock altitude and depth to bedrock maps; and, 11) using the depth to bedrock map and shear wave velocity profiles ascribed to different surficial materials to generate an updated NEHRP soil classification map for Massachusetts.

Bedrock altitudes range from a high of 1059 meters (above NAVD88) at Mount Greylock to a low of -512 meters on Nantucket. Several deep glacially scoured holes exist in the

Connecticut Valley and topographic lows in the bedrock occur also in southwestern Massachsuetts where buried karst topography is suspected. The depth to bedrock ranges from 0 meters at individual bedrock outcrops to a maximum of 511 meters on Nantucket. As expected overburden thicknesses are greatest in southeastern Massachusetts, Cape Cod, Boston and in the larger river valleys. Overburden thickness is very thin in the uplands.

Model prediction errors are less than 5 meters over most of the state and very few are greater than 30 meters. There is one prediction error of 120 meters that occurs in Easthampton, Masschusetts, in an area of sparse data coverage. Approximately 75 percent of the state has observational uncertainties of less than 5 meters. Notable exceptions include the Springfield area and Connecticut River valley where deep boreholes are lacking, and Boston and the Plymouth area of southeast Massachusetts, where the measurement errors are still generally under 10 meters. Measurement errors increase on Cape Cod and the Islands, where geophysical methods, which have a higher uncertainty, were used extensively to gather depth to bedrock data. The highest uncertainties (maximum of 53 meters) were observed on Nantucket. Combined model prediction standard error and observational uncertainty range from 0.2 meters to a maximum of 122 meters (Easthampton area).

The updated NEHRP site class map for Massachusetts indicates that approximately 65 percent of the state has a site class of A or B. However, two of the larger cities, Boston and Springfield, as well as southeast Massachusetts and the heavily populated Cape Cod area, have site classes of D and E.

Meticulous effort was employed to create the “best” model of the bedrock altitude and depth to bedrock based on the currently available data. These models will only improve with additional data. This report and the appendices have been designed so that all process steps are documented. This will allow the entire process to be repeated as more data become available.

The most effective way to use the bedrock altitude or depth to bedrock maps is to use them in conjunction with the error maps, well data, and bedrock outcrops and shallow to bedrock data points. This will provide the user with a probable estimate of bedrock depth with appropriate uncertainties in the depth estimate and the input data values from which these were derived for context and site-specific evaluation.

This page left blank intentionally.

Table of Contents

Technical Report Document Page i
Acknowledgements v
Disclaimer v
Executive Summary vii
Table of Contents xi
List of Tables xiii
List of Figures xiii
List of Acronyms xvii
1.0 Introduction 1
1.1 Purpose and Objectives 1
1.2 Deliverables 2
1.3 Intended Use and Limitations of Work Products 3
1.4 Overview and Previous Work 3
2.0 Research Methodology 7
2.1 Compilation of Existing Borehole, Well and Geophysical Data 7
2.2 Collection of Additional Geophysical Data 8
2.3 Data Validation 16
2.4 Assignment of Observational Uncertainties 22
2.5 Data Processing 24
2.5.1. Overview 24
2.5.2. Data Processing Software 24
2.5.3. Input Data Characteristics 24
2.5.4. Output Data Format 28
2.5.5. Raster Resolution 29
2.5.6. Master Reference Grid 30
2.5.7. 100-meter Topography 31
2.5.8. Preparation of Surficial Geology Proxy Data 32
2.5.9. Bedrock Outcrops (bk) 32
2.5.10. Abundant Outcrops and Shallow to Bedrock Areas (sb) 34
2.5.11. Final Preparation of Drill Hole, Geophysical, Bedrock Outcrop and Shallow to Bedrock Point Data 38
2.6 Modeling the Bedrock Surface: Overview of Approaches, Problems and Solutions 40
2.7 Modeling of Bedrock Altitude 44
2.7.1. Testing Interpolation Methods 44
2.7.2. Modeling Bedrock Altitude with Overburden Constraints 51
2.7.3. Modeling Bedrock Depth 51
2.7.4. Blending Altitude-based and Depth-based Models 53
2.7.5. Patching Kriging Artifacts and Contour Adjustments 55
2.7.6. Modeling Input Data Uncertainty 59
2.7.7. Final Altitude, Depth, and Error/Uncertainty Rasters and Contours 60
2.8 Discussion of Bedrock Altitude and Depth Models 61
2.8.1. Model Evaluation Criteria 61
2.8.2. Summary and Rationale for Data Processing Steps 61
2.8.3. Discussion and Examples of Raster Relationships 63

2.8.4. Modeled Bedrock Altitude Above Topography – Blending Altitude- and Depth-Based Rasters 64
2.8.5. Kriging Artifacts (Depressions) 66
2.8.6. Manual Contouring 68
2.8.7. Areas of Shallow to Bedrock 72
2.9 NEHRP Classification Map of Massachusetts 74
3.0 Results 77
3.1 Discussion of Alternative Depth Models, Errors and Uncertainties 81
3.2 NEHRP Site Class Results 84
4.0 Implementation and Technology Transfer 87
5.0 Conclusions 89
6.0 References 91
7.0 Appendices 95
7.1 Appendix A: A Data Set of Depth to Bedrock Described in Drill Holes and Geophysical Surveys for Massachusetts – Release 1 95
7.2 Appendix B: HVSR – Simple Theory to Finding Depth to Bedrock 111
7.3 Appendix C: Data Processing Steps 115
7.4 Appendix D: Python Script for Filling Kriging Artifacts 137
7.5 Appendix E: NEHRP Site Class Map Development 141

List of Tables

Table 2.1: Name and description of all drill hole and geophysical data contained in the master spreadsheet 17
Table 2.2: Observational uncertainties assigned to each data set 23
Table 2.3: Raster cell and point statistics for various raster resolutions 30
Table 2.4: NEHRP Soil Classifications 75
Table 3.1: Correlation of project deliverables, report name or file type, and file name or folder for data download 77
Table 3.2: Distribution of NEHRP cite classes across Massachusetts 84
Table 7.1: Vs30-based seismic site classification 141
Table 7.2: Surficial geologic groupings of the Massachusetts units into 4 groups of similar mechanical properties 145
Table 7.3: Mean, median and estimated Vs_{avg} values for the four geologic groupings. 145

List of Figures

Figure 1.1: Map showing the thickness of sand and gravel deposits in Massachusetts 4
Figure 1.2: Map of sediment thickness at 1:5,000,000 scale resolution 5
Figure 2.1: Students collecting HVSR survey data in Northampton, MA. Seismometer is the instrument in the foreground 9
Figure 2.2: Example of plot of H/V versus frequency. 10
Figure 2.3: Map showing the locations of HVSR seismic measurements collected by the project team during he summer of 2021 (N=401) 12
Figure 2.4: Plot of calibration sites categorized by data quality type, excellent, good, fair, and poor. In all plots the blue line is the best fit line through sites categorized as excellent and good; dashed line is the best fit through just the A) excellent, B) good, C) fair and D) poor calibration sites. 13
Figure 2.5: Fundamental frequency (fo) versus depth to bedrock for Massachusetts calibration sites (N=37) 14
Figure 2.6: Example of horizontal to vertical spectral ratio (HVSR) data collected at two sites (Mount Toby and Greenfield) by the two field teams using different Guralp 6TD seismometers 15
Figure 2.7: Results of fundamental frequency(F_0) reproducibility testing for the two Guralp 6TD seismometers (N=12) with solid black line representing the 1 to 1 fit 16
Figure 2.8: Distribution of drill hole and geophysical data point (black dots) locations; the density varies greatly across the state 25
Figure 2.9: Distribution of bedrock points (red) and overburden points (blue); neither is uniformly distributed 26
Figure 2.10: Histogram of observational uncertainty by data type 26
Figure 2.11: Profile along the Ted Williams Tunnel in Boston, MA. Red points are bedrock altitudes from bedrock borings; blue points are altitudes of maximum overburden boring depths; green points are topographic elevation; boring altitudes include vertical lines showing +/- uncertainty ranges. 27
Figure 2.12: Comparison of TIN (top) and raster (bottom) representations of the same area. Black dots are input data points. 29

Figure 2.13: Comparison of original 1-meter resolution LiDAR (top) with 100-meter resolution topography (bottom) 31
Figure 2.14: Example showing how bedrock polygons (red areas) are split along the 100-meter grid cell boundaries (gray lines) to determine bedrock altitude at the centroid (black dots) 34
Figure 2.15: Shallow to bedrock polygons (shaded areas) split along the 100-meter grid cell boundaries (gray lines) to assign a bedrock altitude at the centroid (dots) 38
Figure 2.16: All drill hole, geophysical, bedrock outcrop and shallow to bedrock data points (black dots) 38
Figure 2.17: Image of 1-meter resolution LiDAR topography where the Deerfield River enters the Connecticut valley 41
Figure 2.18: Triangular irregular network (TIN) surface interpolated from bedrock depth control points on the left and right side of the image compared to the lack of bedrock depth control points in the center of the image 42
Figure 2.19: Bedrock surface altitude obtained by subtracting TIN interpolated depths (Figure 2.18) from 100-meter topography which imprints the 50-meter erosional scarp along the Deerfield River seen in Figure 2.17 onto the bedrock surface 43
Figure 2.20: 1-meter LiDAR topography near Hadley, MA with surrounding bedrock control points as described in the text 45
Figure 2.21: Modeled bedrock surface from TIN interpolation of bedrock altitude control points; the modeled surface declines smoothly from the ridge crest (dark blue east west feature) to the distant control points in the valley floor to the north. 46
Figure 2.22: Depth-to-bedrock obtained by subtracting the modeled altitude of the bedrock surface from the current topography; lightest shading (yellow and orange) are areas where bedrock is above the land surface 47
Figure 2.23: Cumulative distributions of errors between different models and the 10% set-aside test points for a selection of interpolation methods 48
Figure 2.24: Cumulative distributions of errors between the modeled values and the 90% interpolation control points for a selection of interpolation methods. 49
Figure 2.25: Selected shaded-relief maps of modeled bedrock altitude for central Connecticut River Valley using different interpolation methods 50
Figure 2.26: Selected shaded-relief maps of modeled bedrock depth for central Connecticut River Valley using different interpolation methods 52
Figure 2.27: Shading indicates places where the bedrock altitude in the ALT3 model is above the land surface (i.e., above the TOPO100 surface model). 54
Figure 2.28: Purple cells indicate areas where replacement and blending of the two models occurred 55
Figure 2.29: An example of a kriging artifact 57
Figure 2.30: Contours before (left) and after (right) manual adjustments to create a single continuous linear depression linking the isolated individual depressions from the kriging model 58
Figure 2.31: Map of cross section showing bedrock model above topography in Boston area 65
Figure 2.32: Cross section from Figure 2.31 showing bedrock model above topography 66
Figure 2.33: Map of two cross sections in the Deerfield, Massachusetts, area 67
Figure 2.34: Cross section of the northern Deerfield line in Figure 2.33 showing the altitude-based model (medium dashed line) daylighting on the valley margins, and the resulting blended/final model to correct the errors 68
Figure 2.35: Cross section of southern Deerfield line in Figure 2.33; two kriging artifacts are visible in the upper chart where the blended-altitude (thick dashed line) model shows depressions that have been smoothed-over in the final (thick solid line) bedrock altitude model. 69
Figure 2.36: Cross section locations across manually-contoured region in the northern Connecticut River valley 70
Figure 2.37: Northern cross section shown in Figure 2.36 71

Figure 2.38: Southern cross section shown in Figure 2.36 72
Figure 2.39: Map of cross section in region of shallow bedrock in the Williamstown-Adams area 73
Figure 2.40: Cross section in shallow to bedrock areas—all models coincide well 74
Figure 2.41: Overburden structure of the layer-over-halfspace model 76
Figure 3.1: Map of depth to bedrock (meters) derived from modeling the depth to bedrock values for all bedrock wells, bedrock outcrops and shallow to bedrock areas 78
Figure 3.2: Map of the bedrock altitude 78
Figure 3.3: Map of depth to bedrock (meters) derived from subtracting the bedrock altitude from topography 79
Figure 3.4: Map of kriging prediction standard errors in meters—Martha's Vineyard and Nantucket not included 80
Figure 3.5: Map of measurement uncertainty (meters) 81
Figure 3.6: Map and histogram of differences between DTB and DTBALT models for depth to bedrock 82
Figure 3.7: Map showing the range in depth estimates (meters) by the two methods—Martha's Vineyard and Nantucket not included 83
Figure 3.8: Map showing the combined model prediction standard error and observational uncertainty (meters) 83
Figure 3.9: Cumulative histogram of combined error and measurement uncertainty 84
Figure 3.10: Distribution of NEHRP site classes across the state 85
Figure 7.1: The area covered by the reference grid (black) and state land mask (green) 116
Figure 7.2: Gridlines of the 100-meter raster grid cell boundaries 117
Figure 7.3: Original LiDAR 1-meter resolution data (top) and mean elevation at 100-meter resolution (bottom). The flat surfaces on the right side of the top image is part of the Quabbin Reservoir, which have been filled in the bottom image with gridded bathymetry data for the reservoir. .. 118
Figure 7.4: Bedock polygons (red areas) split along the 100-meter grid cell boundaries (light gray lines); each (new) polygon is converted to a point located at it's centroid (black dots) and assigned a depth (DTB) value of zero meters and an altitude (ALT) value of the (mean) 1-meter LiDAR values in the polygon. 119
Figure 7.5: Shallow to bedrock polygons (shaded areas) split along the 100-meter grid cell boundaries (light gray lines), with bedrock polygons erased (holes in shaded areas); each (new) polygon is converted to a point located at it's centroid (dots) and assigned a depth to bedrock (DTB) value of zero meters and an altitude (ALT) value 124
Figure 7.6: Bedrock wells (circles) and overburden wells (squares) with their altitude values displayed; black lines indicate raster cell boundaries, with the modeled bedrock altitude values posted in the cell (large italic lettering); background is LiDAR shaded-relief. These overburden wells were NOT included in the second round of altitude kriging because their maximum altitude values are already higher than the modeled bedrock altitude 128
Figure 7.7: Shaded areas indicate places where ALT3 model of bedrock altitude is higher than TOPO100; darker shades indicate greater excess altitude 129
Figure 7.8: Purple cells indicate blending factor; darker shades indicate areas where the depth-based altitudes will be weighted more relative to the altitude-based cells 130
Figure 7.9: Some examples of kriging artifacts to be filled by inverse-distance weighting of the outlined perimeter cells; markers are well and bk and sb data—note there are no points within these depressions 132
Figure 7.10: Contours before (left) and after (right) manual adjustments to create a single continuous deep depression linking the three separate depressions from the kriging model 133
Figure 7.11: Combined prediction errors and input data measurement uncertainties from 0.2 meters (blue) to 120 meters (orange-red) 135
Figure 7.12: Depth to bedrock determined by subtracting the altitude-based model from the topography. 136

Figure 7.13: Range of depth estimates by two different methods (absolute difference of depth models) from zero (white) to 122 meters (red) 136
Figure 7.14: Overburden structure of the layer-over-halfspace model 142
Figure 7.15 Massachusetts depth to bedrock map used to determine d_s for Equation 2 143
Figure 7.16: Locations of the shear wave velocity profile stations used to estimate Vs_{avg} in this study 143
Figure 7.17: Vs_{avg} values of each station within each grouping with the median (red line) computed from the Vs_{avg} values and the assigned Vs_{avg} value used in the study (purple line) listed in Table 7.3 146
Figure 7.18: Raw shear wave velocity profiles for the four geologic groupings and each median and estimate value as a vertical line 147
Figure 7.19: Final *Vs30*-based seismic site classification map using the *Vs30* groupings in Table 7.1 148
Figure 7.20: a) Layer over halfspace model with the overburden velocity = 220 m/s. b) Three-layer velocity model with layer thicknesses. c) Linearly increasing model 149

List of Acronyms

Acronym	Expansion
ALT	Altitude
ALT1	First Altitude Raster
ALT2	Second Altitude Raster
ALT3	Third Altitude Raster
ALTERR	Altitude Kriging Prediction Standard Error Raster
BLEND	Blended Bedrock Altitude Raster
BLENDDIST	Blend Distance Raster
BLENDERR	Blended Altitude Kriging Prediction Standard Error Raster
BLENDFAC	Blending Factor Raster
BOR_FLAG	Flag indicating the type of boring, well or data point
BOS	Boston
BSP	Boston Subsurface Project
CC	Cape Cod
CENTROID_X	X Coordinate of a Polygon Centroid
CENTROID_Y	Y Coordinate of a Polygon Centroid
CO-K	Co-Kriging
CONTALT	Contoured Altitude Raster
DEM	Digital Elevation Model
DTB	Depth to Bedrock
DTBALT	Altitude Raster Derived from Depth to Bedrock
DTBCHECK	Depth to Bedrock Check Raster
DTBERR	Depth to Bedrock Kriging Prediction Standard Error Raster
EBK	Empirical Bayesian Kriging
EEA	Executive Office of Energy and Environmental Affairs
ESRI	Environmental System Research Institute
FEMA	Federal Emergency Management Agency
FGDC	Federal Geospatial Data Committee
FHWA	Federal Highway Administration
FID	Feature Identification Number
FINALALT	Final Bedrock Altitude Raster of entire state including islands
FINALDTB	Final Depth to Bedrock Raster of entire state including islands
FINALDTBALT	Final Altitude raster derived from Depth to Bedrock
FINALERRUNC	Final Kriging Prediction Standard Error and Observational Uncertainty
FINALUNC	Final Observational Uncertainty Raster
FIPS	Federal Information Processing Standard
GeoTIFF	TIFF file with embedded georeferencing tags
GIS	Geographic Information System
GQ	Geologic Quadrangle
GWSI	Ground Water Site Inventory
H/V	Horizontal to Vertical

Acronym	Expansion
HDR	Hydrologic Data Report
HVSR	Horizontal to Vertical Spectral Ratio
IDW	Inverse Distance Weighting
ISLANDALT	Altitude Raster for the Islands (Martha's Vineyard and Nantucket)
LiDAR	Light Detection and Ranging
MADEP	Massachusetts Department of Environmental Protection
MAINALT	Mainland Altitude Raster excludes Martha's Vineyard and Nantucket
MassDOT	Massachusetts Department of Transportation
MassGIS	Massachusetts Geographic Information System
MWRA	Massachusetts Water Resources Authority
NAD27	North American Datum 1927
NAD83	North American Datum 1983
NAVD88	North American Vertical Datum 1988
NED	National Elevation Dataset
NED	National Elevation Data Set
NEHRP	National Earthquake Hazards Reduction Program
NGVD29	National Geodetic Vertical Datum 1929
NOBLEND	No Blend Raster
NRCS	National Resources Conservation Service
NWIS	National Water Information System
PAEK	Polynomial Approximation with Exponential Kernal
PATCHALT	Patched Altitude Raster
PATCHCONTALT	Patched Contour Altitude Raster
QA/QC	Quality Assurance/Quality Control
REPALT3	Raster of Cells Requiring Repair on the Third Altitude Raster
REPDIST	Repair Distance Raster
SE	Southeast
SEMA	Southeast Massachusetts
SESAME	Site Effects Assessment using Ambient Excitations
SIR	Scientific Investigations Report
SITE_ID	Site Identification
SPR	State Planning and Research
TFW	Tag Image File Format World File
TIFF	Tag Image File Format
TIN	Triangular Irregular Network
TOPO100	Topography Raster at 100-meter Resolution
UK	Universal Kriging
UK-D	Universal Kriging with Default Parameters
UK-O	Universal Kriging with Optimized Parameters
UNC	Uncertainty
USE_ALT_M	Use Altitude Value in Meters
USE_DTB_M	Use Depth to Bedrock Value in Meters
USGS	United States Geological Survey

Acronym	Expansion
WELL_ID	Well Identification
WRI	Water Resources Investigations
WRIR	Water Resources Investigation Report

This page left blank intentionally.

1.0 Introduction

This study of the Massachusetts Depth to Bedrock was undertaken as part of the Massachusetts Department of Transportation (MassDOT) Research Program. This program is funded with Federal Highway Administration (FHWA) State Planning and Research (SPR) funds. Through this program, applied research is conducted on topics of importance to the Commonwealth of Massachusetts transportation agencies.

Fundamental to any transportation planning and engineering activity is having a reasonable estimate of the depth to bedrock. Knowing the bedrock depth not only influences cost but may also affect selection of the appropriate foundation system for a particular structure. Furthermore, estimates of the bedrock depth, along with the type of overburden (e.g., glacial till, varved clay, sand and gravel) help determine the most appropriate subsurface investigation method to use during project planning, and reduces construction delays and claims brought forward by contractors. Accordingly, there is some uncertainty in planning subsurface investigations that trend towards an ad hoc approach for any transportation project.

1.1 Purpose and Objectives

Massachusetts has several existing data sets containing thousands of borehole and well logs with depth to bedrock measurements that have never been assembled in one place and made readily accessible. The purpose of this project is to compile these data and build a high-resolution data layer of the varying depth to bedrock across the entire state. The overall goal is to help reduce the uncertainty in highway projects by providing a rational approach to clarifying bedrock depth during project planning and design development.

The research has the following objectives:

1. Identify and acquire borehole and geophysical data from existing sources and assemble this information in a spreadsheet for modeling depth to bedrock.

2. Collect HVSR (Horizontal to Vertical Spectral Ratio) survey data in areas where borehole data are sparse and also prepare a calibration curve of depth to bedrock versus fundamental frequency for Massachusetts.

3. Combine bedrock depth, LiDAR data (which provides a high-resolution data layer of the ground surface), and mapped outcrop and shallow bedrock areas from the statewide surficial materials map *(3)* to create continuous bedrock depth and altitude of the top-of-bedrock data layers using appropriate geostatistical methods. Accompany each layer with data quality confidence maps.

4. Use the depth to bedrock model developed above, existing surficial geologic mapping and shear wave velocity data to generate a revised NEHRP soil classification map for Massachusetts.

The main outcomes of this project are resource maps prepared as raster images showing the altitude of the top of bedrock and depth to bedrock as well as a shapefile of the NEHRP soil classifications that can be imported directly into MassDOT's Geographic Information System (GIS) for use in planning and designing transportation projects in Massachusetts.

1.2 Deliverables

Specific deliverables include the following:

1. Master spreadsheet of all drill hole and geophysical data collected as part of Objective 1 above.

2. Statewide calibration curve relating HVSR fundamental frequency and depth to bedrock as part of Objective 2 above

3. All drill hole, geophysical data, bedrock outcrops and shallow to bedrock area data points used to model the altitude of the top of the bedrock surface and the depth to bedrock.

4. 100-meter resolution GeoTIFF image of the depth to bedrock (Version 1) derived from bedrock depth measurements in a data set of drill holes, bedrock outcrops and shallow to bedrock areas using co-universal kriging.

5. 100-meter resolution GeoTIFF image of the altitude of the bedrock surface derived from bedrock altitude determinations in a data set of drill holes, bedrock outcrops and shallow to bedrock areas using empirical Bayesian kriging.

6. 100-meter resolution GeoTIFF image of the depth to bedrock (Version 2). This map is created by subtracting the altitude values in (5) above from a 100-meter resolution LiDAR DEM of surface topography.

7. 100-meter resolution GeoTIFF image of kriging prediction standard errors.

8. 100-meter resolution GeoTIFF image of observational uncertainties.

9. 100-meter resolution GeoTIFF image of combined model prediction process errors and observational uncertainty.

10. 100-meter resolution GeoTIFF image of depth to bedrock ranges (Ver. 1 – Ver. 2).

11. Shapefile of NEHRP site classes (A, B, C, D and E) for Massachusetts at 100-meter resolution plus associated metadata.

1.3 Intended Use and Limitations of Work Products

The new GeoTIFF images provided here are intended for use only as a guide. They are not intended for site-specific engineering design or construction. They can be used for planning purposes and for prioritizing areas that might be examined for targeted subsurface data acquisition and analysis. The work products in no way guarantee the modeled depth to bedrock is accurate; input data uncertainties, estimated modeling errors, and modeled depth ranges are provided as indicators of known uncertainty and error in the modeled estimates, but unknown uncertainties and errors may remain.

Although the data used to make these work products have been processed successfully on a computer, no warranty, expressed or implied, is made by the Massachusetts Geological Survey, University of Massachusetts, Tufts University, GISmatters, Inc., or the Massachusetts Department of Transportation (MassDOT) regarding the utility of the data on any other system, nor shall the act of distribution constitute any such warranty. Every reasonable effort has been made to ensure the accuracy of the information on which the work products are based; however, the Massachusetts Geological Survey, University of Massachusetts, Tufts University, GISmatters, Inc., or MassDOT do not warrant or guarantee that there are no errors or inaccuracies. Efforts have been made to ensure that the interpretation conforms to sound geologic and cartographic principles. No claim is made that the interpretation shown is correct. The Massachusetts Geological Survey, University of Massachusetts, Tufts University, GISmatters, Inc., or Mass DOT disclaim any responsibility or liability for interpretations from these work products or digital data, or decisions based thereon.

1.4 Overview and Previous Work

In glaciated environments, such as Massachusetts, the depth to bedrock can be extremely variable ranging in depth from 0 meters (0 feet) at outcrops to more than 500 meters (1600 feet). These depths can change drastically over short lateral distances. Accordingly, to derive a practical, 2-dimensional understanding of the spatial variability in bedrock depth with reasonable confidence requires an adequate density of point data.

Massachusetts is fortunate to have a wealth of drill hole and geophysical data residing in existing, publicly available data sets. However, these data have never been examined closely or assembled in one place. In addition, MassDOT has seismic refraction data available for various projects that provide bedrock depth. Passive seismic data (Horizontal to Vertical Spectral Ratio, HVSR) are also available, especially in the Boston area. Therefore, one of the main tasks of this project is to assemble as much existing data as reasonably possible into a single, self-consistent, quality-controlled database.

The second major task is to convert all the discrete drill hole and geophysical data into a two-dimensional surface. This requires a model to interpolate the point data. Accordingly, a

portion of this research project examines different methods of interpolation to determine which model produces the least error and honors the data points best.

As far as previous work is concerned, Byron Stone at the USGS developed a map showing the thickness of overburden in 1986 (Stone, unpublished map, 1986) (Figure 1.1). This map was prepared as part of the New England Governor's Conference to study the availability of sand and gravel in the six-state New England region. This map was developed at a scale of 1:250,000 and was based on available surficial geologic mapping and borehole data available at the time. The map only shows the thickness of sand and gravel deposits, which do not cover the entire state. In addition, the thickness data are categorical with only four depth ranges 0-50, 50-100, 100-200 and >200 feet. Thus, the map is very general.

Soller and Garrity published a map of sediment thickness and bedrock topography at a scale of 1:5,000,000 for all the glaciated regions of the U.S. east of the Rockies (Figure 1.2) *(4)*. Soller and Garrity used Stone's 1986 map as the basis for their map *(4)*. However, the map is too small scale to be of much practical value and presents no new data in the analysis.

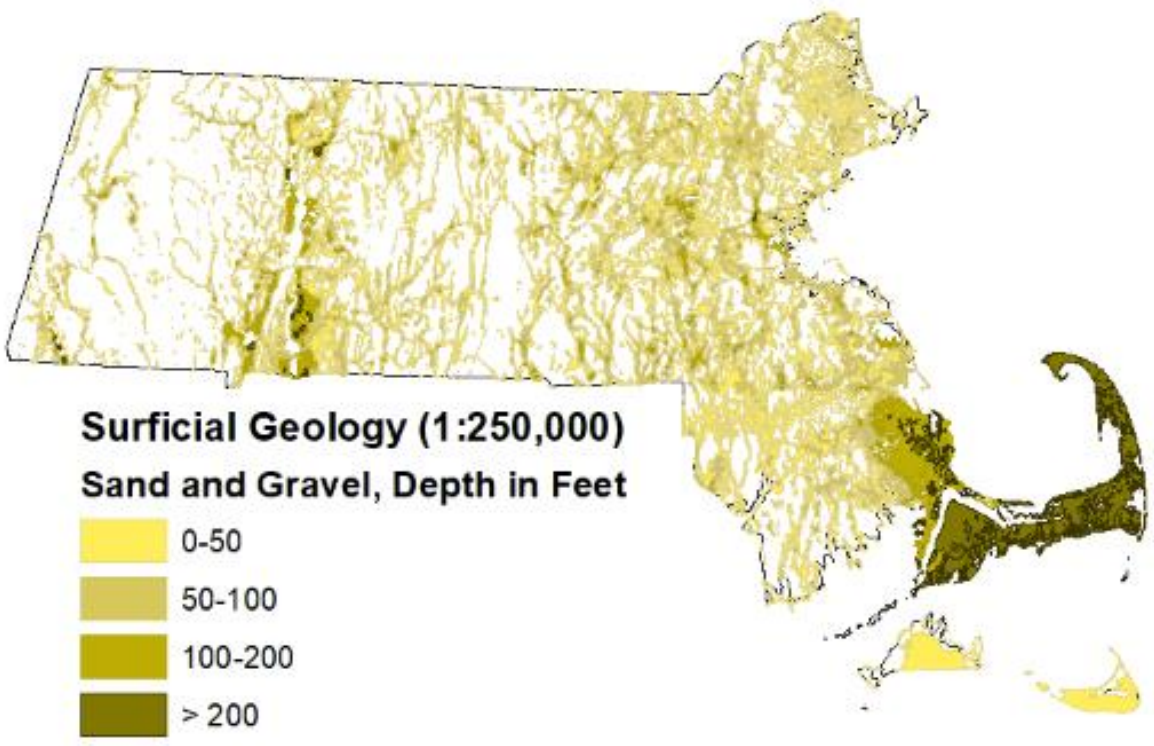

Figure 1.1: Map showing the thickness of sand and gravel deposits in Massachusetts

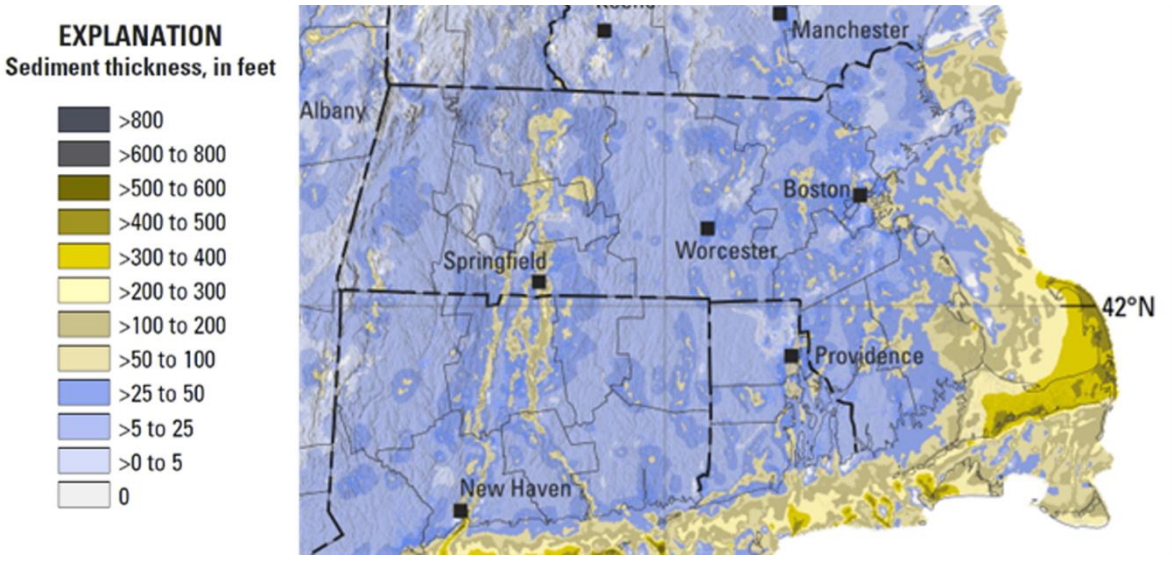

Figure 1.2: Map of sediment thickness at 1:5,000,000 scale resolution

This page left blank intentionally.

2.0 Research Methodology

The research methodology involved several steps. This included 1) compilation of existing borehole, well and geophysical data, 2) collection of additional geophysical field data, 3) data validation, 4) assignment of observational uncertainties, 5) data processing, and 6) modeling. Details of the research methodology are provided below.

2.1 Compilation of Existing Borehole, Well and Geophysical Data

Over a period of 1.5 years, borehole, well and geophysical data were collected from several existing sources. These sources included MassDOT bridge and highway borings and seismic refraction surveys, Massachusetts Water Resources Authority (MWRA) project borings through 2014, data downloads from the USGS National Water Information System (NWIS) and Ground Water Site Inventory (GWSI) databases, USGS Hydrologic Data Reports, borings shown on 1:24,000 scale surficial geologic quadrangle maps, some limited seismic survey data collected by Hager Geoscience, various USGS Scientific Investigation Reports, Water Resources Investigation Reports and Open-File Reports, the Well Driller's Well Completion Report database maintained by the Massachusetts Department of Environmental Protection (MADEP), published and unpublished Horizontal to Vertical Spectral Ratio (HVSR) survey data and, offshore analog seismic survey data collected by the USGS and reinterpreted by Janet Stone (USGS) and Ralph Lewis (marine geologist). There are 28 different data sets.

The data have been compiled into a Master Spreadsheet with 33 sheets and contains a total of 107,702 unique records. There are 61,531 records that provide the depth to bedrock and 41,171 records that are considered overburden points that terminate within the overburden. For the purposes of this study, borings, test holes or wells that met refusal (wells that encounter something hard but it is not confirmed if it is a boulder or bedrock) are assumed to have reached bedrock. FGDC-compliant metadata (Federal Geospatial Data Committee) accompanies the Master Spreadsheet.

Some of the data sources were previously published or were publicly available, some were provided via personal communication while other data were collected as part of this project (see Section 2.2). There is some limited stratigraphic data contained within the data sources.

Coordinate pairs specifying the location of each borehole, well or geophysical data point are in the Mass State Plane coordinate system (NAD83) and all elevations are in NAVD88. Coordinate pairs in NAD27 were converted using the appropriate transformation in ArcGIS 10.8.1. Coordinates expressed in feet were converted to meters using the U.S. Survey foot to metric conversion (Massachusetts uses the U.S. survey foot convention rather than the international foot; 1 U.S. Survey Foot = 1200/3937 meters). When needed elevations were converted from NGVD29 to NAVD88 using the National Geodetic Survey Coordinate

Conversion and Transformation Tool. Latitudes and Longitudes have 6 decimal places of precision. Northings and Eastings have 3 decimal places of precision. A conversion factor of 3.281 feet per meter was used for all conversions of depth from feet to meters. For consistency all units are expressed in meters.

Surface elevations for each data point were determined one of two ways. Some data sets provided surveyed elevations. These were used when available and converted to NAVD88 as needed. Most surface elevations were extracted from the 1-meter resolution LiDAR DEM (digital elevation model) available from MassGIS. Note: the newest version of the Massachusetts statewide LiDAR coverage released in January 2022 provides elevations as integers rather than floating point numbers. The January 2002 LiDAR DEM was used for this project.

A report describing each individual data set is provided in Appendix A. The Master Spreadsheet containing all the data, report and associated metadata can be downloaded here from Dropbox.

2.2 Collection of Additional Geophysical Data

During the summer of 2021, two teams consisting of two students each, equipped with Guralp 6TD seismometers, fanned out across Massachusetts (excluding the Cape and Islands) to collect HVSR survey data at locations where well coverage was relatively sparse. HVSR is a non-invasive technique that is increasing in popularity as a technique to estimate the depth to bedrock. It works well in New England because of the strong impedance contrast between the soft, unconsolidated glacial sediments that overlie hard bedrock. The method determines the resonance frequency of the sediments, which is used to find sediment thickness.

The technique employs a three-component seismometer to record ambient seismic signals in the earth. The seismometer records ambient noise from ocean waves, large storms, tectonic sources, wind and human activity. The seismometer is leveled, oriented to north and allowed to record ambient seismic energy for approximately 30 minutes (Figure 2.1). The seismometer communicates with a laptop using Guralp's Scream software. Data are analyzed using Geopsy software (version 2.7.0).

The north-south, east-west and vertical spectra are found using a fast Fourier transform of each component. The ratio is found using equation 1.

$$\mathrm{HVSR} = \sqrt{\frac{(S(\omega)_{NS}^2 + S(\omega)_{EW}^2)}{2S(\omega)_V^2}}$$

(1)

Figure 2.1: Students collecting HVSR survey data in Northampton, MA. Seismometer is the instrument in the foreground

where $S(\omega)^2_{NS}$ is the north-south spectrum, $S(\omega)^2_{EW}$ is the east-west spectrum and $2S(\omega)^2_V$ is twice the vertical spectrum. Plot HVSR (or H/V) as a function of frequency and a peak will occur at the resonance frequency for the sediment, also referred to as the fundamental frequency (f_0) (Figure 2.2). In Figure 2.2, H/V is the dimensionless ratio of the the horizontal spectra divided by twice the vertical spectrum, the different colored lines on the graph represent the H/V ratio for each 30 to 60 second window of data analysis, and the numbers from top to bottom represent the instrument serial number, station number, frequency in Hertz of the maximum amplitude and depth to bedrock in meters and feet determined by three different regression methods. The heavy black line is the average spectra and the heavy dashed lines represent one standard deviation.

The fundamental frequency depends on the shear wave velocity of the sediment and the wavelength of the seismic wave (Equation 2).

$$\lambda = V_S/f_0 \quad (2)$$

where, λ is wavelength in meters, V_S is shear wave velocity in meters per second and f_0 is fundamental frequency in Hertz. It is well known in geophysics and seismology that the minimum thickness of a layer that can be identified in the subsurface is equal to ¼ of the wavelength *(5, 6)*. So depth, *Z*, is related to wavelength by Equation 3.

$$Z = \lambda/4 \quad (3)$$

Equation 2 then simplifies to,

$$f_0 = V_S/4Z \quad (4)$$

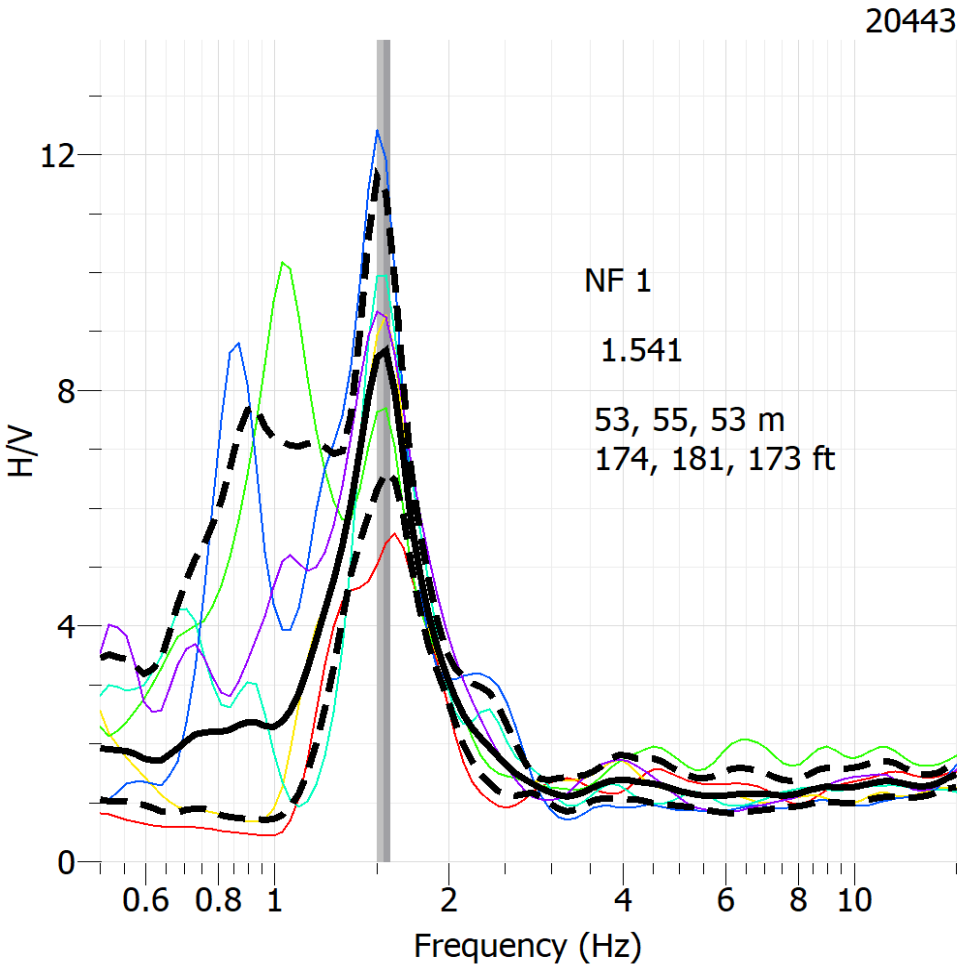

Figure 2.2: Example of plot of H/V versus frequency.

Since V_S and Z are unknown, a calibration curve can be developed by measuring the fundamental frequency at locations where the sediment thickness is known. The relationship is a power law function *(7)* (Equation 5).

$$Z = af_0^b \qquad (5)$$

where, a and b are constants found by fitting a curve to a log-log plot of Z versus f_0. A full explanation can be found in Appendix B.

For this project, a total of 505 HVSR seismic measurements were taken across Massachusetts. Of these, 401 measurements (79%) were accepted as valid measurements (Figure 2.3). Twenty-one percent of the measurements were omitted due to a lack of a clear peak, excessive anthropogenic noise, multiple peaks, the measurement was inconsistent with the local geology and depth to bedrock observed in nearby borings or it fared poorly in the Quality Assurance/Quality Control (QA/QC) testing.

Processing and QA/QC testing involved identifying the fundamental frequency and making sure that it stood out above background noise and was not affected by anthropogenic interference. As a guide to QA/QC evaluation, the SESAME (Site EffectS Assessment using AMbient Excitations) Guidelines for the Implementation of the H/V Spectral Ratio Technique on Ambient Vibrations: Measurement, Processing and Interpretation was used to evaluate the quality of the data *(8)*. The guidelines establish criteria for determining the conditions for peak reliability (i.e., is the peak stable and robust if parameters are changed slightly) and conditions for establishing a clear peak (i.e., does the peak exhibit a clear peak that stands out above the noise). If 6 out of 8 criteria are met the analysis passes. If 4 to 5 of the criteria are met, the plots are examined by the geophysicist. If the peak is clear to the eye and the peak falls within the expected frequency range for bedrock depths in the area, then the site is accepted. All others are rejected.

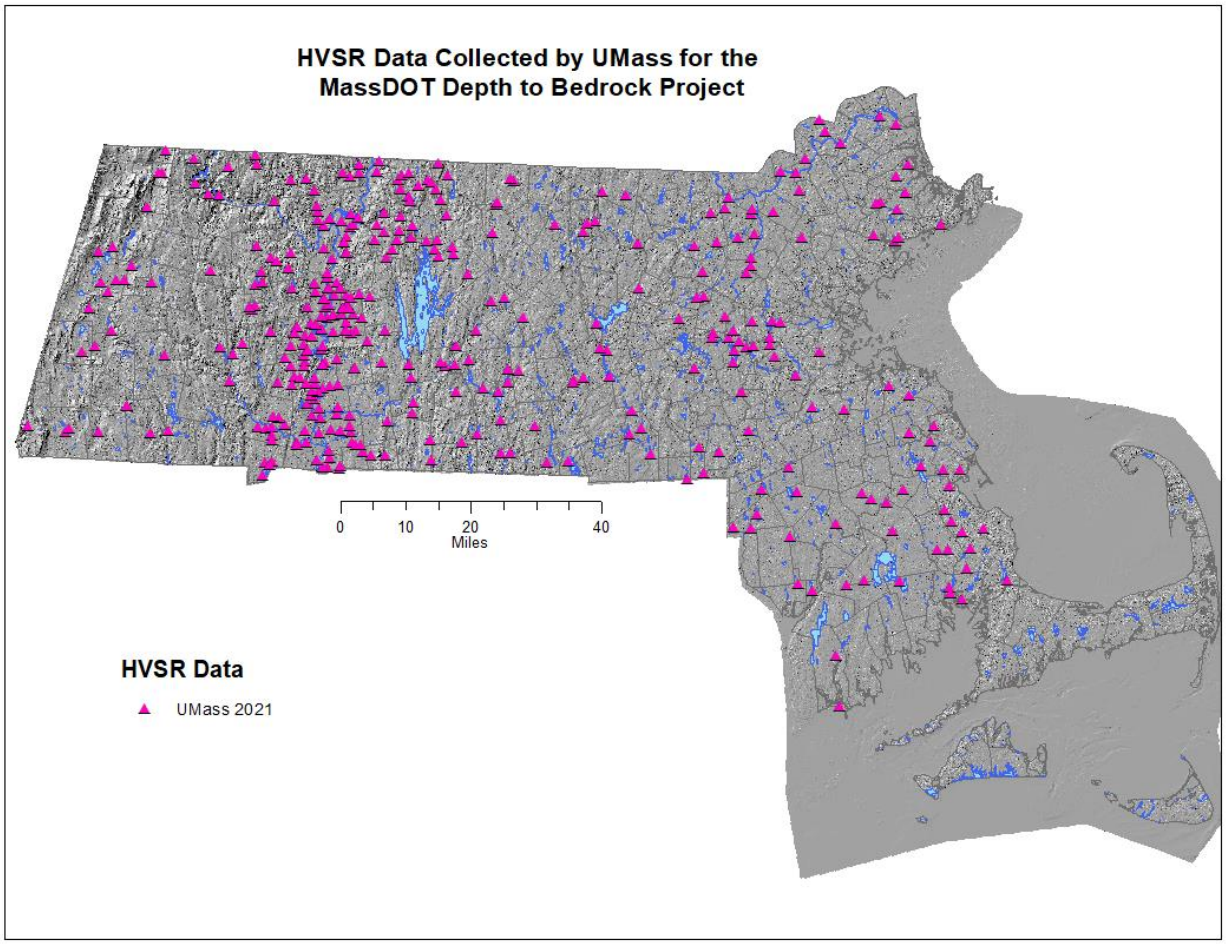

Figure 2.3: Map showing the locations of HVSR seismic measurements collected by the project team during he summer of 2021 (N=401)

During the collection of passive seismic data, 106 sites were used to develop a MA-specific calibration curve of fundamental frequency vs. depth. Calibration involved visiting sites at locations where the depth to bedrock was known. Data from the calibration sites were divided into four categories – excellent, good, fair and poor (Figure 2.4). Several factors were used to determine the data's category. These include: 1) was there a clear, single fundamental frequency peak; 2) how close to the well was the measurement taken; could the field team find the well in the field and set the instrument next to the well; 3) did the measurement pass the QA/QC protocol; 4) what was the level of bedrock measurement reported for a particular well (for example, MassDOT borings have a higher degree of confidence in determining depth to bedrock because typically a geologist or engineer is on site); and, 5) was the depth measurement consistent with the expected depth based on the geology (for example, a measurement of 400 m to bedrock based on passive seismic data next to a well in an upland area of thin glacial till with a depth to bedrock measurement of 4 m is inconsistent and must be considered poor). The calibration curve developed for this project is based on 37 measurements that were categorized as excellent or good (Figure 2.5). In Figure 2.5, pass means the data passed the QA/QC protocol. The best fit calibration curve is estimated depth to bedrock, $Z = 102.07 * fo^{-1.24}$.

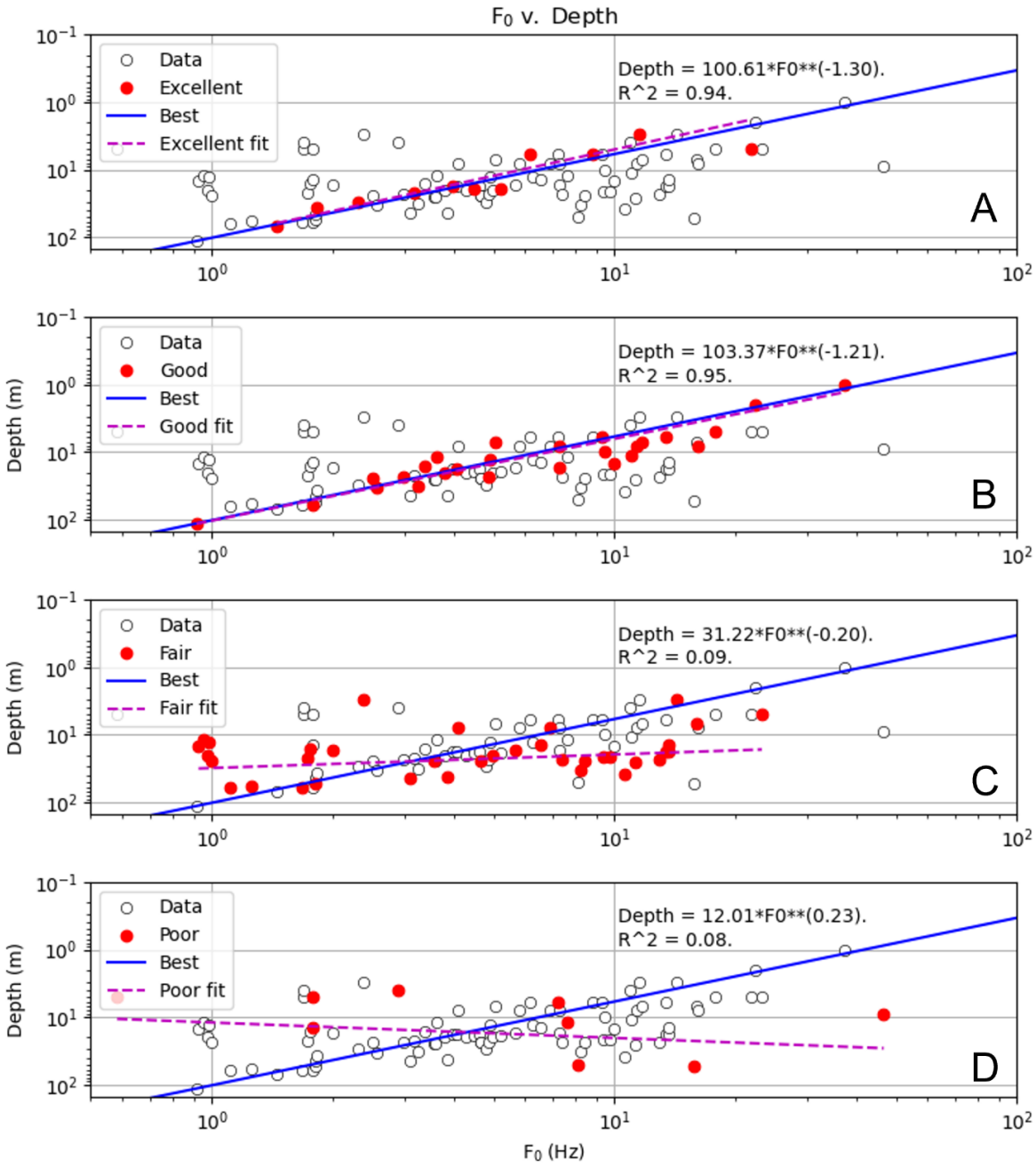

Figure 2.4: Plot of calibration sites categorized by data quality type, excellent, good, fair, and poor. In all plots the blue line is the best fit line through sites categorized as excellent and good; dashed line is the best fit through just the A) excellent, B) good, C) fair and D) poor calibration sites.

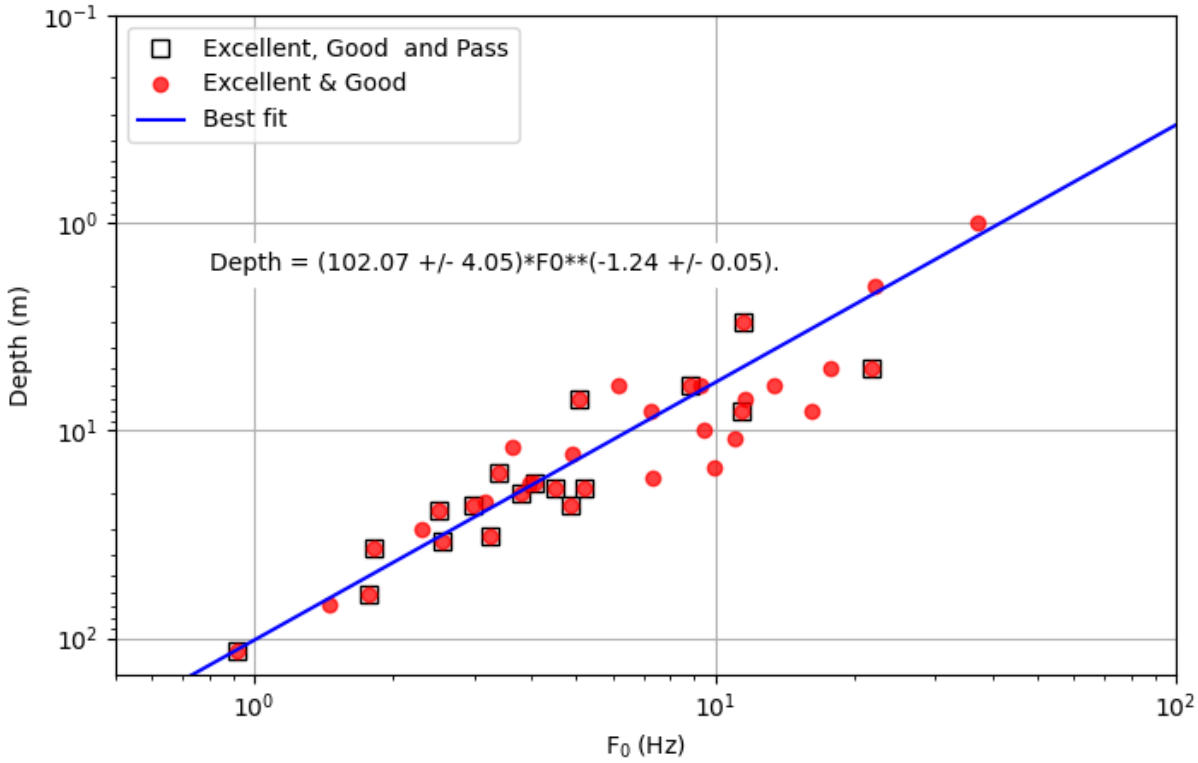

Figure 2.5: Fundamental frequency (fo) versus depth to bedrock for Massachusetts calibration sites (N=37)

Other researchers have developed similar calibration curves. Parolai and others developed a relationship between sediment thickness and resonance frequency in sediments in Cologne, Germany *(9)*. Ibs-von Seht and Wohlenberg *(10)* also developed a similar relationship in the western lower Rhine Embayment in Germany. Some frequency versus depth relationships are very local rather than regional *(11)*. The approach in this study was to develop a regional Massachusetts-specific calibration curve for the entire state.

As an additional quality control check, reproducibility testing was also conducted at 16 sites (Figures 2.6 and 2.7). These are sites where the two field teams went into the field and set the seismometers side by side. In Figure 2.6. the results are compared at two sites, Mount Toby and Greenfield. The x-axis is the frequency in Hertz and the y-axis (H/V) is the ratio of the amplitudes of the horizontal spectra divided by twice the vertical spectrum. The different colored lines on the graph represent the H/V ratio for each 30 to 60 second window of data

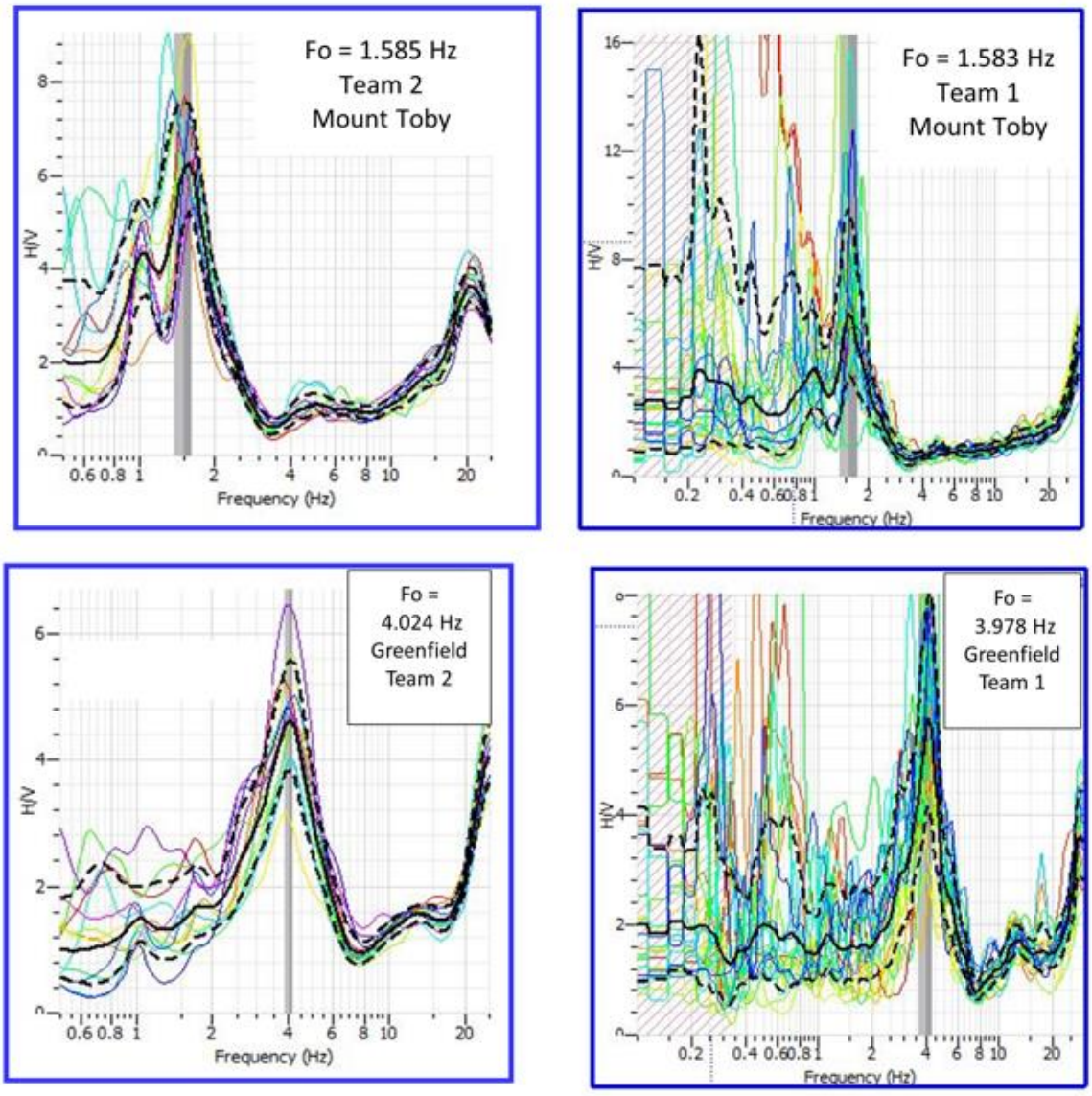

Figure 2.6: Example of horizontal to vertical spectral ratio (HVSR) data collected at two sites (Mount Toby and Greenfield) by the two field teams using different Guralp 6TD seismometers

analysis, and the text on the graphs indicate the frequency (Fo) in Hertz of the maximum amplitude, the team collecting the data, and the location of the measurement. The heavy black line is the average spectra and the heavy dashed lines represent one standard deviation. Comparison of the two seismometers indicated good reproducibility (Figure 2.7). There were 4 exceptions where the automated peak selection tool in the Geopsy software picked different peaks.

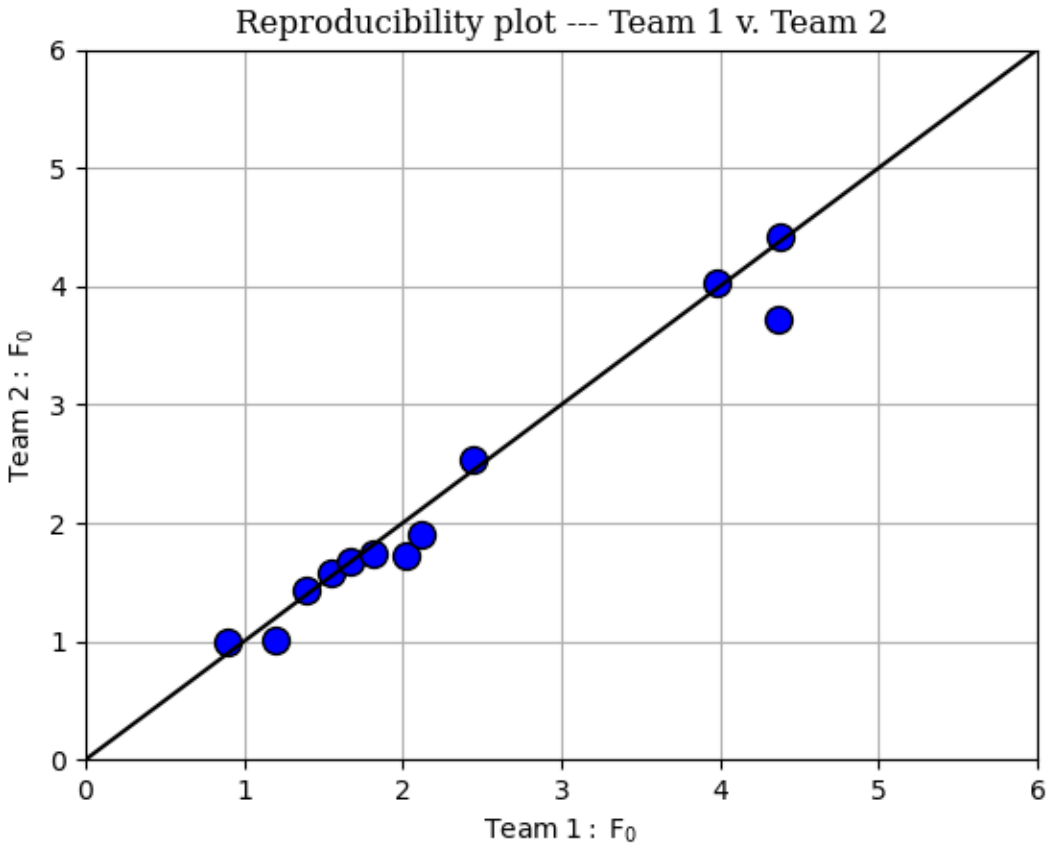

Figure 2.7: Results of fundamental frequency(F_0) reproducibility testing for the two Guralp 6TD seismometers (N=12) with solid black line representing the 1 to 1 fit

2.3 Data Validation

Table 2.1 provides a listing of all the drill hole and geophysical data sets contained in the Master Spreadsheet. Each individual data set was formatted identically with consistent field names and a script prepared to look for within-file inconsistencies such as duplicate site IDs and locations. These inconsistencies were resolved by examining the source data, repairing transcription errors or deleting duplicates as necessary. In addition, surface elevations, depths to bedrock and bedrock altitudes for each record were examined by computing z-errors (surface elevation – depth – altitude = 0). Any non-zero z-error was inspected, evaluated and resolved.

This exercise was repeated to evaluate across-file inconsistencies. A close inspection of the GWSI_Borings, NWIS_Borings, HDR_Borings, GQ_Borings, WRIR03_4320_Borings and Hansen_WRI84_4106_Borings data sets (Nos. 5, 6, 8, 19, 26 and 27 in Table 2.1) was completed to remove duplicate values . Many wells were repeated across these data sets. The

Table 2.1: Name and description of all drill hole and geophysical data contained in the master spreadsheet

No.	Data Set	Description
1	BSP_Borings	Boston Subsurface Project - a database compiled by Dr. Laurie Baise, Tufts University, of borings drilled as part of the depression of the central artery and construction of the Ted Williams Tunnel in Boston, MA; downloaded 1/31/2019
2	BSP_Stratigraphy	Boston Subsurface Project Stratigraphy - contains stratigraphic information including tops and bottoms for select borings in the BSP_Borings data set; Site_ID and Boring_ID are the linking fields
3	Fairchild_Borings	Borings completed as part of studies at the Massachusetts Military Reservation on Cape Cod and contained in Fairchild, Lane, Voytek and LeBlanc, 2103, SIM 3233 *(12)*
4	Fairchild_HVSR	Horizontal to Vertical Spectral Ratio (passive seismic) data collected as part of studies at the Massachusetts Military Reservation on Cape Cod and contained in Fairchild, Lane, Voytek and LeBlanc, 2013, SIM 3233 *(12)*
5	GQ_Borings	Borings included on Geologic Quadrangle maps that were not captured from any other data set including the Massachusetts Hydrologic Data Reports, the Ground Water Site Inventory database, the National Water Information System database
6	GWSI_Borings	Data pull of borings from the Ground Water Site Inventory database provided by Janet Stone (USGS, personal communication on 2/15/2019); contains wells not already in the Massachusetts Hydrologic Data Reports, National Water Information System Database or geologic quadrangle maps; date of data download unknown
7	Hansen_WRI84_4106_Seismic	Seismic refraction surveys collected by Bruce Hansen and contained in WRI84-4106
8	HDR_Borings	Borings from the 27 Massachusetts Hydrologic Data Reports that are not already included in the Ground Water Site Inventory database, National Water Information System database or on the geologic quadrangles
9	USGS_BOS_SE_MA_HVSR	Horizontal to Vertical Spectral Ratio (passive seismic) data provided by B.D. Stone (USGS, personal communication, 12/17/2021); data collected by John Mullaney and Byron Stone

No.	Data Set	Description
10	Pontrelli_2021_HVSR	Horizontal to Vertical Spectral Ratio (passive seismic) data collected and provided by Marshall Pontrelli, Tufts University; data collected in summer 2021
11	UMass_2017_2019_HVSR	Horizontal to Vertical Spectral Ratio (passive seismic) data collected and provided by Bill Clement and Steve Mabee between 2017 and 2019
12	UMass_2021_HVSR	Horizontal to Vertical Spectral Ratio (passive seismic) data collected by UMass in the summer of 2021
13	Pontrelli_2020_HVSR	Horizontal to Vertical Spectral Ratio (passive seismic) data collected and provided by Marshall Pontrelli, Tufts University; data collected in 2020
14	Yilar_2017_HVSR	Horizontal to Vertical Spectral Ratio (passive seismic) data from Yilar, Baise and Ebel, 2017 *(13)*
15	MassDOT_Borings_Post1996	Borings provided by MassDOT from 1996 to the present, includes bridge and highway borings; depth to bedrock extracted from boring logs and plans by UMass
16	MassDOT_Borings_Pre1996	MassDOT Borings that were originally digitized by Dr. Hon and students at Boston College and held at the Massachusetts Water Resources Authority in G-Base; includes borings up to 1996
17	MassDOT_Seismic_Data	Seismic refraction surveys provided by MassDOT and completed in the 1950's and 1960's
18	MWRA_Borings_Pre2015	Massachusetts Water Resources Authority project borings extracted from G-base through 2014; provided by J. Nelson, 12/3/2018; bedrock borings include refusal borings
19	NWIS_Borings	Borings from the National Water Information System database not already included in any other data set including the Ground Water Site Inventory database, Massachusetts Hydrologic Data Reports and geologic quadranlge map; provided by L. Medalie and G. Walsh, 1/21/2021
20	USGS_Offshore_Seismic	Reinterpretation of old, analog seismic data collected by USGS offshore; reinterpretation done by Janet Stone and Ralph Lewis; data provided by J.R. Stone, personal communication, 12/17/2021
21	Oldale_CC_1962_Seismic	Seismic refraction surveys conducted on the outer Cape by Oldale and Tuttle, 1962, Open-File Report 62-95 *(14)*
22	Oldale_CC_1965_Seismic	Seismic refraction surveys conducted on Cape Cod by Oldale and others, 1962, Open-File Report 62-96

No.	Data Set	Description
		and Oldale and Tuttle, 1965, USGS Professional Paper 525D *(14, 15)*
23	Stone_SEMA_Borings_Seismic	Miscellaneous borings and seismic refraction surveys for Cape Cod provided by J.R. Stone, personal communication, 12/17/2021; contains data not included in the USGS_Offshore_Seismic, Oldale_CC_1962_Seismic and Oldale_CC_1965_Seismic data sets, and contains stratigraphic test well on Martha's Vineyard published by Hall and others, 1980 *(16)*
24	SIR2019_5042_Borings	Miscellaneous boring on Cape Cod; Hull and others, 2019, SIR2019-5042 *(17)*
25	Well_Drillers_DB_Borings	Borings from the Massachusetts Department of Environmental Protection Well Driller's Well Completion Report database pulled from the Massachusetts Office of Energy and Environmental Affairs data portal; data retrieval on 5/7/2020
26	Hansen_WRI84_4106_Borings	Borings compiled by Bruce Hansen, 1986, WRI84-4106 and not already included in any other data set; refusal assumed to be bedrock *(18)*
27	WRIR03_4320_Borings	Borings from study by Garabedian and Stone, 2004, WRIR04-4320 not already included in other data sets *(19)*
28	Hager_Geophysical_Data	P-wave and Multi-Analysis of Surface Wave data collected by Hager Geosciences in 2016 as a subcontractor to the Massachusetts Geological Survey. Data were used to develop a National Earthquake Hazard Reduction Program soils map of Massachusetts. Data are contained in Appendix B of final report (Mabee and Duncan, 2017, Preliminary NEHRP Soil Classification Map of Massachusetts, 232 p.) *(20)*

NWIS_Borings data set (No. 19) was taken as the definitive source as it was the most recent data set. In addition, a visual inspection of NWIS boring locations with known wells that had been visited in the field and which are identifiable on the 1-meter LiDAR DEM shows the locations in the NWIS_Borings data set to be accurate; wells plot exactly where the well is on the ground. The GWSI_Borings (No. 6 in Table 2.1) showed a systematic offset to the west southwest of about 40 meters due to a datum shift. The offset was determined at different locations across the state to obtain an average offset and then the correction applied to GWSI_Borings to align them with the NWIS_Borings. Once the GWSI_Borings were shifted, all GWSI wells within a 30-meter search radius of the NWIS wells were selected. GWSI and NWIS Site Names of the selected wells were manually checked and if identical the GWSI boring was removed and the NWIS boring retained.

HDR_Borings (No. 8 in Table 2.1) were inspected visually by comparing the GWSI and NWIS borings with georeferenced boring location plans from the Hydrologic Data Reports. Only those borings in the Hydrologic Data Reports not included in the GWSI_Borings or NWIS_Borings data sets were retained. Any duplicates were removed.

A comparison of Hansen_WRI84_4106_Borings (No. 26 in Table 2.1) and WRIR03_4320_Borings (No. 27 in Table 2.1) with the NWIS_Borings and GWSI_Borings data sets was made by visual inspection and comparison of Site IDs. Only those borings in the Hansen_WRI84_4106_Borings and WRIR03_4320_Borings data sets not included in the GWSI_Borings or NWIS_Borings data sets were retained. Any duplicates were removed.

For MassDOT_Borings_Post1996 (No. 15 in Table 2.1), Pete Connors and Mike Glovasky provided plans showing the locations of boreholes and borehole logs completed for MassDOT projects between 1997 and the present. These included highway, bridge, noise barrier, mast arm, signage and wall borings. Test pits and probes were not tallied. The plans and logs were uploaded to dropbox on May 27, 2021 and organized by contract number or bridge ID. Each boring layout plan and borehole log was examined and the following information manually entered into a spreadsheet: project number, bridge ID number, boring number, Northing, Easting, depth to bedrock (as determined from the boring log), minimum depth to bedrock for overburden borings, surface elevation and any additional information worth noting. Care was needed as some borings used feet while others were in meters. Unfortunately, not all boring logs provided coordinates. Some only provided stationing (surveying term for location along a baseline from a prescribed origin) and could not be tied to geographic coordinates. The total number of borings logs examined was 5,590. However, only 2,516 borings had logs with location information suitable for plotting.

Wherever possible, surface elevations recorded on the boring logs were used when available for the MassDOT_Borings Post1996 data set. This was important for logs taken on bridge decks. The boring must go through the pavement, air and water column before encountering the mud line. Using a LiDAR DEM to establish surface elevations for these borings would have resulted in an error for the depth to bedrock of several tens of meters.

In the 1990s Professor Rudi Hon and students at Boston College digitized the locations of borings and scanned borehole logs for MassDOT highway and bridge projects conducted prior to 1996 (MassDOT_Borings_Pre1996, No. 16 in Table 2.1). The Boston College team digitized thousands of borehole locations. The borings were entered into a database at the Massachusetts Water Resources Authority called G-base. Unfortunately, unique locations were not provided for each individual boring. Sometimes up to 30 borings were placed at the same geographic location. Accordingly, highway borings could not be included in this study because the locations were uncertain. The same problem occurred for bridge borings; several borings were located at the same geographic location. However, because bridges occupy a smaller spatial footprint, the depths to bedrock recorded in the boreholes at each bridge were averaged. If some of the boreholes did not reach bedrock, the deepest boring was selected and retained in the data set. Once this exercise was completed, a second problem emerged. Many borings were assigned to the incorrect bridge and some boreholes were several miles from their assigned bridge. As a remedy, each borehole was moved manually to the correct

bridge using the Bridge ID number. For consistency the borehole was placed at the bridge abutment by the edge of the roadway.

Between 1957 and 1972, MassDOT conducted numerous seismic refraction surveys along many of Massachusetts' transportation corridors (MassDOT_Seismic_Data, No. 17 in Table 2.1). The purpose of these surveys was to determine if rock excavations were needed along proposed roadway cuts. Peter Connors, Massachusetts State Geotechnical Engineer with MassDOT discovered two banker's boxes filled with these old seismic survey reports. All the maps were scanned, georeferenced and shot points digitized. Altitudes of the bedrock surface were interpolated from the seismic survey profiles and entered into the ArcGIS attribute table. Surface elevations were not available in the reports so surface elevations were extracted from the 1-meter resolution LiDAR DEM. Unfortunately, subtracting bedrock altitudes determined decades ago from current day surface topography often leads to negative depths to bedrock because the excavations and rock cuts are now complete. In cases where the depth to bedrock was negative (meaning the bedrock in the past was somewhere above present-day topography) the altitude of the bedrock was assigned the present-day surface elevation.

The Massachusetts Department of Environmental Protection (MassDEP) maintains a well driller's well completion report database (Well_Drillers_DB_Borings, No. 25 in Table 2.1). Well drillers are required to submit a well completion report to the state for every well, exploratory hole, geothermal well or geotechnical boring drilled in Massachusetts. Each well is assigned a Well ID number. Currently there are over 200,000 records in the database. Records can be accessed through the Massachusetts Executive Office of Energy and Environmental Affairs (EEA) data portal: **https://eeaonline.eea.state.ma.us/portal/#!/search/welldrilling**. The SITE_ID in the Well Drillers database contained in this report can be linked directly to the Well ID number in the EEA data portal allowing users to access pdfs of the well logs. For this report, data were downloaded from the EEA data portal on May 7, 2020 and submitted to Peter Grace at MassGIS for street and address verification. MassGIS returned 65,853 records with valid street addresses, or about a third of the total number of records. MassGIS location protocol sites the wells on the centroid of the structure on the parcel and provides a Northing and Easting coordinate. If more than one structure is located on a parcel the location protocol uses an inverse distance weighting based on the area of the footprint of each structure to determine the well's location on a parcel. If no structure appears on the parcel the well is placed on the centroid of the lot. Placing the well on the structure leads to uncertainty in the well location. Typically, the well is located near the structure but not on the structure. Accordingly, well locations may be off by 30 meters or more. Some wells in the Well Drillers database may be duplicated with the NWIS data set. There are no street addresses with the NWIS data set, so it is difficult to identify duplicates with the Well Driller data set. For the time being, any duplicates have been retained in the master spreadsheet.
Once these validation steps were completed to verify locations, remove spurious data and remove duplicates a global unique identifier was assigned to each record. The total number of unique records in the combined data sets is 107,702.

2.4 Assignment of Observational Uncertainties

Uncertainty estimates for each data set reflect the reliability of the depth to bedrock measurement and are provided to give the user some understanding of the level of confidence in any analysis or derivative product based on these data. The assignment of observational uncertainties are summarized in Table 2.2

For any project conducted by MassDOT, verifiable USGS projects or the MWRA (Nos. 1, 3, 15, 18, 24 and 26 in Table 2.2) it is assumed a geologist or engineer was present to log the boring. Accordingly, an uncertainty estimate of 0.6 m (2 feet) is assigned to these records. An exception is MassDOT_Borings_Pre1996 (No. 16 in Table 2.2). Because many of the borings were assigned to the incorrect bridge or were many miles from the bridge, these borings had to be moved manually to the correct bridge using the bridge ID number. For consistency the borehole was placed at the bridge abutment by the edge of the roadway. As a result, there is uncertainty in the location of the borehole which produces greater uncertainty in the depth measurement. For example, the boring may have been constructed near the underpass rather than up near the bridge deck resulting in significant differences in the surface elevation of the borehole. For these reasons an uncertainty of 3 meters was adopted for this data set.

Seismic refraction surveys (Nos. 7, 17, 21, 22 and 28) in Table 2.2 were given an uncertainty of 10% for depths greater than 6 meters (20 feet) and 0.6 meters (2 feet) for depths less than 6 meters (<20 feet). These are the uncertainties suggested by Hager-Richter Geoscience and adopted here (Hager-Richter Geoscience, personal communication, January 2022).

An uncertainty of 6 meters is assigned to HVSR seismic data (Nos. , 9, 10, 11, 12, 13 and 14 in Table 2.2). This uncertainty is based on comparing calculated depth to bedrock determined from HVSR measurements with sites where the depth to bedrock is known. The median of the difference between the actual depth to bedrock and estimated depth to bedrock using HVSR is 6 meters. This uncertainty was determined as part of the calibration exercise conducted during the summer of 2021 and then unilaterally assigned to all HVSR data sets.

GQ_Borings (No. 5 in Table 2.2) were assigned an uncertainty of 2 meters. It is unknown who drilled these wells and whether or not a geologist or engineer was present when the well was drilled. Therefore, these wells were assigned a greater uncertainty.

Table 2.2: Observational uncertainties assigned to each data set

No.	Data Set	Uncertainty (m)
1	BSP_Borings	0.6
2	BSP_Stratigraphy	N/A
3	Fairchild_Borings	0.6
4	Fairchild_HVSR	6
5	GQ_Borings	2
6	GWSI_Borings	5
7	Hansen_WRI84_4106_Seismic	0.6 m for depths < 6 m, otherwise 10%
8	HDR_Borings	5
9	USGS_BOS_SE_MA_HVSR	6
10	Pontrelli_2021_HVSR	6
11	UMass_2017_2019_HVSR	6
12	UMass_2021_HVSR	6
13	Pontrelli_2020_HVSR	6
14	Yilar_2017_HVSR	6
15	MassDOT_Borings_Post1996	0.6
16	MassDOT_Borings_Pre1996	3
17	MassDOT_Seismic_Data	0.6 m for depths < 6 m, otherwise 10%
18	MWRA_Borings_Pre2015	0.6
19	NWIS_Borings	5
20	USGS_Offshore_Seismic	10
21	Oldale_CC_1962_Seismic	0.6 m for depths < 6 m, otherwise 10%
22	Oldale_CC_1965_Seismic	0.6 m for depths < 6 m, otherwise 10%
23	Stone_SEMA_Borings_Seismic	See explanation below
24	SIR2019_5042_Borings	0.6
25	Well_Drillers_DB_Borings	5
26	Hansen_WRI84_4106_Borings	0.6
27	WRIR03_4320_Borings	See explanation below
28	Hager_Geophysical_Data	0.6 m for depths < 6 m, otherwise 10%

Most of the borings contained in the HDR_Borings (Hydrologic Data Reports), GWSI_Borings, NWIS_Borings and Well_Drillers_DB_Borings data sets (Nos. 6, 8, 19 and 25 in Table 2.2) typically come from well drillers. Well drillers typically embed the casing into the bedrock an average of 15 feet (4.5 meters) or more depending on the degree of weathering or fracturing. It is unclear whether the driller noted the top of the bedrock as the point of first encounter while drilling or the depth to competent bedrock (depth of casing). Accordingly, an uncertainty of 5 meters was assigned to this data set.

During the 1960's the USGS conducted numerous cruises in the offshore waters of Massachusetts to collect seismic reflection data (USGS_Offshore_Seismic, No. 20 in Table 2.2). Recently, Janet Stone (USGS, retired) and Ralph Lewis (former state geologist of Connecticut and marine geologist) reinterpreted the analog seismic reflection data for the new Massachusetts statewide Quaternary Geologic Map currently in preparation. Part of that

interpretation included an estimate of the altitude of the crystalline bedrock below the Quaternary and Holocene sediment packages in the offshore areas of Cape Cod Bay and Nantucket Sound. Since the depth to bedrock below the seabed is not known the normal rules for assigning uncertainty to seismic data in terrestrial areas cannot be applied. In this case, an arbitrary uncertainty of 10 meters was ascribed to this data set.

The Stone_SEMA_Borings_Seismic data set (No. 23 in Table 2.2) contains both borings and seismic data. The seismic data are located offshore and are assigned an uncertainty of 10 meters because there is no depth to bedrock information below the seabed. The data set also contains three deep holes in Eastham, Chatham and Martha's Vineyard but it is unclear who logged the holes. Accordingly, an uncertainty of 2 meters is assigned to this data set. Finally, five miscellaneous research holes were constructed by the USGS and given an uncertainty of 0.3 meters (1 foot) because of the level of precision required for research.

WRIR03_4320_Borings data set (No. 27 in Table 2.2) contains borings that were constructed by the USGS or by a consultant installing monitoring wells for the Town of South Hadley. These borings were assigned an uncertainty in the depth estimate of 0.6 meters (2 feet) because it was assumed a geologist or engineer was on site. Two wells in this data set were domestic wells and assumed to be installed by a well driller with no geologist or engineer on site. These latter wells were assigned a depth uncertainty of 5 meters.

The uncertainty information will be used to propagate uncertainty through the modeling process in the steps to follow.

2.5 Data Processing

2.5.1. Overview

The overall goal of the processing is to use the available drill hole and geophysical data to generate the "best" continuous statewide estimates of the depth to bedrock (also equivalent to overburden thickness) and the altitude of the bedrock surface. The word "best" is in quotes because it has no single, objective definition: it depends on a number of factors, including how the results will be represented, how they will be used, and trade-offs between level of detail vs. degree of confidence. Details on data processing are provided in Appendix C.

2.5.2. Data Processing Software

Except where otherwise noted, all processing was performed using ESRI ArcGIS Desktop version 10.8.1, including all available extensions and tools (e.g., Spatial Analyst, Geostatistical Analyst, etc).

2.5.3. Input Data Characteristics

With 107,000+ drill hole and geophysical data points distributed over a statewide land surface area of ~21,000 square kilometers, the *average* well density is roughly 5 wells per

square kilometer, equivalent to an area of about 450x450 meters per well. However, the wells are far from uniformly distributed: they are concentrated in populated and topographically low-lying and gently-sloping areas, and they are much sparser in less-developed and topographically higher and steeper areas. Across the state, observed well densities range from hundreds of wells per square kilometer to tens of square kilometers per well (Figure 2.8).

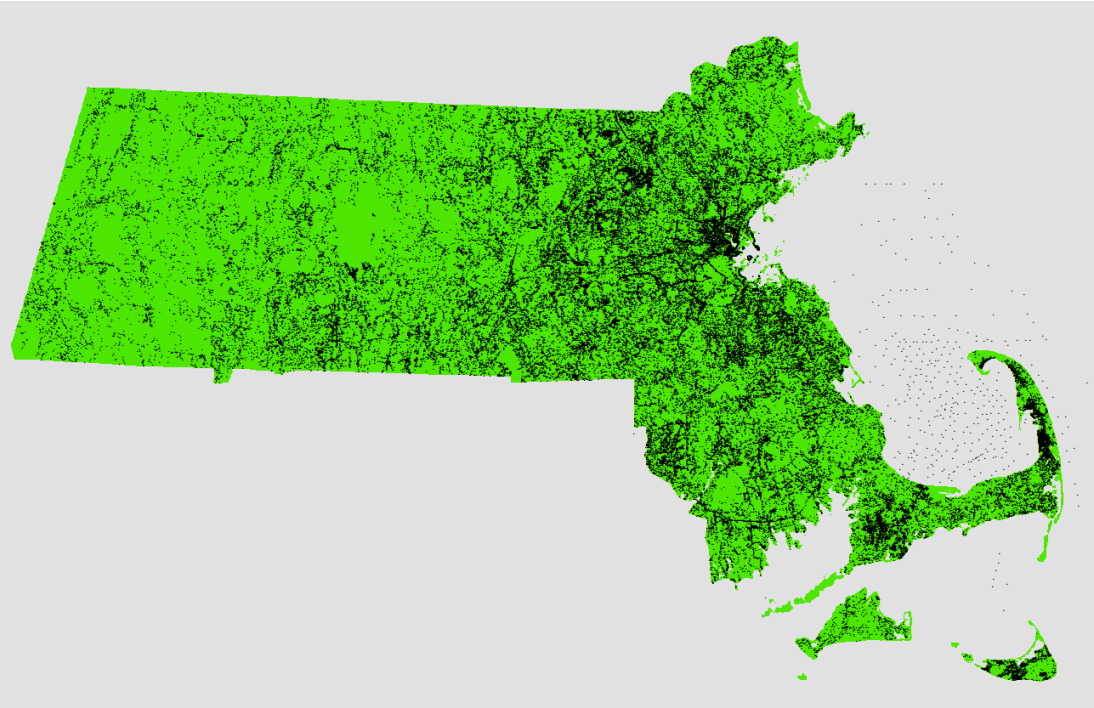

Figure 2.8: Distribution of drill hole and geophysical data point (black dots) locations; the density varies greatly across the state

Data point density is further complicated by consideration of the type of data point: only 57% of the data points reach bedrock or refusal (referred to hereafter as bedrock points or wells); the remaining 43% did not drill deeply enough to encounter bedrock (referred to hereafter as overburden points or wells). Overburden points are not as useful or informative as bedrock points as they provide only a minimum depth-to-bedrock value as a one-sided constraint that is an unknown distance above the actual bedrock surface. The distribution of bedrock vs. overburden wells is not spatially uniform; for example, there is a concentration of overburden wells on Cape Cod where bedrock is much deeper on average (Figure 2.9).

The reliability of the measured depths is a further consideration: estimated uncertainties range from 0.3 meters for high-quality, survey-grade measurements to more than 15 meters for less closely controlled seismic refraction data (Figure 2.10). This variable uncertainty complicates the task of data processing and assessing confidence in the final results.

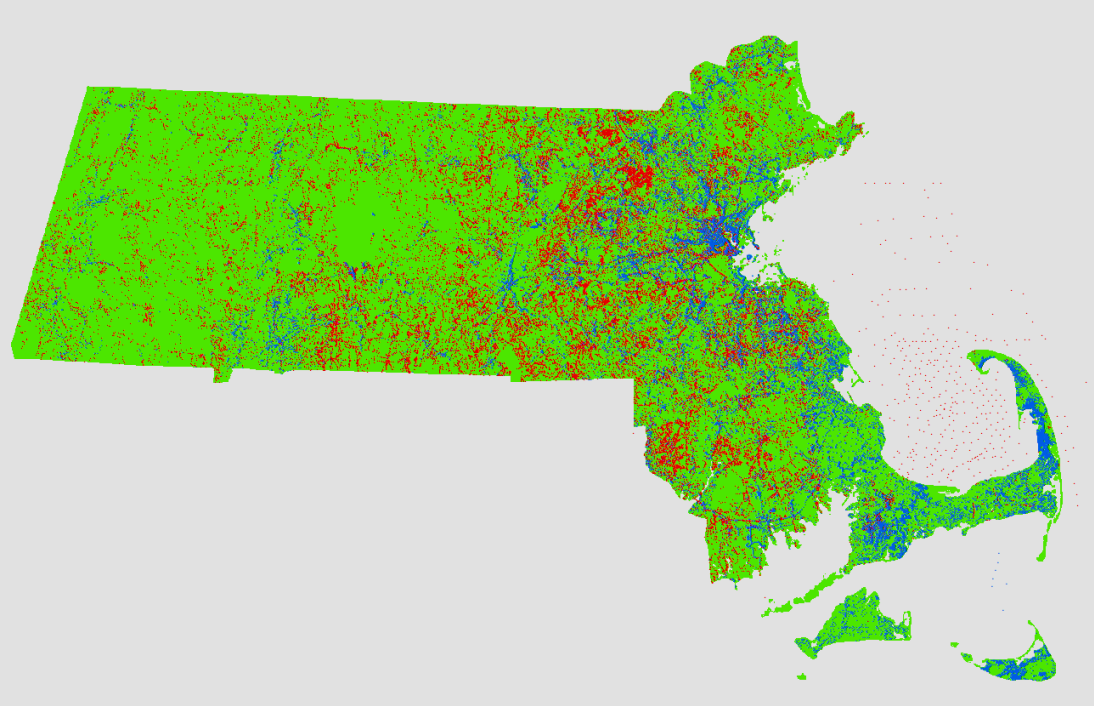

Figure 2.9: Distribution of bedrock points (red) and overburden points (blue); neither is uniformly distributed

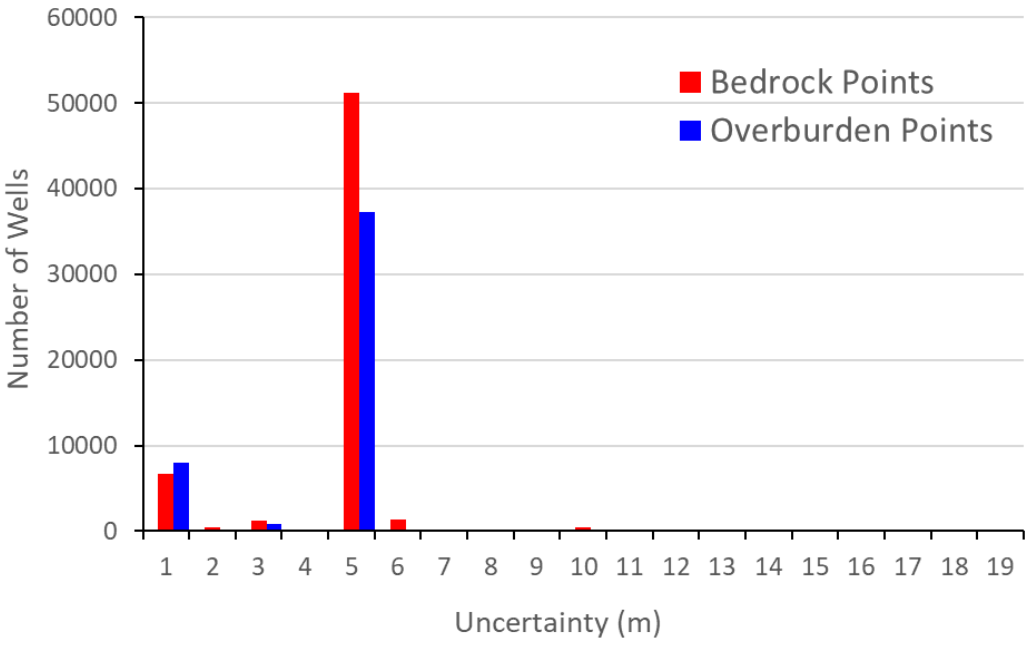

Figure 2.10: Histogram of observational uncertainty by data type

The bedrock depth values exhibit high spatial variability over all horizontal length scales; some of this may reflect data quality issues where wells of different reliability are near to each other, but even in areas with dense, high-quality samples the depth measurements can vary by more than 20 meters across horizontal distances of a few meters, so it is likely that the bedrock surface exhibits abrupt altitude changes (Figure 2.11). The processing approach should be one that permits such variable depth changes in the resulting surface.

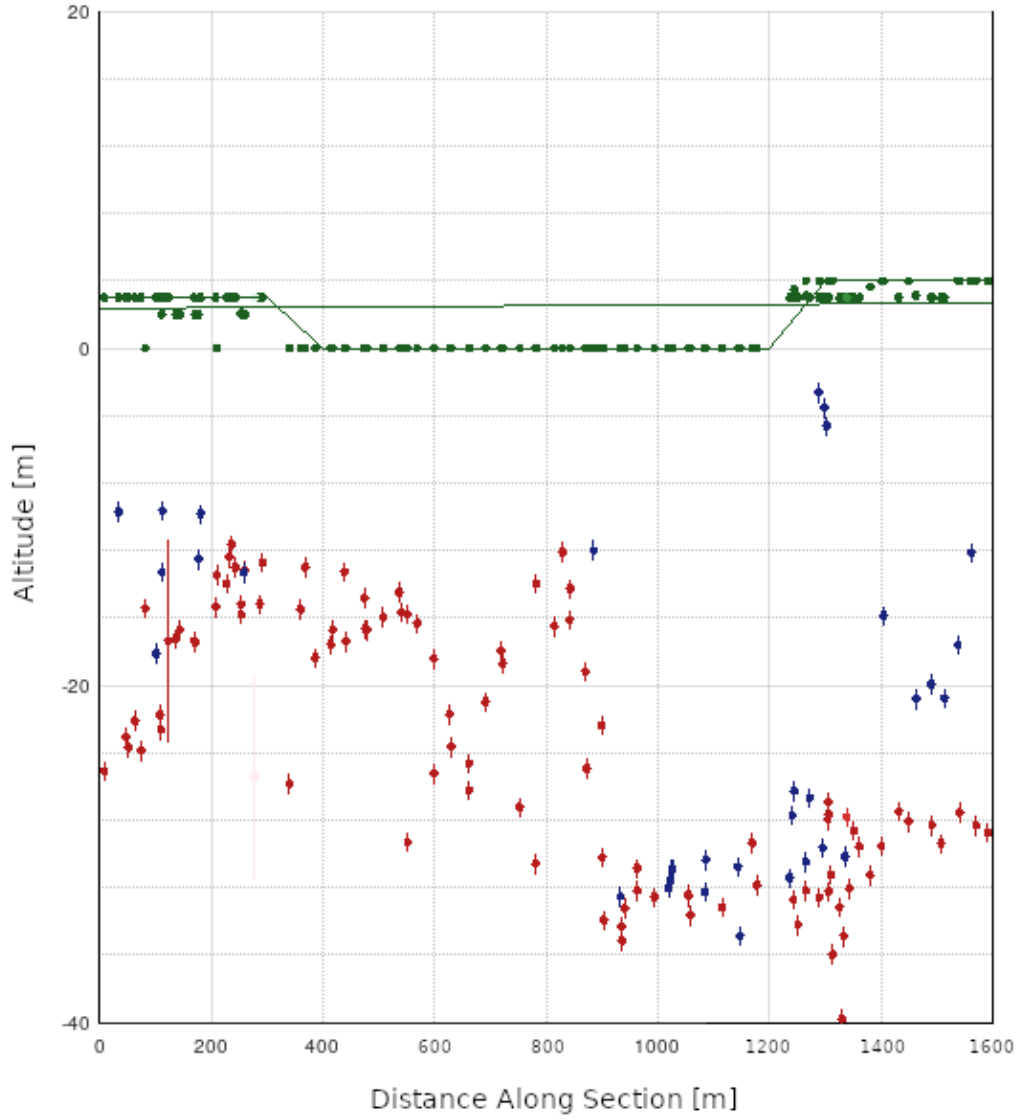

Figure 2.11: Profile along the Ted Williams Tunnel in Boston, MA. Red points are bedrock altitudes from bedrock borings; blue points are altitudes of maximum overburden boring depths; green points are topographic elevation; boring altitudes include vertical lines showing +/- uncertainty ranges.

2.5.4. Output Data Format

The selection of an output data format or representation affects all other processing considerations. The requirement of continuity—that is, of having an estimated value of bedrock altitude/depth at every location throughout the state—can only be met with two available data structures: a raster with estimated values on a uniform grid of locations (square cells), or a triangular irregular network (TIN) with estimated values at irregularly-distributed point locations and implicitly defined between those points by triangular planar surfaces passing through neighboring triplets of points. Each data structure format has advantages and disadvantages in the context of this project that need to be considered when choosing which to use.

One advantage of a TIN is that it can operate on and represent data values in the exact locations where they were measured; it naturally adapts to any arbitrary spatial distribution of measurement points. TINs are also better at representing linear surface features such as ridgelines or stream channels, assuming the data are collected along those lines (in this study, that is not the case). TINs can be very efficient in terms of the number of data points needed to define surface morphology, but only when the input points have been carefully selected to coincide with surface breaks, peaks, sinks, and other features (again, the data used for this study were not collected in this manner). Overall, however, the TIN representation of surfaces as a collection of planar elements is not ideal, particularly as point density decreases and the linear interpolation between control points becomes increasingly unrealistic as a model of the bedrock surface.

Rasters have a number of advantages over TINs: they are much better suited for performing computations involving multiple variables ("map algebra"); they can represent more complex (e.g., curved, noisy, or discontinuous) surfaces; they are better able to generate and make use of statistical characteristics of data; their uniform size facilitates consistent error estimation and propagation; they are a supported output format for all the Geostatistical Analyst modeling tools in ArcGIS (TINs are not); and they can be displayed and used (when formatted as GeoTIFF images) without specialized GIS software.

An important disadvantage of the raster model that must be recognized and accounted for in the data processing is that it implicitly generalizes input information: if there is more than one input value within a raster cell (for example, an outcrop and a couple of borings), that information is lost as the multiple values are reduced in some way (averaging, taking the max or min, etc) to a single value for the cell. Positional information is also lost: an input value in a corner of a raster cell will be moved implicitly to the center of the cell. When working with data of varying type (point, line, raster), relationships among data values can be altered through the process of representing and operating on the values as rasters. For example, in this project, a bedrock outcrop on a steep hillslope in the corner of a raster cell might cause the bedrock altitude to be estimated near the outcrop's elevation, which is higher than the mean elevation of the raster cell; when compared with topography, this cell would have an invalid bedrock elevation above the cell's topography, even though it is based on a valid bedrock observation within that cell. These sorts of discrepancies, though generally small in magnitude, occurred throughout the course of this project and required periodic adjustments to be made to maintain different datasets in a valid relationship with each other.

For this project it was concluded that raster output is the better choice for representing the estimated bedrock surface (Figure 2.12).

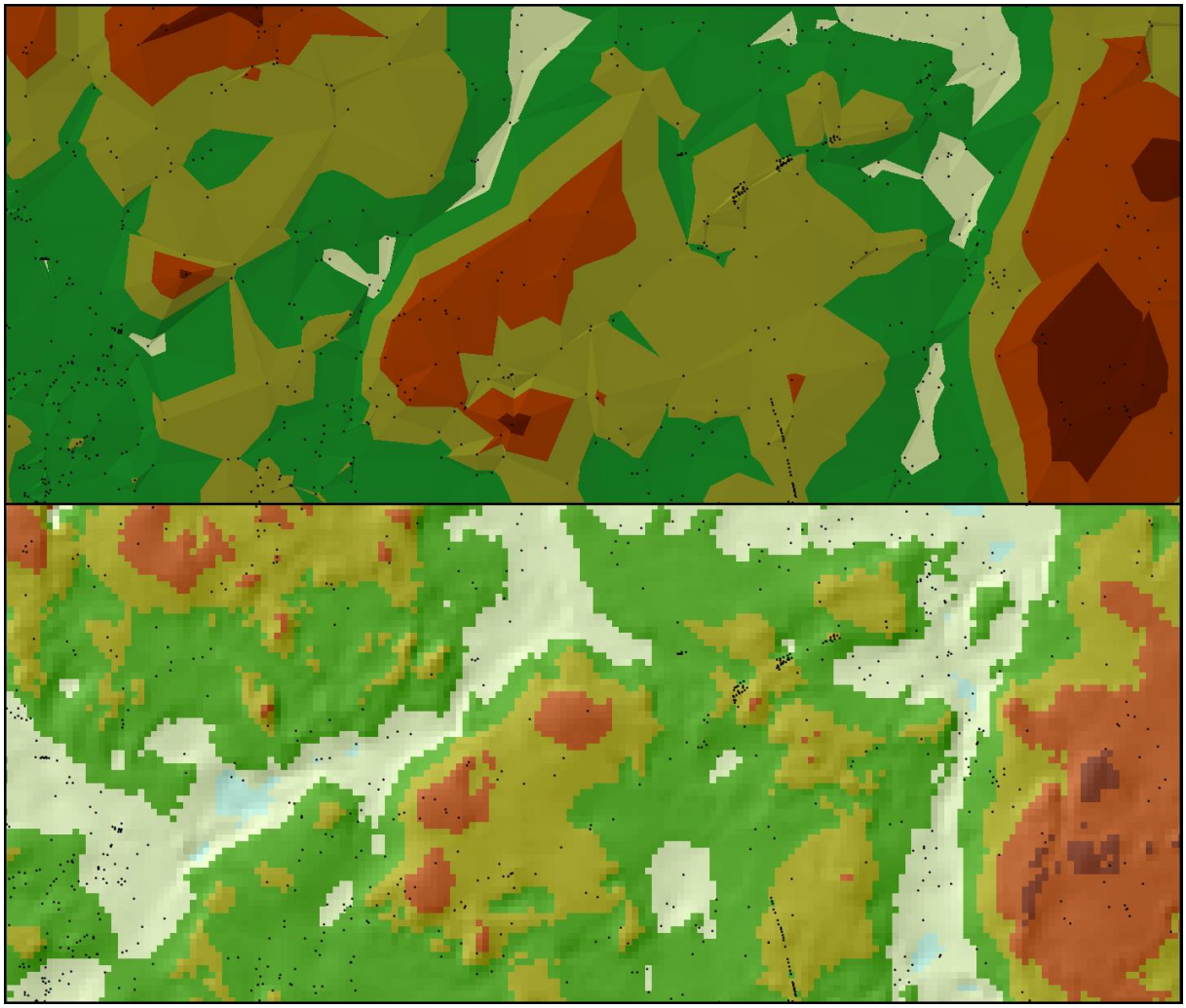

Figure 2.12: Comparison of TIN (top) and raster (bottom) representations of the same area. Black dots are input data points.

2.5.5. Raster Resolution

With the selection of a raster format to represent the bedrock surface and related variables (depth, uncertainty, etc), the next step involved choosing the best resolution—raster grid cell size—to use. This decision required finding some reasonable balance between several competing considerations: larger cell sizes lose more information as multiple wells fall within a single cell and must be averaged together into a single value; higher resolution (smaller cell sizes) can preserve and convey more detailed information about the bedrock surface, but at the cost of more poorly-constrained interpolation in areas of sparse input data, larger data volumes to manage, and exponentially-increasing processing times. The benefits of increasing the resolution also start to decline as there become fewer and fewer areas with

sufficient input data density to take advantage of reduced cell sizes. A final, more qualitative consideration is the relationship between the vertical accuracy of the results vs the horizontal level of detail: with input data uncertainties and prediction errors reaching tens of meters in some areas there is little value in making horizontal scales of a similar or smaller size.

To apply the above considerations and guide the choice of raster resolution, Table 2.3 examines how raster cell size would affect the distribution of well counts within the cells and the number of cells and data points that would be created, stored, managed, and processed. Table 2.3 shows some of these numbers for cell sizes ranging from 10 kilometers down to 20 meters. The columns give the number of cells that would cover Massachusetts' land area, the percent of land cells having no wells (% empty), the percent of the remaining (i.e., well-containing) cells having exactly 1 well, the percent of remaining cells containing more than 5 wells, and estimates of the number of bedrock outcrop (*bk*) and shallow to bedrock (*sb*) data points that would have to be managed. The shaded row highlights the chosen resolution of 100 meters as the best balance between preserving information (almost 88% of the non-empty cells have just one well in them, and less than 1% have more than 5 wells) without excessive waste (for smaller cell sizes over 99% of the cells are empty) and unmanageable data volumes (cell counts and *bk* and *sb* data points climb exponentially with each decrease in cell size). This strikes a reasonable balance of the competing factors that captures sufficient detail where data density is high without adding lengthy processing time but still produces reasonable interpolation in areas of sparse data coverage.

Table 2.3: Raster cell and point statistics for various raster resolutions

Cell Size	# Land Cells	% Empty	% 1 Well	% >5 Wells	# bk Points	# sb Points
10km	264	1.9%	1.2%	94.2%	35,776	16,416
5km	1,006	8.2%	2.5%	91.1%	66,145	17,878
2km	6,349	23.9%	8.1%	68.1%	67,256	22,639
1km	25,560	44.8%	23.5%	30.8%	69,128	31,822
500m	101,741	70.6%	47.3%	8.0%	72,950	54,866
200m	637,314	91.9%	74.4%	1.2%	85,032	161,423
100m	2,547,629	97.5%	87.7%	0.3%	107,226	463,776
50m	10,193,766	99.3%	95.8%	0.1%	159,325	1,536,315
20m	63,711,283	99.9%	99.0%	0.0%	377,316	8,496,611

2.5.6. Master Reference Grid

For internal consistency and compatibility with drill hole and geophysical data, all data were processed using the NAD 83 Massachusetts State Plane Mainland FIPS 2001 coordinate system. Any data obtained that were not already in this coordinate system were re-projected before use.

To ensure consistent handling of all input data, especially with respect to correct co-registration of all location data, a statewide master 100-meter reference grid clipped to the

state boundary was defined. This insures that any rasters produced from the data will co-register perfectly with each other. The reference grid is converted to a shapefile in ArcGIS. The resulting shapefile contains roughly 2.1 million polygons of 100 x 100 meters, corresponding to approximately 21,000 square kilometers of land surface area in the state.

2.5.7. 100-meter Topography

The current land surface plays a crucial role in this project: it places a continuous upper bound on the allowable altitude of the modeled bedrock surface, and serves as a reference for depth-to-bedrock analysis. To obtain a downsampled topography raster on the 100-meter reference grid the latest statewide 1-meter LiDAR raster was used. Using statistics tools in ArcGIS, the mean elevation within each 100 x 100 meter cell was calculated from the 10,000 indiviudal 1 x 1 meter cells within each reference grid. This generates a 100-meter topography raster in which each cell's value is the mean elevation of the 1-meter LiDAR elevations within it. This 100-meter resolution raster is designated as TOPO100 for later use.

The surfaces of lakes, ponds, and reservoirs in the LiDAR dataset are assigned constant elevation values. In most cases these features are small enough that the effect of using the water surface instead of the lake-bed elevation is negligible. In the case of the Quabbin Reservoir, however, the surface area is quite large, and moreover, well data are virtually absent throughout the region. To obtain a more useful constraint on bedrock altitudes in this region, MassGIS bathymetry contours of the Quabbin were rasterized using the ArcToolbox "Topo To Raster" tool. This 100-meter Quabbin bathymetry raster was substituted for the LiDAR cells (Figure 2.13). In figure 2.13, the flat surfaces on the right side of the top image are parts of the Quabbin Reservoir, which have been filled in the bottom image with gridded bathymetry data for the reservoir.

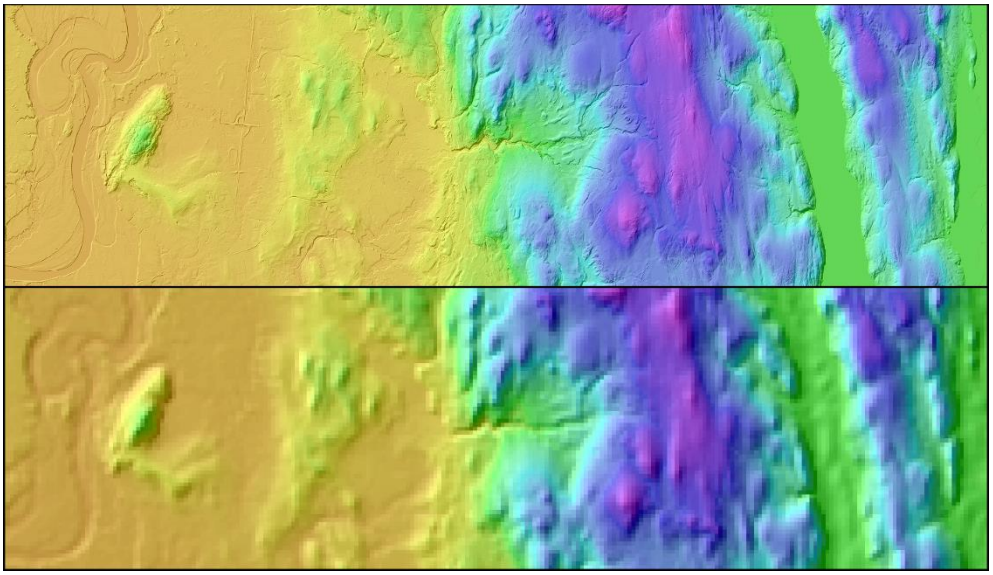

Figure 2.13: Comparison of original 1-meter resolution LiDAR (top) with 100-meter resolution topography (bottom)

2.5.8. Preparation of Surficial Geology Proxy Data

In 2018, the USGS published the new surficial materials map of Massachusetts *(3)*. This map was produced at a 1:24,000 scale level of detail and was based on field mapping conducted over many decades beginning in 1938. The map contains two map units that can provide additional information on the depth to bedrock. First, many of the geologists mapped individual outcrops. The outcrops appear as solid red polygons on the geologic map and a total of 65,409 polygons have been mapped (bk is the map unit symbol). Each bedrock outcrop provides a known altitude for the bedrock surface and a known depth to bedrock because they are at the ground surface. In addition, many of the outcrops occur in the higher terrain where well data are sparse.

The second map unit on the new statewide surficial materials map is “shallow to bedrock areas” (sb is the map unit symbol). Shallow to bedrock areas are defined as a region where bedrock is generally less than 3.5 meters deep (10 feet) or there are too many individual outcrops to map at a scale of 1:24,000. Some mappers took the time to map individual outcrops whereas others tended to lump these areas into one larger polygon of shallow to bedrock areas. Approximately 15% of Massachusetts is mapped as shallow to bedrock and most of these areas occur in higher terrain where well data is relatively sparse.

2.5.9. Bedrock Outcrops (bk)

The bedrock outcrop polygons indicate the extent of observed bedrock outcrops. To convert these to point values with bedrock altitude and depth-to-bedrock values, the following steps were performed to create point data for each polygon or portion of a polygon within each 100-meter grid cell:

1. Any outcrop polygon that intersected the 100-meter gridlines were split using the ArcToolbox "Intersect" tool.

2. The ArcToolbox "Add Geometry Attributes" tool was used to add CENTROID_X and CENTROID_Y attributes to the polygon attribute table, containing the computed area centroid for each polygon.

3. Three attributes were manually added to the polygon layer's attribute table: ALT for the polygon's (mean) altitude; DTB for the depth to bedrock; and UNC for uncertainty.

4. Mean elevations for these newly split bedrock polygons were computed by running the ArcToolbox "Zonal Statistics As Table" with the polygons as zones and the 1-meter LiDAR raster as values.

5. To move the mean elevations from the table back into the polygon layer, the zonal statistics table was joined to the polygon features using the FID field. The field calculator was used to set the ALT field equal to the MEAN value column in the joined zonal statistics table.

6. The DTB field was assigned zero (0) for all features.

7. The UNC field was assigned a value of 0.3 meters for all features.

There were some bedrock polygons too small to be given a value by the Zonal Statistics tool; these were identified by the absence of assigned ALT values from step 5. To get altitudes for these points, the attribute table for these selected records was exported and converted to a point shapefile; the ArcToolbox "Extract Multi Values To Points" was run to extract the altitude for these small polygons from the 1-meter resolution LiDAR data. Figure 2.14 shows an example of how bedrock polygons (red areas) are split along the 100-meter grid cell boundaries (gray lines). Each polygon is assigned the mean altitude at its centroid (black dots) determined from the 1-meter LiDAR data. A value of zero for depth to bedrock and an uncertainty of 0.3 m (1 foot) is also assigned to each point.

At the end of this processing the 65,409 original bedrock polygons are now split into 111,495 smaller polygons, each with a mean or a point LiDAR value assigned as the ALT attribute, zero assigned to the DTB attribute, 0.3 meters for all UNC values, and point locations in the CENTROID_X and CENTROID_Y attributes.

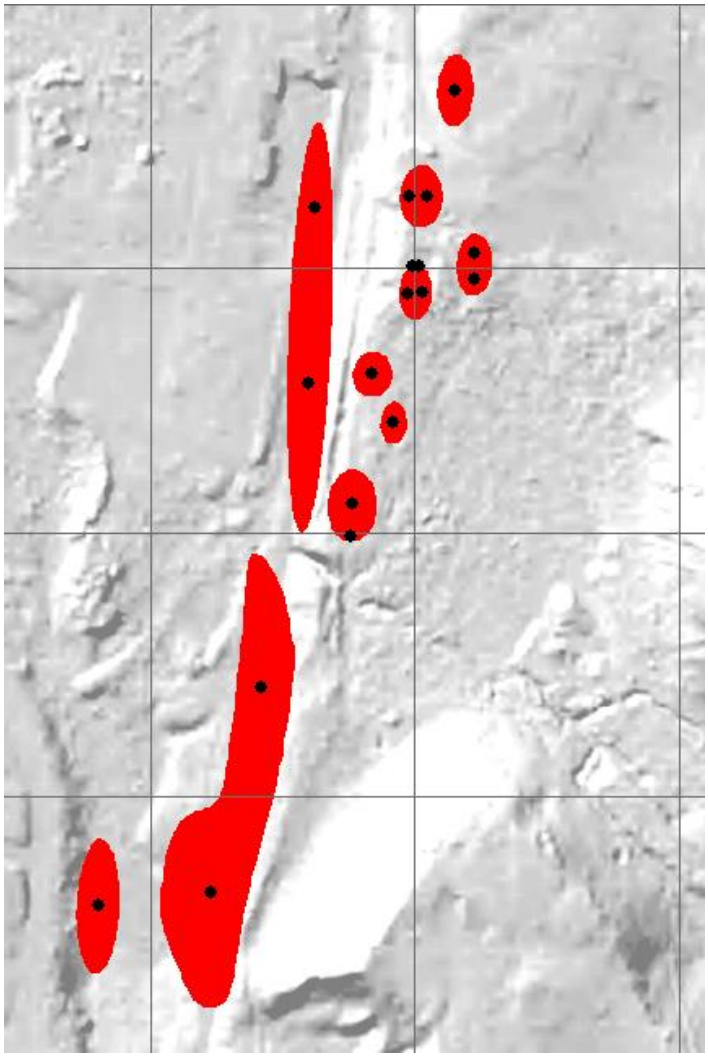

Figure 2.14: Example showing how bedrock polygons (red areas) are split along the 100-meter grid cell boundaries (gray lines) to determine bedrock altitude at the centroid (black dots)

2.5.10. Abundant Outcrops and Shallow to Bedrock Areas (sb)

To convert shallow to bedrock areas, which are defined as areas with depths to bedrock of less than 3.5 meters, to point values, a slope-curvature soil thickness model was developed. Topography was processed to determine curvature and slope using the National Resources Conservation Service (NRCS) slope categories (0-3%, 3-8%, 8-15%, 15-25%, 25-35%, 35-50% and >50%). The concept relies on the notion that the flatter the slope, the thicker the soil is likely to be up to a maximum thickness of 3.5 meters. Accordingly, a set of rules were established as follows:

For ridgecrests and summits where the curvature is positive (convex) and slope is <15%, a depth to bedrock of 0.5 meters was set. Otherwise, if the slope was 0-3% the depth to bedrock was set at 3.5 meters, for 3-8%, 3 meters, 8-15%, 2.5 meters, 15-25%, 2.0 meters,

25-35%, 1.5 meters, 35-50%, 0.5 meters and for slopes greater than 50% the depth to bedrock was set at 0 meters as these were generally cliffs or rock faces.
To use these rules mean slope and curvature values were needed for the 100-meter grid cells. Because the ArcGIS tools for computing topographic slope and curvature only use fixed 3x3-cell neighborhoods, neither the 1-meter LiDAR (computing slopes and curvature over 3x3-meter areas) nor the 100-meter mean elevations (300x300-meter areas) was possible. The use of small 3x3-meter areas, plus the presence of noise, vegetation, and development artifacts in the 1-meter LiDAR yielded 3x3 slope and curvature values that did not adequately capture meaningful hillslope and topographic curvature.

To obtain meaningful hillslope and curvature values, an intermediate-resolution topographic dataset, the National Elevation Dataset (NED) DEM at 1/3 arc-second resolution (roughly 7.5x10 meters at 42 degrees north latitude) was used. The NED data was re-projected to a regular 7.5-meter grid for use as the input to slope and curvature functions; the 3x3 cells used in those functions gives an ~25-meter support basis that is a more appropriate size for measuring slope and curvature at a scale that will relate meaningfully to the hillslope processes affecting soil-depth.

The following steps detail the process of preparing the depth values according to this model:

1. Run ArcToolbox "Slope" on the 7.5-meter NED data, using the "percent rise" and "planar" output options to get a 7.5-meter slope raster (with slopes computed over 22.5x22.5-meter areas).

2. Run ArcToolbox "Curvature" on the 7.5-meter NED data to get a 7.5-meter curvature raster (with curvatures computed over 22.5x22.5-meter areas).

3. Use the ArcToolbox "Raster Calculator" to apply the slope-curvature soil-depth model to create a 7.5-meter raster of soil depths. Using "slp.tif" and "crv.tif" for the 7.5-meter slope and curvature rasters for brevity, the expression to compute is:

```
Con(("crv.tif" > 0) & ("slp.tif" < 15),

  0.5,
  Con("slp.tif" < 3,
    3.5,
    Con("slp.tif" < 8,
    3.0,
    Con("slp.tif" < 15,
      2.5,
      Con("slp.tif" < 25,
        2.0,
        Con("slp.tif" < 35,
          1.5,
          Con("slp.tif" < 50,
            0.5,
            0.0
            )
          )
        )
      )
    )
  )
)
```

4. Use the ArcToolbox "Raster Calculator" to compute uncertainties for the 7.5-meter raster of soil depths where the uncertainty is assigned as 10% of the depth for depths >= 3 meters and 0.3 meters elsewhere—using "dtb.tif" as the 7.5-meter soil-depth raster for brevity, the expression to compute is:

```
Con(("dtb.tif" < 3),
  0.3,
  "dtb.tif" * 0.1
)
```

The following steps were performed to create point data for each shallow to bedrock polygon or portion of a polygon within each 100-meter grid cell:

1. The ArcToolbox "Erase" tool was used to remove all bedrock polygons from the shallow to bedrock polygons, since the bedrock polygons are handled separately (see section 2.5.9).

2. The shallow to bedrock polygons were split along the 100-meter gridlines using the ArcToolbox "Intersect" tool (although some of these small polygons were not intersected by any of the lines and were simply copied across to the new polygon output layer).

3. The ArcToolbox "Add Geometry Attributes" tool was used to add CENTROID_X and CENTROID_Y attributes to the polygon attribute table, containing the computed area centroid for each polygon.

4. Four attributes were manually added to the polygon layer's attribute table: LIDAR for the polygon's (mean) LiDAR elevation; ALT for the polygon's (mean) altitude; DTB for the (mean) soil depth (depth to bedrock); and UNC for (mean) uncertainty.

5. Mean elevations for these new shallow to bedrock polygons were computed by running the ArcToolbox "Zonal Statistics As Table" with the polygons as zones and the 1-meter LiDAR raster as values for computing the mean.

6. To get these mean elevations from the table back into the polygon layer, the zonal statistics table was joined to the polygon features using the FID field. The Field Calculator was used to set the LIDAR field equal to the MEAN value column in the joined zonal statistics table.

7. Mean depth values for these new shallow to bedrock polygons were computed by running the ArcToolbox "Zonal Statistics As Table" with the polygons as zones and the 7.5-meter soil-depth raster as values to be averaged within each polygon.

8. Mean uncertainty values for these new shallow to bedrock polygons were computed by running the ArcToolbox "Zonal Statistics As Table" with the polygons as zones and the 7.5-meter uncertainty raster as values to be averaged within each polygon.

9. The shallow to bedrock polygon layer was joined to the depth and uncertainty zonal statistics tables and the Field Calculator used to set the DTB field in the polygon layer to the MEAN column of the depth statistics table and likewise the UNC field to the MEAN column of the uncertainty statistics table.

10. There were some shallow to bedrock polygons too small to be given values by the Zonal Statistics tool; these were identified by the absence of assigned LIDAR values from step 6. To get values for these points, the attribute table for these selected records was exported and converted to a point shapefile; the ArcToolbox "Extract Multi Values To Points" was run to extract the altitude for these small polygons from the 1 meter LiDAR data.

11. With all records populated with values from the rasters, the ALT field for each point was computed using the Field Calculator by subtracting the DTB field from the LiDAR field.

At the end of this processing the 15,016 original shallow to bedrock polygons had been split into 492,120 smaller shallow to bedrock polygons, each with a mean (or, for small ones, point) surface elevation value, depth to bedrock, computed bedrock altitude and uncertainty values, and point locations in the CENTROID_X and CENTROID_Y attributes (Figure 2.15). These were added to the drill hole and geophysical master spreadsheet spreadsheet.

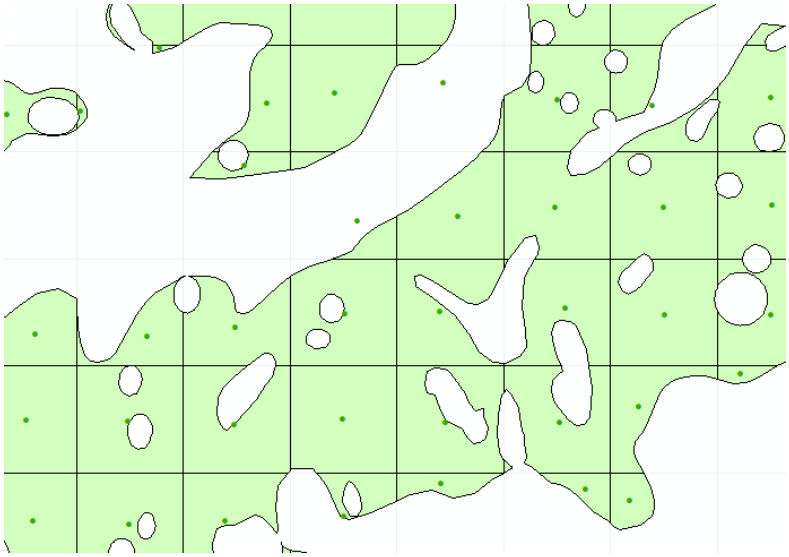

Figure 2.15: Shallow to bedrock polygons (shaded areas) split along the 100-meter grid cell boundaries (gray lines) to assign a bedrock altitude at the centroid (dots)

2.5.11. Final Preparation of Drill Hole, Geophysical, Bedrock Outcrop and Shallow to Bedrock Point Data

The final point data layer to be used for modeling the bedrock surface consists of 107,702 drill hole and geophysical data points, 111,495 bedrock outcrop points, and 492,120 shallow to bedrock data points for a total of 711,317 points (Figure 2.16).

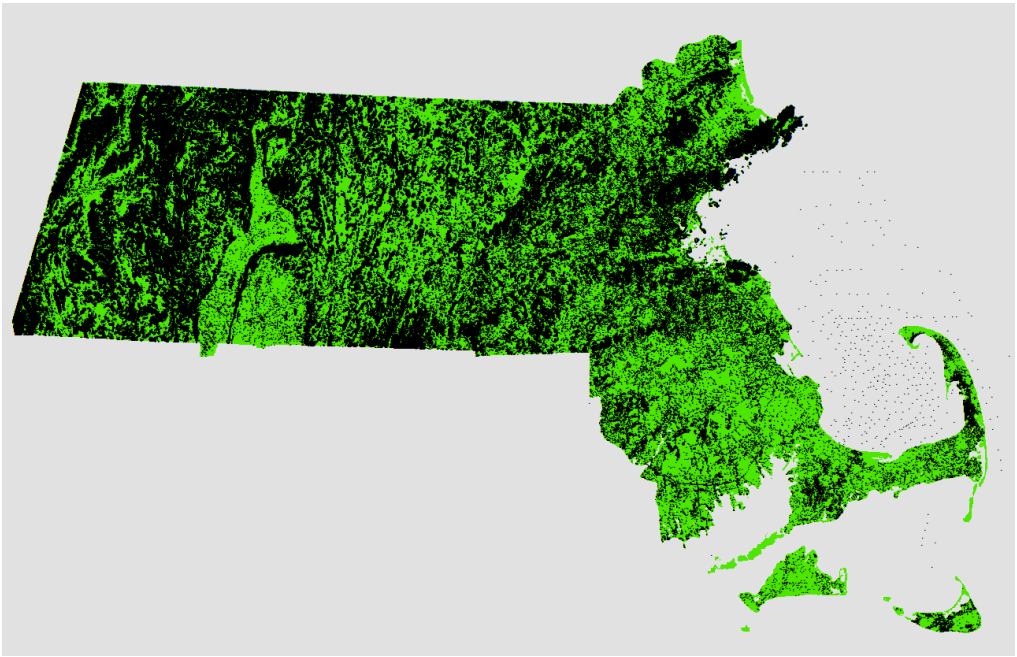

Figure 2.16: All drill hole, geophysical, bedrock outcrop and shallow to bedrock data points (black dots)

Some final steps were taken to prepare the data for ingestion into GIS before modeling the bedrock surface:

1. All bedrock outcrops and shallow to bedrock areas were assigned a boring type flag (BOR_FLAG) of "bedrock".

2. Borings that met refusal were interpreted as bedrock wells so the boring type flag (BOR_FLAG) was changed to “bedrock”. Accordingly, there are only two types of subsurface data points throughout the data set, “bedrock” and “overburden”.

3. The USGS_Offshore_Seismic records only have altitude data. The surface elevation and depth to bedrock were set to zero.

4. The overburden well depths are a minimum constraint on bedrock depth—they do not reach bedrock, so bedrock depth is at some depth below the bottom of the well. To make the use of these wells more effective in conditioning the bedrock depth, the total depth of the overburden well or boring was increased by 5% (this may be a slight over-estimate of depth for a few wells, but is likely to be an underestimate for the vast majority of them).

5. Added two new columns to the spreadsheet: USE_ALT_M and USE_DTB_M, where USE_ALT_M is the altitude to the bedrock or altitude of the bottom of the boring in the case of an overburden well, in meters, and USE_DTB_M is the depth to bedrock below the ground surface expressed in meters. These two columns will be used for modeling bedrock altitude and depth, respectively.

6. Any columns that will not be needed for modeling in GIS are removed to save on memory.

7. The finalized spreadsheet of drill hole, geophysical, bedrock outcrops and shallow to bedrock data points is imported into ArcGIS and exported as a point shapefile. In addition, two other shapefiles are exported from ArcGIS, one for overburden wells in grid cells only containing overburden points and another containing only bedrock points.

The final point files used for the bedrock surface modeling exclude any data for the islands of Nantucket and Martha's Vineyard; there is insufficient data—no bedrock wells and no bedrock outcrops or shallow to bedrock occurrences—to successfully model these areas. Instead, the bedrock contours for the islands prepared by Oldale will be used *(21)*. The contours, which are represented as depth to bedrock below sea level, were converted to a 100-meter raster using the ArcToolbox "Topo to Raster" tool, clipped to the outline of the islands, and converted to bedrock altitudes. The island bedrock altitude raster is designated ISLANDALT for later reference.

2.6 Modeling the Bedrock Surface: Overview of Approaches, Problems and Solutions

With a perfect data set, one in which a well with a reliable depth-to-bedrock value was located in every 100-meter grid cell, this project would involve only simple math and mapping: the bedrock altitude for each cell could be computed as topography minus depth, and the two rasters—depth and altitude—could be rendered by choosing some simple display options.

With incomplete data, overburden wells, and data uncertainties, however, the process is much more complex. The obvious approach would be to model a continuous depth-to-bedrock raster based on the available values, interpolating by some appropriate method for all the cells where there is no data, then subtracting this raster from topography to obtain the bedrock altitude surface. This approach is referred to as the "depth-based" approach. However, the depth-based approach has issues in that it tends to translate or imprint the details of the surface topography on to the modeled bedrock, including surface features such as scarps. The geologic process that formed the bedrock surface in the larger valleys involved glacial scouring and is an erosional surface whereas the landforms observed at the land surface are constructional formed by deposition from glacial meltwater streams. The two processes that formed these surfaces are independent and should not mimic each other particularly in the deeper valleys.

This problem can occur wherever bedrock depth values are interpolated across large distances; it is likely to occur and to be serious where those data-free regions are in valley floors. For example, in the Connecticut River Valley of Massachusetts, there is a lack of bedrock well data in the valley floor, often because bedrock is buried more deeply there and not easily reached by most borings. A common pattern is to have bedrock wells—or, similarly, bedrock outcrop or shallow-bedrock proxy data—along the valley sidewalls where bedrock depth is relatively shallow, and little to no data in the middle of the valley. When interpolating across the valley, the shallow depths from the valley sides are the control points and so the interpolated depth is shallow right across the valley. Not only does this typically underestimate the bedrock depth in the middle of the valley, it also results in relatively uniform interpolated bedrock depths that are insensitive to surface morphology within the valley that represent varying thicknesses of overburden. This means that when computing a bedrock surface altitude by subtracting modeled depth from topography, details of the surface features will be echoed in the computed bedrock surface, when in fact they are due to varying overburden thicknesses rather than bedrock relief.

An example to illustrate this is taken from the area where the Deerfield River enters the Connecticut River valley and turns north, passing alongside the town of Deerfield. As is visible in the 1-meter LiDAR topography (Figure 2.17), the Deerfield River has eroded an older alluvial surface, creating steep erosional scarps as much as 50 meters in height in the center of the image. In Figure 2.17, the dots represent shallow to bedrock areas, bedrock outcrops, and bedrock wells. Note the plethora of data on either side of the valley but very little data in the center of the valley. The scarps shown in Figure 2.17 have nothing to do with the buried erosional bedrock surface, yet interpolating across the valley yields a fairly

uniform estimated depth across the valley (Figure 2.18); when subtracted from the depicted topography, it results in a modeled bedrock surface that has the same 50-meter scarp in it, just 10 or 20 meters below the surface (Figure 2.19).

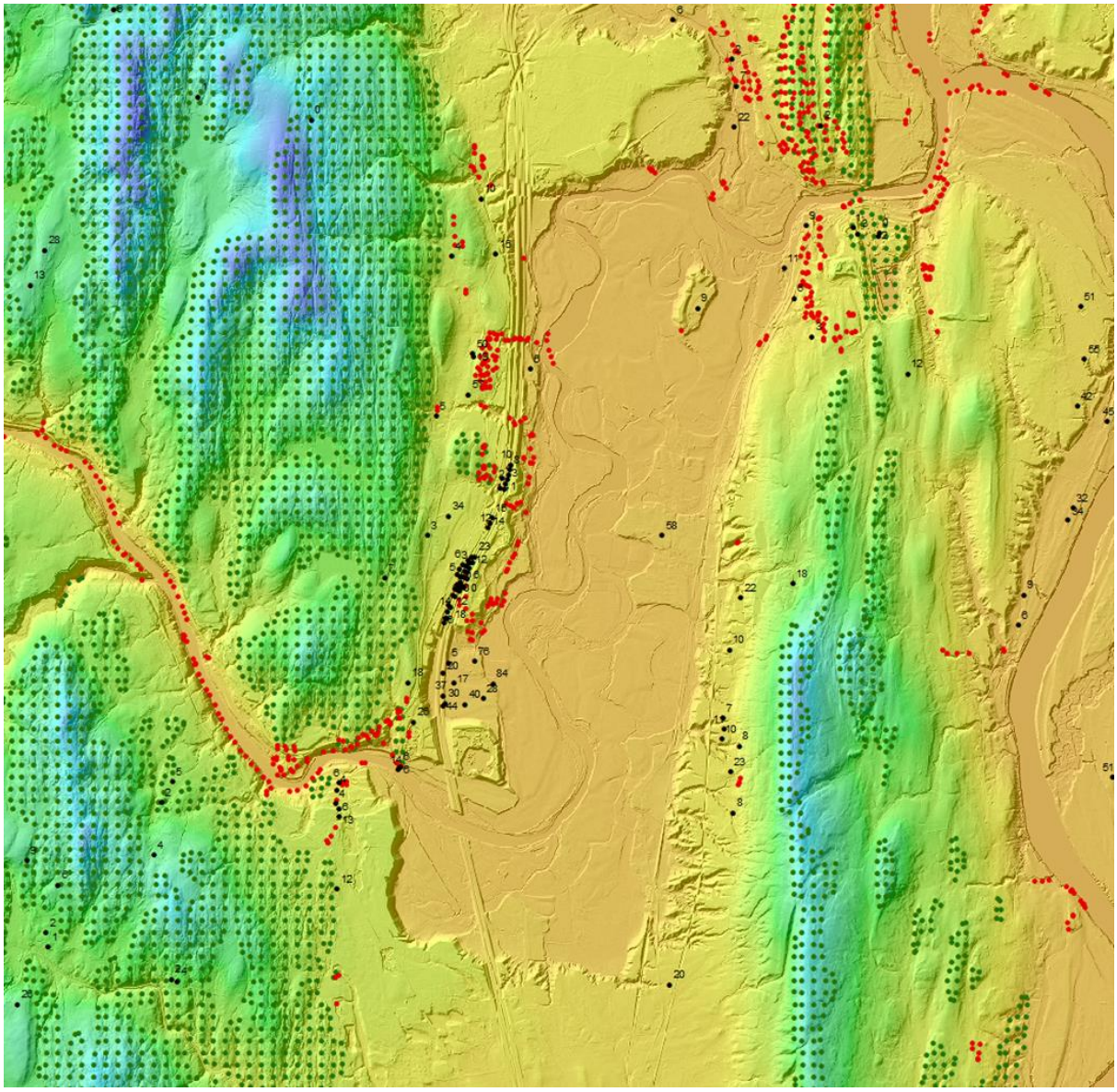

Figure 2.17: Image of 1-meter resolution LiDAR topography where the Deerfield River enters the Connecticut valley

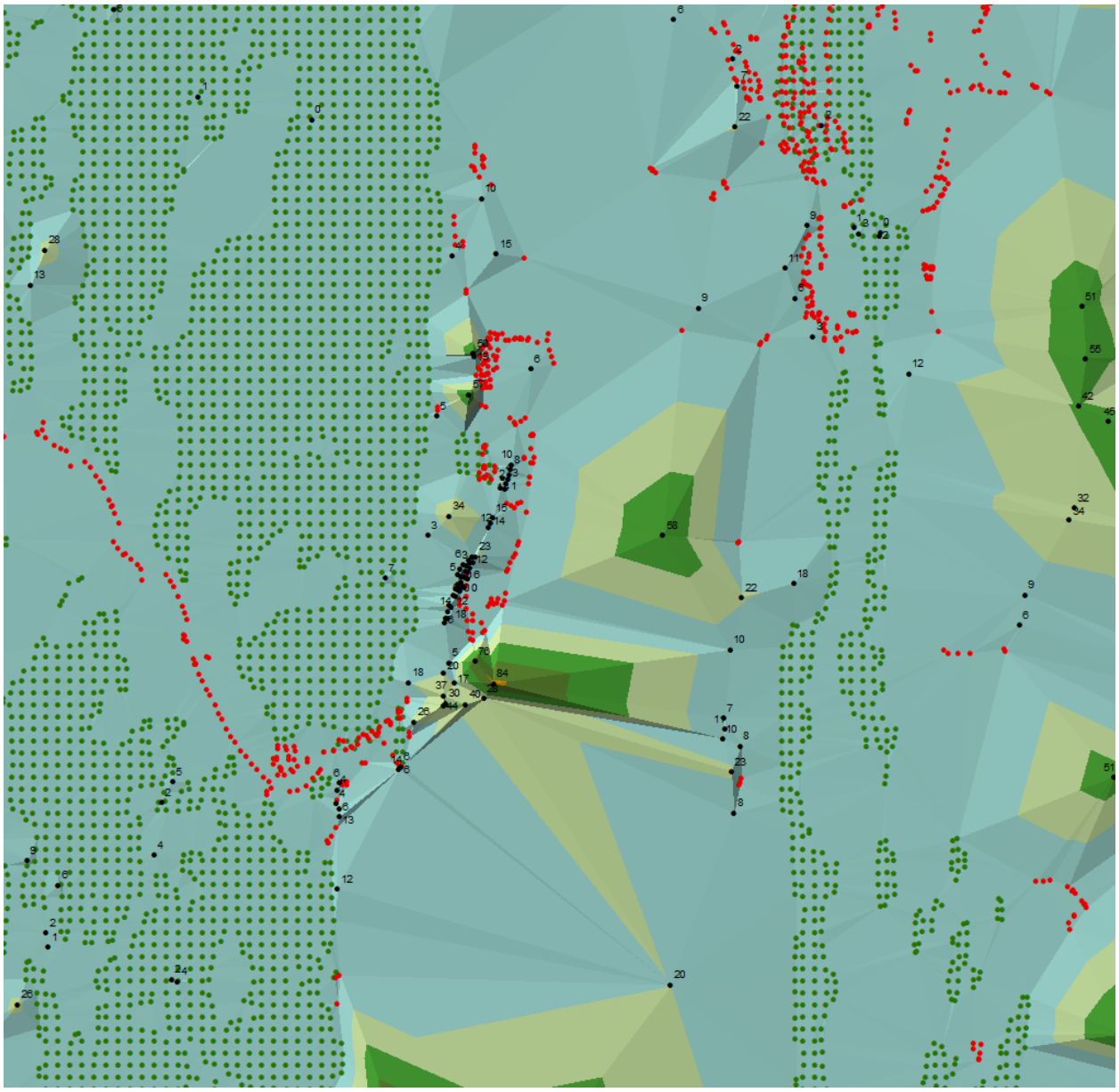

Figure 2.18: Triangular irregular network (TIN) surface interpolated from bedrock depth control points on the left and right side of the image compared to the lack of bedrock depth control points in the center of the image

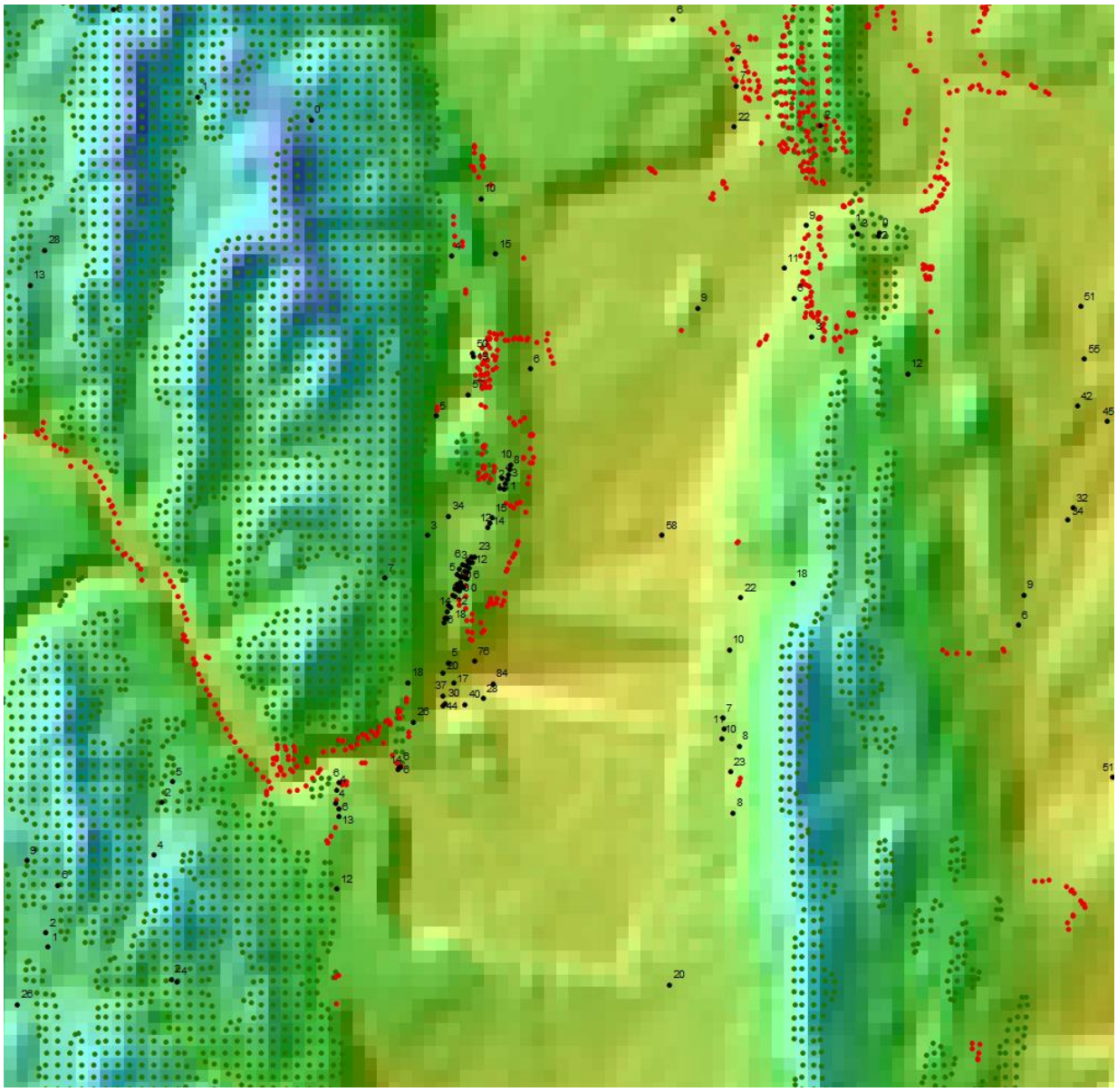

Figure 2.19: Bedrock surface altitude obtained by subtracting TIN interpolated depths (Figure 2.18) from 100-meter topography which imprints the 50-meter erosional scarp along the Deerfield River seen in Figure 2.17 onto the bedrock surface

An obvious alternative approach that should avoid this problem of imprinting overburden features onto the bedrock surface is to interpolate directly from bedrock altitude values rather than bedrock depth values, and then to subtract the resulting bedrock surface from the current topography to obtain an estimate of overburden thickness (depth to bedrock). This is referred to as the "altitude-based" approach.

This approach has its own shortcoming, however: in areas of high topographic relief and sparse point data—for example, in narrow valley floors or adjacent to steep hillsides and

ridges—the interpolated bedrock surface tends to "bridge" between the control points (usually bedrock outcrops or shallow to bedrock areas) of the ridges and hillsides and the sparse points (usually bedrock wells) scattered in the adjacent valley floor. There are not enough control points to constrain the interpolated surface to stay below the rapidly-decreasing topography and so the modeled bedrock surface "daylights" or "bridges" across the area in front of the hills, creating impossible "negative" depth-to-bedrock values. In other words, the bedrock is above the ground surface where it should not be.

To illustrate this problem more clearly, using data from the north side of the Holyoke Range in Hadley, MA: there is abundant control of bedrock elevation from outcrops and shallow bedrock regions along the Holyoke Range ridgecrest and even down some of the interfluves on the north side of the ridge (Figure 2.20); in the valley floor north of the range, however, bedrock altitudes are only available from sparse and distant bedrock wells. In Figure 2.20, the dots represent bedrock outcrops, shallow to bedrock areas and bedrock wells or points. Interpolating between the elevated ridgecrest altitudes and the valley floor altitudes tends to produce an inclined plane for the modeled bedrock surface that decreases more slowly than the current topography, causing the modeled bedrock surface to bridge the topography and produce an impossible zone where bedrock is higher than topography (Figures 2.21 and 2.22). In Figure 2.22, the lighter shading (yellow and orange areas) shows areas where the bedrock is exposed above the land surface where it should not be.

Given these problems with the altitude-based and depth-based modeling approaches, we adopt a hybrid strategy that blends these two approaches—substituting depth-based results where the altitude-based model exceeds topography—followed by some targeted mitigations of secondary issues that remain after blending. The next sections present the details of the processing sequence developed to obtain the best model of the bedrock surface. After detailing the processing, a discussion follows of the pros and cons of the final bedrock model and several of the intermediate results—including consideration of cases where the use of one map product might be preferred over another—and an analysis of uncertainties and errors and when/where/how caution should be employed when using the results.

2.7 Modeling of Bedrock Altitude

2.7.1. Testing Interpolation Methods

Modeling begins with bedrock altitude values rather than depth values for two reasons: 1) to avoid, as much as possible, the imprinting of surface topography on to the bedrock surface because the "bridging" problem of the altitude-based approach can be mitigated more easily than avoiding the imprinting errors of the depth-based approach; and, 2) there is a rational, quantitative basis for selecting overburden wells when modeling altitude first but not when modeling depth, so it makes sense to identify the useful overburden wells through the altitude-based approach so the same overburden wells can be used in the later depth-based approach.

There are many ways to interpolate point data. In order to select the most appropriate method to use, all the bedrock wells, bedrock outcrops and shallow to bedrock data points were divided randomly into two groups: 90% of the points were used to generate interpolated surfaces, and 10% set aside for evaluating how well each approach performed in estimating the correct values at these test points (Figure 2.23). Several models were evaluated including triangular irregular networks (TIN), inverse distance weighting (IDW), universal kriging (UK) and empirical Bayesian kriging (EBK). In addition, each model was evaluated using different input options. In Figure 2.23, the x-axis is the error between the modeled values and the test points, in meters. Dotted, dashed and solid lines are based on bedrock wells only whereas solid lines with markers are based on bedrock wells, bedrock outcrops and shallow to bedrock data points. The numbers next to the letters in the explanation represent different input options. EBK and IDW interpolation methods performed best with approximately 70% of the errors less than 5 meters

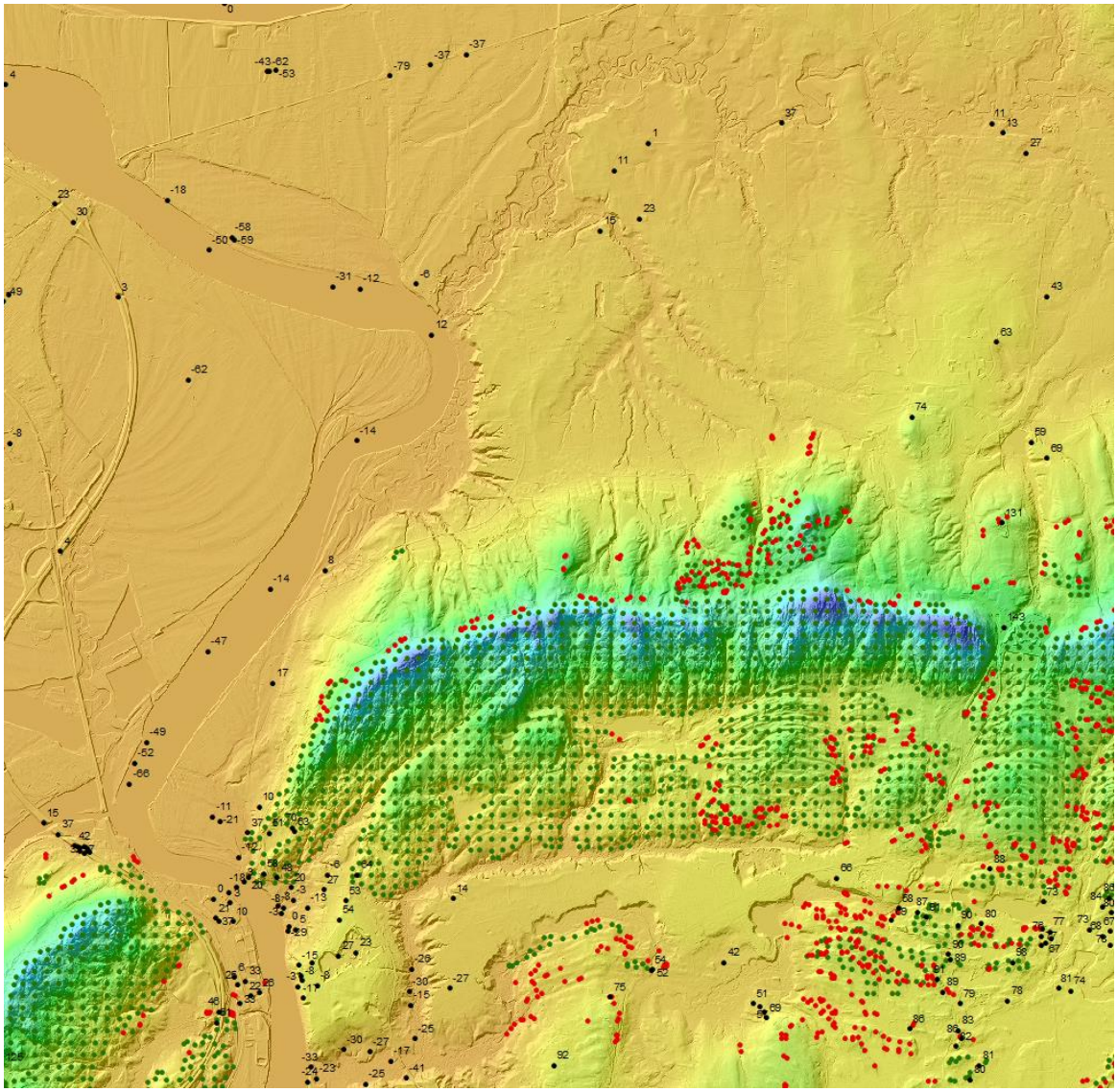

Figure 2.20: 1-meter LiDAR topography near Hadley, MA with surrounding bedrock control points as described in the text

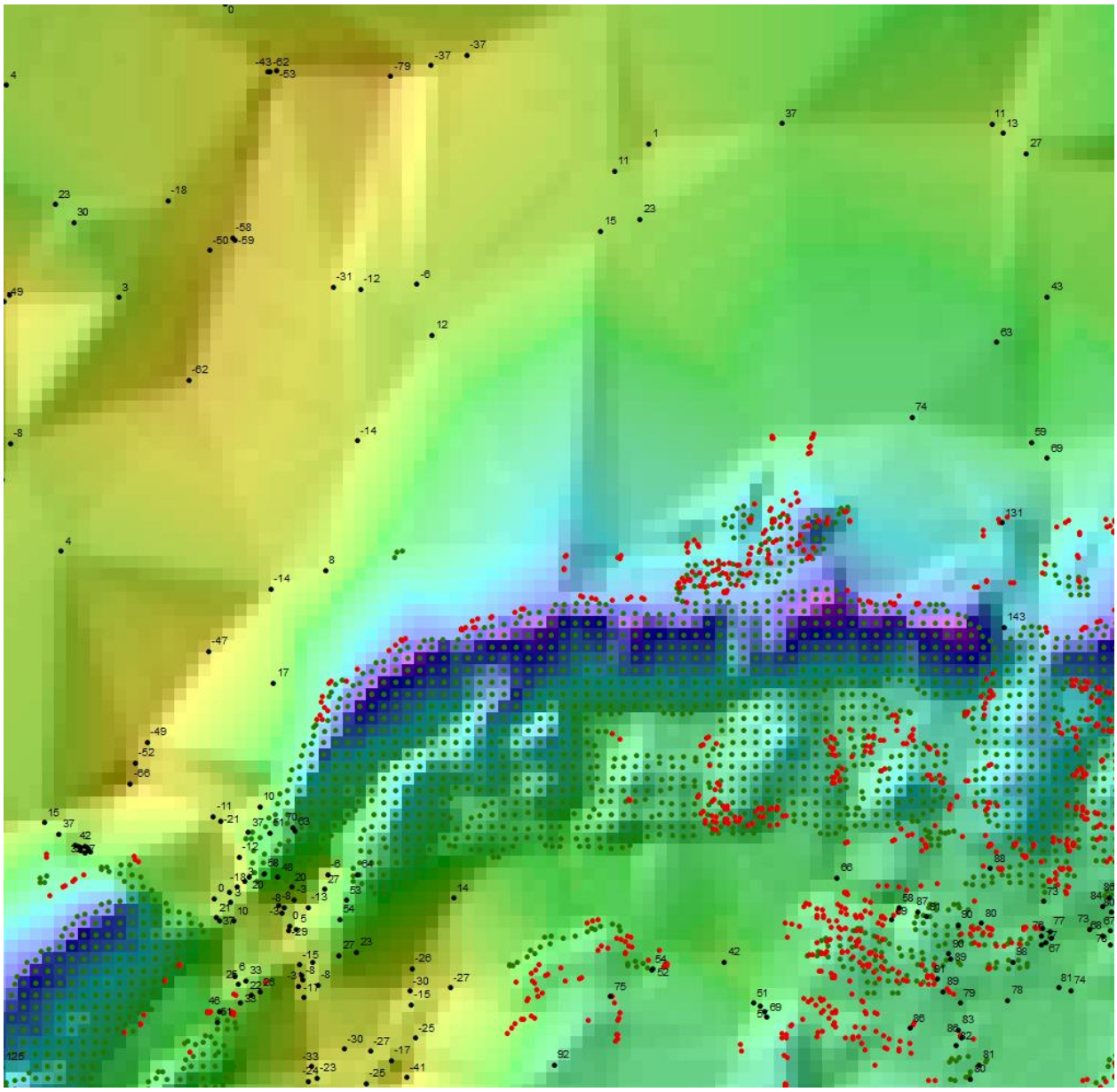

Figure 2.21: Modeled bedrock surface from TIN interpolation of bedrock altitude control points; the modeled surface declines smoothly from the ridge crest (dark blue east west feature) to the distant control points in the valley floor to the north.

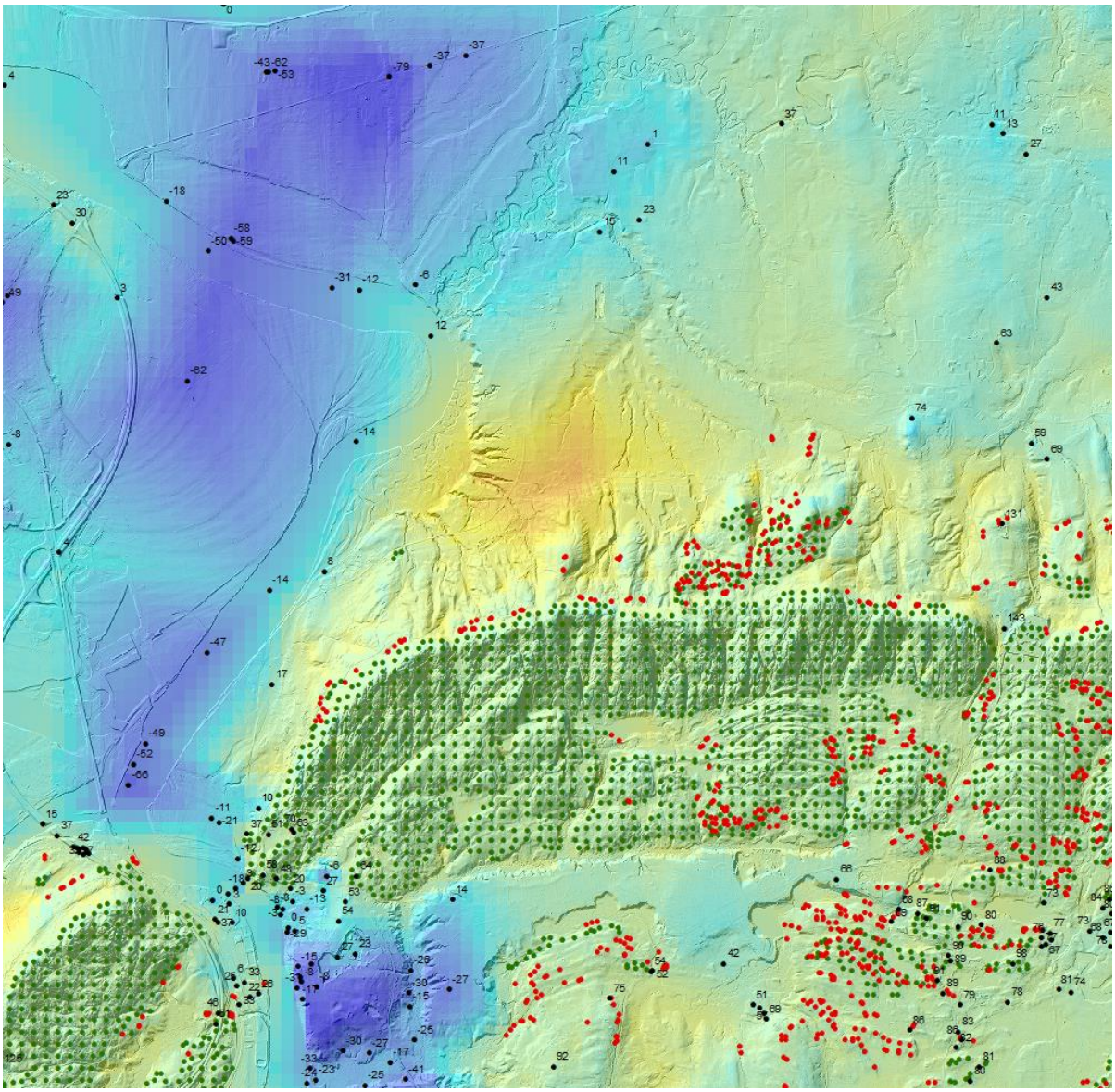

Figure 2.22: Depth-to-bedrock obtained by subtracting the modeled altitude of the bedrock surface from the current topography; lightest shading (yellow and orange) are areas where bedrock is above the land surface

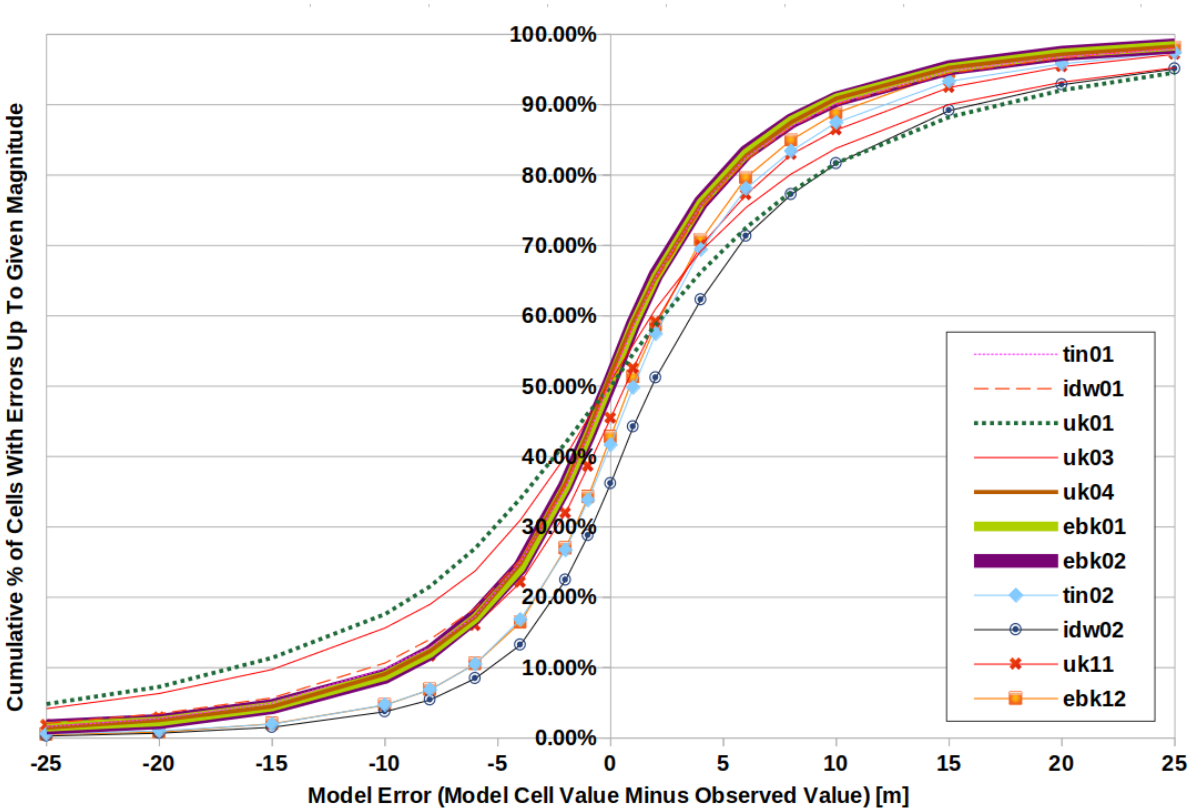

Figure 2.23: Cumulative distributions of errors between different models and the 10% set-aside test points for a selection of interpolation methods

Some interpolators are exact—they result in surfaces that pass exactly through the interpolation points—while others allow the result to diverge more or less from these points. Therefore, a comparison of how closely each interpolation method reproduced the values at the 90% interpolation control points (i.e., in addition to their performance at the 10% test points) is shown in Figure 2.24. The same interpolators were tested again: integrated irregular networks (TIN), inverse distance weighting (IDW), universal kriging (UK), empirical Bayesian kriging (EBK). In addition, each model was evaluated using different input options, which are represented by the numbers next to the letters in the explanation. In Figure 2.24, the x-axis is the error between the modeled values and the observed value at the bedrock data points, in meters. Dotted, dashed and solid lines are based on bedrock wells only, whereas methods based on bedrock wells plus bedrock outcrops and shallow to bedrock data points are shown as solid lines with markers. For each model, the distribution of errors was assessed at the interpolation points (90% of the input data) and at the test points (10% of the data). For most models, approximately 90% of the errors are less than 4 meters.

In addition to these quantitative tests, qualitative criteria were also used as a guide; for example, a TIN surface is an exact interpolator that passes directly through each control point—meaning it will score well in tests of how closely it matches the point data—yet the surface it produces, consisting of planar triangular facets, is completely unrealistic for bedrock topography. More subtly, a number of kriging-based interpolations yield quite similar performance scores on the point data, but have different appearances—some much

more spiky (and pit-ty) than others—and we used these characteristics to guide the choice between such models (Figure 2.25). In Figure 2.25, UK-D equals universal kriging with default parameters, IDW equals inverse distance weighting, EBK equals empirical Bayesian kriging, TIN equals triangular irregular networks, and UK-O equals universal kriging with optimized parameters.

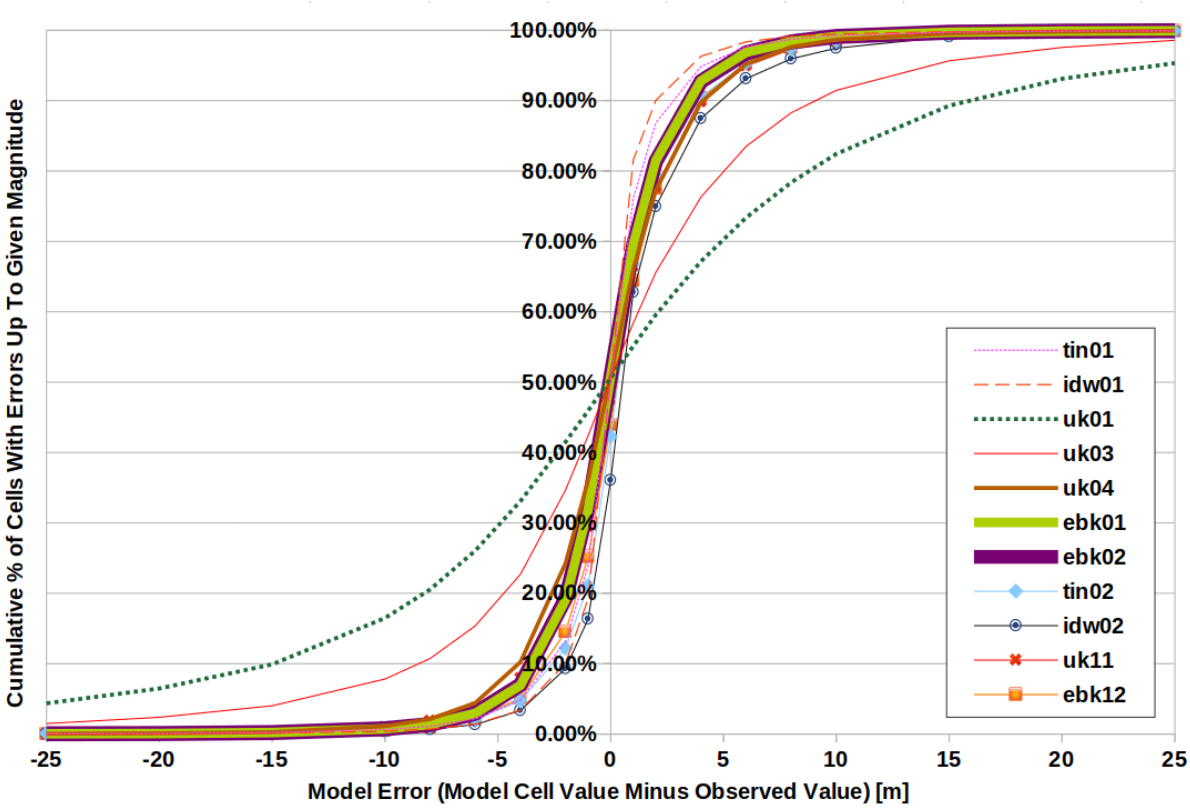

Figure 2.24: Cumulative distributions of errors between the modeled values and the 90% interpolation control points for a selection of interpolation methods.

More than half a dozen distinct types of interpolation were performed on the data, with varied parameters for each type, to create and evaluate a couple dozen different bedrock altitude models. Interpolators used included triangular irregular networks (TIN), inverse-distance weighting (IDW), global and local polynomial functions, kriging, and co-kriging. In addition, each model was evaluated using different input options.

As expected, exact or near-exact interpolators such as TIN- and IDW-based methods performed better than other methods at the control points, but more poorly for test points. In general, best performance was observed from the various kriging approaches (ordinary kriging, universal kriging, empirical Bayesian kriging, co-kriging), although in some cases these methods needed optimizing (using the built-in optimization options) before they

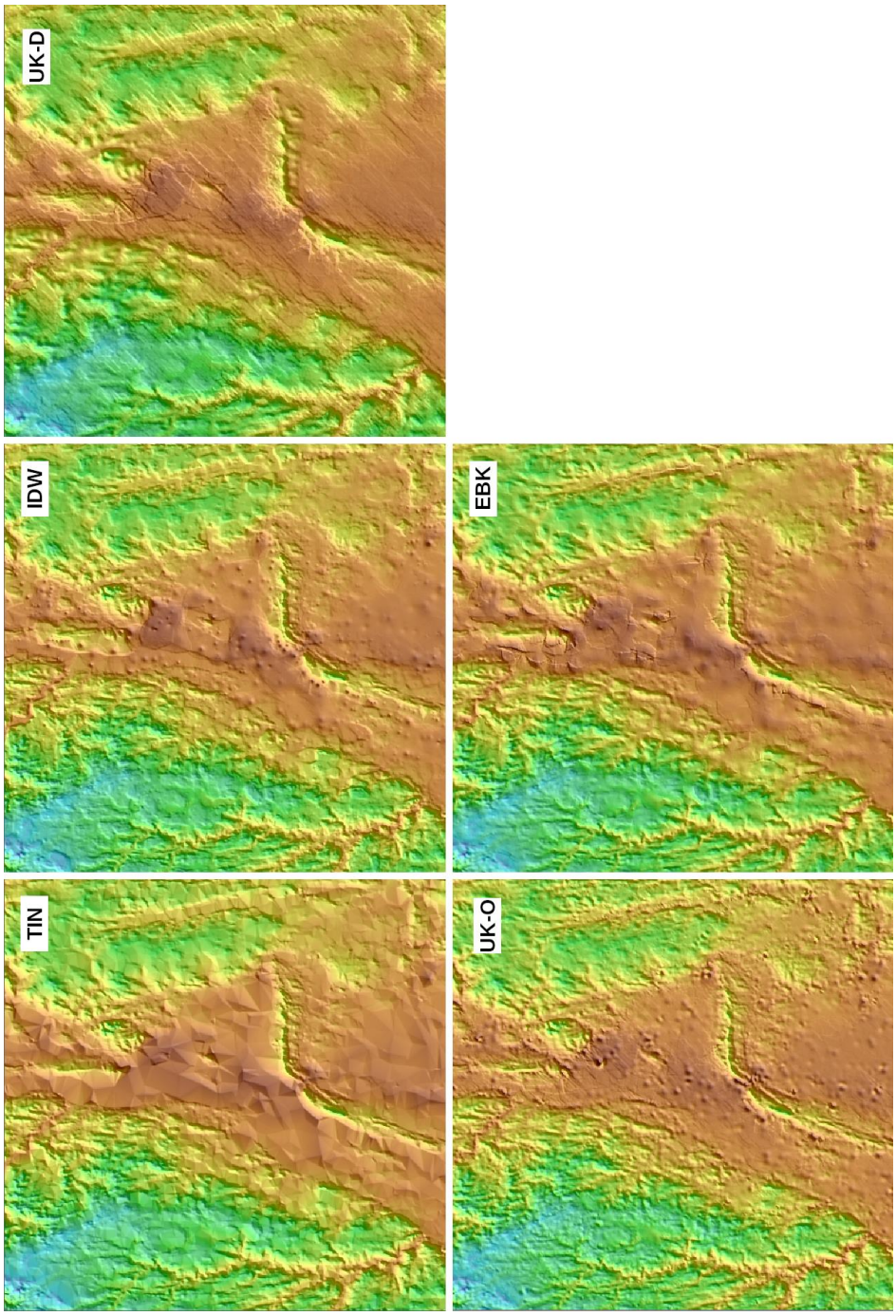

Figure 2.25: Selected shaded-relief maps of modeled bedrock altitude for central Connecticut River Valley using different interpolation methods

performed well. In the end the best overall result was obtained from empirical Bayesian kriging (EBK) using a search radius of 1000 meters (although the difference between that radius and the default value of ~85 meters was negligible).

2.7.2. Modeling Bedrock Altitude with Overburden Constraints

Having selected an interpolation approach, a bedrock altitude model was developed using an iterative approach to incorporate useful overburden well data. EBK interpolation was performed first on the entire set of mainland bedrock wells (Nantucket and Martha's Vineyard are excluded at this point) and bedrock outcrop and shallow to bedrock data points (665,082 points). The resulting bedrock altitude surface model (named ALT1) was compared against all of the overburden wells (wells that occur in grid cells only containing overburden wells) to identify overburden wells whose USE_ALT_M attribute (105% of the well's reported maximum depth) was below the modeled bedrock surface—these are places where the overburden information indicates the bedrock is deeper than the model predicted, even though the exact depth is unknown. Overburden wells whose total depth is above the modeled altitude are ignored because they provide no useful additional information about the bedrock surface.

This step identified 13,566 overburden wells whose maximum depth was below the modeled surface. These wells were added to the bedrock well, outcrop and shallow to bedrock data set and the EBK model re-run. This creates a new surface (named ALT2) with lower altitudes where the new overburden well constraints were added. This essentially pushes the bedrock surface down. A comparison of the ALT2 surface with remaining overburden wells was repeated to identify any new overburden wells whose USE_ALT_M value is below the new model surface. A total of 188 additional wells were found and added to the data set. It may be surprising that new overburden wells were found in this second round that were not selected in the first round; this is because the modeled surface from one round to the next may either increase or decrease in altitude in areas between control points, depending on the geostatistical properties of the points used. Adding the overburden wells changed the geostatistics and caused the predicted altitude to increase in a few areas where it had previously been lower than the overburden well depths.

Adding these 188 new overburden wells and performing a third EBK interpolation resulted in a model (named ALT3) that honored all remaining overburden wells. This final altitude model and the associated kriging prediction standard errors (ALTERR) were saved for further development. As discussed above, although the altitude-based approach honors the bedrock well, bedrock outcrops, shallow to bedrock data points, and selected overburden wells, it "daylights" above the current topography in many places, a condition that is addressed by substituting depth-based results in those areas.

2.7.3. Modeling Bedrock Depth

As with the altitude models, dozens of interpolation methods using the depth to bedrock values for all the bedrock wells, bedrock outcrops and shallow to bedrock points were performed using the same quantitative/qualitative approach as outlined in section 2.7.1. It

was found that a co-kriging approach using each point's surface elevation as the co-variable performed best. The co-kriging result was nearly identical to EBK in performance, and was selected over the EBK result based on the qualitative characteristics (Figure 2.26). In Figure 2.26, TIN equals triangular irregular networks, UK-D equals universal kriging with default

parameters, UK-O equals universal kriging with optimized parameters, EBK equals empirical Bayesian kriging, and CO-K equals co-kriging with elevation as the co-variable.

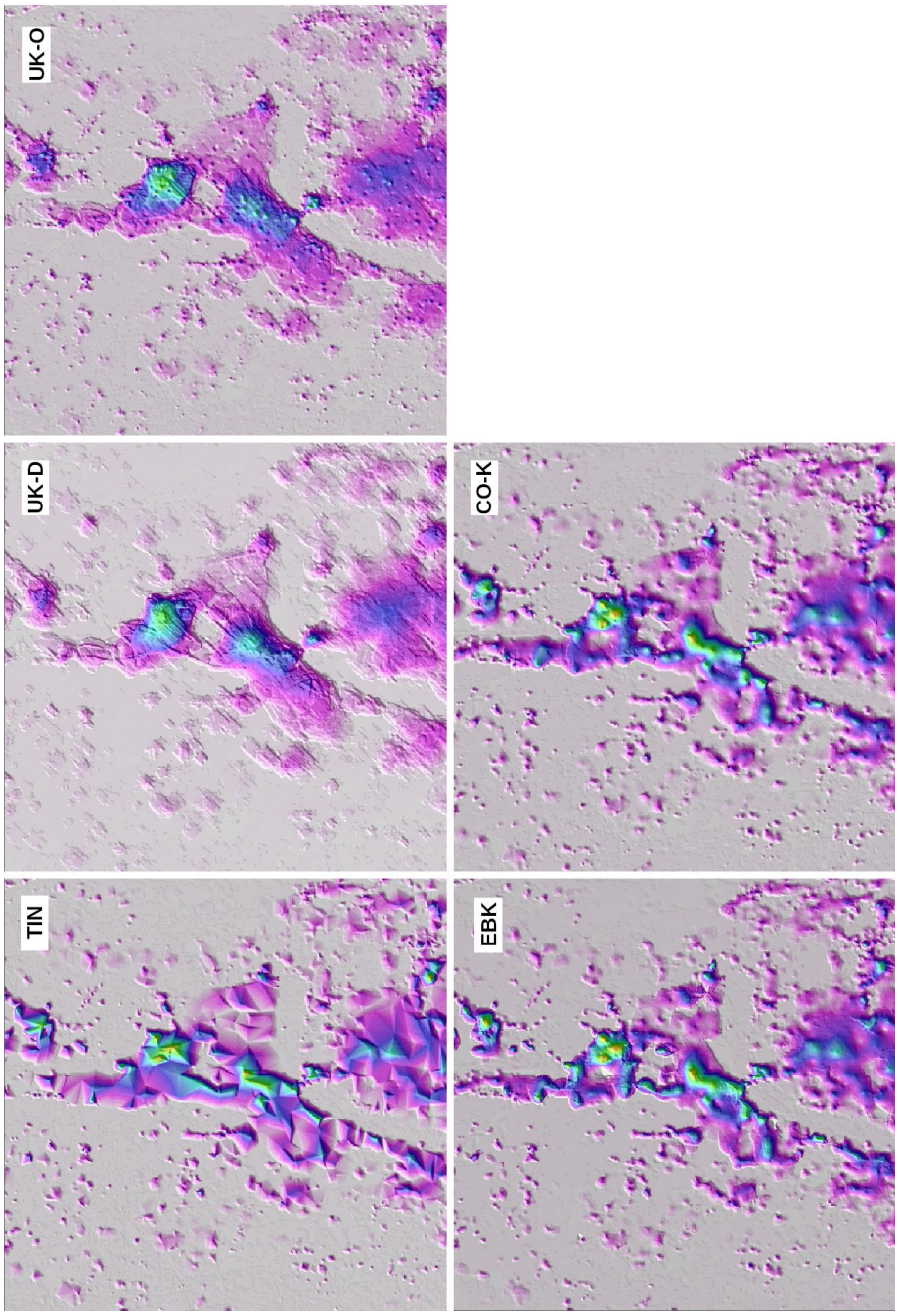

Figure 2.26: Selected shaded-relief maps of modeled bedrock depth for central Connecticut River Valley using different interpolation methods

It is worth noting that unlike altitude modeling, depths must be a one-sided distribution, bounded on the low end by a value of zero depth—there should be no negative depth values (areas where the bedrock is above the ground surface). In general, however, the interpolation

methods do result in small negative depths in some locations, typically where control points are sparse. Before evaluating each result, therefore, the interpolation output was processed to set all negative depth values to zero.

The co-kriging model result, referred to as DTB, is saved along with the associated kriging prediction errors (referred to as DTBERR). The DTB model is then used to compute an equivalent altitude model, designated as DTBALT using the ArcToolbox "Raster Calculator" to subtract DTB values from TOPO100 values.

To summarize, two models of the altitude of the surface of the bedrock have been created statewide at a 100-meter resolution. One is a model (ALT3) created of just bedrock altitudes (a combination of altitudes from bedrock wells, bedrock outcrops, shallow to bedrock areas and selected overburden wells) using empirical Bayesian kriging as the interpolator (altitude-based approach). The second model (DTBALT) uses the same input data but instead uses the depth to bedrock (not altitude) values and maximum depth of selected overburden wells (same overburden wells as in the ALT3 model) to first create a depth to bedrock model (DTB) using co-kriging as the interpolator. The DTB model is then subtracted from the 100-meter resolution topography (TOPO100) to produce a second estimate of the altitude of the surface of the bedrock (DTBALT). This is the depth-based approach. Along the way an interim model of the depth to bedrock is created (DTB). In addition, for each altitude model (ALT3 and DTBALT) corresponding model prediction standard error rasters are produced (ALTERR and DTBERR).

2.7.4. Blending Altitude-based and Depth-based Models

Blending begins by first identifying the cells in the ALT3 model where bedrock lies above the ground surface. This is done by comparing the ALT3 model against the TOPO100 model of surface elevation and creating a raster designated as REPALT3 (replace ALT3). REPALT3 identifies the specific cells in ALT3 that need to be replaced by the cells from the DTBALT model (Figure 2.27). Darker shading in Figure 2.27 indicates greater excess bedrock altitude.

In order to avoid abrupt discontinuities at the substitution boundaries, the ALT3 and DTBALT values are blended in the 300-meter zone surrounding the replaced cells. The blending zone uses a linear weighted averaging where the cells to be replaced are weighted 100% toward DTBALT model. In the next set of cells outside the boundary, for example, the DTBALT model is weighted 66% and the ALT 3 model weighted 33%. In the cells located 200 meters from the boundary the DTBALT model is weighted say 33% and the ALT3 model weighted 66%. Finally, in cells 300 meters away or further from the boundary the cells are weighted 100% by the ALT3 model.

The procedure for blending is as follows. To create the blending zone, the ArcToolbox "Euclidean Distance" tool is used on the REPALT3 raster with a limiting distance of 300 meters; this yields a raster REPDIST with cell values of zero (0) over all the REPALT3 cells,

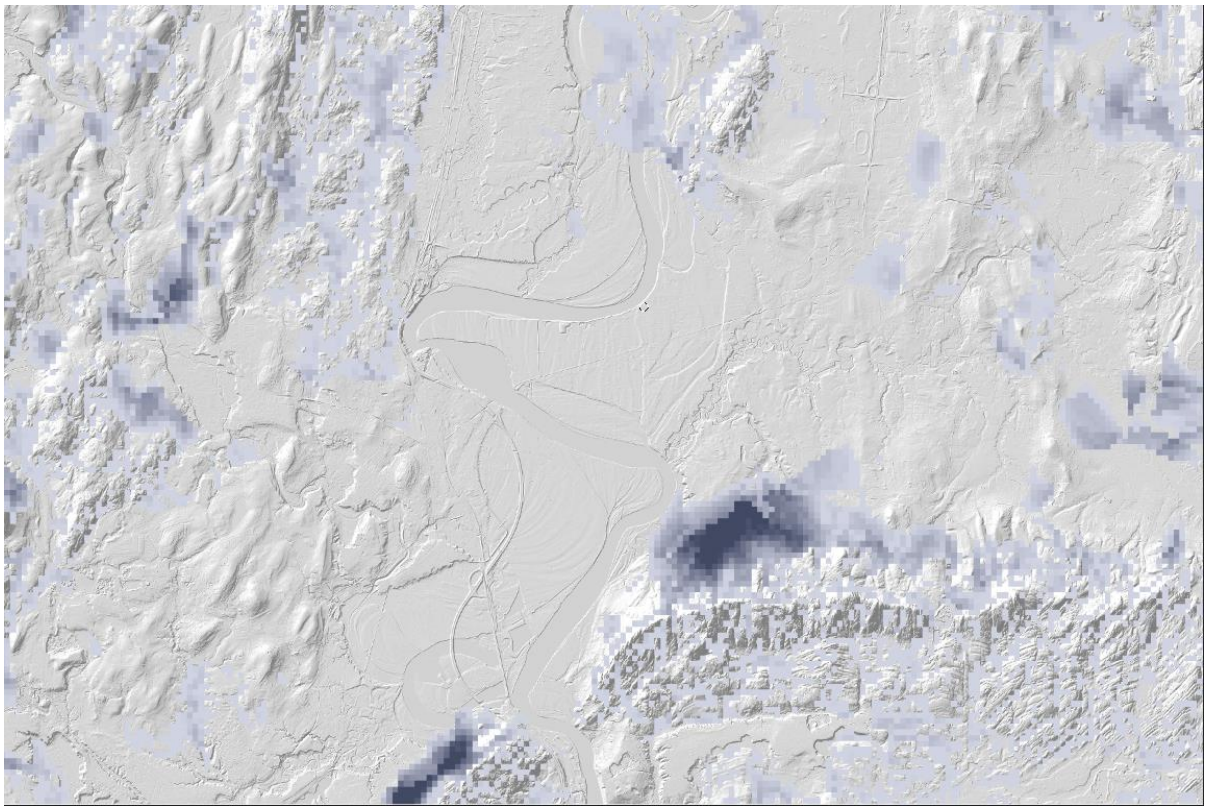

Figure 2.27: Shading indicates places where the bedrock altitude in the ALT3 model is above the land surface (i.e., above the TOPO100 surface model).

surrounded by cells with values increasing up to 300 (meters). Beyond that distance all cell values are null (nodata).

REPDIST is converted to a blending-factor raster BLENDFAC using the "Raster Calculator" with this expression: 1.0 - (REPDIST / 300.0), resulting in a value of 1.0 over all the cells to be completely replaced, grading down to zero (0.0) beyond 300 meters away (Figure 2.28). Darker shades in Figure 2.28 indicate areas where the depth-based altitudes will be weighted more relative to the altitude-based cells.

The "Raster Calculator" was used to do the actual blending with this nested conditional expression:

```
Con ( IsNull ( BLENDFAC ) ,
      ALT3,
      Con ( BLENDFAC < 1.0 ,
            ALT3 * ( 1.0 - BLENDFAC ) + DTBALT * BLENDFAC ,
            DTBALT
      )
)
```

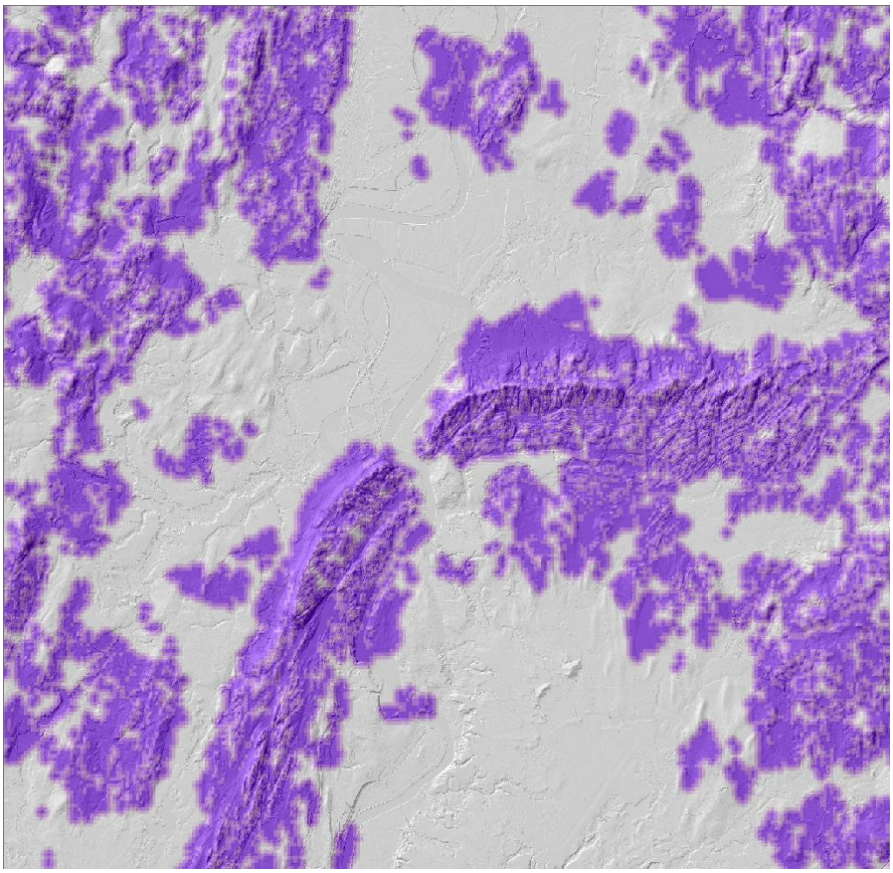

Figure 2.28: Purple cells indicate areas where replacement and blending of the two models occurred

In words, this says "outside the blend zone, just use the ALT3 model; inside the blend zone, wherever the blend factor is less than 1.0, compute a blended value of ALT3 and DTBALT, otherwise just use DTBALT model values."

The resulting raster is referred to as BLEND. The companion blended model prediction standard error raster is referred to as BLENDERR and uses a similar "Raster Calculator" expression:

```
Con ( IsNull ( BLENDFAC ) ,
      ALTERR,
      Con ( BLENDFAC < 1.0 ,
            ALTERR * ( 1.0 - BLENDFAC ) + DTBERR * BLENDFAC ,
            DTBERR
      )
)
```

2.7.5. Patching Kriging Artifacts and Contour Adjustments

The blended model for bedrock altitude (BLEND) exhibits some isolated problems requiring additional processing. In some of the larger spaces lacking any well data, bedrock outcrops or shallow to bedrock areas the EBK kriging produced artifacts in the form of deep local

depressions. Typically, the depressions are deep (>40 m), have steep sides with multiple concentric contours but not always, are unnatural in appearance and cannot be explained by underlying bedrock features (e.g., karst). The shape of the hole is not necessarily symmetrical, often one side is steeper than the other. These appear to be transitions in the middle of large data-free areas where the kriging predictions propagated from data points on a slope on one side of a valley meet kriging predictions propagated from data points on a different slope on the opposite side of a valley; the predictions more or less continue the downward data trends into the data-free region until they meet, resulting in these steep-walled depressions (Figure 2.29). In Figure 2.29, the squares are bedrock wells, circles are bedrock outcrops or shallow to bedrock areas. Values posted next to the circles and squares are bedrock altitudes in meters. The thin black lines are 20-meter computer-generated bedrock altitude contours. The thick line in the center of the image outlines the rim of the hole and overlies the grid cell altitudes that will be used to produce an inverse distance-weighted patch to remove the model artifact.

The entire BLEND raster was scanned systematically by a geologist at 1:50,000 scale to look for kriging artifacts. Once identified a polygon was created defining the boundary of the artifact. A total of 100 such kriging artifacts were found. A python geoprocessing script (Appendix D) was developed to replace the interiors of these polygons with surfaces interpolated using inverse-distance weighting of the boundary cell values. This has the effect of "filling" these depressions with smoothly-varying elevations controlled by the perimeter points. The resulting patched altitude raster is designated PATCHALT. No corresponding adjustments were made to the prediction standard error raster, which has high values in these artifact regions due to their greater distance from control points.

A 20-meter bedrock altitude contour layer was developed from the PATCHALT raster. To simplify and generalize this, all contours with a total line length less than 500 meters were removed. Contour smoothing was performed using the Polynomial Approximation with Exponential Kernal (PAEK) algorithm with a 500 meter smoothing tolerance. This provided a reasonably smoothed contour that generally honors the data points. These contours were also inspected by a geologist across the state at 1:50,000 scale to identify any anomalies. In 6 areas the contours were manually re-drawn either to remove some details of topographic imprinting within DTBALT areas (3 instances), or to make a continuous set of parallel contours out of a series of isolated depressions within narrow valley floors (3 instances). Figure 2.30 shows an example of these adjustments before and after manual contouring. .In Figure 2.30, the left image shows a series of isolated depressions in the valley that need to be connected. The image on the right in Figure 2.30 shows the new contour after manual manipulaton connecting the isolated depressions into a series of longer troughs. The bold line surrounding the valley indicates the 500-meter buffer around the adjusted contour lines within which the updated altitudes will be blended.

In order to update the bedrock altitude raster to include these manual contour adjustments, a statewide 100-meter raster was created from the 20-meter contours (CONTALT). Another blending was performed using the PATCHALT raster with a 300-meter blend zone inside of

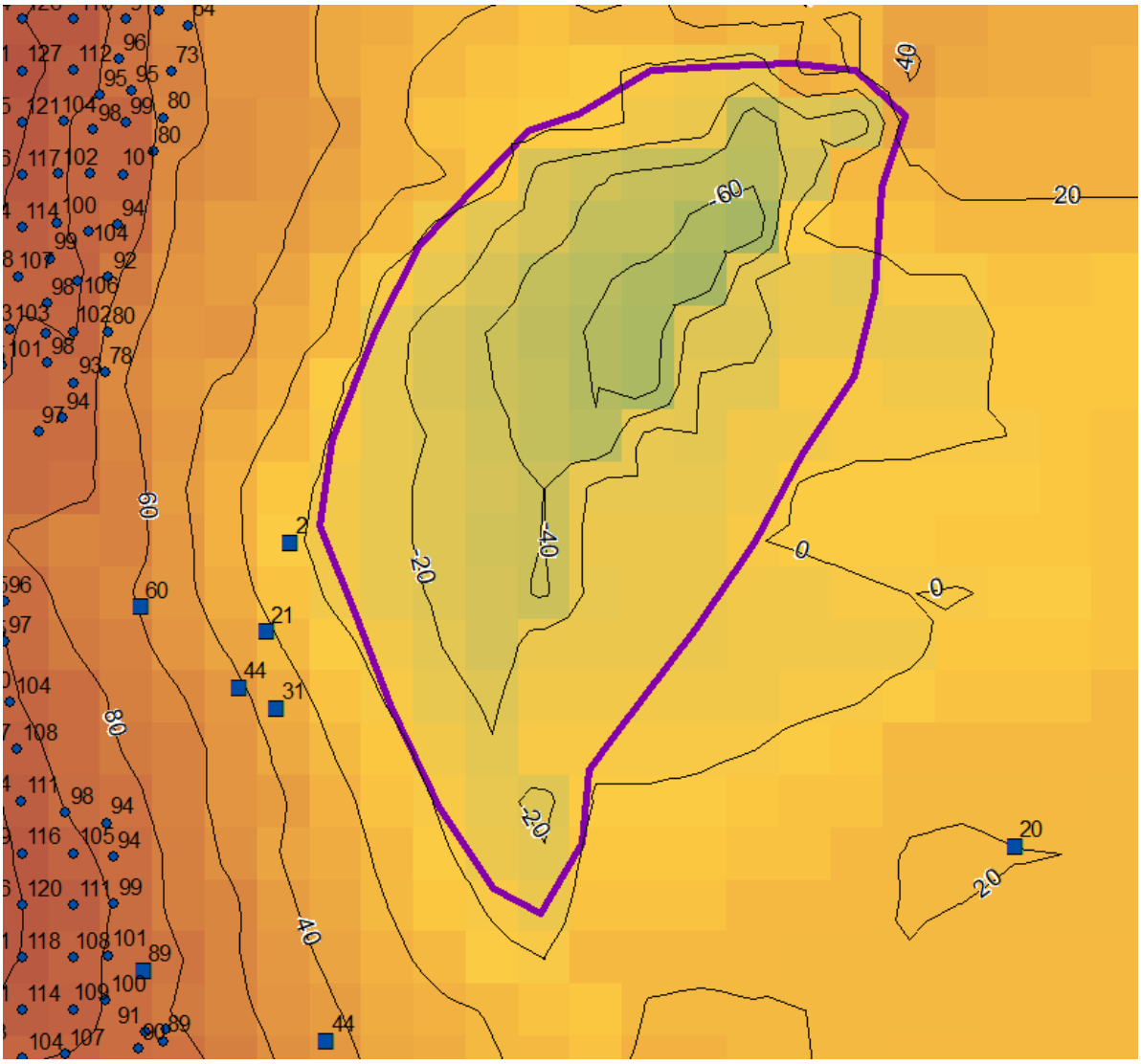

Figure 2.29: An example of a kriging artifact

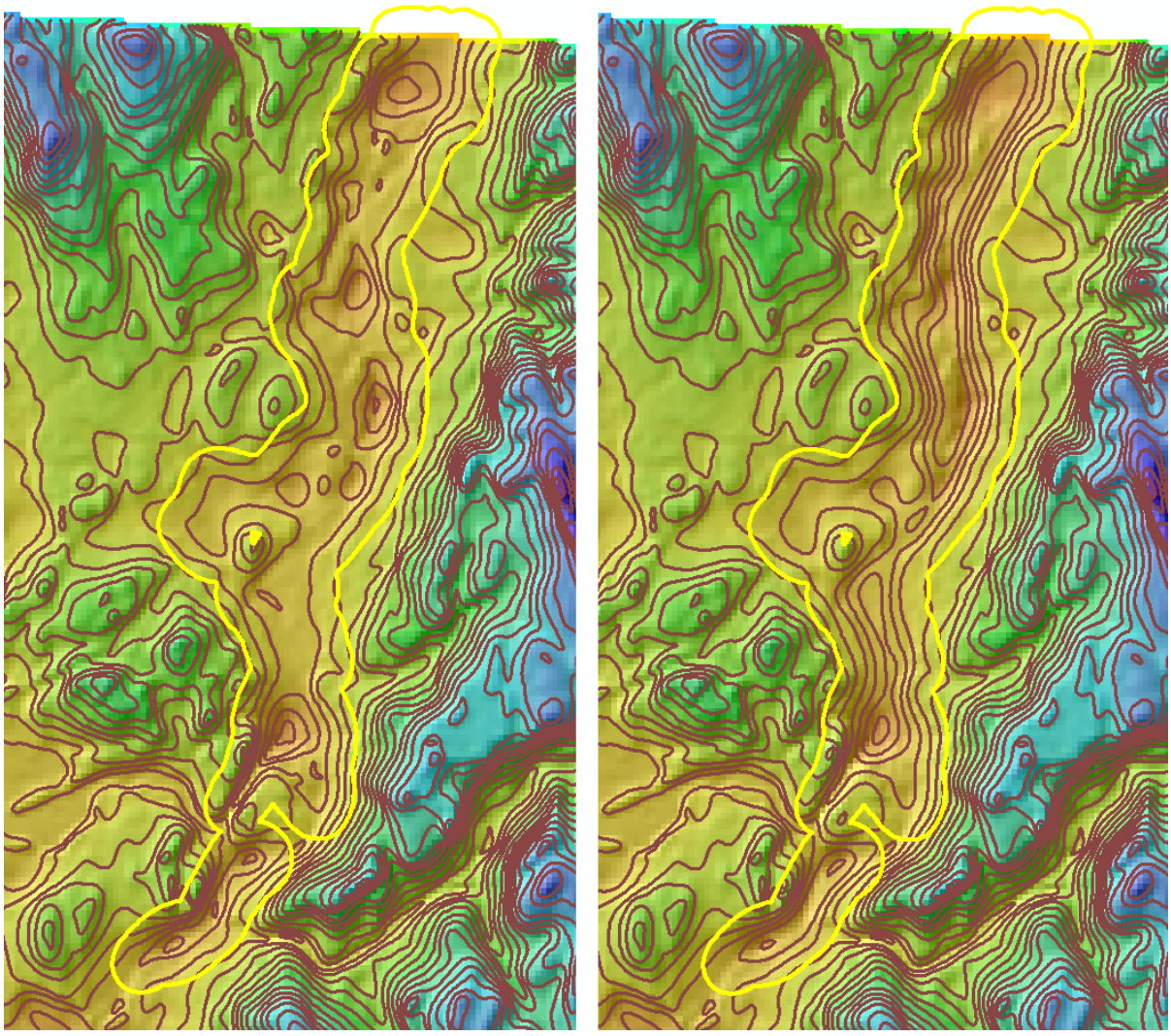

Figure 2.30: Contours before (left) and after (right) manual adjustments to create a single continuous linear depression linking the isolated individual depressions from the kriging model

a 500-meter buffer of the altered contour lines. In detail, this sequence involved using the following ArcToolbox tools:

1. "Topo to Raster" to convert the edited 20-meter contours to a 100-meter altitude raster.

2. Buffer" to map 500-meter buffer polygons around the manual contours.

3. "Polygon to Raster" to create a 100-meter raster of zones using each polygon's FID.

4. "Raster Calculator" to create a NOBLEND raster of ones (1s) outside the polygon zones.

```
Con ( IsNull ( CONTFIDZONES ) , 1 )
```

5. "Euclidean Distance" on the NOBLEND raster to get BLENDDIST.

6. "Raster Calculator" to compute a new BLENDFAC raster:

```
Con(BLENDDIST > 0, Con(BLENDDIST <= 300, BLENDDIST/300.0, 1.0))
```

7. "Raster Calculator" to blend CONTALT values into PATCHALT to create PATCHCONTALT:

```
Con(IsNull(BLENDFAC),
        PATCHALT,
        (1.0 - BLENDFAC) * PATCHALT + BLENDFAC * CONTALT
)
```

8. "Raster Calculator" to check for any remaining bedrock altitudes above topography from the patching and manual contouring processes by creating raster DTBCHECK:

```
TOPO100 -  PATCHCONTALT
```

9. "Raster Calculator" to remove any negative depths found in DTBCHECK:

```
Con(DTBCHECK < 0, PATCHCONTALT + DTBCHECK, PATCHCONTALT)
```

The resulting bedrock altitude raster is designated MAINALT, the bedrock altitude raster for the mainland after applying all adjustments and corrections and ensuring it is everywhere at or below the altitude of the current topography.

2.7.6. Modeling Input Data Uncertainty

All of the interpolation methods available in ArcGIS operate (implicitly) on the assumption of perfect input data; that is, they do not offer a way to incorporate constant nor per-point measurement uncertainties in the interpolation process and propagate that uncertainty into the predicted standard error. Rather, the predicted standard error results represent only the uncertainty at each location due to the geostatistical model and nearby control points being used to estimate the model at that point. Whether the input control values are known perfectly or with uncertainties of 100’s of meters, the output models from the Geostatistical Analyst are identical. Therefore, to have a complete picture of the uncertainty in the modeled bedrock altitude, the input measurement uncertainties must also be assessed in addition to the kriging prediction standard errors.

To estimate the spatial distribution of measurement uncertainty, the EKB kriging process is repeated using the point uncertainty attribute UNCERT_M rather than the bedrock altitude attribute. EKB was used with the same 1000-meter search radius used for altitude kriging. As

with bedrock depth, uncertainty must be everywhere a non-negative value, so any negative uncertainty cells are replaced with zero. The resulting raster is designated as UNC.

2.7.7. Final Altitude, Depth, and Error/Uncertainty Rasters and Contours

The bedrock altitude for the islands was added to the mainland altitude raster to create a FINALALT raster in "Raster Calculator" with this expression:

```
Con(IsNull(MAINALT), ISLANDALT, MAINALT)
```

In addition, the ISLANDALT raster was used to add the islands to the DTB raster to create the FINALDTB raster for the entire state:

```
Con(IsNull(DTB), TOPO100 - ISLANDALT, DTB)
```

An alternate raster of depth-to-bedrock was also created by subtracting the final altitude raster (FINALALT) from topography to create FINALDTBALT:

```
TOPO100 - FINALALT
```

In a similar vein, the uncertainties in the rasterized contours for the islands provided by Oldale were added to the mainland UNC raster *(21).* Since Oldale's work is based on seismic data and the depth to bedrock is very deep in this area, an uncertainty of 10% of the total depth was applied to the data *(21).* In the "Raster Calculator" the FINALUNC raster is computed with:

```
Con(IsNull(UNC), 0.1 * FINALDTBALT, UNC)
```

Finally, we combined the blended kriging prediction standard errors and the kriged measurement uncertainties into a FINALERRUNC raster, assigning a value of zero to the prediction standard errors for the islands where we did not use any kriging results. The procedure for combining independent measures of uncertainty/error is to convert the measures from standard deviations to variances by squaring them, then add the variances together, then take the square root of the sums to convert back to combined standard deviations:

```
SquareRoot(Power(FINALUNC,2) + Con(IsNull(BLENDERR), 0, Power(BLENDERR,2))
```

Final contour lines corresponding to the final bedrock altitude raster (FINALALT) were generated using the "Contour" tool with an interval of 20 meters and a reference altitude of zero. These contours were simplified and generalized by removing any contour lines with total lengths less than 500 meters, and then using the "Smoothline" tool to apply a 500 meter PAEK tolerance to the remaining lines.

2.8 Discussion of Bedrock Altitude and Depth Models

As detailed above, the processing of all the input data to obtain bedrock altitude and depth to bedrock models was an involved and complex sequence of steps. However, each model was evaluated to make sure it endeavored to meet certain criteria. Below is a recapitulation of the model criteria and the steps taken, including the rationale, to meet those criteria.

2.8.1. Model Evaluation Criteria

Conceptually, the process is simple enough: use all available data to estimate the best bedrock surface that meets the following criteria:

- passes as closely as possible to the observed bedrock altitudes of the bedrock wells.
- passes as closely as possible to the topographic surface at the locations of mapped bedrock outcrops.
- passes as closely as possible to the estimated bedrock altitudes beneath mapped shallow to bedrock regions.
- does not exceed the altitude of the maximum depth of any overburden well.
- does not exceed the altitude of the topography.
- displays as few modeling artifacts as possible (local spikes/pits associated with erroneous data points; lineations, linear ridges/valleys, linear slopes; significant rises or depressions that are unconstrained by interior data points).
- looks as plausible as possible for a bedrock surface subject most recently to glacial erosion and scour and is consistent with the structure and physical properties of the underlying bedrock formations.

These criteria are in some tension with each other—trying to meet one can make it more difficult to meet another—and the means for evaluating them fall along a spectrum from completely quantitative to highly qualitative. Nonetheless, they provide the framework for working from raw data to a final model that can be labeled "best" given the currently available data.

2.8.2. Summary and Rationale for Data Processing Steps

Beginning with a cleaned, curated, internally-consistent data set converted to centroid points on a 100-meter grid, here is a summary of the processings steps and a brief rationale for each step.

1. Exclude marine and island points; work only with data over the Massachusetts mainland and within Cape Cod Bay or within a few kilometers of the Cape. ***Rationale:*** **point density is very low beyond the Cape, bedrock depths decline rapidly off the Cape (including beneath the islands), and there is only one bedrock well on each island; these data serve only to confuse and complicate efforts at geostatistical modeling of the bedrock surface.**

2. Separate the data into two groups: bedrock observations (including bedrock outcrops and shallow to bedrock areas) and overburden wells (but only those overburden wells in cells lacking any bedrock data). ***Rationale:*** **the overburden wells cannot be used to estimate bedrock altitudes, *per se*, only to enforce a one-sided maximum-altitude constraint; removing them from the initial modeling ensures robust and consistent geostatistics of bedrock altitudes.**

3. After testing and evaluating to decide the best-performing interpolation method for bedrock altitude, apply that method to all bedrock data points (including bedrock outcrops and shallow to bedrock areas). Use the resulting bedrock surface to find any overburden wells whose maximum-altitude value is below the bedrock surface, and add them to the interpolation input. Repeat these steps (interpolate-select-add) until no overburden well altitudes are violated by the result. This is the altitude-based model. ***Rationale:*** **initial goal is to estimate the bedrock surface from known bedrock altitude values, but where such values are missing, the overburden wells can be used to condition the model towards the (unknown) correct solution.**

4. Identify model cells that violate the topographic constraint, and prepare a raster of blending factors to replace these invalid cells and smoothly feather their immediate neighbors by weighted averaging of the altitude-based model cells and depth-based altitude model cells (see next step). ***Rationale:*** **bedrock altitude cannot exceed topography, and replacing invalid cells with values derived from depth-to-bedrock measurements is a better option than simply setting all invalid cells equal to the topography.**

5. After testing and evaluating to decide the best-performing interpolation method for bedrock depth, use the bedrock depth values (rather than bedrock altitude) for all the input data used in step 3 to make a raster model of bedrock depth. Convert this depth model to an altitude model by subtracting from topography. This is the depth-based model. ***Rationale:*** **while obtaining a bedrock surface by subtracting estimated bedrock depths from topography is prone to errors (see Section 2.4 above, *Overview of Approaches, Problems, and Solutions*), it is a better approximation for repairing the altitude model than the alternative of assuming zero depth in those regions.**'

6. Using the raster of blending factors, blend the depth-based model from step 5 with the altitude-based model from step 3. ***Rationale:*** **this replaces known-invalid altitude model cells with data-driven alternative values that do not violate the topographic constraint.**

7. Using the same blending factors raster, blend the prediction standard errors from the altitude-based model (step 3) and the depth-based model (step 5) to create standard errors reflecting the blended data sources. ***Rationale:*** **the prediction errors from the altitude-based model where they lie above the topography and are replaced by depth-based values should reflect the prediction errors of that depth-based model.**

8. Manually inspect the blended bedrock altitude model for additional problems according to the criteria listed above; apply manual and semi-automated corrections to these isolated regions. ***Rationale:*** **where known problems or model artifacts can be identified, and a method devised to eliminate or reduce the problem, the result is an improved bedrock altitude model.**

9. Look for any remaining bedrock altitude cells exceeding topography and set them to the topographic altitude. ***Rationale:*** **the corrections applied in step 7 introduce minor/isolated violations of the topographic constraint; the final bedrock altitude raster should be everywhere at or below the topographic raster.**

10. Add bedrock altitude estimates for the islands based on contours from Oldale *(21)*. ***Rationale:*** **the statewide final product must include the islands and this is the best available source for bedrock altitude beneath the islands.**

11. Compute a depth-to-bedrock model by subtracting the final blended bedrock altitude model from topography. ***Rationale:*** **the depth model described in step 5, derived by interpolating depth values at the input points, is likely to underestimate overburden thickness in places as described in Section 2.4, *Overview of Approaches, Problems, and Solutions,* and is not consistent with the bedrock altitude model and topography; this step produces a depth model consistent with those two data layers.**

12. Use the same interpolation method, parameters, and input points from the last iteration of step 3 (modeling bedrock altitude) to generate a continuous raster of input data uncertainty values. ***Rationale:*** **the interpolation methods do not take into account uncertainties in the input data values; in order to fully represent uncertainties and errors in the final data products, we need to generate a continuous estimate of the measurement uncertainties of the input values behind the model.**

13. Combine the uncertainty model from step 12 with the blended prediction errors from step 7 to produce a combined errors and uncertainties raster. ***Rationale:*** **the input data uncertainties and modeling prediction errors are independent of each other and their variances are additive.**

2.8.3. Discussion and Examples of Raster Relationships

To understand better the relationships among the intermediate and final rasters and how the various modeling and correction steps affect them, illustrative cross-sections are provided below for specific scenarios. All of the examples use a shared basemap and chart symbology, with a few additional visual elements added as described for specific examples.

The basemap for each example consists of: shaded-relief 1-meter LiDAR topography; small black dots depict wells, bedrock outcrops or shallow to bedrock data points; the smooth curvilinear lines are bedrock altitude contours derived from the final bedrock altitude model, with labels in meters; raster cells with shading indicate theamount by which the original

bedrock-altitude model exceeds topography (and therefore required blending with depth-based values); the darker the shading the more bedrock rises above the topography. The thick straight line indicates the location of the cross section(s).

The accompanying cross-sections are displayed as line graphs, with altitude in meters above sea level on the y-axis and distance along the cross section line on the x-axis, expressed in meters. In these graphs, the 100-meter raster cells are readily apparent in the 100-meter-wide stair-step shapes of all the plotted curves. The fine smoothly varying dotted line represents the 1-meter LiDAR topography. It is also apparent from these curves that all the raster layers have been co-registered; that is, they all use the same 100-meter master reference grid as their basis.

The graph depicts the altitudes of six raster layers, as indicated in its legend: 1-meter (fine dotted line) and 100-meter (fine solid line) topography; the initial bedrock altitude model from the kriged altitude (medium dashed line); the bedrock altitude derived from interpolating depths and subtracting from topography (medium solid line); the blended bedrock altitude (bold dashed line), which may match (overprint) parts of both the kriged altitude-based and kriged depth-based lines; the final bedrock altitude (bold solid line), including any manual alterations made to address model artifacts, which will match (overprint) the blended altitude except where such alterations were made.

2.8.4. Modeled Bedrock Altitude Above Topography – Blending Altitude- and Depth-Based Rasters

A simple illustration of the "daylighting" of the altitude-based bedrock interpolation model (ALT3) where it rises above topography is shown in Figures 2.31 and 2.32, taken from an area just south of the Mass Pike near the Newton-Boston municipal boundary. The line of cross section traverses three topographic highs and intervening lows. In Figure 2.31, the shading indicates areas where the bedrock rise above the land surface; the darker the shading the greater the excess bedrock topography. In Figure 2.32, the bedrock altitudes measured in the nearby wells result in a bedrock surface that trends lower from south to north (medium dashed line), roughly paralleling the topographic trend. This surface daylights in the topographic lows, bridging across them from one hill to the next.

Clearly this is invalid behavior for the bedrock surface, which must be at or below topography everywhere. These areas require blending with the depth-based altitude (medium solid line). One can see how the blending works: for all of the altitude-based (medium dashed line) cells that are actually above topography, they are replaced in the blended (bold dashed line, hidden in most places) and final (bold solid line, overprints bold dashed line) results by the depth-based (medium solid line) surface.

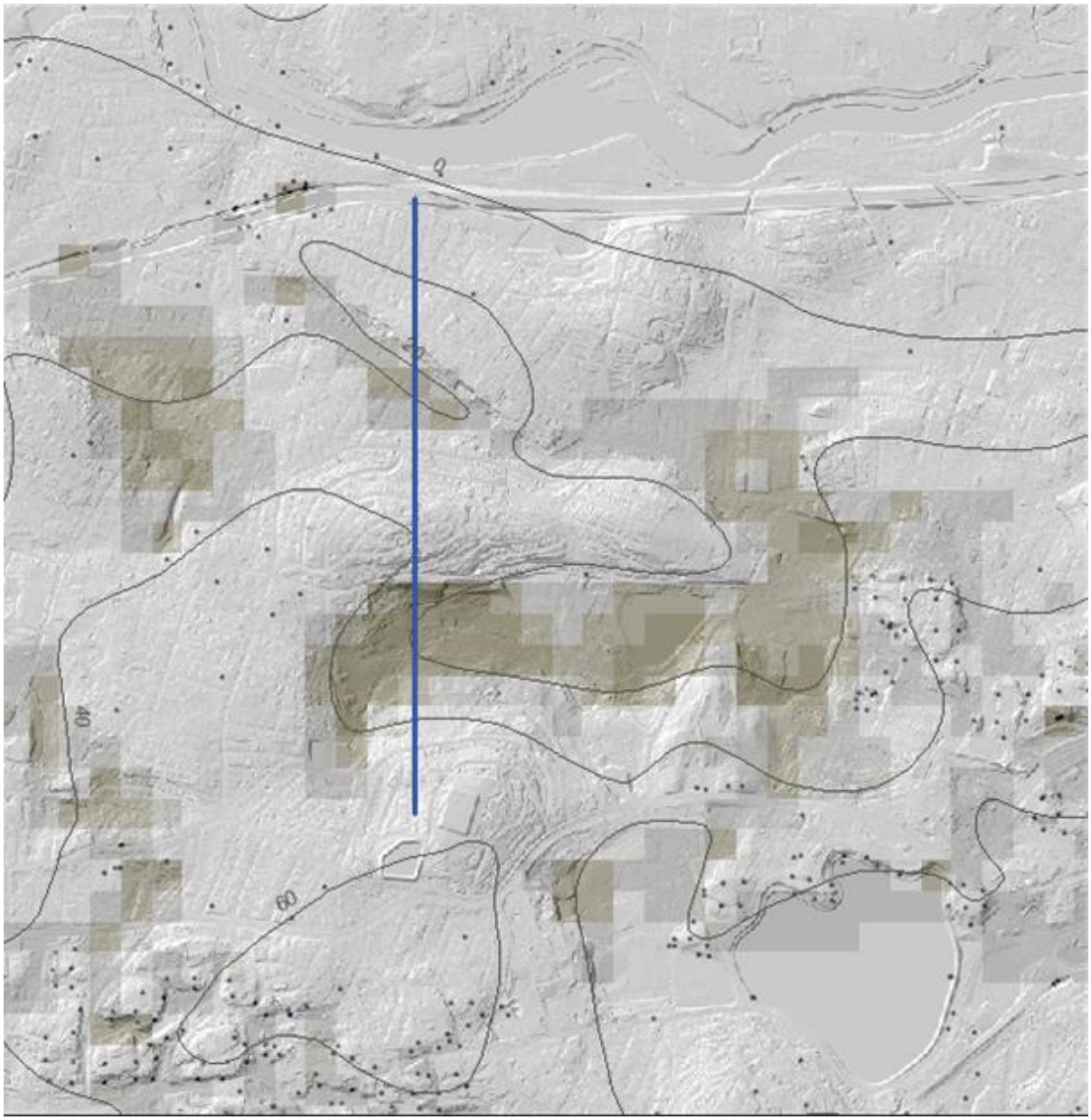

Figure 2.31: Map of cross section showing bedrock model above topography in Boston area

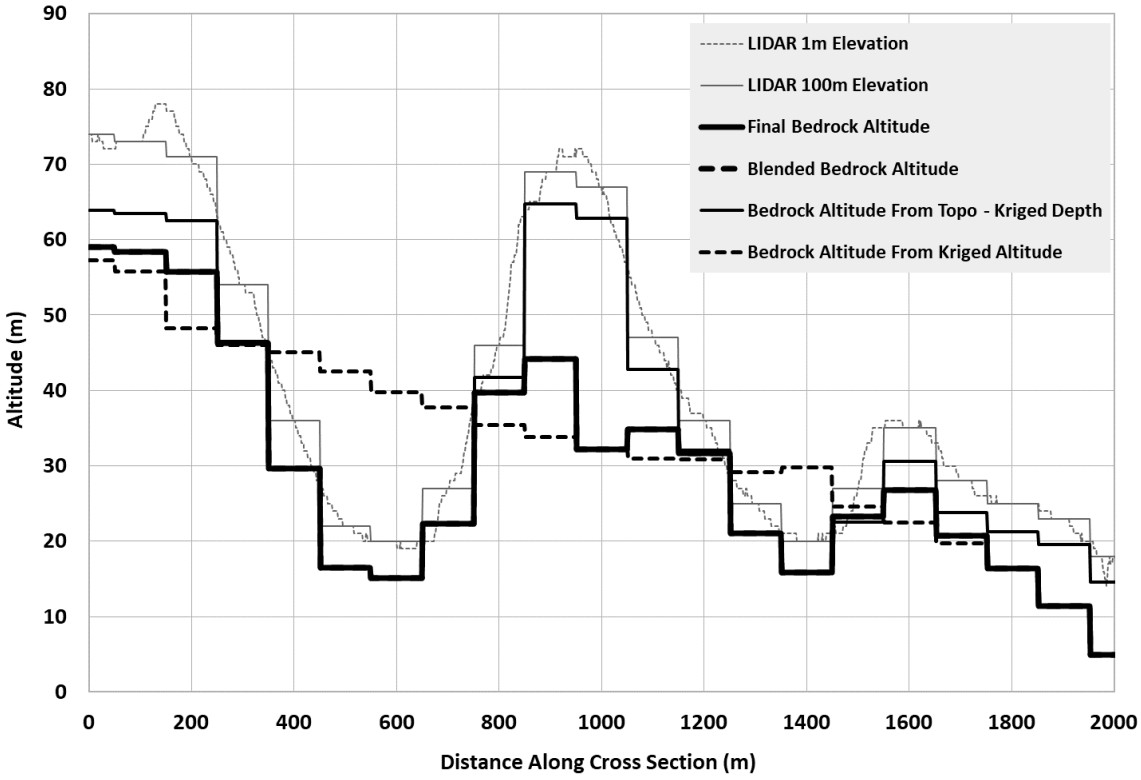

Figure 2.32: Cross section from Figure 2.31 showing bedrock model above topography

Another example of the altitude-based model daylighting occurs near Deerfield, in this case along the margins of the broad valley floor (Figures 2.33 and 2.34; Figure 2.34 is the cross-section along the northern line in Figure 2.33). The altitude model, controlled by bedrock outcrops and shallow to bedrock area data points (black dots) on the hillsides and only one or two points in the middle of the valley, approximates a broad, open "V" shape, somewhat steeper on the east, but not as steep as the topography, so the bedrock winds up emerging above the topography in the corners along the edges of the broad, flat valley floor. Where these errors occur, the blended (bold dashed line, hidden) and final (bold solid line) follows the depth-based surface, with the 200-meter transition zone on either side.

2.8.5. Kriging Artifacts (Depressions)

There are several kriging errors (artifacts) in the Deerfield region (Figure 2.33, light-colored, outlined polygons). About 100 of these artifacts were identified and corrected in the state. These are areas where the kriging interpolation output shows a depression, typically with steep sides, without any well data, bedrock outcrops, shallow to bedrock data points or geologic reason to justify the anomalously low bedrock altitudes.

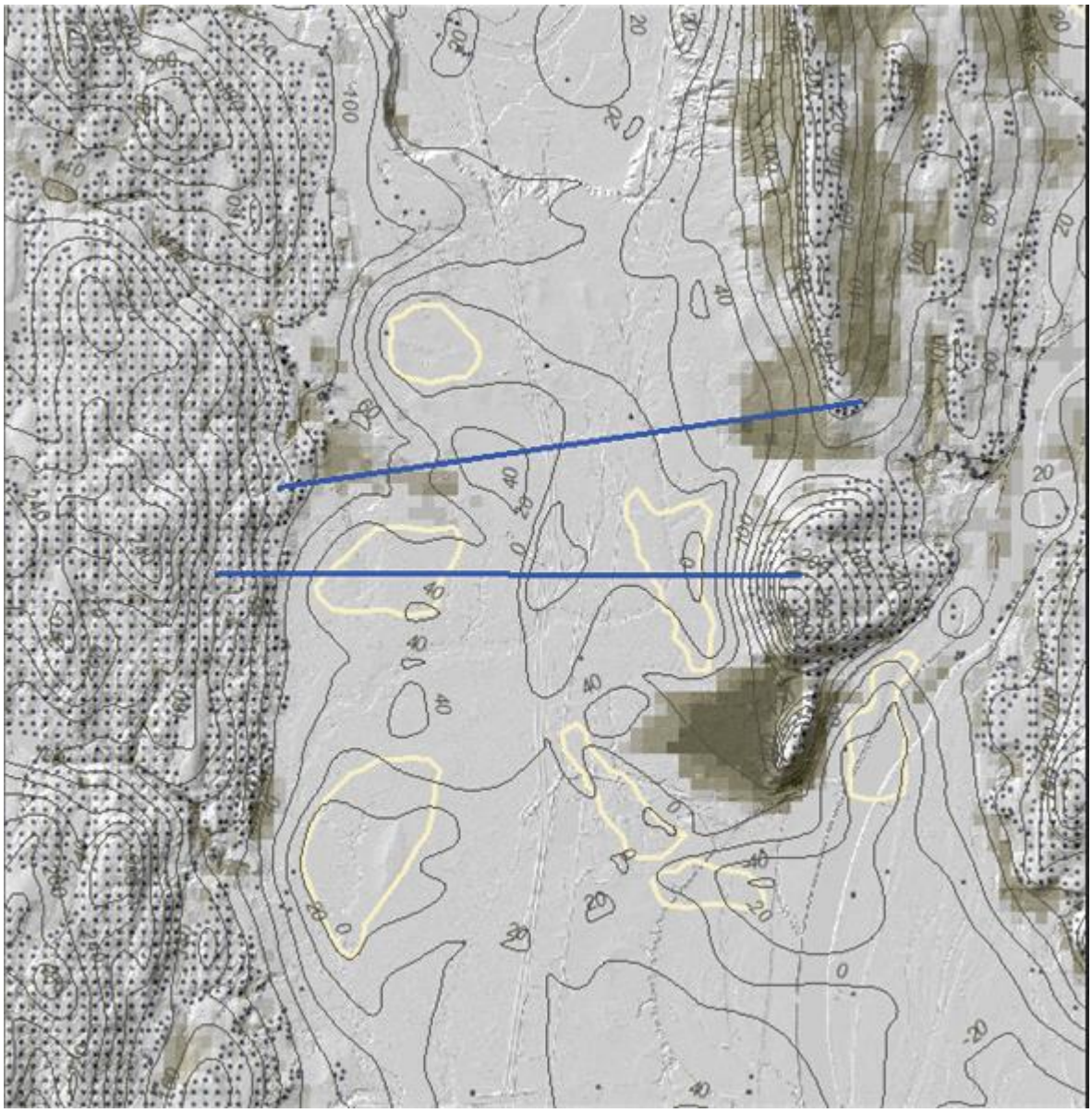

Figure 2.33: Map of two cross sections in the Deerfield, Massachusetts, area

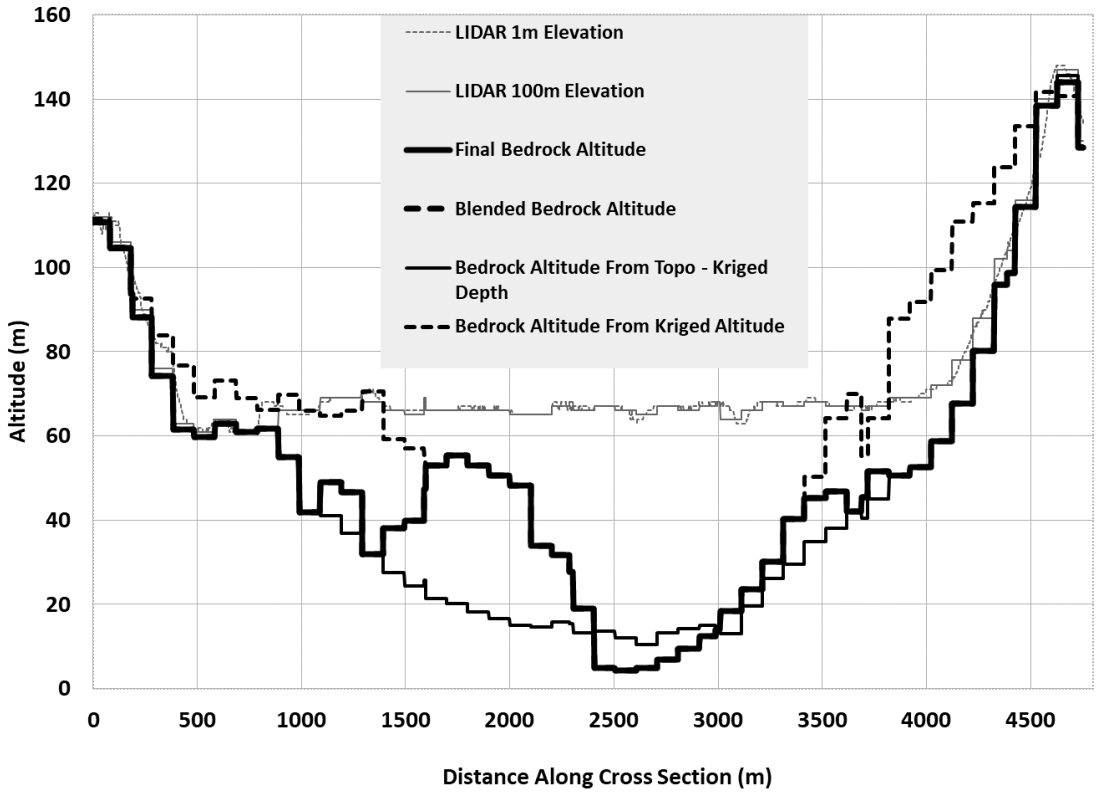

Figure 2.34: Cross section of the northern Deerfield line in Figure 2.33 showing the altitude-based model (medium dashed line) daylighting on the valley margins, and the resulting blended/final model to correct the errors

These errors were addressed by replacing the cells interior to the outlined artifacts with inverse-distance-weighted values of the model elevations around the perimeter of the artifact. This has the effect of removing the depression and replacing it with a gently- and smoothly-varying surface across it. The cross-section in Figure 2.35 shows the results of this correction for two of the artifacts visible in the cross section in Figure 2.33.

2.8.6. Manual Contouring

Manual contours were drawn to address two distinct problems: in three instances (one illustrated here), deep valleys in the bedrock altitude model appeared as a series of disconnected closed depressions; the manual contours were drawn to link these separate depressions into a through-going trough in the bedrock altitude model. In three other instances (not illustrated here), manual contours were drawn to replace contours depicting (incorrectly) features of the overburden rather than the bedrock surface (See section 2.4, Overview of Approaches, Problems, and Solutions for details).

Figure 2.36 shows the location of two cross-sections in the upper Connecticut River Valley where contour lines were manually adjusted to create a through-going trough. The contours of the altitude-based interpolation model (thin gray lines) depict a series of isolated closed depressions. The manually-redrawn contours (thick curvilinear lines) depict a single trough.

The thick black lines are the 500-meter buffer around the manually rendered contour lines, within

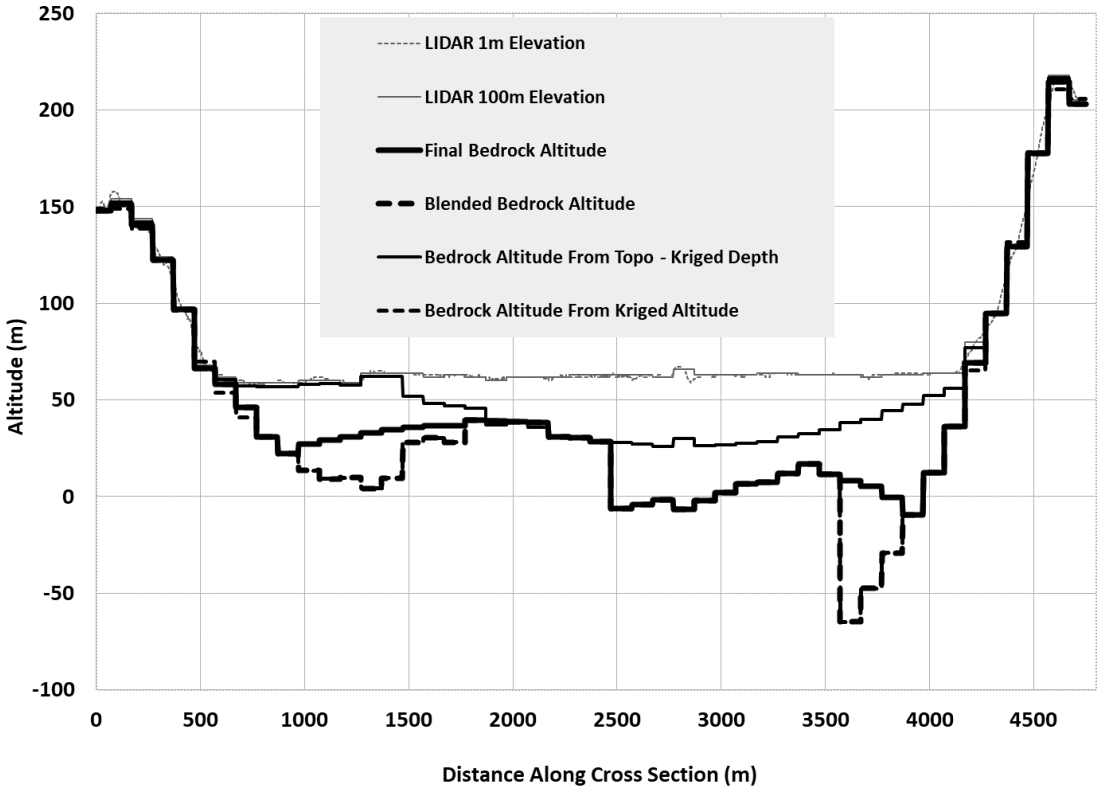

Figure 2.35: Cross section of southern Deerfield line in Figure 2.33; two kriging artifacts are visible in the upper chart where the blended-altitude (thick dashed line) model shows depressions that have been smoothed-over in the final (thick solid line) bedrock altitude model.

which the rasterized manual contours are blended with the altitude-based model to produce the final result. Black dots are bedrock altitude points. Straight lines are cross sections.

The two cross-sections in this region (Figures 2.37 and 2.38) were chosen to illustrate the effects due to integration of manual contouring into the altitude model. In Figure 2.37, the differences between the pre-manual-contoured blended surface (thick dashed line) and post-manual-contoured surface (thick solid line) are minimal. In Figure 2.38, the effects are substantial, with the final altitude (thick solid line) 40-80 meters lower than the blended altitude (thick dashed line).

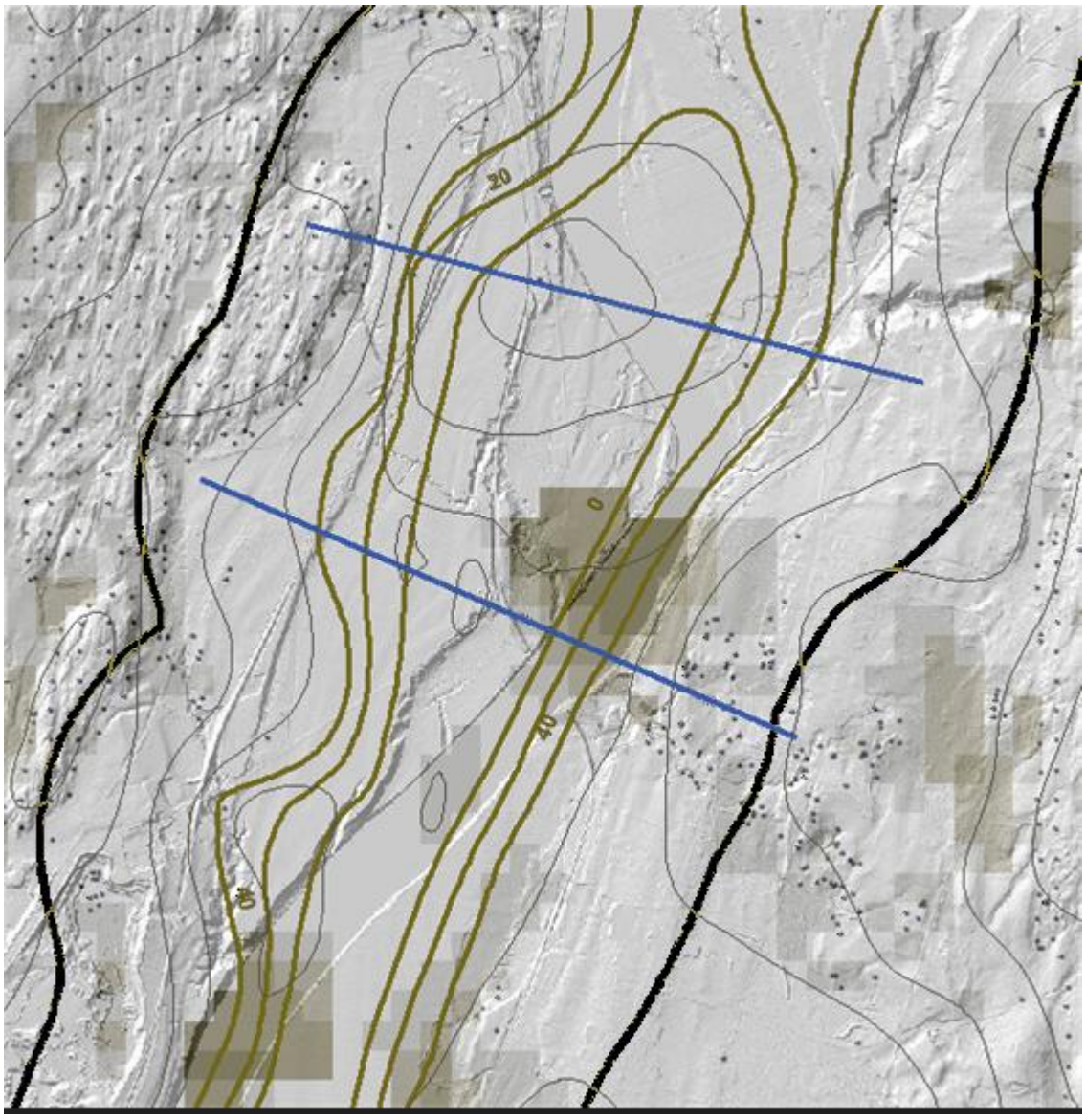

Figure 2.36: Cross section locations across manually-contoured region in the northern Connecticut River valley

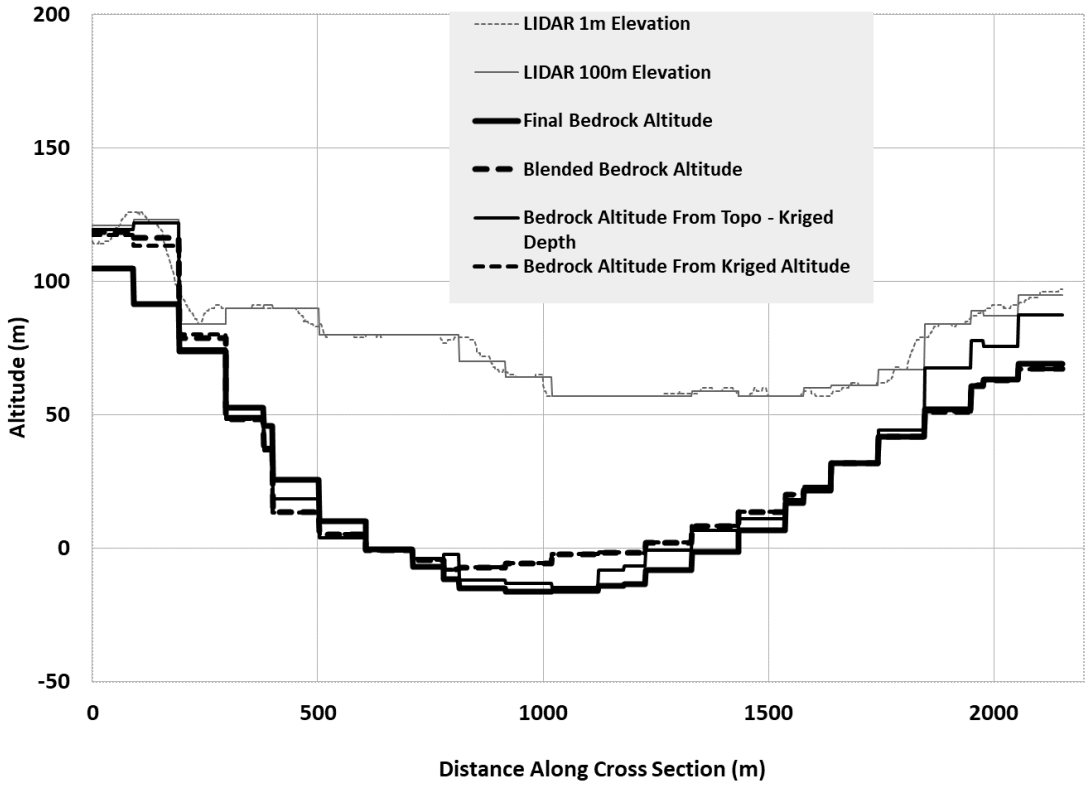

Figure 2.37: Northern cross section shown in Figure 2.36

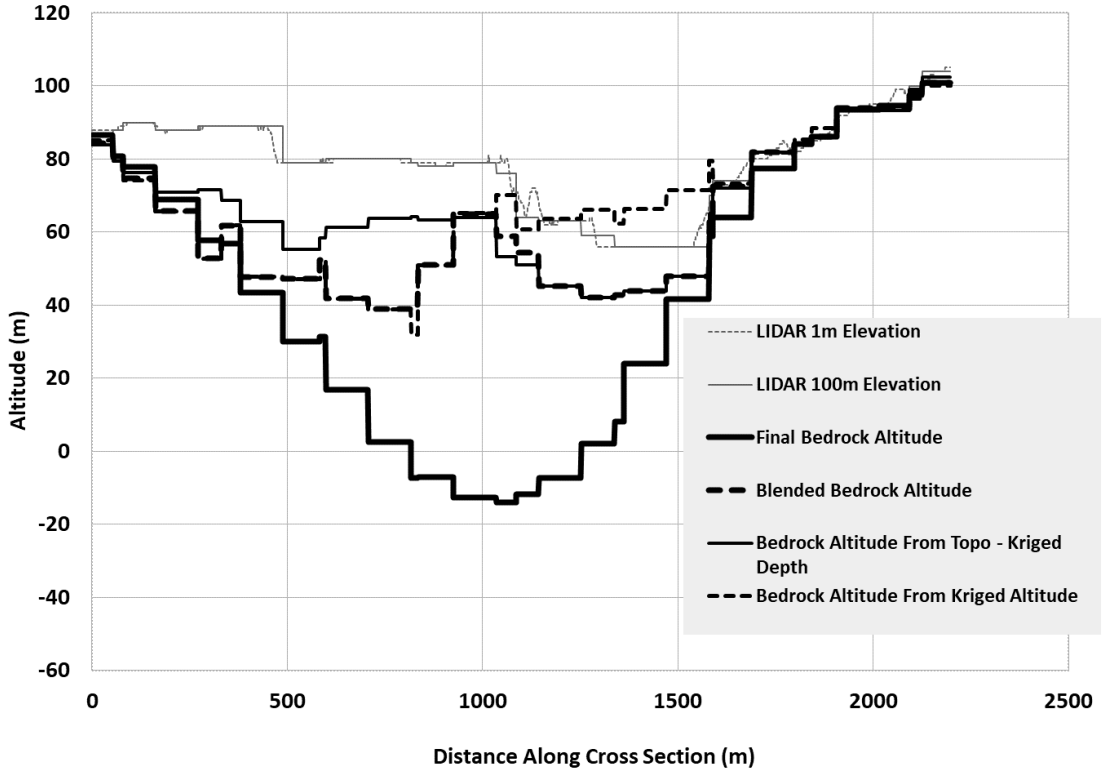

Figure 2.38: Southern cross section shown in Figure 2.36

2.8.7. Areas of Shallow to Bedrock

In contrast to the above examples, regions of shallow bedrock or abundant bedrock outcrops show little difference among the various bedrock altitude models. Figures 2.39 and 2.40 illustrate this from a region in the Williamstown-Adams area. These figures show how in areas of abundant point control, the two interpolation approaches (medium dashed line vs medium solid line, mostly hidden and under the bold solid line for the final bedrock altitude) differ very little, and so the need for blending is minimal and its consequences negligible.

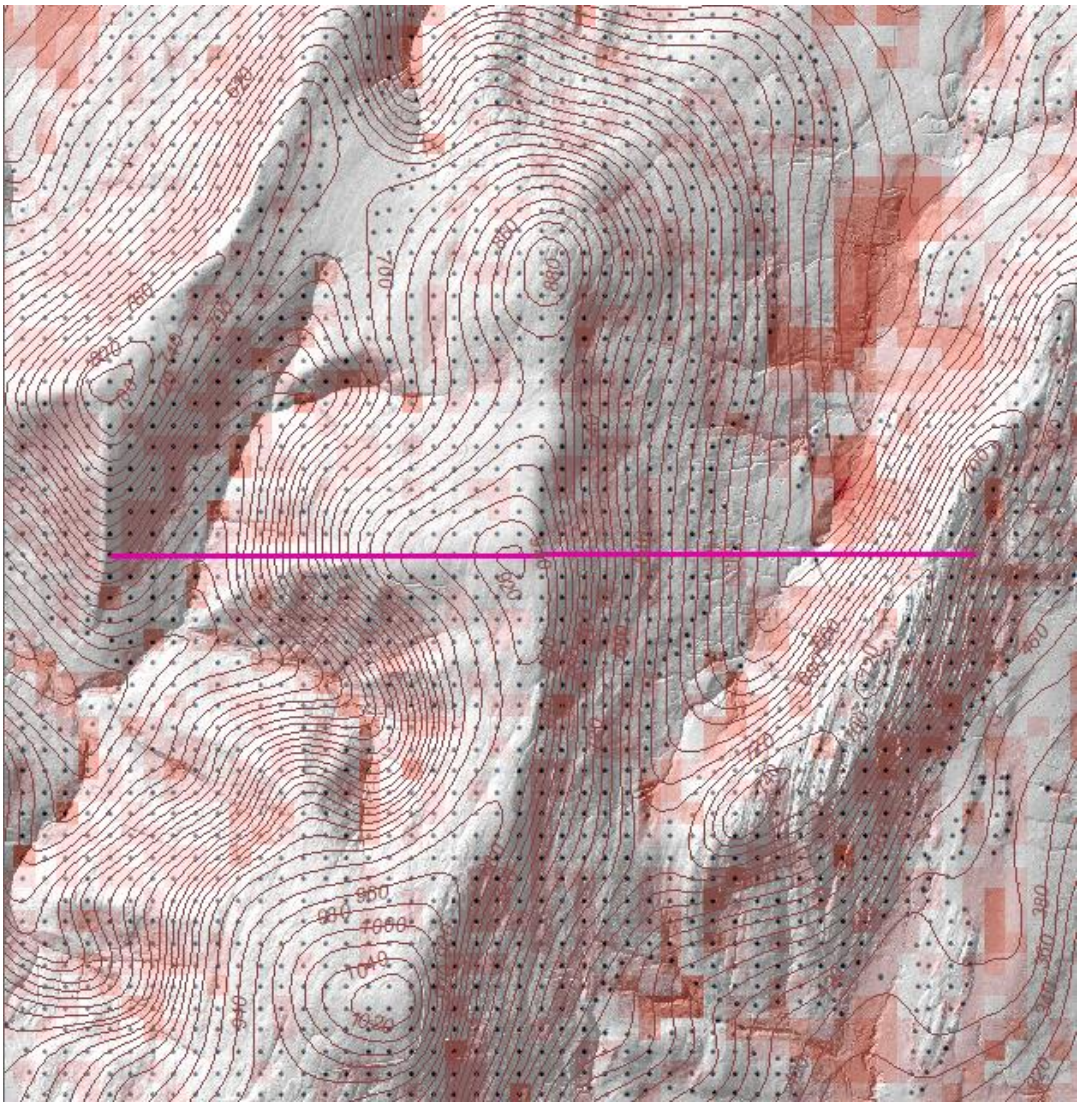

Figure 2.39: Map of cross section in region of shallow bedrock in the Williamstown-Adams area

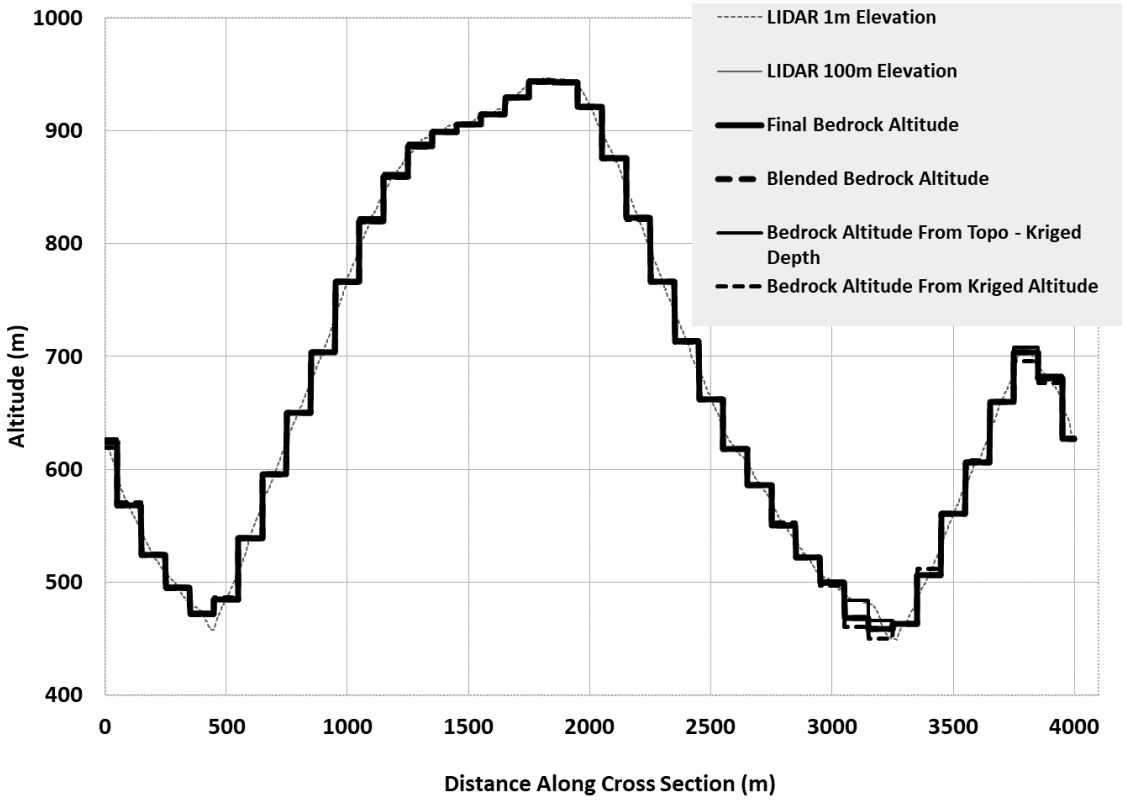

Figure 2.40: Cross section in shallow to bedrock areas—all models coincide well

2.9 NEHRP Classification Map of Massachusetts

The purpose of this section is to provide an updated, statewide NEHRP site classification map for Massachusetts at a 100-meter resolution and integrate the final depth to bedrock map (FINALDTB raster) into the classification processing. The Federal Emergency Management Agency (FEMA) classifies soil into five NEHRP categories and are defined based on the average shear wave velocity (*Vs30)* down to a depth of 30 meters (100 feet) (Table 2.4).

Table 2.4: NEHRP Soil Classifications

NEHRP Site Classification Category	Description	Mean Shear Wave Velocity to 30 m Depth
A	Hard Rock	>1500 m/s
B	Firm to Hard Rock	760–1500 m/s
C	Dense Soil, Soft Rock	360–760 m/s
D	Stiff Soil	180–360 m/s
E	Soft Clays	<180 m/s

Vs30 is a weighted average shear wave velocity over the top 30 meters of a geotechnical profile *(1, 2)* and is calculated using the equation:

$$Vs30 = \sum_{i=1}^{n} \frac{d_i}{\frac{d_i}{V_i}} \quad (1)$$

where d_i is the thickness and V_i is the shear wave velocity of the i^{th} geotechnical layer and $\sum_{i=1}^{n} d_i$ = 30 meters. Seismic site classes simplify the continuous *Vs30* variable into ranges represented by 5 classes (A-E) of increasing seismic site response hazard (Table 2.4).

Massachusetts was a glaciated state and typically has soft, unconsolidated glacial sediments overlying hard bedrock. During the Wisconsinan glaciation, the Laurentide ice sheet covered the state, clearing most of the existing pre-glacial materials and depositing glacial sediments on the cleared bedrock surface. With this unique high impedance contrast structure – soft, low velocity sediment over hard, high velocity bedrock – a simple layer-over-halfspace model can be employed, which is composed of an average overburden velocity (Vs_{avg}), a depth to bedrock (d_s) and a bedrock velocity (V_R) (Figure 2.41). Average overburden velocity is computed using equation 1 where $\sum_{i=1}^{n} d_i$ = the depth to the impedance contrast (the sediment-bedrock interface). The *Vs30* calculation simplifies to

$$Vs30 = \frac{30}{\left(\frac{d_S}{Vs_{avg}} + \frac{d_R}{V_R}\right)} \quad (2)$$

Where d_R is the thickness of the basement rock layer and is equal to 30 – d_s. This equation is valid for d_s <= 30 m. When d_s > 30 m, $Vs30 = Vs_{avg}$. Equation 2 is essentially Equation 1 where instead of *i* layers, there are 2 layers, one overburden layer and one basement rock layer, each with a thickness and a shear wave velocity. The thickness of the bedrock layer is 30 minus the thickness of the overburden sediment.

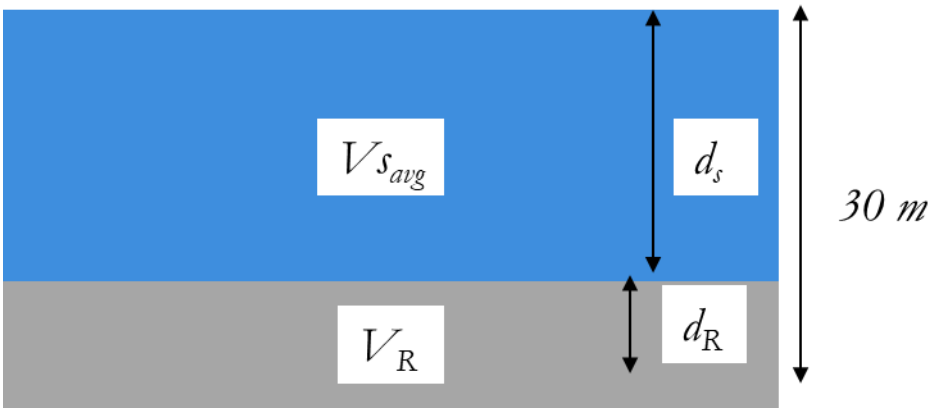

Figure 2.41: Overburden structure of the layer-over-halfspace model

A total of 35 shear wave velocity profiles were collected from , Mabee and Duncan, Thompson and others, and Pontrelli and others *(20, 22,23)*. Next, the surficial geologic map units from Stone and others were lumped into four groups based on their similar mechanical properties *(3)*. The shear wave velocity profiles were then assigned to these groups and plotted to determine the mean and median shear wave velocity for each group. This establishes a correlation between the surficial geologic map unit and shear wave velocity and assigns an average shear wave velocity for each map unit at every cell in the 100-meter resolution grid.

With the depth to bedrock map and a map of Vs_{avg} values, *Vs30* is calculated by applying Equation 2 to the two maps. For this calculation, bedrock shear wave velocity is assumed to be 2500 meters/second *(24, 25, 26, 27, 28)*). Details of the methodology are provided in Appendix E.

The method provided here uses a simple layer-over-halfspace model for the entire state and assigns a Vs_{avg} value based on the sediments exposed at the surface. In reality, the subsurface is more complex, likely with multiple layers and multiple velocities above the bedrock. Despite this limitation, estimating *Vs30* using the simple layer over halfspace model produces useful, reproduceable and conservative results.

3.0 Results

Table 3.1 presents the final products for this project. The links to the final products are embedded in the table (third column).

Table 3.1: Correlation of project peliverables, report name or file type, and file name or folder for data download

Project Deliverables	Report NAME of GeoTIFF image or File Type	File Name or Folder for Download
Master Spreadsheet	Spreadsheet	Final Data Release
HVSR Calibration Curve	Document	Calibration Curve
Data Used for Modeling	Shapefile	Wells_and_sg_used_for_kriging
Depth to Bedrock Version 1	DTB	Final_bedrock_depth_from_dtb_values
Bedrock Altitude	FINALALT	Final_bedrock_altitude
Depth to Bedrock Version 2	FINALDTBALT	Final_bedrock_depth_from_topo_minus_altitude
Model Prediction Errors	BLENDERR	Final_bedrock_altitude_prediction_standard_error
Observational Uncertainties	FINALUNC	Final_measurement_uncertainties
Combined Errors	FINALERRUNC	Final_combined_uncertainties_and_errors
Depth to Bedrock Ranges	GeoTIFF image	Final_bedrock_depth_range
NEHRP Site Class Map	Shapefile	MA_site_class_updated_MAP_2_16_2023

The Master Spreadsheet contents have been described in detail in Sections 2.1, 2.3, 2.4 and Appendix A of this report. The Calibration Curve has been described in Section 2.2 and Appendix B. The Data Used for Modeling is described in detail in Section 2.5. These will not be repeated here.

GeoTIFF images of each of the maps can be downloaded using the links in Table 3.1 and can be imported into GIS software directly for analysis. Small scale images and a short description of each map are provided below.

Figure 3.1 is a map of the depth to bedrock produced by modeling the depth to bedrock values for all bedrock wells, bedrock outcrops, shallow to bedrock areas, and a subset of overburden wells. Depth to bedrock ranges from 0 meters at individual outcrops to a maximum of 531 meters on Nantucket. As expected the thickness of the overburden is greatest in southeast Massachusetts, Cape Cod, Boston, and the larger river valleys and thin in the uplands.

Bedrock altitude ranges from a maximum of 1059 meters above NAVD88 to a minimum of -511 meters on Nantucket (Figure 3.2). There are several deep depressions in the Connecticut River Valley in central Massachusetts. One is observed on the either side of the gap where the Connecticut River passes through the Holyoke Range just north of Springfield. A few isolated depressions occur in the Housatonic River valley in extreme southwest Massachusetts that are likely the result of karst topography in the Stockbridge marble. As

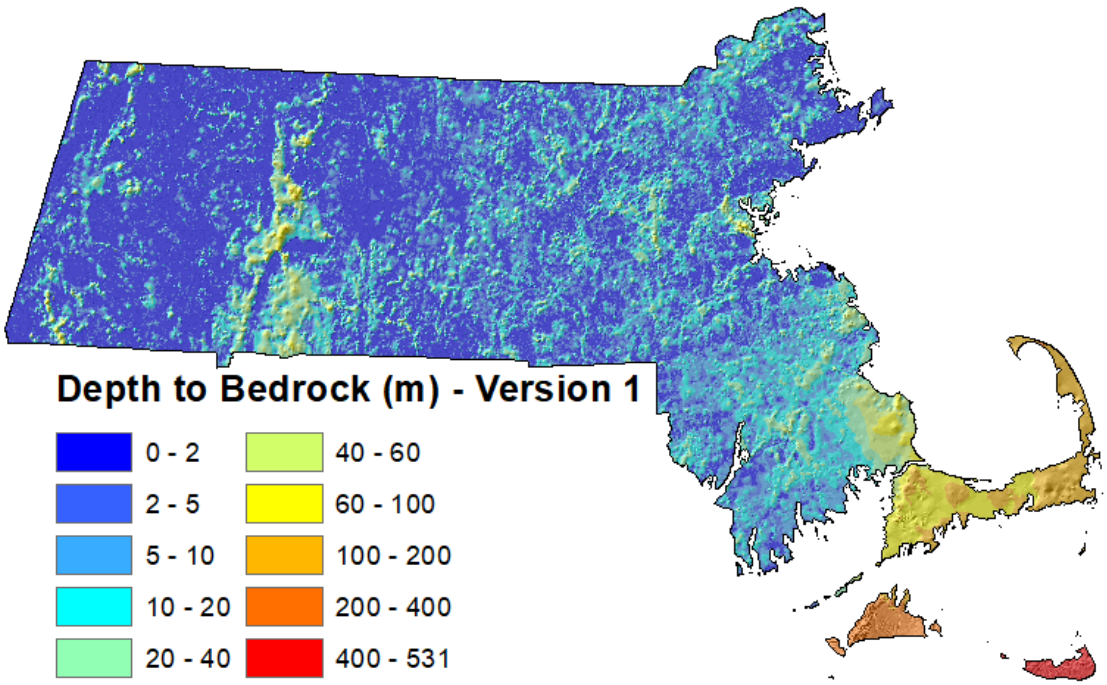

Figure 3.1: Map of depth to bedrock (meters) derived from modeling the depth to bedrock values for all bedrock wells, bedrock outcrops and shallow to bedrock areas

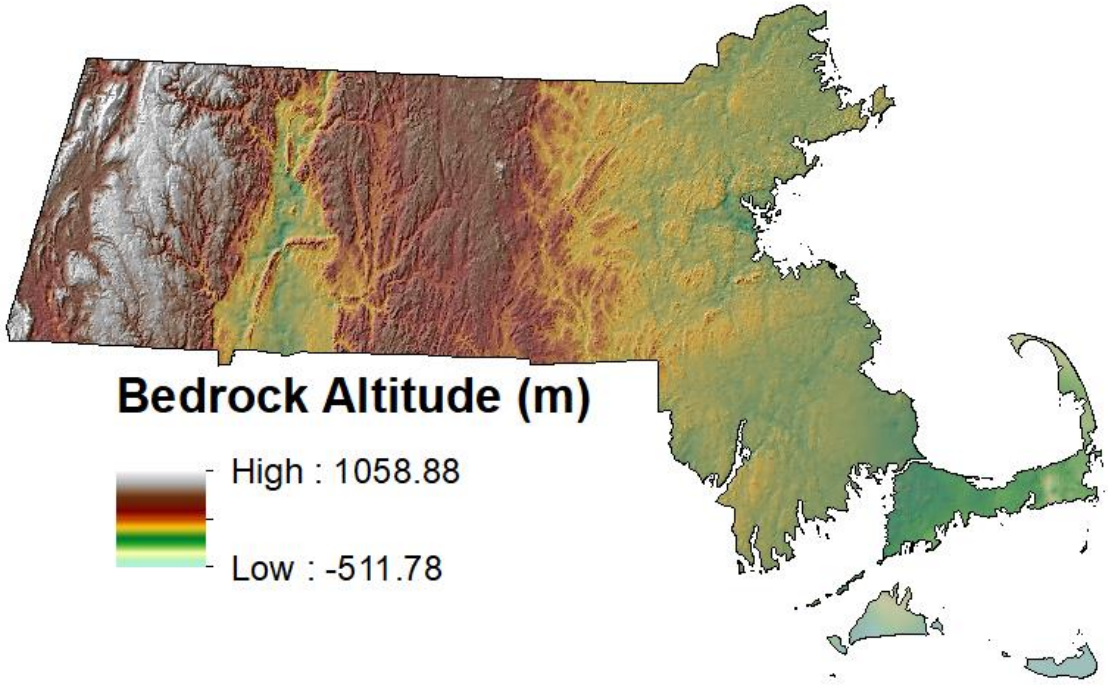

Figure 3.2: Map of the bedrock altitude

expected the altitude of the bedrock drops quickly in a southeastward direction from the Plymouth area.

Figure 3.3 shows a second version of the depth to bedrock. This version was derived by subtracting the altitude of the bedrock surface (Figure 3.2) from topography. Ideally this makes intuitive sense since the bedrock surface is an independent surface created by glacial scour. Accordingly, it should be modeled independently and then subtracted from topography to obtain the true thickness of the overburden. While this rendition looks very similar to the depth to bedrock version 1 map (Figure 3.1), there are differences; some are very subtle and others are significant. Some of these differences are described below.

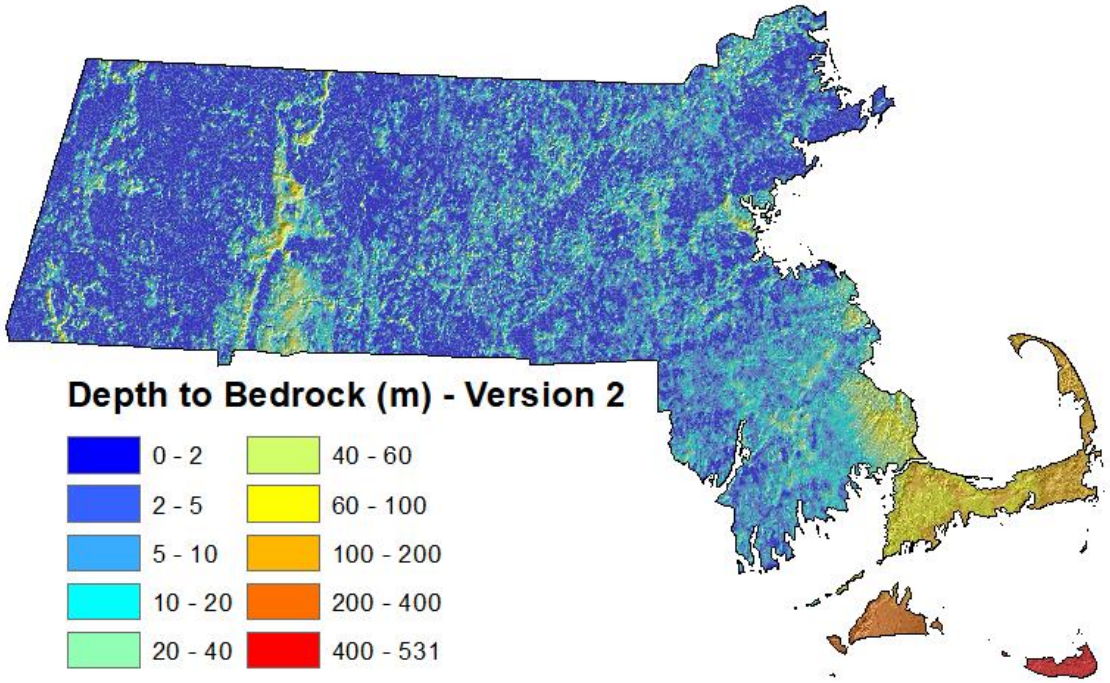

Figure 3.3: Map of depth to bedrock (meters) derived from subtracting the bedrock altitude from topography

There are two types of errors introduced into the modeling, prediction errors associated with the modeling and uncertainties associated with the depth measurements in the input data. For this project, three maps have been provided, a map of model prediction standard errors, which are output directly from the modeling, a map of measurement uncertainties, that is, the uncertainties assigned to the input data, and a combined error map where the prediction error and observational uncertainties are added.

Figure 3.4 shows the model prediction standard errors. Most of the state has a prediction error of less than 5 meters and very few are greater than 30 meters. The largest error is 120 meters and is located in the Connecticut Valley in an area of sparse well coverage.

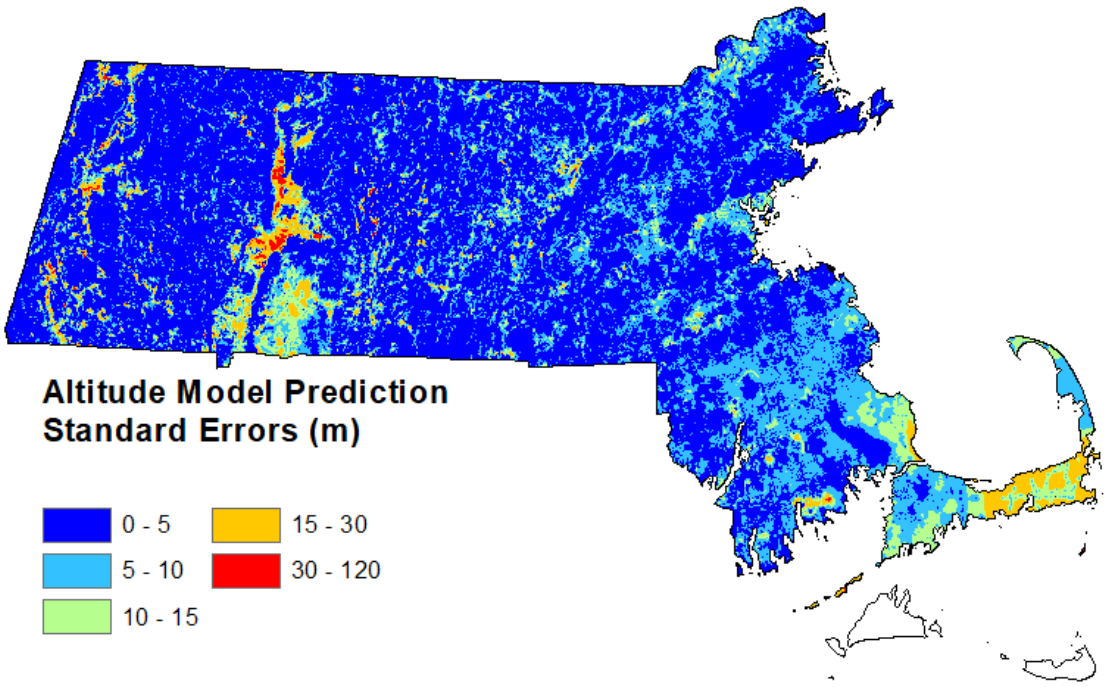

Figure 3.4: Map of kriging prediction standard errors in meters—Martha's Vineyard and Nantucket not included

Figure 3.5 shows the measurement uncertainty of the input data. For most of the state the measurement uncertainty is less than 5 meters. Notable exceptions include the Springfield area and Connecticut River valley where deep boreholes are lacking, and Boston, Plymouth area of southeast Massachusetts, Cape Cod and the Islands, where geophysical methods, which have a higher uncertainty, were used extensively to gather depth to bedrock data. The highest uncertainties were observed on Nantucket.

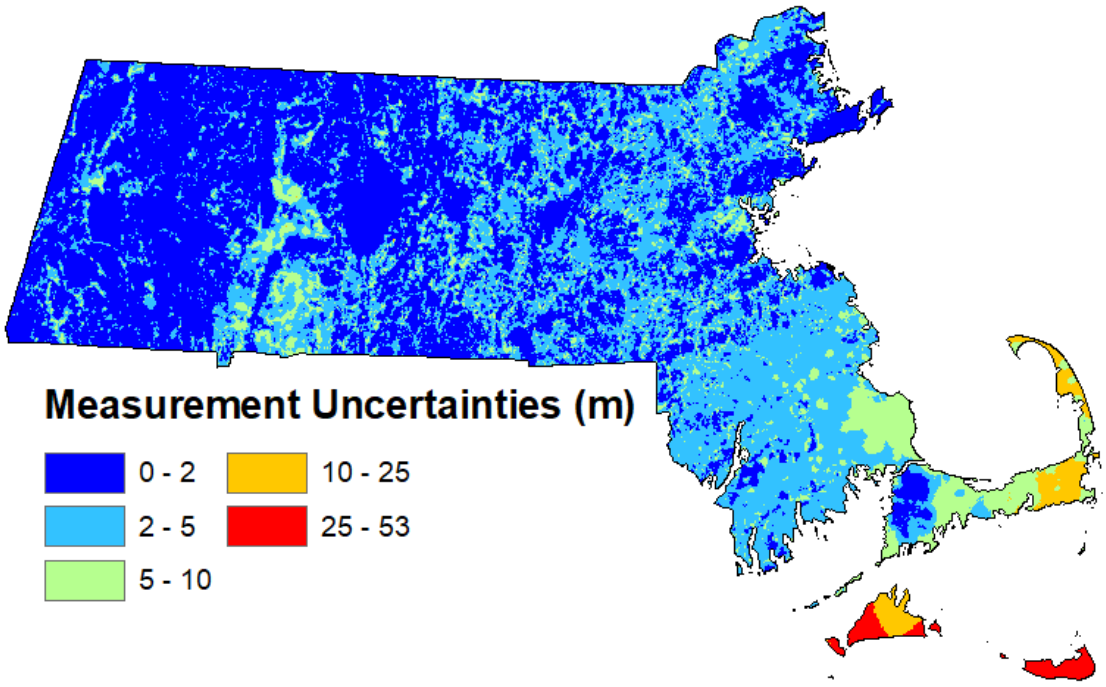

Figure 3.5: Map of measurement uncertainty (meters)

3.1 Discussion of Alternative Depth Models, Errors and Uncertainties

In the process of generating the best bedrock surface model two versions of a depth-to-bedrock model were created, one (designated DTB) interpolated directly from depth values at well, bedrock outcrops and shallow to bedrock data points, the other (designated DTBALT) created by subtracting the final bedrock altitude model from topography. These two models for depth to bedrock differ, primarily in areas of lower input data density and corresponding higher prediction errors.

Figure 3.6 shows the differences between the two depth models, obtained by subtracting DTBALT from DTB. In Figure 3.6, the differences shown as -123 to -10 (blues) are areas where the indirectly-determined (DTBALT) depths are greater, and differences showns as 10 to 60 (reds) are areas where the directly-determined (DTB) depths are greater; white was used for all differences smaller than +/- 2 meters.It is immediately apparent that the differences are slight for much of the state. In general, DTBALT depths tend to be deeper in mountainous areas (or areas with many bedrock outcrops or shallow to bedrock points), whereas DTB depths tend to be deeper in low-lying areas such in the Springfied area (south-central Massachusetts) and in the southeastern portion of the state and Cape Cod. Some of

the differences—for example the dark strip in north central Massachusetts—are due to manual alterations of contours that were only applied to the final bedrock altitude model, not to the direct DTB model.

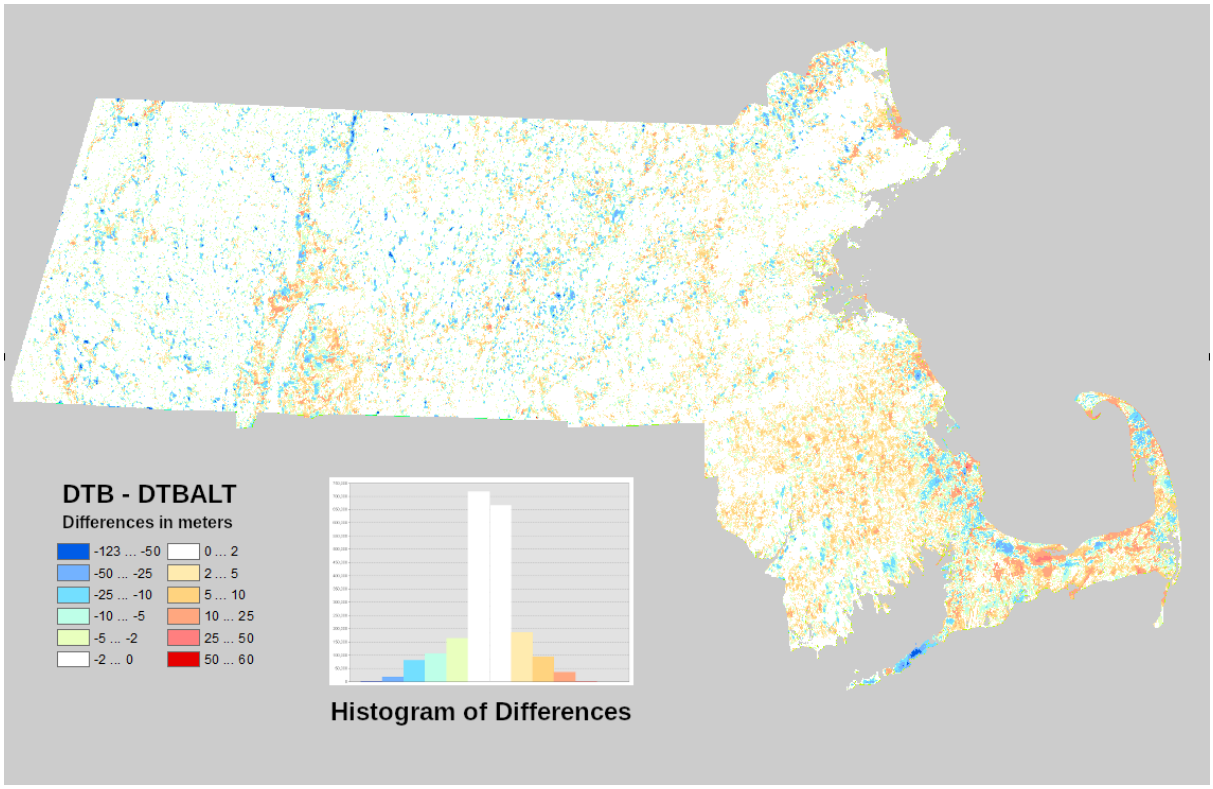

Figure 3.6: Map and histogram of differences between DTB and DTBALT models for depth to bedrock

Another way to portray the difference is to map the absolute value of the difference between the two depth models (Figure 3.7). For most of the state the difference is less than 5 meters. There are only a few outliers greater than 25 meters. The largest differences occur where model prediction standard errors and observational uncertainties are greatest (Figure 3.8).

A cumulative histogram of the combined errors (Figure 3.9) indicates that 95% of the combined errors are less than 18 m and 70% are less than 7 meters. There are 169 cells out of ~2.1 million 100 x 100-meter cells that have a combined error greater than 60 meters. This represents 0.008% of the area in Massachusetts. Most of these large errors occur in valleys in areas where there is sparse well coverage.

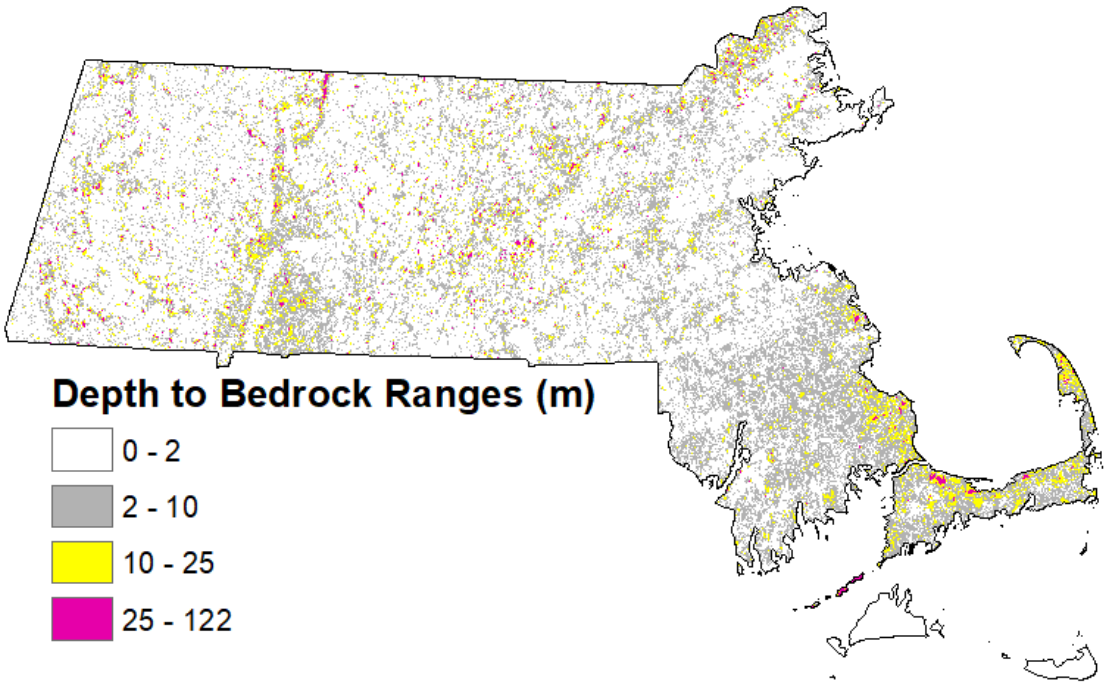

Figure 3.7: Map showing the range in depth estimates (meters) by the two methods—Martha's Vineyard and Nantucket not included

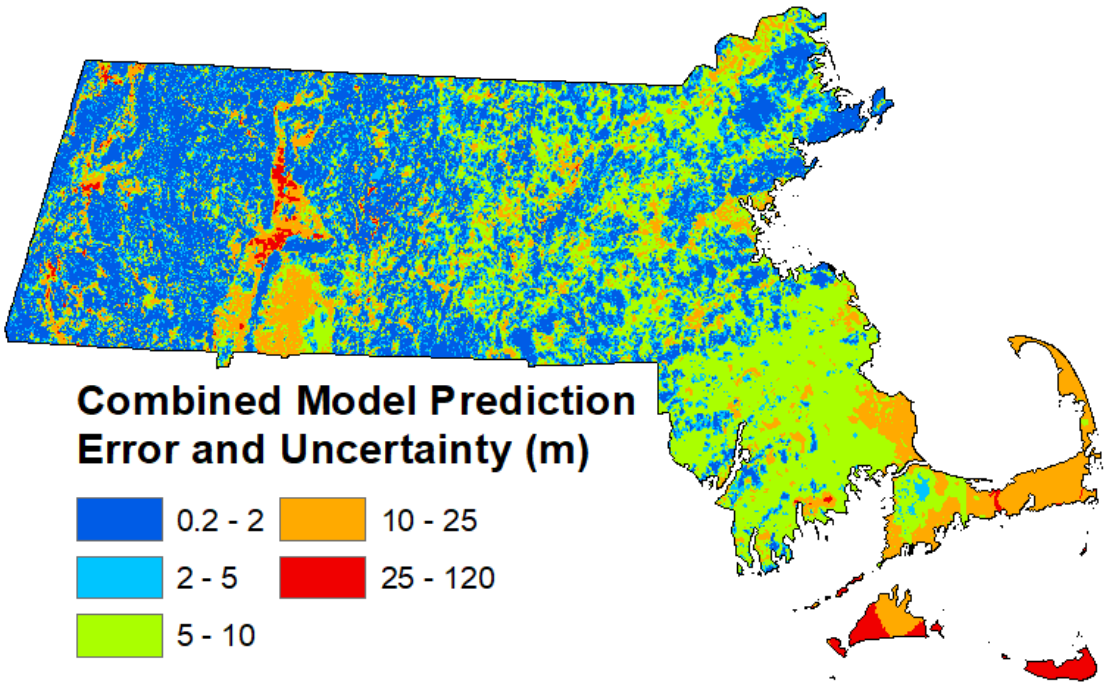

Figure 3.8: Map showing the combined model prediction standard error and observational uncertainty (meters)

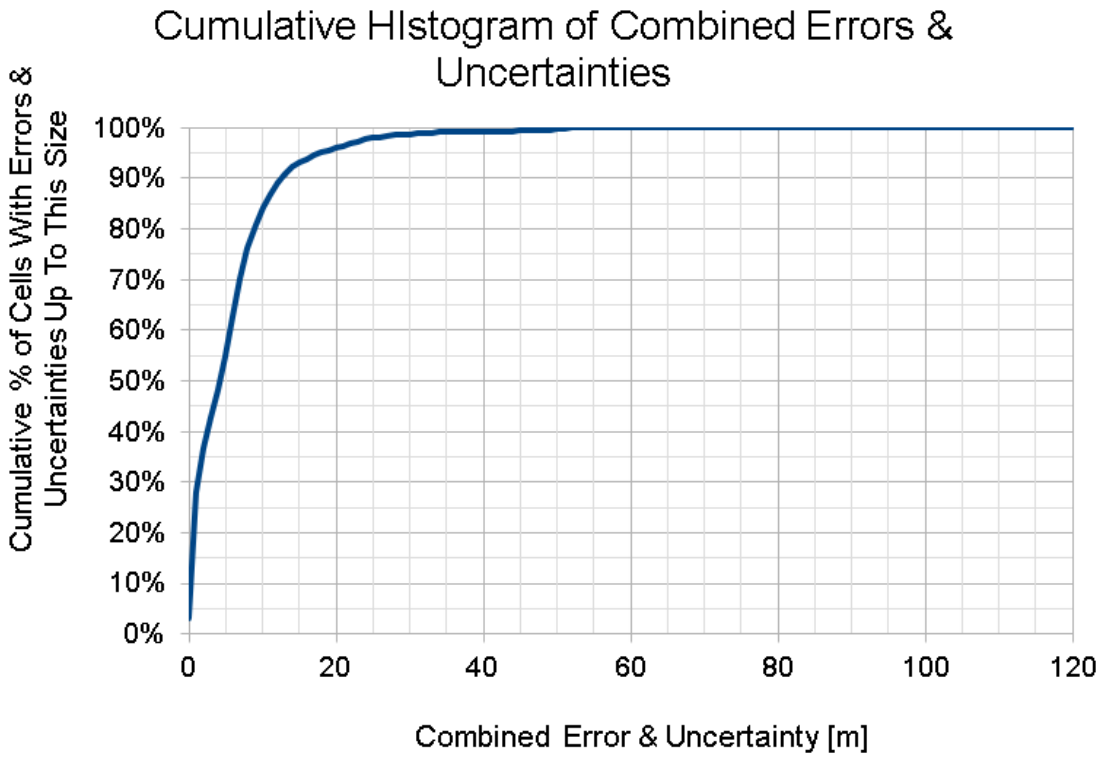

Figure 3.9: Cumulative histogram of combined error and measurement uncertainty

3.2 NEHRP Site Class Results

Approximately 40% of Massachusetts is classified as site classA, 25% as B, 21% as C, 14% as D and 1% as E (Table 3.2). While a high percentage of Massachusetts is classified as site class A or B (65%), two of the larger cities, Boston and Springfield, as well as southeast Massachusetts and Cape Cod are located in areas classified as site class D and E (Figure 3.10).

Table 3.2: Distribution of NEHRP cite classes across Massachusetts

NEHRP	Sq km	% Total
A	8350	40
B	5289	25
C	4323	20
D	2863	14
E	202	1

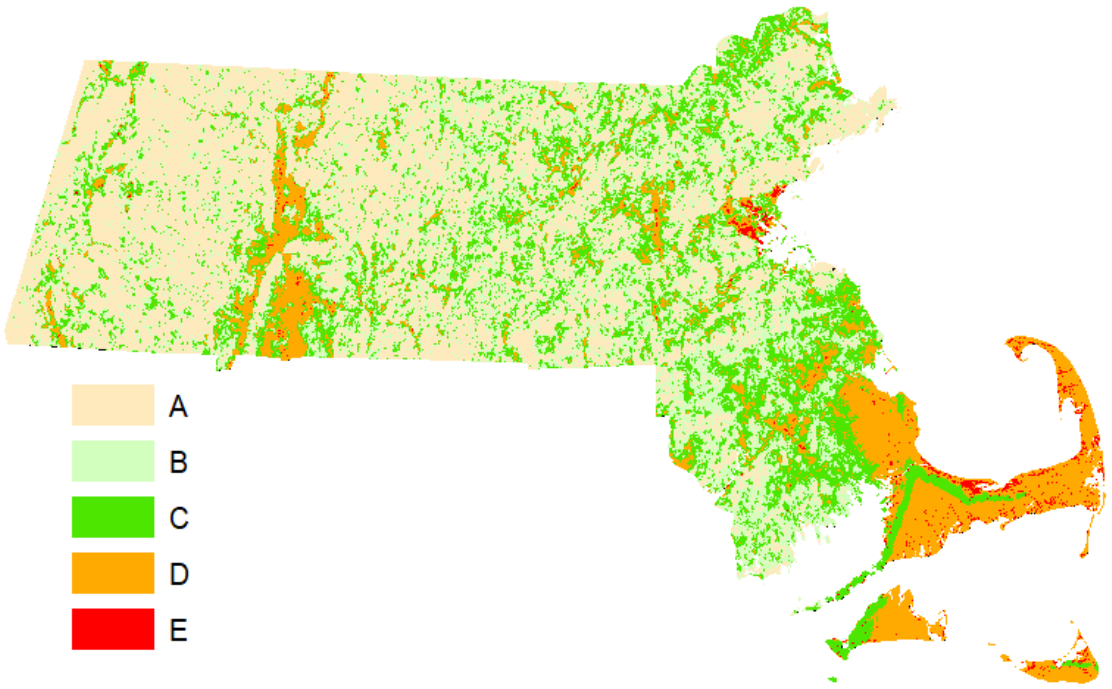

Figure 3.10: Distribution of NEHRP site classes across the state

In the Connecticut River valley and in Boston bedrock depth decreases as one moves from the center of the basin to the basin edges. Site classes change from class E or D in the basin center to a band of class C along the basin margin as the bedrock depth shallows ultimately to classes A or B in the uplands where compact tills are the dominant materials and the depth to bedrock is shallow.

This page left blank intentionally.

4.0 Implementation and Technology Transfer

All deliverables can be downloaded from the links provided in Table 3.1. The maps are all in GeoTIFF image format (the tfw world file is also provided) so the images can be imported directly into any GIS software. The maps are in Mass State Plane coordinates so they can be used with any other data layers from MassGIS and easily applied for any type of analysis. Proper use of these files does require some level of GIS proficiency. The shapefile for the NEHRP site classes and the shapefile for wells, bedrock outcrops and shallow to bedrock data points can also be imported directly into GIS. In addition, the Master Spreadsheet can likewise be imported into GIS by using the AddXY function and loading the the XY coordinates as either Northings and Eastings or Latitudes and Longitudes.

This page left blank intentionally.

5.0 Conclusions

The depth to bedrock is perhaps one of the most important surfaces that is fundamental to many practical engineering and geological problems. Yet it is not well understood everywhere. Knowing the depth to bedrock not only influences cost but may also affect selection of the appropriate foundation system for a particular structure. Furthermore, estimates of the bedrock depth, along with the type of overburden (e.g., glacial till, varved clay, sand and gravel) help determine the most appropriate subsurface investigation method to use during project planning, and reduces construction delays and claims brought forward by contractors. Accordingly, there is some level of uncertainty in planning subsurface investigations for any transportation project when depth to bedrock information is lacking.

This project is an attempt to reduce the uncertainty in highway project planning by providing interpolated statewide data layers of the depth to bedrock and bedrock altitude at 100-meter resolution based on currently available data. In addition, maps depicting the level of confidence in the estimate of bedrock altitude and depth are also provided. The confidence is based on both the interpolated prediction standard error as well as the measurement uncertainties associated with the input data.

Bedrock altitudes range from a high of 1059 meters (above NAVD88) at Mount Greylock to a low of -512 meters on Nantucket. The depth to bedrock ranges from 0 meters at individual bedrock outcrops predominantly located in the higher elevations to a maximum of 531 meters on Nantucket. As expected, overburden thicknesses are greatest in southeastern Massachusetts, Cape Cod, Boston and in the larger river valleys. Overburden thickness is very thin in the uplands.

Model prediction errors are less than 5 meters over most of the state and very few are greater than 30 meters. Approximately 75 percent of the state has observational uncertainties of less than 5 meters. Notable exceptions include the Springfield area and Connecticut River valley where deep boreholes are lacking, and Boston and the Plymouth area of southeast Massachusetts, where the measurement errors are still under 10 meters. Measurement errors increase on Cape Cod and the Islands, where geophysical methods, which have a higher uncertainty, were used extensively to gather depth to bedrock data. The highest uncertainties (maximum of 53 meters) were observed on Nantucket. Combined model prediction standard error and observational uncertainty range from 0.2 meters to a maximum of 122 meters.

The updated NEHRP site class map for Massachusetts indicates that approximately 65 percent of the state is classified as site class A or B. However, two of the larger cities, Boston and Springfield, as well as southeast Massachusetts and the heavily populated Cape Cod area, are located in areas classified as site class D and E. This map is greatly improved with better constraints on the depth to bedrock.

All maps are in formats that allow them to be imported directly into any GIS software. Meticulous effort was employed to create the “best” model of the bedrock altitude and depth to bedrock. These models will only improve with additional data. This report and the

appendices have been designed so that all process steps are well documented. This will allow the entire process to be repeated as more data become available.

The most effective way to use the bedrock altitude or depth to bedrock maps is to use them in conjunction with the error maps, well data, and bedrock outcrop and shallow to bedrock data points. This will provided the user with a probable estimate of bedrock depth with appropriate uncertainties in the depth estimate and the input data values from which these were derived for context and site specific evaluation.

6.0 References

1. Borcherdt, R.D., 1994. Estimates of Site-Dependent Response Spectra for Design (Methodology and Justification). Earthquake Spectra, Vol 10, No. 4.
2. Borcherdt, R.D., 1992. Simplified site classes and empirical amplification factors for site-dependent code provisions. NCEER, SEAOC, BSSC workshop on site response during earthquakes and seismic code provisions, Univ. Southern California, Los Angeles, California, Nov. 1992
3. Stone, J.R., B.D. Stone, M.L. DiGiacomo-Cohen and S.B Mabee, comps., 2018. Surficial materials of Massachusetts – A 1:24,000-scale geologic map database. U.S. Geological Survey Scientific Investigations Map 3402, 189 sheets, scale 1:24,000, index map, scale 1:250,000, 58 page pamphlet and geodatabase files, https://doi.org/10.3133/sim3402.
4. Soller, D.R. and C.P. Garrity, 2018. Quaternary sediment thickness and bedrock topography of the glaciated United States east of the Rocky Mountains: U.S. Geological Survey Scientific Investigations Map 3392, 2 sheets, scale 1:5,000,000, https://doi.org/10.3133/sim3392
5. Rial, J.A., 1989. Seismic wave resonance in 3-D sedimentary basins. Geophysical Journal International, v. 99, pp. 81-90.
6. Rial, J.A., N.G. Saltzman and H. Ling, 1992. Earthquake-induced resonance in sedimentary basins. American Scientist, v. 80, pp. 566-578
7. Delgado, J., C. Lopez Casado, J. Giner, A. Estevez, A. Cuenca and S. Molina, 2000. Microtremors as a geophysical exploration tool: Applications and limitations. Pure and Applied Geophysics, v. 157, pp. 1445-1462.
8. Site Effects Assessment Using Ambient Excitations (SESAME), 2004. Guidelines for the implementation of the H/V spectral ratio technique on ambient vibrations: Measurements, processing and interpretation. SESAME European Research Project WP12 – Deliverable D23.12, 62p.
9. Parolai, S, P. Bormann and C. Milkert, 2002. New relationships between Vs, thickness of sediments, and resonance frequency calculated by the H/V ratio of seismic noise for Cologne area (Germany). Bulletin of the Seismological Society of America, v. 92, pp. 2521-2527.
10. Ibs-von Seht, M., and Wohlenberg, J., 1999, Microtremors measurements used to map thickness of soft soil sediments: Bulletin of the Seismological Society of America, v. 89, p. 250-259.
11. Johnson, C.D. and J.W. Lane, 2016. Statistical comparison of methods for estimating sediment thickness from horizontal-to-vertical spectral ratio (HVSR) seismic methods: An example from Tylerville, Connecticut, in Symposium on the Application of Geophysics to Engineering and Environmental Problems, March 20-24, 2016, Denver Colorado, Proceedings of the Environmental and Engineering Geophysical Society, 7p.

12. Fairchild, G.M., Lane, J.W., Jr., Voytek, E.B., and LeBlanc, D.R., 2013, Bedrock topography of western Cape Cod, Massachusetts, based on bedrock altitudes from geologic borings and analysis of ambient seismic noise by the horizontal-to-vertical spectral-ratio method: U.S. Geological Survey Scientific Investigations Map 3233, 1 sheet, maps variously scaled, 17-p. pamphlet. (Also available at http://pubs.usgs.gov/sim/3233.)
13. Yilar, E., L.G. Baise and J.E. Ebel, 2017. Using H/V measurements to determine depth to bedrock and Vs30 in Boston, Massachusetts. Engineering Geology, v. 2017, pp. 12-22.
14. Oldale, R.N., C.R. Tuttle and L.W. Currier, 1962. Preliminar report on the seismic investigations in the Harwich and Dennis quadrangles, Massachusetts. U.S. Geological Survey Open-File Report 62-96.
15. Oldale, R.N. and C.R. Tuttle, 1965. Seismic investigations in the Harwich and Dennis quadrangles, Cape Cod, Massachusetts. U.S. Geological Survey Professional Paper 525D, pp. D101-D105.
16. Hall, R.E., Poppe, L.J., and Ferrebee, W.M., 1980, A stratigraphic test well, Martha's Vineyard, Massachusetts: U.S. Geological Survey 1488, 19 p. Also available at https://pubs.er.usgs.gov/publication/b1488.
17. Hull, R.B, Johnson, C.D., Stone, B.D., LeBlanc, D.R., McCobb, T.D., Phillips, S.N., Pappas, K.L., and Lane, J.W., 2019, Lithostratigraphic, geophysical, and hydrogeologic observations from a boring drilled to bedrock in glacial sediments near Nantucket sound in East Falmouth, Massachusetts: U.S. Geological Survey Scientific Investigations Report 2019–5042, 27 p., https://doi.org/10.3133/sir20195042.
18. Hansen, B.P., 1986. Exploration for areas suitable for ground-water development, central Connecticut Valley lowlands, Massachusetts. U.S. Geological Survey Water-Resources Investigation WRI84-4106, 41p. https://pubs.usgs.gov/wri/1984/4106/report.pdf
19. Garabedian, S.P. and J.R. Stone, 2004. Delineation of areas contributing water to the Dry Brook public-supply well, South Hadley, Massachusetts. Water-Resources Investigations Report 03-4320, 56p.
20. Mabee, S.B. and C.C Duncan, 2017. Preliminary NEHRP soil classification map of Massachusetts, Appendix B Hager Geoscience shear wave velocity data and analyses. Prepared for the Massachusetts Emergency Management Agency and Federal Emergency Management Agency, 232p.
21. Oldale, R.N., 1969. Seismic investigations on Cape Cod, Martha's Vineyard, and Nantucket, Massachusetts and a topographic map of the basement surface from Cape Cod Bay to the islands, in Geological Survey Research 1969, Chapter B, Scientific notes and summaries of investigations in geology, hydrology and related fields: U.S. Geological Survey Professional Paper 650-B, pp. B122-B127.
22. Thompson, E.M., B. Carkin, L.G. Baise and R.E. Kayen, 2014. Surface wave site characterization at 27 locations near Boston, Massachusetts, including 2 strong-motion stations. U.S. Geological Survey Open-File Report 2014-1232.
23. Pontrelli, M., S.B. Mabee and W.P. Clement, 2023. MA seismic site class map development from the state 100-m resolution depth to bedrock map. Unpublished notes, 12p.

24. Stewart, J.P., G.A. Parker, G.M. Atkinson, D.M. Boore, Y.M.A. Hashash and W.J. Silva, 2020. Ergodic site amplification model for central and eastern North America. Earthquake Spectra, v. 36, no. 1, pp. 42-68. https://doi.org/10.1177/8755293019878185
25. Goulet CA, Bozorgnia Y, Abrahamson NA, and others, 2018. Central and eastern North America ground—motion characterization—NGA-East final report. PEER report 2018/08. Berkeley, CA: Pacific Earthquake Engineering Research Center.
26. Goulet CA, Bozorgnia Y, Kuehn N, and others, 2017. NGA-East ground-motion models for the U.S. Geological Survey National Seismic Hazard Maps. PEER report no. 2017/03. Berkeley, CA: Pacific Earthquake Engineering Research Center.
27. Pacific Earthquake Engineering Research Center (PEER), 2015a. NGA-East: Median ground-motion models for central and eastern North America. PEER Report No. 2015/04, Berkeley, CA, PEER, University of California.
28. Pacific Earthquake Engineering Research Center (PEER), 2015b. NGA-East: Adjustments to median ground-motion models for central and eastern North America. PEER Report No. 2015/08. Berkeley, CA, PEER, University of California

This page left blank intentionally.

7.0 Appendices

7.1 Appendix A: A Data Set of Depth to Bedrock Described in Drill Holes and Geophysical Surveys for Massachusetts – Release 1

By: Stephen B. Mabee, William P. Clement, Christopher Duncan, Maya Pope, Keegan Moynahan, Ryan Miller, Hannah Davis and Alex Low

Abstract

This data set is a spreadsheet that contains borehole and geophysical data compiled from several available sources. These sources include MassDOT bridge and highway borings and seismic refraction surveys, Massachusetts Water Resources Authority project borings through 2014, data downloads from the USGS National Water Information System (NWIS) and Groundwater Site Inventory (GWSI) databases, Hydrologic Data Reports, surficial geologic quadrangle maps, seismic survey data collected by Hager Geoscience, various USGS Scientific Investigation Reports, Water Resources Investigation Reports and Open-File Reports, the Well Driller's Well Completion Report Database maintained by the Massachusetts Department of Environmental Protection, published and unpublished Horizontal to Vertical Spectral Ratio (HVSR) data and, offshore analog seismic survey data reinterpreted by Janet Stone and Ralph Lewis. There are 28 different data sets contained in the spreadsheet. The data sets include borings that go to bedrock and those that terminate in the overburden. Sheet 1 provides a description of the various data sets. Sheet 2 describes the source of the elevation data. Some data sets rely on the Massachusetts statewide 1-m resolution LiDAR DEM to determine surface elevation of a borehole or shot point whereas others use the surface elevation provided on the log of the borehole when available or from the original data source. Others have only the altitude of the bedrock. Sheet 3 is a compilation containing all 107,702 records for immediate plotting. Sheets 4 and 5 are for points that reach bedrock (N=61,531) and points that do not reach bedrock (N=46,171), respectively. Sheets 6 through 33 are the individual data sets. Stratigraphic information is limited.

Introduction

This data set provides depth to bedrock information assembled from various available data sources. The source data include borings, test wells, water wells and seismic data, specifically seismic refraction and reflection surveys and horizontal to vertical spectral ratio (HVSR) data. The data set is compiled as a spreadsheet with 33 sheets and contains a total of 107,702 unique records. There are 61,531 records that provide the depth to bedrock and 41,171 records that are considered overburden points that terminate within the overburden. For the purposes of this data release, borings or test wells that met refusal (wells that

encounter something hard but it is not confirmed if it is a boulder or bedrock) are assumed to have reached bedrock.

Purpose and Scope

The purpose of this data release is to provide data to the public to build maps of the altitude of the top of the bedrock surface and thickness of the overburden across the state for use by all stakeholders. For example, MassDOT will use this information as a tool for planning subsurface investigations and developing preliminary designs. The Massachusetts Emergency Management Agency will use overburden thickness to help assess seismic risk. Others may use the information for estimating the volume of aquifer storage. A second purpose of this data release is to provide data to generate structure contours of the bedrock surface for the new statewide Quaternary Geologic Map of Massachusetts currently under development.

Data Set

The data are presented as a Master Spreadsheet in Microsoft Excel 2007-2010 .xlsx format. FGDC-compliant metadata (Federal Geospatial Data Committee) accompanies the spreadsheet in htm, xml and txt formats. The data were compiled from a variety of data sources. Some data sources were previously published or were publicly available, some were provided via personal communication while other data were collected as a part of this project. This data set contains stratigraphic information only in a few limited instances.

Fields (labeled column headings in the spreadsheet) that are generally common to all data sets are identified with all caps. All other fields that are unique to each individual data set are indicated by lower case field names.

All coordinates are in the Mass State Plane coordinate system (NAD83) and all elevations are in NAVD88. Coordinate pairs in NAD27 were converted using the appropriate transformation in ArcGIS 10.8.1. Coordinates expressed in feet were converted to meters using the U.S. Survey foot to metric conversion (Massachusetts uses the U.S. survey foot convention rather than the international foot; 1 U.S. Survey Foot = 1200/3937 meters). When needed elevations were converted from NGVD29 to NAVD88 using the National Geodetic Survey Coordinate Conversion and Transformation Tool. Latitude and Longitudes have 6 decimal places of precision. Northing and Eastings have 3 decimal places of precision. A conversion factor of 3.281 feet per meter was used for all conversions of depth from feet to meters.

Surface elevations for each data point were determined one of two ways. Some data sets provided surveyed elevations. These were used when available and converted to NAVD88 as needed. Most surface elevations were extracted from the 1-meter resolution LiDAR DEM (digital elevation model) available from MassGIS. Note: the newest version of the Massachusetts statewide LiDAR coverage released in January 2022 provides elevations as integers rather than floating point numbers. The January 2002 LiDAR DEM was used for this project.

Uncertainty estimates for each data set reflect the reliability of the depth to bedrock estimate. For example, borings or test holes for which a geologist or engineer was present were given an uncertainty estimate of 0.6 meters (2 feet) in the depth to bedrock measurement. In contrast, depth estimates for borings drilled by well drillers were given an uncertainty of 5 meters. Seismic refraction surveys were given an uncertainty of 10% for depths greater than 6 meters and 0.6 meters for depths less than 6 meters (Hager-Richter Geoscience, personal communication, January 2022). Uncertainties are provided to give the user some understanding of the confidence in any analysis or derivative product based on these data.

The original source of the data contained in each data set is also provided along with any explanatory comments.

Great effort was made to verify locations, remove spurious data, or eliminate duplicates, however, there is no guarantee there will not be some duplicates or inconsistencies. Although these data and associated metadata have been reviewed for accuracy and completeness and approved for release, no warranty expressed or implied is made regarding the display or utility of the data for other purposes, nor on all computer systems, nor shall the act of distribution constitute any such warranty.

Description of the Data Sets

The following presents a more detailed description of each sheet in the data set.

Sheet 1 – DataSets: This sheet provides a brief description of each data set. It provides the abbreviated name of the data set, a fuller description of the data set (who created it, date of publication, or date data were collected or acquired). It also lists the number of points or wells that reached bedrock in each data set as well as the number of points or wells that did not reach bedrock (overburden points). Finally, a note is provided to indicate if stratigraphic information is affiliated with the data set.

Sheet 2 – Elevation: This sheet summarizes how surface elevations, depths and altitudes were determined. Column A lists each data set. Column B indicates whether or not the surface elevation for each point was acquired from the Massachusetts statewide LiDAR DEM (denoted by the X). Column C indicates the data sets for which surface elevations were provided from the original source data and not the LiDAR DEM. Column D indicates if the depth data were used to calculate altitudes whereas Column E indicates those data sets where altitude was provided and used to calculate depth. Note that GQ_Borings have both altitudes and depths provided in the source data. In some surficial geologic quadrangles the authors provided altitudes whereas in others the authors provided depths. Column F indicates how the altitudes or depths were computed for each data set. Altitudes were computed by subtracting depth from the surface elevation. Sometimes altitudes were given and depths were computed by subtracting altitude from surface elevation.

Sheet 3 – Compilation: This sheet contains all 107,702 records for easy plotting of the data set. The following fields are common to all the data tables. Therefore, they will only be described here. SITE_UID is the global unique identifier used for all the data in this project; there is only one occurrence of each SITE_UID in the compiled data tables, although they

may repeat in the source data tables where source-specific data occupies more than one row (e.g., information for multiple lithologic layers for one well). DATASET contains the name of the Data Set which allows for expedited filtering. This field does not occur in the individual data sets. SITE_ID is the local site identifier. In some cases, this identifier comes directly from the source data, in other cases it is a concatenation of several fields to obtain a unique local site ID and eliminate duplicate IDs. The next four fields are LATITUDE and LONGITUDE in decimal degrees and NORTHING_M and EASTING_M in meters. HOR_DATUM and VERT_DATUM are the horizontal and vertical datums, respectively. In all cases the horizontal datum is North American Datum 1983, and the vertical datum is North American Vertical Datum 1988. SURF_EL_M is the surface elevation of the measurement point in meters either extracted from the LiDAR DEM or provided in the source data. Points that fall within marine water bodies are given a default value of zero unless a surveyed elevation is provided. The DB_MN_RF_M field indicates the depth to bedrock or the minimum depth to bedrock in the case of overburden wells or the depth to refusal, in meters. ALT_MX_M is the altitude of the top of the bedrock surface or the depth of the borehole, which represents the maximum possible altitude of the bedrock in the case of overburden wells. UNCERT_M is the uncertainty in the depth estimate assigned to an individual record within a data set, in meters. For example, a MassDOT bridge boring with a depth to bedrock of 30 meters will have an uncertainty of plus or minus 0.6 meters. Details of how this uncertainty was determined is provided in the discussion of each individual data set. BOR_FLAG is a flag that identifies whether a boring or subsurface measurement point reached bedrock, met refusal or was an overburden well. This flag is useful for filtering the data. SGUNIT identifies the surficial geologic map unit in which the subsurface measurement point is located. Definitions for the unit labels can be found either in the metadata or in Stone and others (2018). SGISSB is a flag that identifies if the measurement point is located in a shallow to bedrock area or not. A “0” means the subsurface point is not located in a shallow to bedrock area whereas a “1” means the subsurface point is located within a shallow to bedrock area. A shallow to bedrock area is a polygon that overlies the surficial geology and indicates that the depth to bedrock is likely between 0 and 3.5 meters deep or there are so many bedrock outcrops within the polygon overlay that they are too numerous to map at 1:24,000 scale. LIDAR_M is the extracted surface elevation of the subsurface measurement point from the Massachusetts 1-meter resolution LiDAR DEM. This integer value is provided here because in some instances the surface elevation (SURF_EL_M, Column I) provided on borehole logs or source data publications differs significantly from the LiDAR estimate. For example, borings taken from bridge decks over water bodies go through the air, then the water column before reaching the mudline. In this case, using the surface elevation on the borehole log to calculate the bedrock altitude is appropriate rather than the LiDAR surface elevation, which often is taken at the water surface. In these cases, the difference in surface elevation values can be tens of meters.

Sheet 4 – Bedrock: This sheet contains all the subsurface measurement points that reached bedrock. It also includes those borings classified as meeting refusal. The field names are identical to the Compilation sheet. There are 61,531 records in this sheet.

Sheet 5 – Overburden: This sheet contains all the subsurface measurement points that did not reach bedrock. Field names are identical to the Compilation sheet. There are 46,171 records in this sheet.

Sheet 6 – BSP_Borings: This sheet represents a collection of 1,885 borings assembled by Dr. Laurie Baise and colleagues at Tufts University. The borings were drilled by MassDOT as part of the design and construction of the Ted Williams Tunnel under Boston Harbor and the depression of the central artery through Boston from the late 1980's into the 1990's. Dr. Baise called it the Boston Subsurface Project. The data were provided on 1/31/2019. Surface elevations for each boring were originally referenced to the Central Artery/Third Harbor Tunnel base. This base is 30.726 meters below 0 meters NAVD88. Other data provided with this data set include the original Northing and Easting coordinate pairs in feet, surface elevations relative to the Central Artery/Third Harbor Tunnel base in feet and the depths in feet. The uncertainty assigned to this data set is 0.6 m as an engineer or geologist was present when the borings were drilled.

Sheet 7 – BSP_Stratigraphy: This data set has 11,199 records listing the stratigraphic information for many of the borings in the BSP_Borings sheet. It contains the gINT (geotechnical integrator) record number, Boring ID, geologic sequence number, geologic description of the material, depth to the top of the geologic material interval, depth the bottom of the geologic material interval and thickness of the interval, all in feet. The stratigraphic information can be linked to the BSP_Borings through the SITE_ID field.

Sheet 8 – Fairchild_Borings: This data set contains 998 borings assembled and published by Fairchild and others (2013) at the Massachusetts Military Reservation and former site of Otis Air Force Base on Cape Cod. The site has recently been renamed Joint Base Cape Cod. The borings were drilled over a period of years for the U.S. Air Force. Surface elevations provided in the source data were used and converted to NAVD88. An uncertainty value of 0.6 meters was assigned to this data set as most of the borings were conducted by the USGS or consultants and it is assumed a geologist or engineer was on site during drilling. Also included in this data set are the original Northing and Easting coordinate pairs in feet (NAD27), the surface elevation and depth of the boring in feet and the original vertical datum (NGVD29).

Sheet 9 – Fairchild_HVSR: In addition to borings, Fairchild and others (2013) also collected Horizontal to Vertical Spectral Ratio (HVSR) method seismic data at 183 sites. They used a Guralp 6TD three-component seismometer to collect ambient noise measurements using Guralp's Scream software. Data were analyzed using Geopsy software (version 2.7.0). An uncertainty of 6 meters is assigned to HVSR seismic data. This uncertainty is based on comparing calculated depth to bedrock determined from HVSR measurements with sites where the depth to bedrock is known. The median of the difference between the actual depth to bedrock and estimated depth to bedrock using HVSR is 6 meters. Other fields in this data set include the observed fundamental frequency (Hz), original Northing and Easting coordinate pairs (NAD27) and surface elevation (NGVD29) in feet, date of the measurement and the depth and calculated altitude of the bedrock in feet.

Sheet 10 – GQ_Borings: Surficial geologic mapping of 7.5-minute quadrangles in Massachusetts was conducted over many decades starting in 1938. Some of these mappers included borehole data and/or seismic refraction data on the published geologic maps. This data set contains 305 borings and 13 seismic survey shot points from several published geologic quadrangle maps (Campbell and Hartshorn, 1980; Koteff and Stone, 1990; Nelson, 1974; Pomeroy, 1977; Chute, 1965; Hartshorn and Koteff, 1967; Hildreth and Colton, 1982; Stone, 1980; Hartshorn, 1967; Oldale, 1985; Holmes and Newman, 1971). Borings and shot points were digitized into ArcGIS 10.8.1 from georeferenced GQ-series maps. The attribute table was populated by hand entering the boring ID, depth or altitude measurements and other pertinent information into the table. The maps were downloaded from the National Geologic Map Database. Only borings not already included in the other data sets were digitized. The uncertainty assigned to these wells is 2 meters. It is unknown who drilled these wells and whether or not a geologist or engineer was present when the well was drilled. Therefore, these wells were assigned a greater uncertainty. For the points from seismic surveys, an uncertainty of 0.6 m was used for estimated depths to bedrock of 6 m or less or an uncertainty of 10% of the total depth for estimated depths to bedrock of greater than 6 meters. The data set also includes the surface elevation, original depth or altitude of the bottom of the boring in feet, the original horizontal and vertical datums, subsurface measurement point type (well, wash boring, seismic shot point) if known, town name and quadrangle name.

Sheet 11 – GWSI_Borings: This data set contains 8,499 records representing 8,268 unique boreholes. Some of the borings have stratigraphic information resulting in duplicate Site IDs for those wells (i.e., one boring site ID might have two or more records, one record for each lithologic unit). A PlotFlag field is provided with this data set to facilitate plotting in ArcGIS and avoid duplicate labeling of individual wells. This data set comes from the older USGS Ground Water Site Inventory (GWSI) database and was provided by Janet Stone (USGS) to the Massachusetts Geological Survey (MGS) on 2/15/2019. She collected this information for other projects. The date of the original download from the GSWI database is unknown. Most of the information in this data set comes from well driller data compiled in Hydrologic Data Reports. Well drillers typically embed the casing into the bedrock an average of 15 feet or more depending on the degree of weathering or fracturing. It is unclear whether the driller noted the top of the bedrock as the point of first encounter while drilling or the depth to competent bedrock (depth of casing). Accordingly, an uncertainty of 5 meters was assigned to this data set. Surface elevations for this data set were extracted from the 1-m resolution LiDAR DEM. Other fields provided in this data set include latitude and longitude (degrees, minutes, seconds), original horizontal datum, quadrangle name, surface elevation in feet, original vertical datum, topographic setting, construction date, primary use of site, hole depth (feet), well depth (feet), depth to the top of the casing (feet), depth to the bottom of the casing (feet), diameter of the casing (inches), depth to the top of the open interval (feet), depth to the bottom of the open interval (feet), type of opening, aquifer code, lithology code, discharge (gallons per minute), date of water level measurement, depth to the water table (feet), depth to the bedrock or depth of the well (feet), state code (25 for Massachusetts), county code and description.

Sheet 12 – Hansen_WRI84_4106_Seismic: Hansen (1986) collected seismic data in the Connecticut valley lowlands while exploring for areas suitable for ground water development. The map showing the location of the seismic survey lines was scanned from the report, georeferenced in ArcGIS and the endpoints, quarter points and midpoints along the survey lines digitized by MGS. Altitudes were interpolated from the seismic profiles for each point and entered into the attribute table. There are a total of 46 records in this data set. Uncertainty was assigned using 0.6 meters for estimated depths to bedrock of less than 6 m or 10% of the total depth for estimated depths to bedrock greater than 6 meters. Other fields in the data set include the seismic survey line identifier or number, location on the seismic survey line, original vertical datum and comments.

Sheet 13 – HDR_Borings: Between 1961 and 1989 a series of Hydrologic Data Reports were prepared for 27 watersheds in Massachusetts. These reports, sometimes referred to as Basic Data Reports, were the precursors to the Hydrologic Atlas series. The hydrologic data reports contained tables filled with borehole and well data from a variety of sources arranged by town. Many of these boreholes are what constitute the USGS Ground Water Site Inventory database. This data set contains 1127 records. The maps in the reports were georeferenced by MGS and boreholes and wells not already contained in other data sets were digitized and entered in the attribute table in ArcGIS. Surface elevations were extracted from the 1-meter resolution LiDAR DEM and the uncertainty assigned to the data set was 5 meters because most of the wells were installed by well drillers. Additional fields in the data set include town name, watershed name and depth to bedrock in feet. The comment section contains some limited stratigraphic information.

Sheet 14 – USGS_BOS_SE_MA_HVSR: This data set contains 113 HVSR measurements collected in southeast Massachusetts and the Boston area by John Mullaney and Byron Stone. Data were provided to MGS by Byron Stone on December 17, 2021. Data were collected with a Guralp 6TD three-component seismometer operated with Scream software. The data were analyzed using Geopsy software. Uncertainty assigned to this data set is 6 meters as described previously in the Fairchild_HVSR data set. Surface elevations were extracted from the 1-meter resolution LiDAR DEM.

Sheet 15 – Pontrelli_2021_HVSR: This data set contains 40 HVSR measurements and was collected by Marshall Pontrelli, Ph.D. student with Dr. Laurie Baise at Tufts University. He collected this data during the summer of 2021 and shared the results with MGS for this project. The instrument used to collect the data was a CMG-40t broadband seismometer with a Reftek 130 digitizer. The data were analyzed using his own code (available at https://github.com/mpontrelli/HVSR). Surface elevations were extracted from the 1-meter resolution LiDAR DEM and the uncertainty assigned is 6 meters as described in the Fairchild_HVSR data set. Additional fields in this data set include the observed peak frequency (Hz), amplitude of the peak frequency, prominence of the peak (does the peak stand out above background), half power bandwidth (defined as the frequency width at $(1/\sqrt{2})$*amplitude, sigma (median standard deviation between frequency values at the half power bandwidth) and date measurement was taken.

Sheet 16 – UMass_2017_2019_HVSR: This data set was collected by Steve Mabee and Bill Clement in the Connecticut and Housatonic River valleys during 2017 and 2019. A total of 44 measurements were collected. Data were collected using a Guralp 6TD three-component seismometer with Scream software. Data were processed using Geopsy software. Surface elevations were extracted from the 1-meter resolution LiDAR DEM and the uncertainty assigned to this data set was 6 meters as described previously in the Fairchild_HVSR data set. Additional fields in the data set include peak frequency (Hz), a description of the measurement location, the date the measurement was collected and comments.

Sheet 17 – UMass_2021_HVSR: During the summer of 2021 field teams from the MGS fanned out across Massachusetts to collect HVSR data in areas where well coverage was sparse. This data set contains 401 measurements. Data were collected with a Guralp 6TD three-component seismometer using Scream software. Data were analyzed with Geopsy software. Surface elevations were extracted from the 1-meter resolution LiDAR DEM and the uncertainty assigned to this data set was 6 meters as described previously in the Fairchild_HVSR data set. Additional fields include the peak frequency (Hz), description of the location of the measurement, date of the measurement and comments.

Sheet 18 – Pontrelli_2020_HVSR: This data set contains 22 HVSR measurements and was collected by Marshall Pontrelli, Ph.D. student with Dr. Laurie Baise at Tufts University. He collected this data during the summer of 2020 and shared the results with MGS for this project. The instrument used to collect the data was a CMG-40t broadband seismometer with a Reftek 130 digitizer. The data were analyzed using his own code (available at https://github.com/mpontrelli/HVSR). Surface elevations were extracted from the 1-meter resolution LiDAR DEM and the uncertainty assigned is 6 meters as described in the Fairchild_HVSR data set. Additional fields in this data set include a description of the location of the measurement, the observed peak frequency (Hz), amplitude of the peak frequency, prominence of the peak, half power bandwidth (defined as the frequency width at $(1/\sqrt{2})$*amplitude, sigma (median standard deviation between frequency values at the half power bandwidth), collector and date measurement was taken.

Sheet 19 – Yilar_2017_HVSR: The data contained in this data set were collected and published by Yilar and others (2017). The data set contains 564 HVSR measurements from the greater Boston area and was provided to MGS by Marshall Pontrelli at Tufts University. Data were collected with a Guralp 6TD three-component seismometer. Surface elevations were extracted from the 1-meter resolution LiDAR DEM and the uncertainty assigned is 6 meters as described in the Fairchild_HVSR data set. Additional fields in this data set include a description of the measurement location, peak frequency (Hz), collector, date of collection as well as comments.

Sheet 20 – MassDOT_Borings_Post1996: Pete Connors and Mike Glovasky provided plans showing the locations of boreholes and borehole logs completed for MassDOT projects between 1997 and the present. These included highway and bridge borings. The plans and logs were uploaded to dropbox on May 27, 2021 and organized by contract number or bridge ID. MGS examined each boring layout plan and borehole log and manually entered the following information into the spreadsheet: project number, bridge ID number, boring

number, Northing, Easting, depth to bedrock (as determined from the boring log), minimum depth to bedrock for overburden borings, surface elevation and any additional information worth noting. Care was needed as some borings used feet while others were in meters. Not all boring logs provided coordinates. Some only provided stationing (surveying term for location along a baseline from a prescribed origin) and could not be tied to geographic coordinates. A total of 2,516 borings are included in this data set. Surface elevations were obtained from the borehole logs. An uncertainty of 0.6 meters was assigned as a geologist or engineer was assumed to be present during drilling operations. Additional fields in this data set include whether or not a boring layout plan was included with the borehole log and any additional comments such as bridge name, route number, road name, name of the water body the bridge is crossing and bridge ID for bridges in adjoining towns (in instances where a bridge crosses from one town to another).

Sheet 21 – MassDOT_Borings_Pre1996: In the 1990's Professor Rudi Hon and students at Boston College digitized the locations of borings and scanned borehole logs for MassDOT highway and bridge projects conducted prior to 1996. The Boston College team digitized thousands of borehole locations. The borings were entered into a database at the Massachusetts Water Resources Authority called G-base. Unfortunately, unique locations were not provided for each individual boring. Sometimes up to 30 borings were placed at the same geographic location. Accordingly, highway borings could not be included in this study because the locations were uncertain. The same problem occurred for bridge borings; several borings were located at the same geographic location. However, because bridges occupy a smaller spatial footprint, the depths to bedrock recorded in the boreholes at each bridge were averaged. If some of the boreholes did not reach bedrock, the deepest boring was selected and retained in the data set. Once this exercise was completed, a second problem emerged. Many borings were assigned to the incorrect bridge and some boreholes were several miles from their assigned bridge. MGS manually moved each borehole to the correct bridge. For consistency the borehole was placed at the bridge abutment by the edge of the roadway. As a result, there is uncertainty in the location of the borehole which produces greater uncertainty in the depth measurement. For example, the boring may have been constructed near the underpass rather than up near the bridge deck resulting in significant differences in the surface elevation of the borehole. For these reasons an uncertainty of 3 meters was adopted for this data set. There are 1,942 records in this data set. Surface elevations were extracted from the 1-meter resolution LiDAR DEM. Additional fields in this data set include original surface elevation (feet) of the borehole (even though the surface elevation was provided in the source data this information was not used because the datum was not available nor was the location known precisely), and depth to bedrock or minimum depth to bedrock in the case of overburden wells.

Sheet 22 – MassDOT_Seismic_Data: Between 1957 and 1972, MassDOT conducted numerous seismic refraction surveys along many of Massachusetts' transportation corridors. The purpose of these surveys was to determine if rock excavations were needed along proposed roadway cuts. Peter Connors, Massachusetts State Geotechnical Engineer with MassDOT discovered two banker's boxes filled with these old seismic survey reports. MGS scanned and georeferenced all the maps and digitized the shot points. Altitudes of the bedrock surface were interpolated from the seismic survey profiles and entered into the

ArcGIS attribute table. Surface elevations were not available in the reports so surface elevations were extracted from the 1-meter resolution LiDAR DEM. Unfortunately, subtracting bedrock altitudes determined decades ago from current day surface topography often leads to negative depths to bedrock because the excavations and rock cuts are now complete. In cases where the depth to bedrock was negative (meaning the bedrock in the past was somewhere above present-day topography) the altitude of the bedrock was assigned the present-day surface elevation. This data set contains 1,292 records. An uncertainty of 0.6 meters was assigned if the depth to bedrock was less than 6 meters or 10% of the total depth if the depth to bedrock was greater than 6 meters. Additional fields in the data set include estimated altitude of the bedrock before excavation, seismic line ID, contract number, if known, date of the seismic survey, name of the seismic survey report and shot point ID.

Sheet 23 – MWRA_Borings_Pre2015: This data set contains 8,301 borings from various Massachusetts Water Resources Authority (MWRA) projects. It was exported from G-base and provided to MGS by John Nelson on December 3, 2018. The data set contains project borings completed by 2014. Surface elevations were extracted from the 1-meter resolution LiDAR DEM and an uncertainty of 0.6 meters was assigned to the data set because it was assumed a geologist or engineer was on site during drilling operations. Additional fields in the data set include Northing and Easting in feet, original horizontal datum, and depth to bedrock, depth to refusal or total depth, all in feet.

Sheet 24 – NWIS_Borings: This data set contains 16,232 records representing 13,221 unique boreholes. Some of the borings have stratigraphic information resulting in duplicate Site IDs for those wells (i.e., one boring site ID might have two or more records, one record for each lithologic unit). A PlotFlag field is provided with this data set to facilitate plotting in ArcGIS and avoid duplicate labeling of individual wells. This data set comes from the National Water Information System (NWIS) database and was provided by Laura Medalie (USGS) to the Massachusetts Geological Survey (MGS) on January 21, 2021. It is assumed that most of the data in this data set comes from well drillers. Well drillers typically embed the casing into the bedrock on average 5 meters (15 feet) or more depending on the degree of weathering or fracturing. It is unclear whether the driller noted the top of the bedrock as the point of first encounter while drilling or the depth to competent bedrock (depth of casing). Accordingly, an uncertainty of 5 meters was assigned to this data set. Surface elevations for this data set were extracted from the 1-meter resolution LiDAR DEM. Other fields provided in this data set include original coordinate method code, original coordinate accuracy code, original horizontal datum (NAD27), type of site code, well depth in feet, hole depth (hole depth is the depth the hole was drilled and well depth is the depth to which the well was set; they are not always the same) in feet, aquifer code, geologic sequence number, lithology code, depth to the top of a geologic material interval (feet), depth to the bottom of a geologic material interval (feet), lithologic unit code, lithologic description (when available), contributing unit code, notes and yield (gallons per minute), when available. All codes are defined in the metadata.

Sheet 25 – USGS_Offshore_Seismic: During the 1960's the USGS conducted numerous cruises in the offshore waters of Massachusetts to collect seismic reflection data. Recently, Janet Stone (USGS, retired) and Ralph Lewis (former state geologist of Connecticut)

reinterpreted the analog seismic reflection data for the new Massachusetts statewide Quaternary Geologic Map currently in preparation. Part of that interpretation included an estimate of altitude of the crystalline bedrock below the Quaternary and Holocene sediment packages. Janet Stone provided this data to MGS on December 7, 2021. This data set contains 355 points that provide the altitude of the bedrock surface and 7 points where the bedrock is undefined. Since the depth to bedrock below the seabed is not known (denoted by N/A) the normal rules for assigning uncertainty cannot be applied. In this case, an arbitrary uncertainty of 10 meters was ascribed to this data set. No surface elevations were determined for these records (denoted by N/A). Additional fields in this data set include original altitude in meters (NGVD29) and any additional comments.

Sheet 26 – Oldale_CC_1962_Seismic: This data set was collected and published by Oldale and Tuttle (1962). It consists of seismic refraction surveys conducted on outer Cape Cod. The data set contains 18 records. Maps from this publication were georeferenced in ArcGIS and shot points were digitized. Depths to bedrock were read directly from the data table and entered into the attribute table in ArcGIS. Surface elevations were taken from the data table in the publication. Uncertainty was assigned using 0.6 meters for estimated depths to bedrock of less than 6 m or 10% of the total depth for estimated depths to bedrock greater than 6 meters. Additional fields in the data set include shot point ID, Traverse ID, brief description of the location of the seismic survey line, town in which the survey line was located and the date the seismic data were collected.

Sheet 27 – Oldale_CC_1965_Seismic: This data set consists of seismic refraction data and comes from two sources: Oldale, Tuttle and Currier (1962) and Oldale and Tuttle (1965). The data were collected primarily in the Harwich and Dennis quadrangles on Cape Cod. The map from Oldale and others (1962) was georeferenced in ArcGIS and shot points were digitized. Depth to bedrock, altitude of the bedrock surface and surface elevation of the shot point in feet, were extracted directly from the data tables in the publications and used to populate the attribute table in ArcGIS. A few shot points included in the Oldale and Tuttle (1965) come from Weston Geophysical, Inc, a consulting firm. The 1-meter resolution LiDAR DEM was used to determine shot point elevations for the seismic data from Weston Geophysical (Oldale and Tuttle, 1965). The data set contains 110 records. Uncertainty was assigned using 0.6 meters for estimated depths to bedrock of less than 6 m or 10% of the total depth for estimated depths to bedrock greater than 6 meters. Additional fields in the data set, if available, include report number, shot point ID, Traverse ID, street name, town in which the surveys were conducted, and date seismic data were collected.

Sheet 28 – Stone_SEMA_Borings_Seismic: This data set is a miscellaneous collection of seismic data and boreholes compiled from several publications (Gerhard and Phillips, 1989; Oldale and Tuttle, 1962; Oldale and others, 1962; Oldale and Tuttle, 1965; Hall and others, 1980) as well as other miscellaneous boreholes from the USGS. It also includes seismic refraction surveys collected on land by the USGS and reinterpreted by Janet Stone and Ralph Lewis for the new Massachusetts Quaternary Geologic Map. This data set was provided to MGS by Janet Stone on December 17, 2021, and only contains data not already included in other data sets. There are 37 records in this data set. Surface elevations from the original publications were used when available; otherwise the surface elevations were extracted from

the 1-meter resolution LiDAR DEM. Uncertainty was assigned using 0.6 meters for estimated depths to bedrock of less than 6 m or 10% of the total depth for estimated depths to bedrock greater than 6 meters.

Sheet 29 – SIR2019_5042_Borings: This data set consists of 1 record and comes from Hull and others (2019). It is a USGS well drilled in East Falmouth. The surface elevation was extracted from the 1-meter resolution statewide LiDAR DEM. An uncertainty of 0.6 meters was assigned to the data set because it was assumed a geologist or engineer was on site during drilling operations. Additional fields in the data set include surface elevation (feet), depth (feet) and town in which the borehole is located.

Sheet 30 – Well_Drillers_DB_Borings: The Massachusetts Department of Environmental Protection (MassDEP) maintains a well driller's well completion report database. Well drillers are required to submit a well completion report to the state for every well, exploratory hole, geothermal well or geotechnical boring drilled in Massachusetts. Each well is assigned a Well ID number. Currently there are over 200,000 records in the database. Records can be accessed through the Massachusetts Executive Office of Energy and Environmental Affairs (EEA) data portal: https://eeaonline.eea.state.ma.us/portal/#!/search/welldrilling. The SITE_ID in the data set contained in this report can be linked directly to the Well ID number in the EEA data portal allowing users to access pdfs of the well logs. For this report, data were downloaded from the EEA data portal on May 7, 2020 and submitted to Peter Grace at MassGIS for street and address verification. MassGIS returned 65,853 records with valid street addresses, or about a third of the total number of records. MassGIS location protocol sites the wells on the centroid of the structure on the parcel and provides a Northing and Easting coordinate. If more than one structure is located on a parcel the location protocol uses an inverse distance weighting based on the area of the footprint of each structure to determine the well's location on a parcel. If no structure appears on the parcel the well is placed on the centroid of the lot. Placing the well on the structure leads to uncertainty in the well location. Typically, the well is located near the structure but not on the structure. Accordingly, well locations may be off by 30 meters or more. Surface elevations were extracted from the 1-meter resolution statewide LiDAR DEM. Well drillers typically embed the casing into the bedrock on average 5 meters (15 feet) or more depending on the degree of weathering or fracturing. It is unclear whether the driller noted the top of the bedrock as the point of first encounter while drilling or the depth to competent bedrock (depth of casing). Accordingly, an uncertainty of 5 meters was assigned to this data set. Additional fields in the data set include the town in which the well is located, street number, street name, date well was completed, type of well, the type of work performed (new well, replacement, irrigation, etc.), total depth of the well (feet), depth to bedrock (feet; blank if overburden well), depth to the water table (feet), date of water level measurement (if available), master address point (concatenation of the Northing and Easting coordinate pair), and the master address ID (unique ID for a standardized address record generated by sequence). Some wells may be duplicated between the Well Driller and NWIS data sets. There are no street addresses with the NWIS data set, so it is difficult to identify duplicates with the Well Driller data set. For the time being, any duplicates have been retained in the master spreadsheet.

Sheet 31 – Hansen_WRI84_4106_Borings: In addition to seismic data, Hansen (1986) also included borehole data in his report. This data set consists of 2 records and only contains boreholes not included in any other data set. The map showing the location of boreholes was scanned from the report, georeferenced in ArcGIS and the boreholes digitized by MGS. Surface elevations were extracted from the 1-meter resolution statewide LiDAR DEM. An uncertainty of 0.6 meters was assigned. These boreholes are both highway borings and it is assumed that a geologist or engineer was present during drilling operations. Additional fields in the data set include total depth and depth to refusal, in feet.

Sheet 32 – WRIR03_4320_Borings: Garabedian and Stone (2004) conducted a ground water study in South Hadley, Massachusetts to delineate areas contributing water to the Dry Brook public-supply well. Part of that study included collecting borehole data to determine the depth to bedrock for ground water modeling purposes. Only those wells not already contained in other data sets are included here. This data set contains 30 records. Surface elevations were extracted from the 1-meter resolution statewide LiDAR DEM. Many of the wells are exploratory holes drilled by the Holyoke Power Company, Town of Hadley or the South Hadley Fire District. These wells are assigned an uncertainty of 0.6 meters because it is assumed a geologist or engineer was on site during drilling operations. Two records are domestic wells drilled by water well drillers. These wells are assigned an uncertainty of 5 meters as described in the Well Drillers data set. Additional fields in the data set include date well was drilled, yield (gallons per minute), total depth (feet) and depth to bedrock (feet).

Sheet 33 – Hager_Geophysical_Data: MGS in cooperation with GISmatters, Inc. and Hager Geoscience, Inc. prepared a preliminary National Earthquake Hazards Reduction Program (NEHRP) soil classification map of Massachusetts in 2017 (Mabee and Duncan, 2017). The work was done on behalf of the Massachusetts Emergency Management Agency and Federal Emergency Management Agency. The purpose of this project was to reclassify the NEHRP soil categories across the state to improve the estimates of damage and losses for different earthquake scenarios. Part of this work involved collecting shear wave velocity data at different locations using various seismic survey techniques (seismic refraction and multi-analysis of surface waves). One outcome of this work was an estimate of the depth to bedrock. Hager Geoscience, Inc. collected the seismic survey data in 2016. Methods are described in Mabee and Duncan (2017). This data set contains 8 records. The endpoints of each seismic survey line were digitized, and the attribute table populated in ArcGIS. Depth to bedrock was determined from the seismic survey profiles. Surface elevations were extracted from the 1-meter resolution statewide LiDAR DEM. Uncertainty was assigned using 0.6 meters for estimated depths to bedrock of less than 6 m or 10% of the total depth for estimated depths to bedrock greater than 6 meters.

References Cited

Campbell, K.J. and J.H. Hartshorn, 1980, Surficial geologic map of the Northfield quadrangle, Massachusetts, New Hampshire and Vermont. U.S. Geological Survey Geologic Quadrangle Map GQ-1440, 1:24,000 scale.

Chute, N.E., 1965, Geologic map of the Duxbury quadrangle, Plymouth County, Massachusetts. U.S. Geological Survey Geologic Quadrangle Map GQ-466, 1:24,000 scale.

Fairchild, G.M., J.W. Lane, E.B. Voytek and D.R. LeBlanc, 2013, Bedrock topography of western Cape Cod, Massachusetts, based on bedrock altitudes from geologic borings and analysis of ambient seismic noise by the horizontal-to-vertical spectral-ratio method. U.S. Geological Survey Scientific Investigations Map 3233, 22-page report, map, data tables.

Garabedian, S.P. and J.R. Stone, 2004, Delineation of Areas Contributing Water to the Dry Brook Public-Supply Well, South Hadley, Massachusetts: U.S. Geological Survey Water-Resources Investigations Report 03-4320, 56 p.

Gerhard, L.W. and J.D. Phillips, 1989, New drill cores in crystalline bedrock on southeastern Cape Cod, Massachusetts [abs.]: Geological Society of America, Northeastern Section, 24th Annual Meeting: abstracts with programs, v. 21, no. 2, p. 28.

Hall, R.E, L.J. Poppe and W.M. Ferrebee, 1980, A stratigraphic test well, Martha's Vineyard, Massachusetts. U.S. Geological Survey Bulletin 1488, 19p.

Hansen, B.P., 1986, Exploration for areas suitable for ground-water development, central Connecticut Valley lowlands, Massachusetts. Water-Resources Investigations Report 84-4106, 41-page report, map.

Hartshorn, J.H., 1967, Geology of the Taunton quadrangle, Bristol and Plymouth Counties, Massachusetts. U.S. Geological Survey Bulletin 1163-D, 71-page report, map.

Hartshorn, J.H. and C. Koteff, 1967, Geologic map of the Springfield South quadrangle, Hampden County, Massachusetts and Hartford and Tolland Counties, Connecticut. U.S. Geological Survey Geologic Quadrangle Map GQ-678, 5-page report, map, 1:24,000 scale.

Hildreth, C.T. and R.B. Colton, 1982, Surficial geologic map of the Hampden quadrangle, Massachusetts and Connecticut. U.S. Geological Survey Geologic Quadrangle Map GQ-1544, 1:24,000 scale.

Holmes, G.W. and W.S. Newman, 1971, Surficial geologic map of the Ashley Falls quadrangle, Massachusetts-Connecticut. U.S. Geological Survey Geologic Quadrangle Map GQ-936, 1:24,000 scale.

Koteff, C and B.D. Stone, 1990, Surficial geologic map of the Townsend quadrangle, Middlesex and Worcester Counties, Massachusetts and Hillsborough County, New Hampshire. U.S. Geological Survey Geologic Quadrangle Map GQ-1677, 1:24,000 scale.

Mabee, S.B. and C.C. Duncan, 2017, Preliminary NEHRP soil classification map of Massachusetts. Prepared for the Massachusetts Emergency Management Agency and Federal Emergency Management Agency, 232 p.

Nelson, A.E., 1974, Surficial geologic map of the Natick quadrangle, Middlesex and Norfolk Counties, Massachusetts. U.S. Geological Survey Geologic Quadrangle Map GQ-1151, 1:24,000 scale.

Oldale, R.N. and C.R. Tuttle, 1962, Preliminary report on the seismic investigations in the Orleans, Wellfleet, North Truro and Provincetown quadrangles, Massachusetts. U.S. Geological Survey Open-File Report 62-95, 1 plate.

Oldale, R.N. and C.R. Tuttle, 1965, Seismic investigations in the Harwich and Dennis quadrangles, Cape Cod, Massachusetts. U.S. Geological Survey Professional Paper 525-D., pp. D101-D105.

Oldale, R.N., 1985, Geologic map of Nantucket and nearby islands, Massachusetts. U.S. Geological Survey Miscellaneous Investigation Series Map I-1580, 48,000 scale.

Oldale, R.N., C.R. Tuttle and L.W. Currier, 1962, Preliminary report on the seismic investigations in the Harwich and Dennis quadrangles, Massachusetts. U.S. Geological Survey Open-File Report 62-96, 1 plate.

Pomeroy, J.S., 1977, Surficial geologic map of the Warren quadrangle, Worcester, Hampden and Hampshire Counties, Massachusetts. U.S. Geological Survey Geologic Quadrangle Map GQ-1357, 1:24,000 scale.

Stone, J.R., B.D. Stone, M.L. DiGiacomo-Cohen, and S.B. Mabee, comps., 2018, Surficial materials of Massachusetts - A 1:24,000-scale geologic map database: U.S. Geological Survey Scientific Investigations Map 3402, 189 sheets, scale 1:24,000; index map, scale 1:250,000; 58-p. pamphlet; and geodatabase files, https://doi.org/10.3133/sim3402.

Stone, B.D., 1980, Surficial geologic map of the Worcester North quadrangle and part of the Paxton quadrangle, Worcester County, Massachusetts. U.S. Geological Survey Miscellaneous Investigation Series Map I-1158, 1:24,000 scale.

Yilar, E., L.G. Baise and J.E. Ebel, 2017, Using H/V measurements to determine depth to bedrock and Vs_{30} in Boston, Massachusetts. Engineering Geology, v. 217, pp. 12-22.

This page left blank intentionally.

7.2 Appendix B: HVSR – Simple Theory to Finding Depth to Bedrock

HVSR — Simple Theory to Finding the Depth-To-Bedrock
William P. Clement
June 23, 2023

We are developing calibration curves for the HVSR so that we can extend from locations where we computed our curves to areas of similar sediment/geology type. We measure ambient seismic vibrations at places where we know the depth to bedrock. The curves are developed from plots of frequency (f) versus thickness (z). The data points are fitted with a power law of the form,

$$z = af_0^b. \qquad (1)$$

Here, z is the (known) thickness of the overlying sedimentary layer and f0 is the (measured) fundamental resonance frequency. a and b are determined by the regression fit to the data, so a and b are site-specific. If we can find these parameters for a number of different sediment/geology types, we can then use the appropriate parameters for areas where we do not have known sediment thickness. If we wanted, we could "backout" the shear velocity from our 2-parameter formula.

To see how the shear velocity enters the calculation, we assume a power law fit to the thickness-depth plot. The assumption for the power law is that the velocity increases with depth in the sediments as (Ibs-von Seht and Wohlenberg, 1999).

$$v_s(z) \approx v_0(1+z)^x, \qquad (2)$$

where vs is shear velocity, v0 is the surface shear velocity, z is the thickness as before, and x is the exponent of the power law.

In general, the frequency of the seismic wave is related to its velocity divided by its wavelength.

$$f = \frac{v_s}{\lambda}, \qquad (3)$$

where λ is the wavelength of the seismic wave. For the fundamental resonance frequency, a well-accepted relation is that the resonance frequency responds to 1/4 wavelength (Rial, 1989). We now have,

$$f_0 = \frac{v_s}{4z} \qquad (4)$$

which leads to,

$$z = \frac{v_s}{4f_0}. \qquad (5)$$

To develop a power law relationship between thickness and frequency, we follow the development in Delgado et al. (2000). Delgado et al. (2000) start with an equation for the shear modulus.

$$G = \frac{(c_2 - p_1)^{c_3}}{1+p_1}(p_2)^{c_4}\left[(\rho - \rho_w)gz\left(\frac{1+2p_3}{3}\right)\right]^{c_5}. \qquad (6)$$

Here, G is the shear modulus of the soil, z is the soil thickness, ρ is the soil density, ρ_w is the water density, g is the acceleration due to gravity, (c_1 to c_5) are constants and (p_1 to p_3) are geotechnical parameters. If these parameters are constant in the soil, then the only variation is with z. We can collect all the constants into one term η and rename the exponent τ to get,

$$G = \eta z^{\tau}. \qquad (7)$$

From seismology, the shear velocity is related to the shear modulus and the density as $v_s = \sqrt{(G/\rho)}$. In our case, we treat ρ as constant.

To derive a formula for shear velocity, we start by squaring both sides of the equation for shear velocity and move G to one side to get,

$$v_s^2 = \frac{G}{\rho} \Rightarrow G = v_s^2\rho. \qquad (8)$$

Substitute equation 8 into 7 to get.

$$v_s^2\rho = \eta z^{\tau}. \qquad (9)$$

Now, let's rearrange and simplify equation 9.

$$v_s^2\rho = \eta z^{\tau}. \qquad (10)$$

$$v_s^2 = \frac{\eta}{\rho}z^{\tau}\tau. \qquad (11)$$

$$v_s = \left(\frac{\eta}{\rho}z^{\tau}\right)^{\frac{1}{2}}. \qquad (12)$$

$$v_s = \left(\frac{\eta}{\rho}\right)^{\frac{1}{2}} z^{\frac{\tau}{2}}. \qquad (13)$$

Now, we rename the coefficient of the z term α and the exponent β to get a power law for the shear velocity.

$$v_s = \alpha z^{\beta}. \qquad (14)$$

Plugging equation 14 into equation 4 we get,

$$f_0 = \frac{v_s}{4z} = \frac{\alpha z^{\beta}}{4z} = \frac{\alpha}{4} z^{\beta-1}. \quad (15)$$

Substitute c for the coefficient of the z-term to get,

$$f_0 = cz^{(\beta-1)} = cz^{-(1-\beta)}. \quad (16)$$

Rearranging to solve for z gives,

$$cz^{-(1-\beta)} = f_0 \quad (17)$$

$$z^{-(1-\beta)} = \frac{f_0}{c} \quad (18)$$

$$z = \left(\frac{f_0}{c}\right)^{-\frac{1}{(1-\beta)}} \quad (19)$$

$$z = \left(\frac{1}{c}\right)^{-\frac{1}{(1-\beta)}} f_0^{-\frac{1}{(1-\beta)}} \quad (20)$$

$$z = (c^{-1})^{-\frac{1}{(1-\beta)}} f_0^{-\frac{1}{(1-\beta)}} \quad (21)$$

$$z = c^{\left(\frac{1}{(1-\beta)}\right)} f_0^{-\frac{1}{(1-\beta)}} \quad (22)$$

$$z = a f_0^{b}, \quad (23)$$

where $a = c^{\left(\frac{1}{1-\beta}\right)}$ and $b = -\frac{1}{1-\beta}$. In this case, b is negative (f_0 is in the denominator).

References

J. Delgado, C. López Casado, J. Giner, A. Estévez, A. Cuenca, and S. Molina. Microtremors as a geophysical exploration tool: Applications and limitations. Pure and Applied Geophysics, 157: 1445–1462, 2000.

M. Ibs-von Seht and J. Wohlenberg. Microtremor measurements used to map thickness of soft sediments. Bulletin of the Seismological Society of America, 88(1):250–259, 1999.

J. A. Rial. Seismic wave resonances in 3-D sedimentary basins. Geophysical Journal International, 99:81 – 90, 1989.

This page left blank intentionally.

7.3 Appendix C: Data Processing Steps

Overview

This Appendix presents the complete details of the data processing beginning with the Master Spreadsheet and resulting in the bedrock altitude, depth, and uncertainty deliverables, with the focus on the nuts and bolts of process—tools used, settings, parameters, map algebra, etc. Some of these steps were included in the main body of this report in Sections 2.5 through 2.7 but are repeated here for completeness. We omit general discussions of approaches considered, evaluation and testing, rationales and results, and so on—for these please refer to Sections 2.5 through 2.8 of the main report.

Data Processing Software

Except where otherwise noted, all processing was performed using ESRI ArcGIS Desktop version 10.8.1, including all available extensions and tools (e.g., Spatial Analyst, Geostatistical Analyst, etc).

Preparation of Reference Data

The project makes frequent use of various reference datasets in addition to the well data; some of these have already been mentioned above. Here we provide details on the processing of these reference data to prepare them for use with the well data analysis.

Coordinate System

For internal consistency and compatibility with other data products, all data used in the project were processed using the NAD 1983 Massachusetts State Plane Mainland FIPS 2001 coordinate system (ESRI:NAD_1983_StatePlane_Massachusetts_Mainland_FIPS_2001, European Petroleum Survey Group:26986). Any data obtained that were not already in this coordinate system were re-projected to it before use.

100-meter Reference Raster

To ensure consistent handling of all input and proxy data, especially with respect to correct co-registration of all location data, we defined a statewide master 100 meter reference grid using the ArcToolbox "Create Constant Raster" tool with a constant value of zero (0), an integer data type, an output cell size of 100, and an output extent of 30,000..340,000 eastings and 770,000..970,000 northings; we used the Environments... settings to specify the Massachusetts State Plane coordinate system.

These settings created a reference raster that is 310 x 200 km in size, with 3100 x 2000 cells, and a cell size of 100 x 100 meters. This raster was then used via the Environments... settings for all further raster computations as the "snap" raster (which determines the origin point for newly-created rasters), the "processing extent" dataset (which determines the spatial extent of new rasters), and the "output coordinates" reference, ensuring that all new rasters would co-register perfectly with each other. Figure 7.1 shows this reference grid along with the state

land mask grid (described next) on top of it to indicate the full extent of the reference grid with respect to the state boundaries—it extends 5-10km beyond the state boundaries.

100-meter State Land Raster Mask

To limit model results to the state boundaries, we created a state land mask raster grid using the ArcToolbox "Polygon To Raster" tool to convert the MassGIS towns polygons to a 100-meter raster with a value of one (1) for all cells within town polygons and null (nodata) everywhere else. The value was obtained by first adding a "MASK" field to the towns polygon layer and assigning this field a value of one (1) for all towns; this MASK field was then used as the raster value source field in the conversion tool.

This new raster state land mask was used throughout the project in the ArcToolbox "Raster Calculator" for masking model outputs: each raster requiring masking was multiplied by the state land mask to get a copy but with values limited to cells within the state's land surface areas (areas where the mask value is 1 are copied to the new raster; values where the mask is null (nodata) are set to null in the new raster). Figure 7.1 shows this land mask grid in green on top of the project 100-meter reference grid.

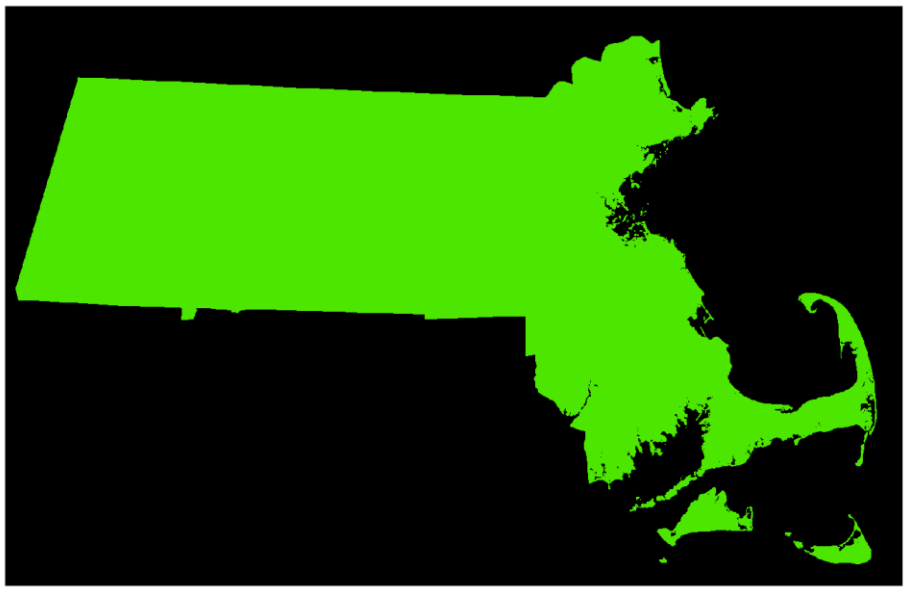

Figure 7.1: The area covered by the reference grid (black) and state land mask (green)

100-meter State Land Polygons

We created a polygon version of the 100-meter state land raster mask in a three-step process (because a direct conversion of individual cells to distinct polygons is not possible unless every raster cell has a unique value, which the land mask does not). Although ESRI has a different three-step process they recommend for this, it seems to reference tools that no longer operate as they once did when the process was documented; in any case, the approach we use here is equally effective and much faster:

First, we generate a grid of random, floating-point values for every cell of the reference grid using the ArcToolbox "Create Random Raster" tool.

Next, we convert these unique floating-point values to unique integers and mask them to the state land cells using the ArcToolbox "Raster Calculator" with an expression like this: Int("rand100m.tif" * 100000000 * "malandmask.tif").

Finally, we generate polygons for these unique masked random values using the ArcToolbox "Raster To Polygon" tool with the "simplify" option disabled to ensure that all the polygon edges conform exactly to raster cell boundaries.

The resulting shapefile contains roughly 2.1 million polygons of 100x100 meters, corresponding to the ~21,000 square kilometers of land surface area in the state. Figure 7.2 shows a portion of the polygon grid overlaid on the state land mask.

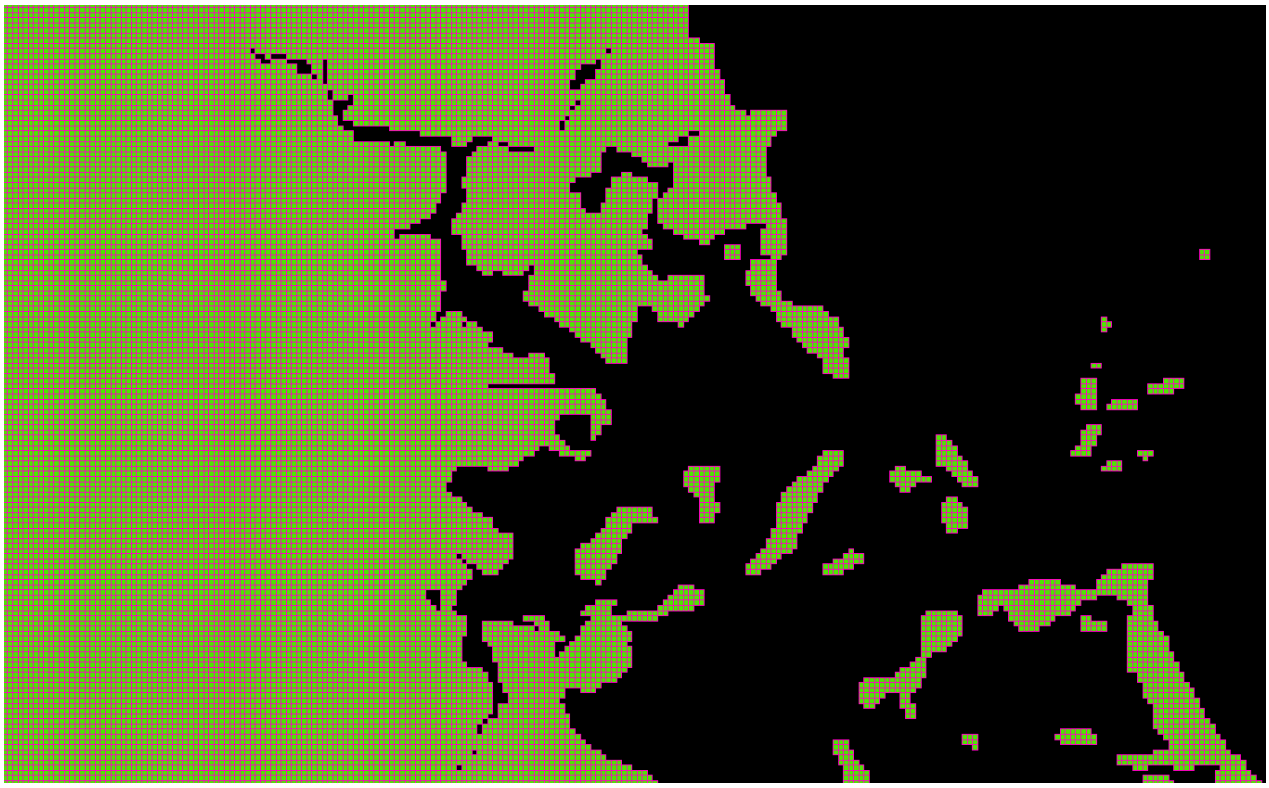

Figure 7.2: Gridlines of the 100-meter raster grid cell boundaries

100-meter Topography

To obtain a topography raster on our 100-meter reference grid we used the latest statewide 1-meter LiDAR raster and the ArcToolbox "Zonal Statistics" tool. We use the feature ID (FID) field of the polygon grid generated in the previous step as the source of the zone data—each 100x100-meter polygon has a unique FID and so will be treated as a unique zone in which to compute LiDAR statistics. The 1-meter LiDAR is used as the input value raster, and we

select MEAN as the statistic type. This generates a 100-meter raster in which each cell's value is the mean elevation of the 1-meter LiDAR elevations within it.

The surfaces of lakes, ponds, and reservoirs in the LiDAR dataset are assigned constant elevation values. In most cases these features are small enough that the effect of using the water surface instead of the lake-bed elevation is negligible. In the case of the Quabbin Reservoir, however, the surface area is quite large, and moreover, well data is virtually absent throughout the region. To obtain a more useful constraint on bedrock altitudes in this region, we rasterized MassGIS bathymetry contours of the Quabbin using the ArcToolbox "Topo To Raster" tool. We substituted this 100-meter Quabbin bathymetry raster for the LiDAR cells for all the constant water-surface cells of the LiDAR-based raster and designated the resulting topography as TOPO100 for later reference (Figure 7.3).

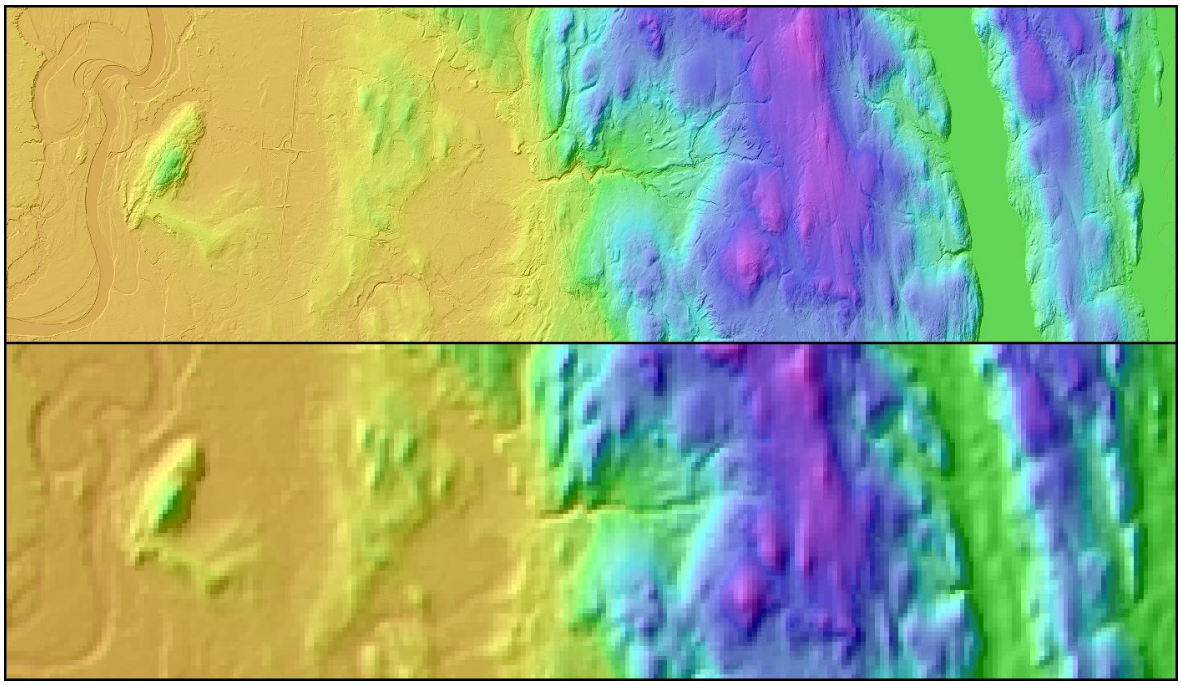

Figure 7.3: Original LiDAR 1-meter resolution data (top) and mean elevation at 100-meter resolution (bottom). The flat surfaces on the right side of the top image is part of the Quabbin Reservoir, which have been filled in the bottom image with gridded bathymetry data for the reservoir.

Preparation of Surficial Geology Proxy Data

As discussed previously, we use two units (data layers) from the digital version of the Surficial Materials of Massachusetts 1:24,000 Map to generate proxy depth-to-bedrock values to supplement the well data: bedrock outcrops (*bk*) and the shallow to bedrock regions (*sb*).

Bedrock Outcrops (bk)

The *bk* polygons of the map indicate the extent of observed bedrock outcrops. To convert these to point values with bedrock altitude and depth-to-bedrock values, the following steps

were performed to create point data for each polygon or portion of a polygon within each 100-meter grid cell:

1. The *bk* polygons were split along the 100-meter gridlines using the ArcToolbox "Intersect" tool (although many of these small polygons were not intersected by any of the lines and were simply copied across to the new polygon output layer) (Figure 7.4).

2. The ArcToolbox "Add Geometry Attributes" tool was used to add CENTROID_X and CENTROID_Y attributes to the polygon attribute table, containing the computed area centroid for each polygon.

3. Three attributes were manually added to the polygon layer's attribute table: ALT for the polygon's (mean) altitude; DTB for the depth to bedrock; and UNC for uncertainty.

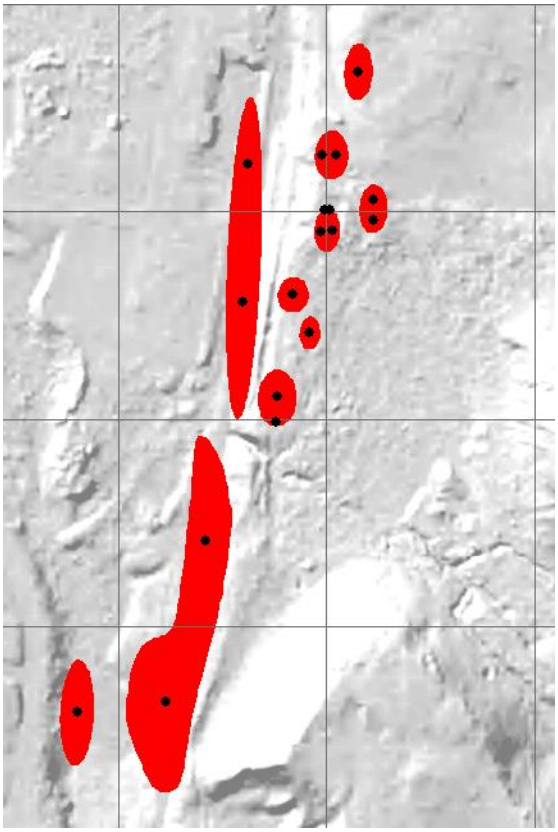

Figure 7.4: Bedock polygons (red areas) split along the 100-meter grid cell boundaries (light gray lines); each (new) polygon is converted to a point located at it's centroid (black dots) and assigned a depth (DTB) value of zero meters and an altitude (ALT) value of the (mean) 1-meter LiDAR values in the polygon.

4. Mean elevations for these new *bk* polygons were computed by running the ArcToolbox "Zonal Statistics As Table" with the polygons as zones and the 1-meter LiDAR raster as values.

5. To get these mean elevations from the table back into the polygon layer, we joined the zonal statistics table to the polygon features by FID, and used the Field Calculator to set the ALT field to the MEAN value column in the joined zonal statistics table.

6. The DTB field was assigned zero (0) for all features.

7. The UNC field was assigned a value of 0.3 meters for all features.

There were some *bk* polygons too small to be given a value by the Zonal Statistics tool; these were identified by the absence of assigned ALT values from step 5. To get altitudes for these points, we exported the attribute table for these selected records, then converted the table to XY data using the CENTROID_X and CENTROID_Y fields to get a point shapefile; the ArcToolbox "Extract Multi Values To Points" was run to add a LIDARALT attribute to the point shapefile populated with the 1-meter LiDAR altitude value for each point; these LIDARALT values were then assigned back to ALT field of the too-small *bk* polygons by joining on the feature IDs of the polygons and the points.

At the end of this processing the 65,409 original *bk* polygons had been split into 111,495 smaller *bk* polygons, each with a mean (or, for small ones, point) LiDAR value assigned as the ALT attribute, zero assigned to the DTB attribute, 0.3 meters for all UNC values, and point locations in the CENTROID_X and CENTROID_Y attributes. These were added to the well data spreadsheet with SITE_UIDs ranging from 200,000 to 311,494 and a DATASET attribute of "bk".

Abundant Outcrops and Shallow Bedrock (sb)

The *sb* polygons of the map indicate regions of abundant bedrock outcrops and/or shallow bedrock (defined as less than 10 feet or 3.5 meters). To convert these to point values with bedrock altitude and depth-to-bedrock values, a procedure similar to that used for *bk* polygons was used, but with additional steps to remove any *bk* polygons inside of *sb* polygons and use of a hillslope and curvature model for soil thickness to compute variable DTB values for each polygon.

Slope-Curvature Soil Thickness (Depth-to-Bedrock) Model and Processing

The model we use distinguishes between ridge crests (regions of positive topographic curvature with slopes less than 15%) where soil thicknesses are very thin (0.5 meters), and hillslopes (regions with neutral or negative curvature of any slope value) where soil thicknesses vary inversely with slope from 3.5 meters for the shallowest slopes (0-3%) down to 0.5 meters for the steepest slopes (35% and above). The specific rules and criteria we used are, in narrative form:

> if it's a ridgecrest (curvature is positive and slope is less than 15%): depth = 0.5 m;
> otherwise:
>
> > if slope is less than 3%: depth = 3.5 m;
> > else if slope is less than 8%: depth = 3.0 m;
> > else if slope is less than 15%: depth = 2.5 m;

else if slope is less than 25%: depth = 2.0 m;
else if slope is less than 35%: depth = 1.5 m;
else if slope is less than 50%: depth = 0.5 m;
else: depth = 0.0 m

To use these rules we need mean slope and curvature values for the 100-meter grid cells. Because the ArcGIS tools for computing topographic slope and curvature only use fixed 3x3-cell neighborhoods, we could use neither the 1-meter LiDAR (computing slopes and curvature over 3x3-meter areas) nor the 100-meter mean elevations (300x300-meter areas). With the 1-meter LiDAR data, the small 3x3-meter areas used, plus the presence of noise, vegetation, and development artifacts in the 1-meter LiDAR yielded 3x3 slope and curvature values that did not adequately capture meaningful hillslope and topographic curvature. With the 100-meter averaged LiDAR, the large 300x300-meter areas were too large and generalized to capture the landscape features underlying the slope-curvature soil model.

To obtain meaningful hillslope and curvature values, we turned to an intermediate-resolution topographic dataset, the National Elevation Dataset (NED) DEM at 1/3 arc-second resolution (roughly 7.5x10 meters at 42 degrees north latitude). We reprojected the NED data to a regular 7.5-meter grid for use as the input to slope and curvature functions; the 3x3 cells used in those functions gives a ~25-meter support basis that is a more appropriate size for measuring slope and curvature at a scale that will relate meaningfully to the hillslope processes affecting soil-depth.

The following steps detail the process of preparing the depth values according to this model:

1. Run ArcToolbox "Slope" on the 7.5-meter NED data, using the "percent rise" and "planar" output options to get a 7.5-meter slope raster (with slopes computed over 22.5x22.5-meter areas)

2. Run ArcToolbox "Curvature" on the 7.5-meter NED data to get a 7.5-meter curvature raster (with curvatures computed over 22.5x22.5-meter areas)

3. Use the ArcToolbox "Raster Calculator" to apply the slope-curvature soil-depth model to create a 7.5-meter raster of soil depths. Using "slp.tif" and "crv.tif" for the 7.5-meter slope and curvature rasters for brevity, the expression to compute is:

```
Con(("crv.tif" > 0) & ("slp.tif" < 15),
   0.5,
   Con("slp.tif" < 3,
      3.5,
      Con("slp.tif" < 8,
      3.0,
      Con("slp.tif" < 15,
         2.5,
         Con("slp.tif" < 25,
            2.0,
            Con("slp.tif" < 35,
               1.5,
               Con("slp.tif" < 50,
                  0.5,
                  0.0
                  )
               )
            )
         )
      )
   )
)
```

4. Use the ArcToolbox "Raster Calculator" to compute uncertainties for the 7.5-meter raster of soil depths where the uncertainty is assigned as 10% of the depth for depths >= 3 meters and 0.3 meters elsewhere—using "dtb.tif" as the 7.5-meter soil-depth raster for brevity, the expression to compute is:

```
Con(("dtb.tif" < 3),
   0.3,
   "dtb.tif" * 0.1
)
```

Converting shallow to bedrock (sb) polygons to point data

The following steps were performed to create point data for each *sb* polygon or portion of a polygon within each 100-meter grid cell:

1. The ArcToolbox "Erase" tool was used to remove all *bk* polygons from the *sb* polygons, since the *bk* polygons are handled separately (see previous section)

2. The *sb* polygons were split along the 100-meter gridlines using the ArcToolbox "Intersect" tool (although some of these small polygons were not intersected by any of the lines and were simply copied across to the new polygon output layer) (Figure 7.5).

3. The ArcToolbox "Add Geometry Attributes" tool was used to add CENTROID_X and CENTROID_Y attributes to the polygon attribute table, containing the computed area centroid for each polygon.

4. Four attributes were manually added to the polygon layer's attribute table: LIDAR for the polygon's (mean) LiDAR elevation; ALT for the polygon's (mean) altitude; DTB for the (mean) soil depth (depth to bedrock); and UNC for (mean) uncertainty.

5. Mean elevations for these new *sb* polygons were computed by running the ArcToolbox "Zonal Statistics As Table" with the polygons as zones and the 1-meter LiDAR raster as values for computing the mean.

6. To get these mean elevations from the table back into the polygon layer, we joined the zonal statistics table to the polygon features by FID, and used the Field Calculator to set the LIDAR field to the MEAN value column in the joined zonal statistics table.

7. Mean depth values for these new *sb* polygons were computed by running the ArcToolbox "Zonal Statistics As Table" with the polygons as zones and the 7.5-meter soil-depth raster as values to be averaged within each polygon.

8. Mean uncertainty values for these new *sb* polygons were computed by running the ArcToolbox "Zonal Statistics As Table" with the polygons as zones and the 7.5-meter uncertainty raster as values to be averaged within each polygon.

9. The shallow to bedrock polygon layer was joined to the depth and uncertainty zonal statistics tables and the Field Calculator used to set the DTB field in the polygon layer to the MEAN column of the depth statistics table and likewise the UNC field to the MEAN column of the uncertainty statistics table.

10. There were some shallow to bedrock polygons too small to be given values by the Zonal Statistics tool; these were identified by the absence of assigned LIDAR values from step 6. To get values for these points, the attribute table for these selected records was exported and converted to a point shapefile; the ArcToolbox "Extract Multi Values To Points" was run to extract the altitude for these small polygons from the 1 meter LiDAR data.

11. With all records populated with values from the rasters, the ALT field for each point was computed using the Field Calculator by subtracting the DTB field from the LiDAR field.

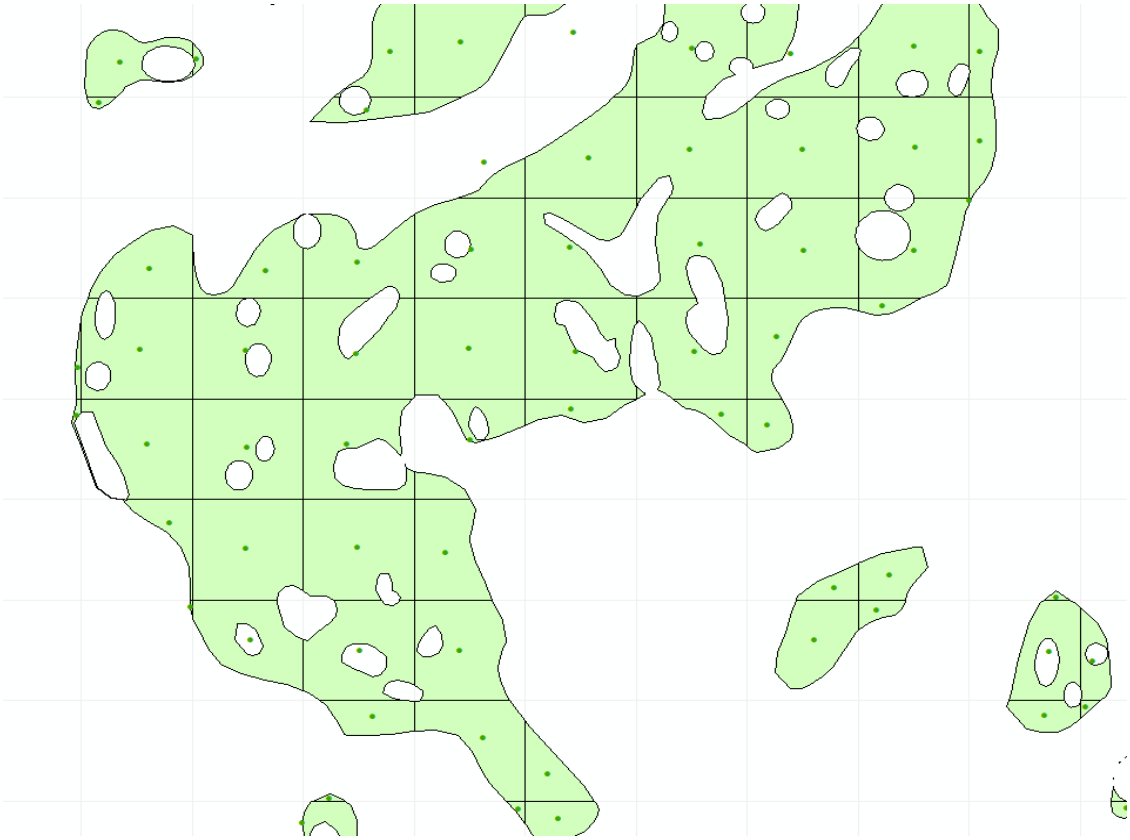

Figure 7.5: Shallow to bedrock polygons (shaded areas) split along the 100-meter grid cell boundaries (light gray lines), with bedrock polygons erased (holes in shaded areas); each (new) polygon is converted to a point located at it's centroid (dots) and assigned a depth to bedrock (DTB) value of zero meters and an altitude (ALT) value

At the end of this processing the 15,016 original shallow to bedrock polygons had been split into 492,120 smaller shallow to bedrock polygons, each with a mean (or, for small ones, point) LiDAR value, computed DTB, ALT, and UNC values, and point locations in the CENTROID_X and CENTROID_Y attributes. These were added to the well data spreadsheet with SITE_UIDs ranging from 400,000 to 892,119 and a DATASET attribute of "sb."

Final Preparation of Well, Bedrock Outcrops, and Shallow to Bedrock, Point Data

Some final steps were taken to prepare for ingestion into GIS before modeling the bedrock surface:

1. all *bk* and *sb* points are assigned a BOR_FLAG of "bedrock"

2. in the well data spreadsheet, some wells have a BOR_FLAG of "refusal"; since these are to be interpreted as bedrock wells, we change their BOR_FLAG to "bedrock" so there are only two point-types in the entire dataset: "bedrock" and "overburden"

3. the USGS_Offshore_Seismic records are missing some elevation-related values; set their SURF_EL_M and DB_MN_RF_M to zero (0)

4. the overburden well depths are a minimum constraint on bedrock depth—they did not reach bedrock, so bedrock depth is an unknown amount greater than the well depth. To make the use of these wells more effective in conditioning the bedrock depth, we use a depth value that is 5% larger than the recorded well depth (this may be a slight over-estimate of depth for a few wells, but is likely to be an underestimate for the vast majority of them). We add two new columns to the spreadsheet: USE_ALT_M and USE_DTB_M and compute them as follows:

```
    USE_ALT_M = IF(BOR_FLAG="bedrock", ALT_MX_M, SURF_EL_M - 1.05 * (SURF_EL_M - ALT_MX_M))
    USE_DTB_M = SURF_EL_M - USE_ALT_M
```

These two columns will be used for modeling bedrock altitude and depth, respectively. The oddly elaborate expression "(SURF_EL_M - ALT_MX_M)" instead of depth in the first calculation is to correctly handle offshore wells where we have no depth data; using this expression gives a correct altitude value for all cases (we exclude offshore wells for any depth-based modeling so the USE_DTB_M expression, which is not correct for offshore wells where there is no meaningful depth value, is irrelevant in those cases).

5. columns that will not be needed for modeling in GIS are removed to save on memory: SITE_ID, LATITUDE, LONGITUDE, HOR_DAT_M, VERT_DAT_M, DB_MN_RF_M, ALT_MX_M, SGUNIT, SGISSB

6. import the spreadsheet values into ArcMap, use the "Display as XY Data" option to render them as mappable points, and then export to a point shapefile *all_wells_and_sg.shp*.

7. delete distant offshore points—retain all the points within the Cape Cod Bay region, plus points within 5 kilometers of the Cape; delete all the points in the islands and in Nantucket Sound; save the remaining points to a point shapefile *wells_and_sg_mainland_ccb.shp*.

8. select by attributes BOR_FLAG = 'bedrock'—save selected points to a point shapefile *bedrock_wells_and_sg_mainland_ccb.shp*.

NB: performance is greatly enhanced by using file geodatabases; we saved copies of these working data shapefiles to a file geodatabase for more rapid processing and display

9. open attribute table for *wells_and_sg_mainland_ccb.shp* and export to *wells_and_sg_mainland_ccb.csv*

10. open *wells_and_sg_mainland_ccb.csv* in a spreadsheet program and make the following changes:

a) delete the OBJECTID column
b) add column K with heading CELL_N and compute its values as:
`=TRUNC(NORTHING_M/100) * 100 + 50`
c) add column L with heading CELL_E and compute its values as:
`=TRUNC(EASTING_M/100) * 100 + 50`
d) Copy, then Paste Special > Number all these computed values to convert the formulas to values
e) sort the whole spreadsheet by CELL_N (descending), CELL_E, SITE_UID
f) add column M with heading CELL_CNT and compute as:
`=IF(AND(K2=K1,L2=L1), M1+1, 1)`
(in words: *if this row's CELL_N and CELL_E are the same as the previous row's, add 1 to this column's value from the previous row, else restart from 1*)
g) add column N with heading OVB_CNT and compute as:
`=IF(G2="overburden", IF(M2=1, 1, N1+1), IF(M2=1, 0, N1))`
(in words: *if this row is an overburden well: if this is the first row for this cell, start initialize the overburden count to 1, else add 1 to the overburden count; if this row is NOT an overburden well: if this is the first row, then set the overburden count to zero, else keep the previous overburden count*)
h) add column O with heading OVB_CELL and compute as:
`=IF(AND(M3<=M2, N2=M2), 1, 0)`
(in words: *if this is the last row for a cell and if all the rows for this cell are overburden wells, set an "is an overburden-only cell" flag to 1 (true), else set the flag to zero (false))*
i) add column P with heading USE_OVB and compute as:
`=IF(M3<=M2, O2, P3)`
(in words: *if this is the last row for a cell, set the "use this overburden cell" flag to the cell's final "is an overburden-only cell" flag, else copy the "use this overburden cell" flag from the FOLLOWING row. In other words, propagate the "is overburden" flag to the "use overburden" flag for all rows that are overburden-only cells)*
j) Copy, then Paste Special > Number all these computed values to convert the formulas to values
k) turn on AutoFilter
l) filter for USE_OVB = 1
m) copy all rows of columns A through J, and Paste to a new spreadsheet
n) save new spreadsheet as *overburden_wells_in_overburden_only_cells.csv*

This new CSV table has all the well records for all overburden wells that are in 100-meter cells containing only other overburden wells—all cells containing any bedrock wells, bk, or sb points have been eliminated.

11. in ArcMap, import the file *overburden_wells_in_overburden_only_cells.csv*, use the "Display as XY Data" option to render them as mappable points, and then export to a point shapefile *overburden_wells_in_overburden_only_cells.shp*

The final point files to be used for the bedrock surface modeling exclude any data for the islands of Nantucket and Martha's Vineyard; there is insufficient data—no bedrock wells and no *bk* or *sb* occurrences—to successfully model these areas. Instead we use the bedrock contours from Oldale (1969) for the islands. We digitized those bedrock depth-below-sea-level contours, converted them to a 100m raster using the ArcToolbox "Topo to Raster" tool, masked them to the 100m state land mask, and converted them to bedrock altitudes by negating them in the "Raster Calculator". We designated his island bedrock altitude raster ISLANDALT for later reference.

Modeling the Bedrock Surface

Modeling of Bedrock Altitude

Modeling Bedrock Altitude with Overburden Constraints

We developed a bedrock altitude model using an iterative approach to incorporate useful overburden well data. We ran the EBK kriging first on the entire set of mainland bedrock well and surficial geology data (665,082 points). We then compared the resulting altitude model (ALT1) against all of the overburden wells in overburden-only cells (refer to previous discussion) and identified overburden wells whose USE_ALT_M attribute (105% of the well's reported maximum depth) was below the modeled bedrock surface—these are places where the overburden information is telling us that bedrock is deeper than the model predicted, even though we don't know exactly how deep. In contrast, we ignore overburden wells whose USE_ALT_M (a *maximum* bedrock altitude value constraint) is above the modeled altitude because these add no useful additional information about the bedrock surface (Figure 7.6).

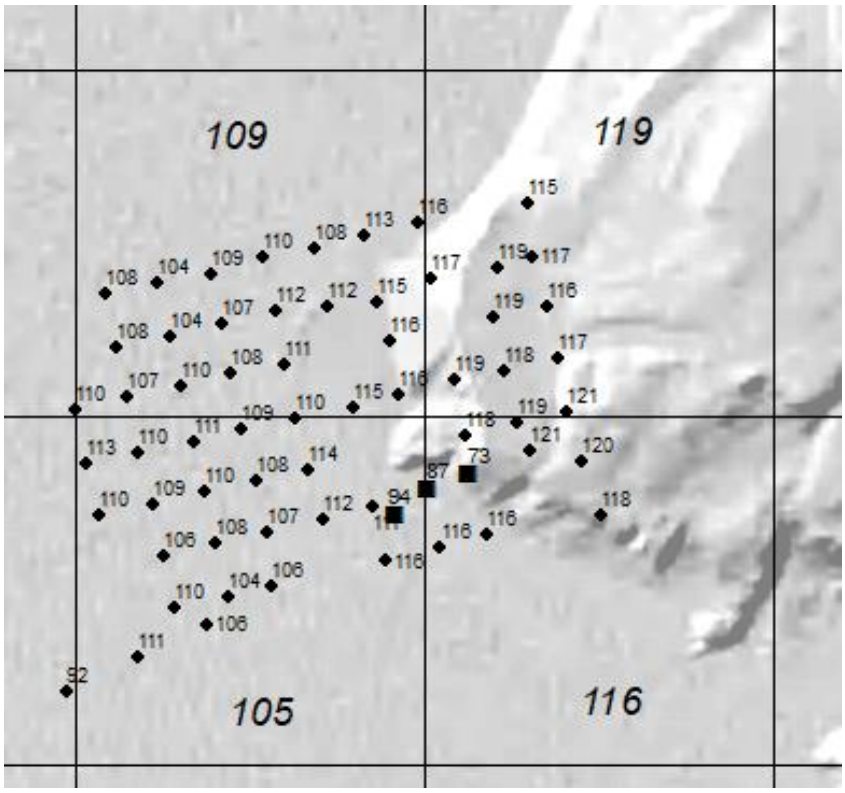

Figure 7.6: Bedrock wells (circles) and overburden wells (squares) with their altitude values displayed; black lines indicate raster cell boundaries, with the modeled bedrock altitude values posted in the cell (large italic lettering); background is LiDAR shaded-relief. These overburden wells were NOT included in the second round of altitude kriging because their maximum altitude values are already higher than the modeled bedrock altitude

We added these 13,566 selected overburden wells to the bedrock and surficial geology points and re-ran the EBK model; this creates a new surface (ALT2) with lower altitudes where we added the new overburden well constraints. We repeated the test of (remaining) overburden wells to find any new ones whose USE_ALT_M is below the new model surface and found an additional 188 wells.

Adding these 188 new overburden wells and performing a third EBK resulted in a model (ALT3) that honored all remaining overburden wells. We saved this altitude model and the associated kriging predicted standard errors (ALTERR) for further development.

Modeling Bedrock Depth

We ran the selected co-kriging process on the depth values of the same wells used for altitude modeling, then post-processed the result to set any negative depth values to zero to obtain the depth-based model designated DTB; we saved the associated kriging prediction standard errors as DTBERR. We then used this model to compute an equivalent altitude model designated DTBALT using the ArcToolbox "Raster Calculator" to subtract DTB values from TOPO100 values.

Blending Altitude and Depth Models

We first identified all the problem cells in the ALT3 model by comparing against TOPO100: we made a raster designated REPALT3 with values of one (1) wherever ALT3 > TOPO100. These cells need replacing with cells from the DTBALT model (Figure 7.7).

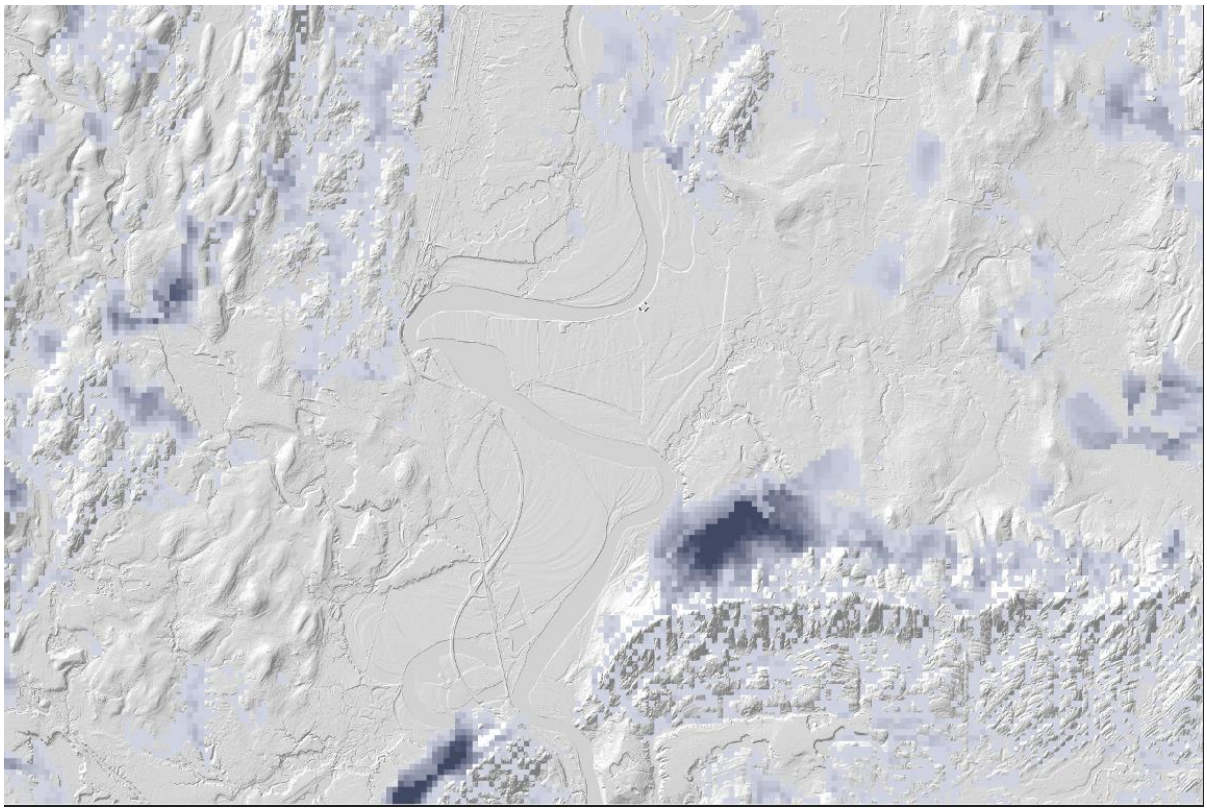

Figure 7.7: Shaded areas indicate places where ALT3 model of bedrock altitude is higher than TOPO100; darker shades indicate greater excess altitude

In order to avoid abrupt discontinuities at the substitution boundaries, we blended the ALT3 and DTBALT values in the 300-meter zone surrounding the replaced cells. To create the blending zone, we ran the ArcToolbox "Euclidean Distance" tool on the REPALT3 raster with a limiting distance of 300 meters; this yields a raster REPDIST with cell values of zero (0) over all the REPALT3 cells, surrounded by cells with values increasing up to 300 (meters); beyond that distance all cell values are null (nodata).

We convert REPDIST to a blending-factor raster BLENDFAC using the "Raster Calculator" with this expression: 1.0 - (REPDIST / 300.0), resulting in a value of 1.0 over all the cells to be completely replaced, grading down to zero (0.0) beyond 300 meters away (Figure 7.8).

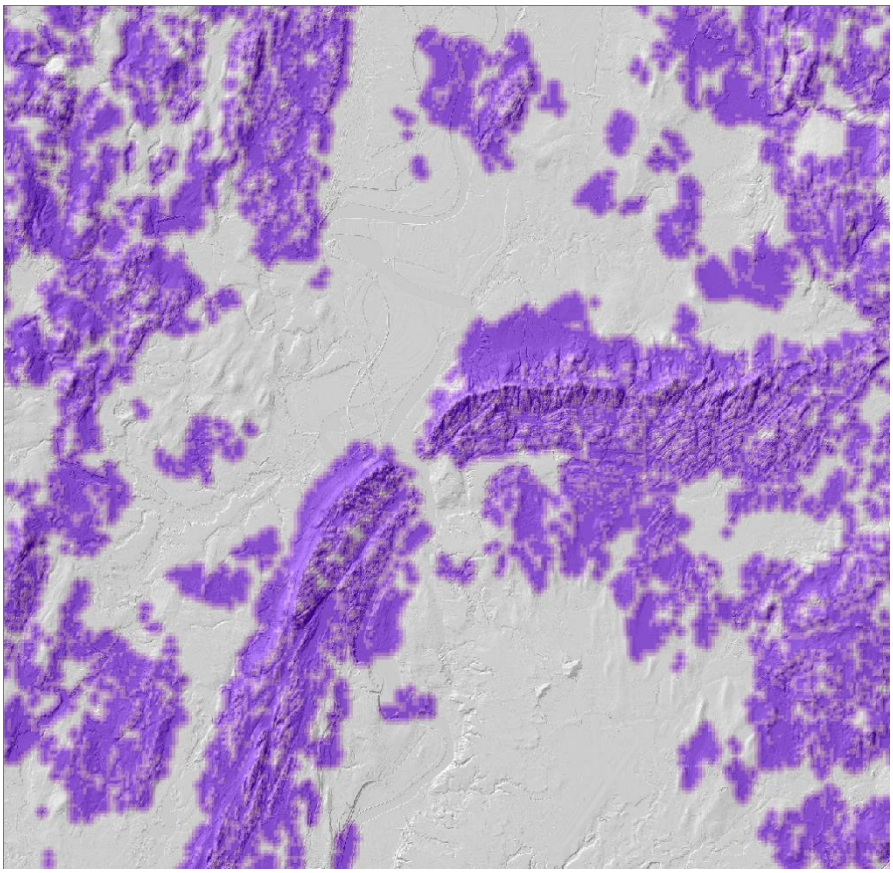

Figure 7.8: Purple cells indicate blending factor; darker shades indicate areas where the depth-based altitudes will be weighted more relative to the altitude-based cells

The "Raster Calculator" was used to do the actual blending with this nested conditional expression:

```
Con ( IsNull ( BLENDFAC ) ,
      ALT3,
      Con ( BLENDFAC < 1.0 ,
            ALT3 * ( 1.0 - BLENDFAC ) + DTBALT * BLENDFAC ,
            DTBALT
      )
)
```

In words, this says "outside the blend zone, just use the ALT3 model; inside the blend zone, wherever the blend factor is less than 1.0, compute a blended value of ALT3 and DTBALT, else just use DTBALT".

We designated the resulting blended raster as BLEND, and computed a companion blended prediction standard error raster BLENDERR using this similar "Raster Calculator" expresion:

```
Con ( IsNull ( BLENDFAC ) ,
      ALTERR,
      Con ( BLENDFAC < 1.0 ,
            ALTERR * ( 1.0 - BLENDFAC ) + DTBERR * BLENDFAC ,
            DTBERR
      )
)
```

Patching Kriging Artifacts and Contour Adjustments

Shaded areas indicate places where ALT3 model of bedrock altitude is higher than TOPO100; darker shades indicate greater excess altitude. We inspected the entire BLEND raster at 1:50,000 scale and created polygons (examples in Figure 7.9) defining the boundaries of 100 kriging artifacts (data-free depressions—see discussion in section 2.7.5). We then ran the python geoprocessing script (Appendix D) to replace the interiors of these polygons with surfaces interpolated using inverse-distance weighting of the boundary cell values. We designated the resulting patched altitude raster PATCHALT. We did not make any corresponding adjustments to the prediction error raster, which has high values in these artifact regions due to their greater distance from control points. We generated a 20-meter bedrock altitude contour layer from the PATCHALT raster. To simplify and generalize this, we removed all contours with a total line length less than 500 meters, and performed PAEK smoothing on the remaining lines with a 500-meter tolerance. These contours were also inspected statewide at 1:50,000 scale and in 6 areas the contours were manually re-drawn either to remove some details of topographic imprinting within DTBALT areas (3 instances), or to make a continuous valley depression out of a series of isolated depressions within narrow valley floors (3 instances). Figure 7.10 shows an example of these adjustments before and after manual contouring. The left image (Figure 7.10) shows a series of isolated depressions in the valley that need to be connected. The image on the right in Figure 7.10 shows the new contour after manual manipulaton connecting the isolated depressions into a series of longer troughs. The bold line surrounding the valley indicates the 500-meter buffer around the adjusted contour lines within which the updated altitudes will be blended.

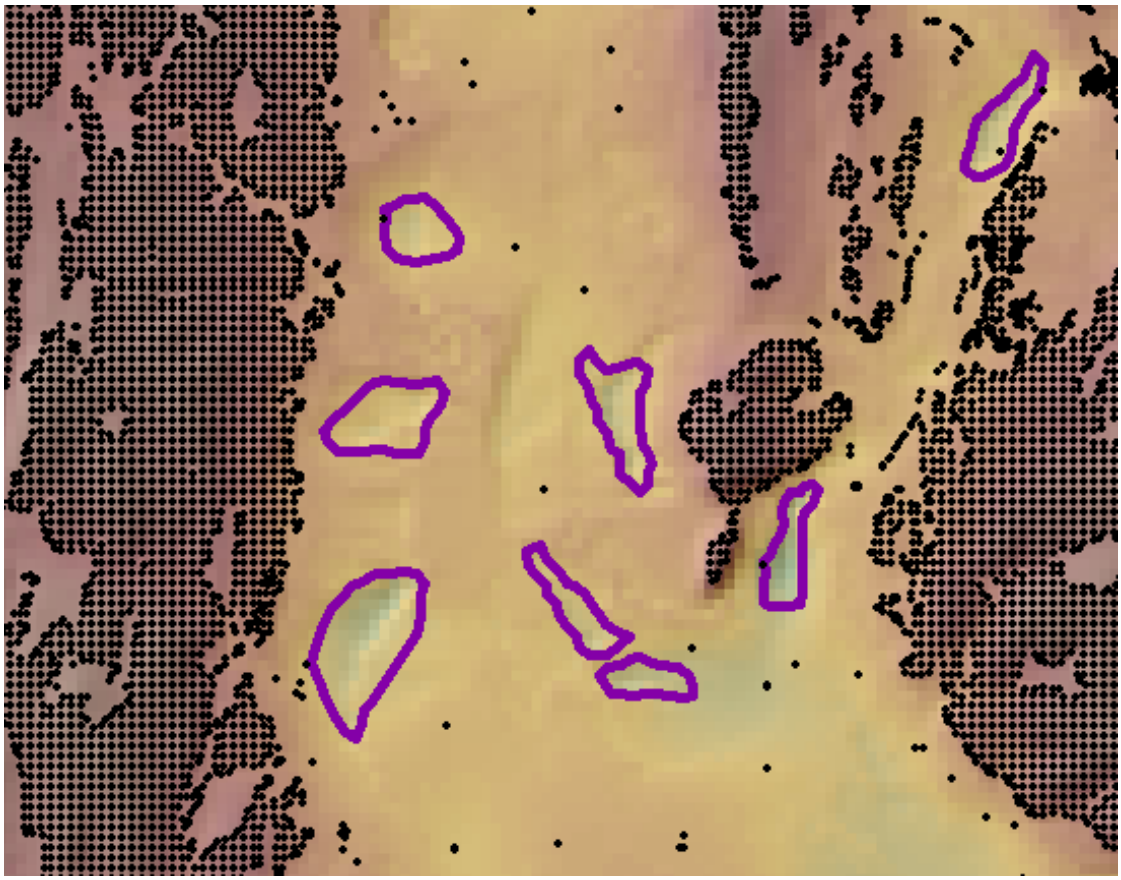

Figure 7.9: Some examples of kriging artifacts to be filled by inverse-distance weighting of the outlined perimeter cells; markers are well and bk and sb data—note there are no points within these depressions

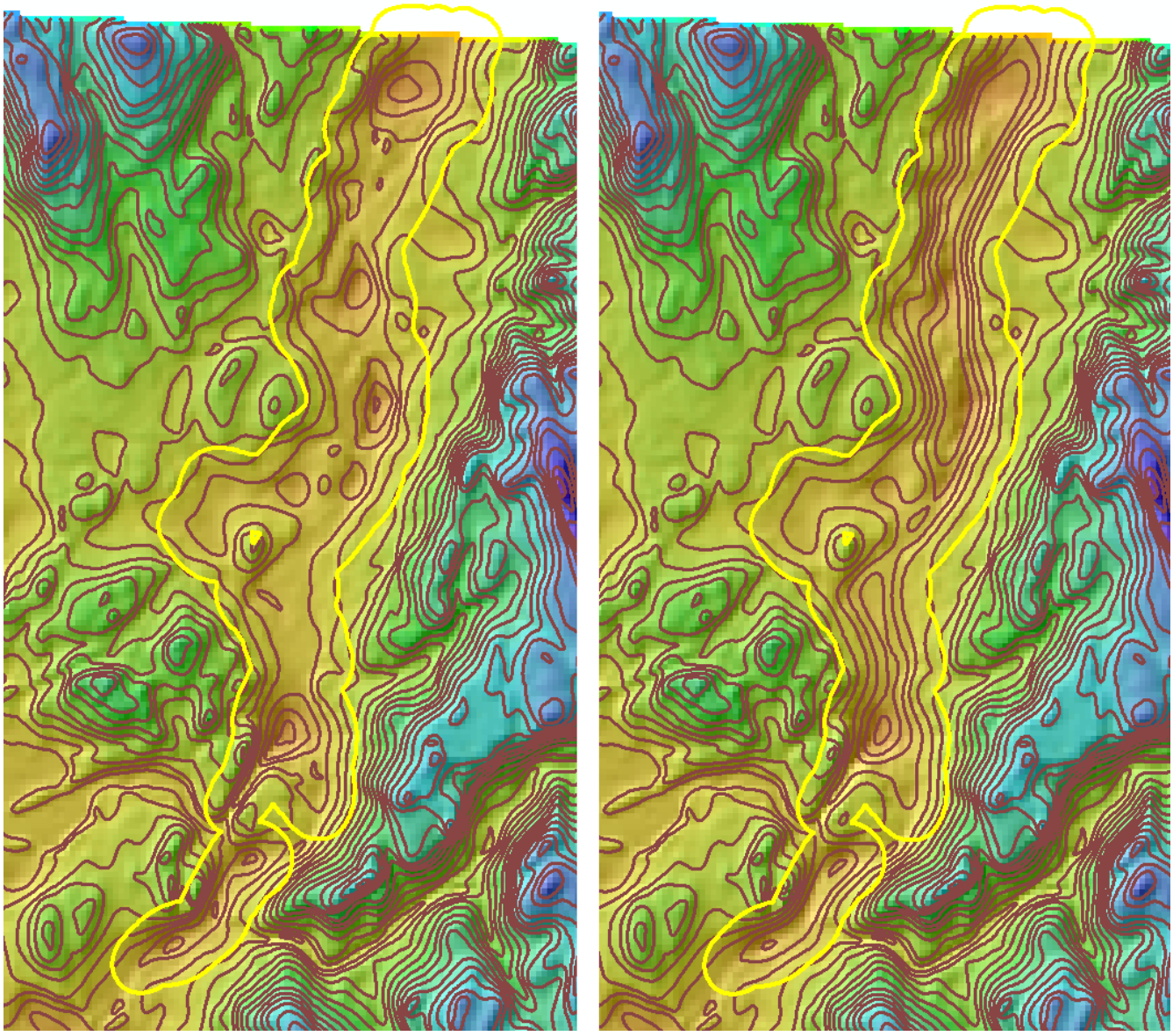

Figure 7.10: Contours before (left) and after (right) manual adjustments to create a single continuous deep depression linking the three separate depressions from the kriging model

In order to update the bedrock altitude raster to include these manual contour adjustments, we created a statewide 100-meter raster from the 20-meter contours (CONTALT), then performed another blending of values from this into the PATCHALT raster with a 300-meter blend zone inside of a 500-meter buffer of the altered contour lines. In detail, this sequence involved using the following ArcToolbox tools:

1. "Topo to Raster" to convert the edited 20-meter contours to a 100-meter altitude raster
2. "Buffer" to map 500-m buffer polygons around the manual contours
3. "Polygon to Raster" to create a 100-meter raster of zones using each polygon's FID
4. "Raster Calculator" to create a NOBLEND raster of ones (1s) outside the polygon zones

```
Con ( IsNull ( CONTFIDZONES ) , 1 )
```

5. "Euclidean Distance" on the NOBLEND raster to get BLENDDIST
6. "Raster Calculator" to compute a new BLENDFAC raster:

```
Con(BLENDDIST > 0, Con(BLENDDIST <= 300, BLENDDIST/300.0, 1.0))
```

7. "Raster Calculator" to blend CONTALT values into PATCHALT to create PATCHCONTALT:

```
Con(IsNull(BLENDFAC),
        PATCHALT,
        (1.0 - BLENDFAC) * PATCHALT + BLENDFAC * CONTALT
)
```

7. "Raster Calculator" to check for any remaining bedrock altitudes above topography from the patching and manual contouring processes by creating raster DTBCHECK:

```
TOPO100 -  PATCHCONTALT
```

8. "Raster Calculator" to remove any negative depths found in DTBCHECK:

```
Con(DTBCHECK < 0, PATCHCONTALT + DTBCHECK, PATCHCONTALT)
```

The resulting bedrock altitude raster is designated MAINALT, the bedrock altitude raster for the mainland after applying all adjustments and corrections and ensuring it is everywhere at or below the altitude of the current topography.

Modeling Input Data Uncertainty

To estimate the spatial distribution of measurement uncertainty, we simply repeated the EKB kriging process using the point uncertainty attribute UNCERT_M rather than the bedrock altitude attribute. We used EKB with the same 1000-meter radius parameter used for altitude kriging. As with bedrock depth, uncertainty must be everywhere a non-negative value, so we replace any negative uncertainty cells with zero. We designate the resulting raster as UNC.

Final Altitude, Depth, and Error/Uncertainty Rasters and Contours

We added the bedrock altitude for the islands to the mainland altitude raster to create a FINALALT raster in "Raster Calculator" with this expression:

```
Con(IsNull(MAINALT), ISLANDALT, MAINALT)
```

Likewise we used the ISLANDALT raster to add the islands to the DTB raster to create FINALDTB:

```
Con(IsNull(DTB), TOPO100 - ISLANDALT, DTB)
```

We also computed an alternate raster of depth-to-bedrock by subtracting our final altitude raster from topography, FINALDTBALT:

```
TOPO100 - FINALALT
```

Refer to the discussion in the next section for the differences between FINALDTB and FINALDTBALT.

In a similar vein we added the islands to the mainland UNC raster using the same estimation approach used for deeper well data, that is, 10% of the depth. In the "Raster Calculator" we computed a FINALUNC raster with:

```
Con(IsNull(UNC), 0.1 * FINALDTBALT, UNC)
```

We combined the blended kriging prediction standard errors and the kriged measurement uncertainties into a FINALERRUNC raster (Figure 7.11) by adding the variances and taking the square root of the sum, assigning a value of zero to the prediction standard errors for the islands where we did not use any kriging results:

SquareRoot(Power(FINALUNC,2) + Con(IsNull(BLENDERR), 0, Power(BLENDERR,2))

Final contour lines corresponding to the final bedrock altitude raster were generated using the "Contour" tool with an interval of 20 meters and a reference altitude of zero. These contours were simplified and generalized by removing any contour lines with total length less than 500 meters, and then using the "Smoothline" tool to apply a 500 meter PAEK tolerance to the remaining lines.

In the process of generating the best bedrock surface model we created two versions of a depth-to-bedrock model, one (DTB) interpolated directly from depth values at well and surficial geology points, the other (DTBALT) indirectly by subtracting the final bedrock altitude model from topography (Figure 7.12). We compute the range of depths between these two models as the absolute value of the differences (Figure 7.13).

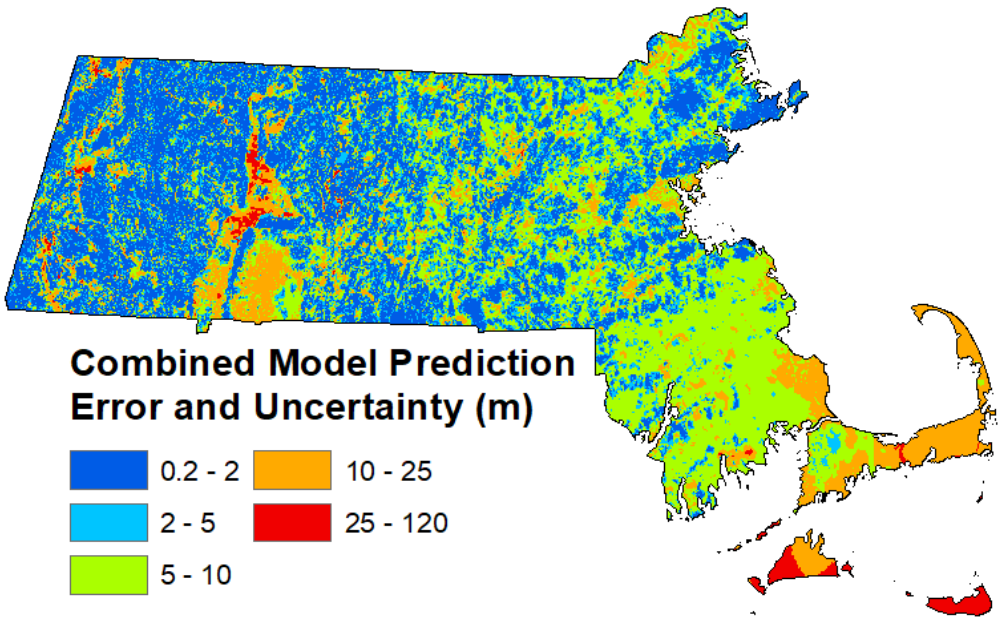

Figure 7.11: Combined prediction errors and input data measurement uncertainties from 0.2 meters (blue) to 120 meters (orange-red)

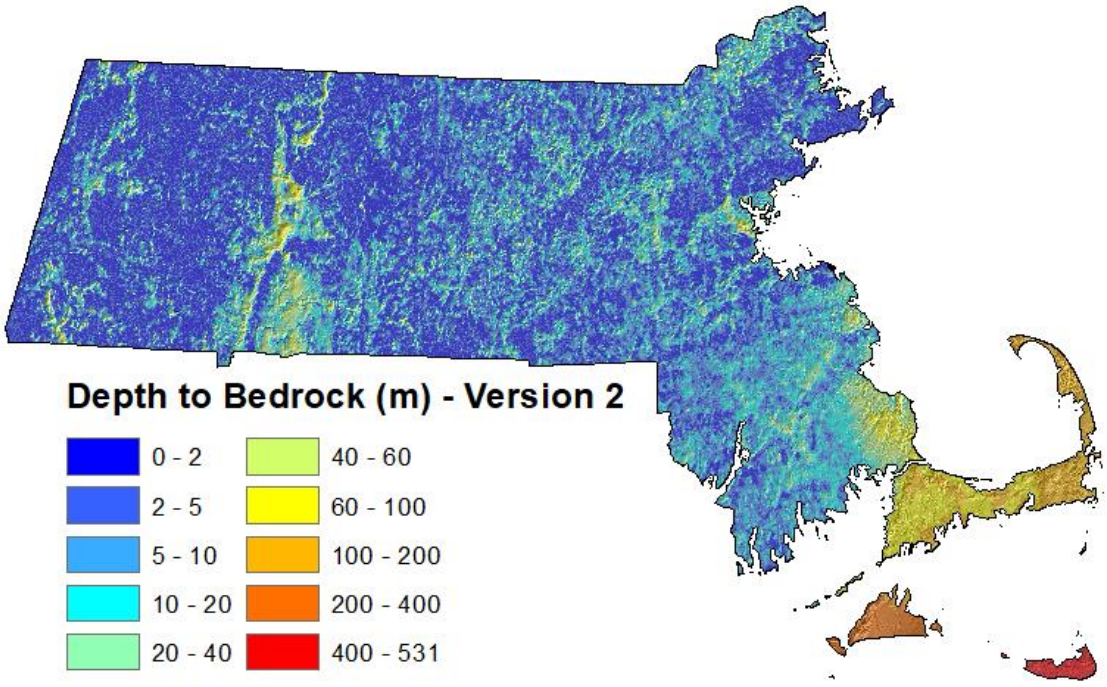

Figure 7.12: Depth to bedrock determined by subtracting the altitude-based model from the topography.

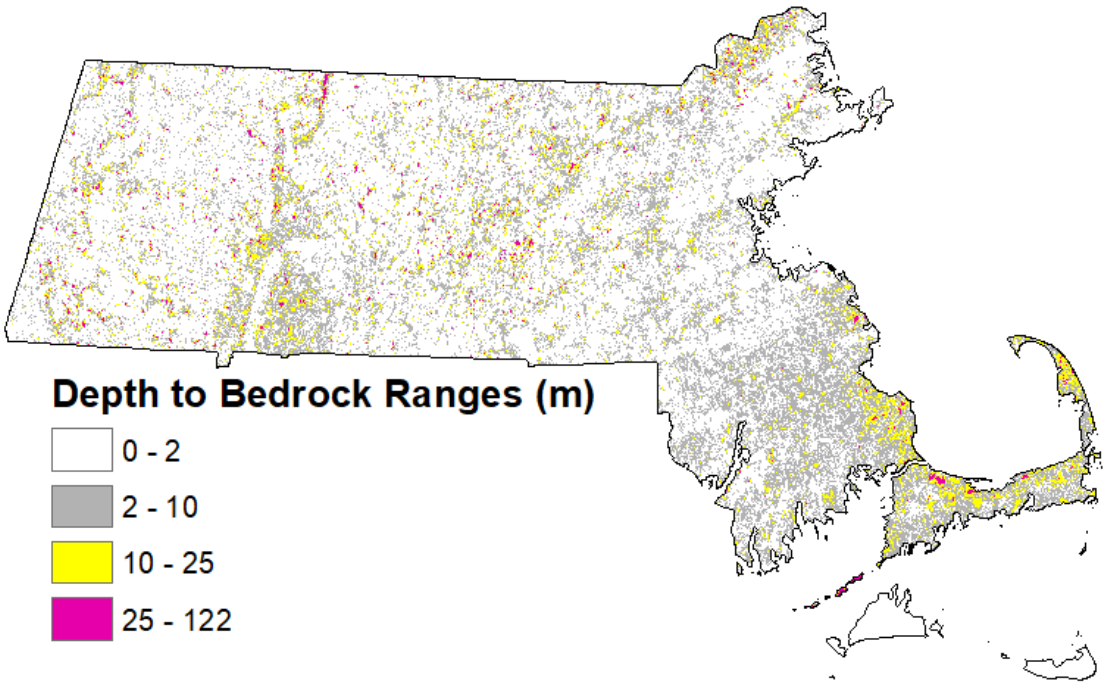

Figure 7.13: Range of depth estimates by two different methods (absolute difference of depth models) from zero (white) to 122 meters (red)

7.4 Appendix D: Python Script for Filling Kriging Artifacts

```
# before running this script, do all prep in final_processing_steps_and_files.txt
#
# setup for this script:
#
# A raster to accumulate the patches on top of the original model:
#   scriptdump.gdb/blended_bedrock_alt_patches, copied from blended altitude tif
#   no need to delete before trying a new run—patches will just be re-applied in the problem
area interiors
# Delete if present:
#   edgepts4idw.shp
#   gdb/outidw
#   gdb/idwpatch


# Import system modules
import sys, string, os, arcgisscripting, arcpy
from arcpy.sa import *

temppath = 'S:/data/Chris/GISmatters/omsg/topofrock/data/release'
tempgdb = temppath + '/scriptdump.gdb'
refraster = temppath + '/blended_bedrock_alt.tif'

arcpy.env.workspace = temppath
arcpy.env.XYResolution = 100
arcpy.env.cellSize = 100
arcpy.env.snapRaster = refraster
arcpy.env.extent = refraster
arcpy.env.overwriteOutput = True

FIDfieldname = 'FID'
FIDfieldindex = 0

idwNumPoints = 150
idwMaxRadius = 5000

# Create the Geoprocessor object
gp = arcgisscripting.create()

mxd = arcpy.mapping.MapDocument("CURRENT")
df = mxd.activeDataFrame

# Load required toolboxes...
```

```
gp.AddToolbox("C:/Program Files (x86)/ArcGis/Desktop10.8/ArcToolbox/Toolboxes/Data Management Tools.tbx")

polylayer = 'problem_areas_type_1'
edgepointslayer = 'problemareainteriors_100m_edge_alt_pts'
pts4idwlayer = "edgepts4idw"
temppts = pts4idwlayer + '.shp'
tempptspath = temppath + '/' + temppts
idwpath = tempgdb + '/outidw'
idwpatchpath = tempgdb + '/idwpatch'
idwRadiusVar = RadiusVariable(idwNumPoints, idwMaxRadius)
cumpatches = tempgdb + '/blended_bedrock_alt_patches'

# clear any selection in problem areas layer or else we won't iterate over all of them
arcpy.SelectLayerByAttribute_management(polylayer, "CLEAR_SELECTION")

# don't know why (memory?), but ArcMap crapped out every ~40 iterations of the loop below;
# so the following sets a starting-point for FID for the run; update for each run as needed
resume_from_FID = 0

i = 0
with arcpy.da.SearchCursor(polylayer, FIDfieldname) as cursor:
    for row in cursor:
        # select one problem polygon to patch
        FID = row[FIDfieldindex]
        if FID < resume_from_FID:
            continue
        query = "" + FIDfieldname + "" = {}'.format(str(FID))
        print(query)
        arcpy.SelectLayerByAttribute_management(polylayer, "NEW_SELECTION", query)
        # select its edge points to get edge altitudes
        arcpy.SelectLayerByLocation_management(edgepointslayer, "WITHIN_A_DISTANCE", polylayer, 100, "NEW_SELECTION")
        # save edge points to temp file and make it a feature layer
        arcpy.FeatureClassToFeatureClass_conversion(edgepointslayer, temppath, temppts)
        arcpy.MakeFeatureLayer_management(tempptspath, pts4idwlayer)
        # compute IDW raster from edge point altitudes and save to disk
        outIDW = Idw(tempptspath, 'grid_code', 100, 2, idwRadiusVar)
        outIDW.save(idwpath)
        # get IDW values only within cells matching this polygon's FID, else the cumul patch layer, and save result
        idwpatch = Con("problemareainteriors_100m.tif", idwpath, cumpatches, "VALUE = " + str(FID))
        idwpatch.save(idwpatchpath)
        # remove intermediate files and replace cumpatches with latest patch output from Con()
```

```
arcpy.Delete_management(tempptspath)
arcpy.Delete_management(idwpath)
arcpy.Delete_management(cumpatches)
arcpy.management.Rename(idwpatchpath, cumpatches)
i += 1
```

This page left blank intentionally.

7.5 Appendix E: NEHRP Site Class Map Development

1/5/2023

MA SEISMIC SITE CLASS MAP DEVELOPMENT FROM THE STATE 100-M RESOLUTION DEPTH TO BEDROCK MAP
By Marshall Pontrelli, Stephen B. Mabee and William P. Clement

1.0 Introduction

We discuss the procedure for creating a *Vs30*-based seismic site classification map for Massachusetts using the State 1:24,000-scale surficial geologic map (Stone and others, 2018) and the State 100-m resolution depth to bedrock map (Mabee and others, 2023). *Vs30* is a weighted average shear wave velocity over the top 30 meters of a geotechnical profile *(1, 2)* and is calculated using the equation:

$$Vs30 = \sum_{i=1}^{n} \frac{d_i}{\frac{d_i}{V_i}} \quad (1)$$

where d_i is the thickness and V_i is the shear wave velocity of the i^{th} geotechnical layer and $\sum_{i=1}^{n} d_i$ = 30 meters. Seismic site classes simplify the continuous *Vs30* variable into ranges represented by 5 classes (A-E) of increasing seismic site response hazard as defined by NEHRP (1994) (Table 7.1).

Table 7.1: Vs30-based seismic site classification

Site Class	Generic Description	Range of *Vs30*
A	Hard Rock	> 1500 m/s
B	Rock	760-1500 m/s
C	Very dense soil and soft rock (firm horizon)	360 < 760 m/s
D	Stiff Soil	180 < 360 m/s
E	Soil profile with soft clay	< 180 m/s

In this work, we produce a regional seismic *Vs30*-based site classification map of Massachusetts. Massachusetts was a glaciated state and typically has soft glacial sediments overlying hard basement rock. During the Wisconsinan glaciation, the Laurentide ice sheet covered the state, clearing most of the existing pre-glacial materials and depositing glacial sediments on the cleared bedrock surface. With this unique high impedance contrast structure – soft, low velocity sediment over hard, high velocity bedrock – we approximate the state using a simple layer-over-halfspace model which is composed of an average overburden

velocity (Vs_{avg}), a depth to bedrock (d_s) and a bedrock velocity (V_R) (Figure 7.14). We compute the average overburden velocity using Equation 1 where $\sum_{i=1}^{n} d_i$= the depth to the impedance contrast (the sediment-bedrock interface). The *Vs30* calculation simplifies to

$$Vs30 = \frac{30}{\left(\frac{d_S}{Vs_{avg}} + \frac{d_R}{V_R}\right)} \quad (2)$$

where d_R is the thickness of the basement rock layer and is equal to 30 – d_s. This equation is valid for d_s <= 30 m. When d_s > 30 m, $Vs30 = Vs_{avg}$. Equation 2 is essentially Equation 1 where instead of *i* layers, there are 2 layers, one overburden layer and one basement rock layer, each with a thickness and a shear wave velocity. The thickness of the bedrock layer is 30 minus the thickness of the overburden sediment (Figure 7.14).

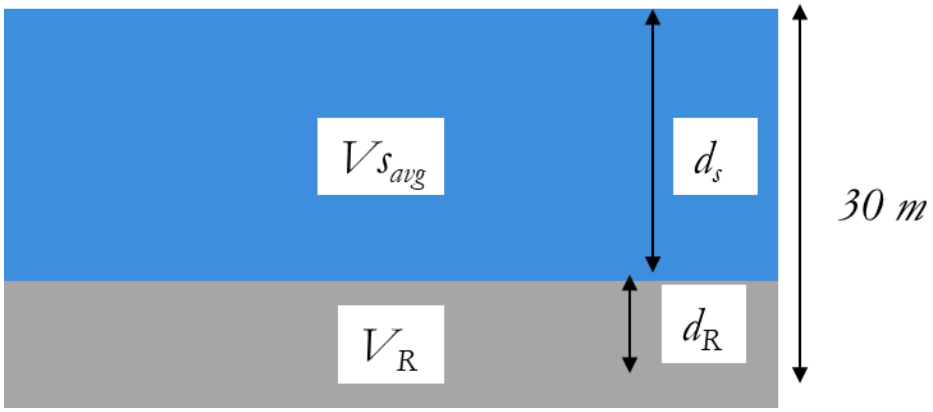

Figure 7.14: Overburden structure of the layer-over-halfspace model

Using Equation 2, we estimate *Vs30* everywhere in the state using a depth to bedrock (d_s) map, a Vs_{avg} map and an estimate of basement shear velocity (V_R) across the state.

2.0 Data

To create a *Vs30*-based site class map across Massachusetts, we use the depth-to-bedrock map (Mabee and others, 2023) to determine d_s (Figure 7.15) and the state 1:24,000 surficial geology map map (https://pubs.er.usgs.gov/publication/sim3402) to come up with geologic correlations for Vs_{avg}. In addition to the mapping layers, our procedure for estimating Vs_{avg} based on surficial geologic classification uses shear wave velocity profiles developed in Thompson and others (2014) (EMT on Figure 7.16), Mabee and Duncan (2017) (HGS on Figure 7.16), and Pontrelli and others (2023) (MAP on Figure 7.16).

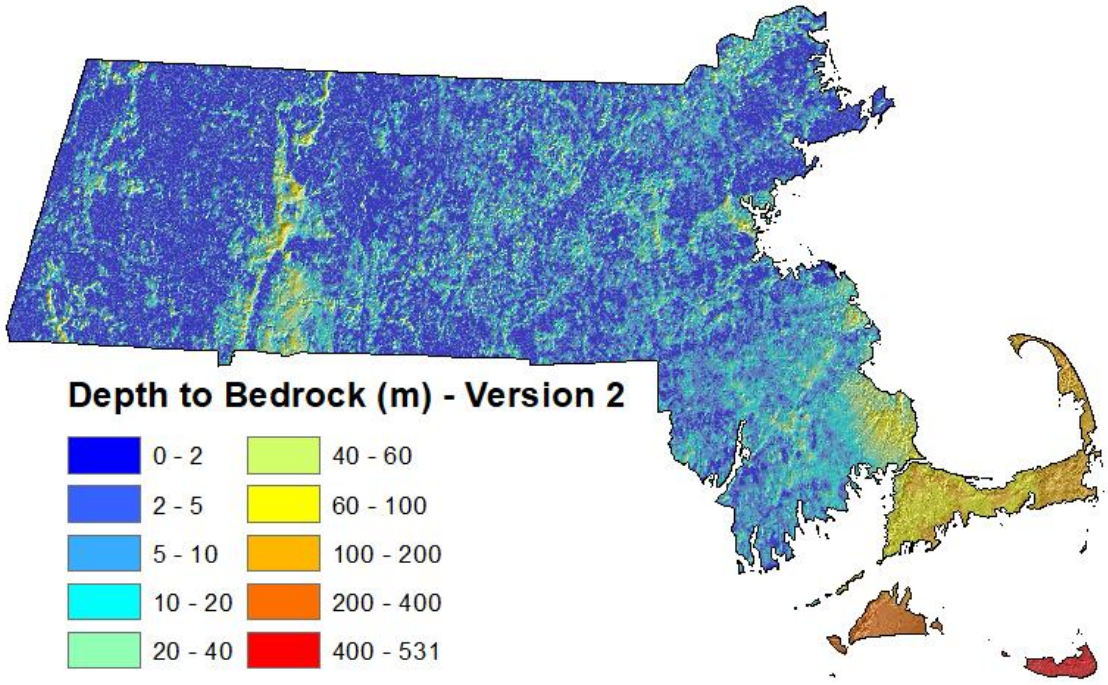

Figure 7.15 Massachusetts depth to bedrock map used to determine d_s for Equation 2.

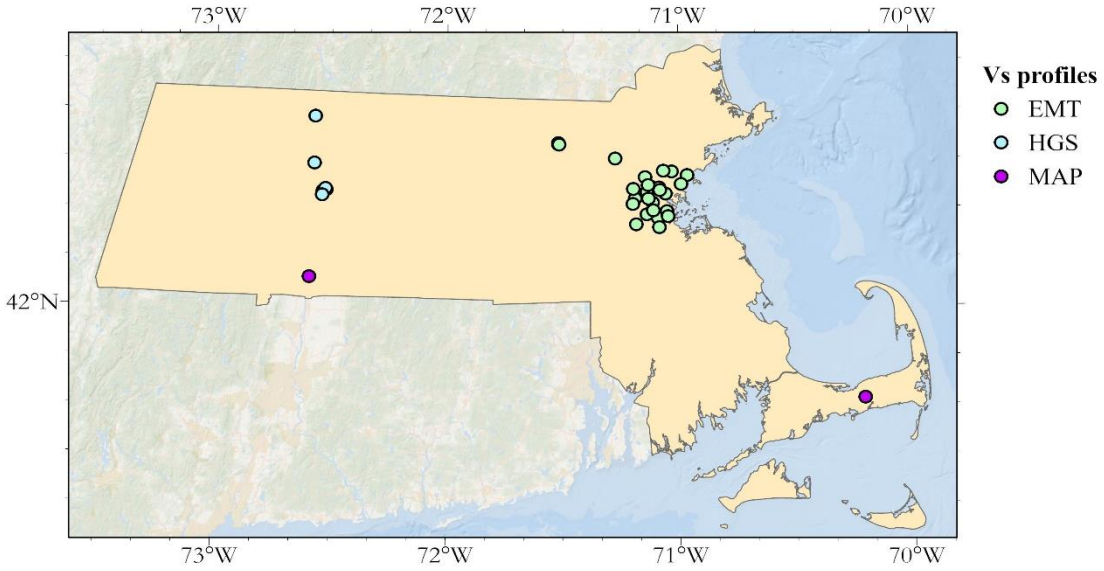

Figure 7.16: Locations of the shear wave velocity profile stations used to estimate Vs_{avg} in this study

3.0 Methods

Methods 3.1 - Estimating Vs_{avg} using geologic correlations.

Our procedure requires a map of Vs_{avg} for the entire state. We use 35 shear wave velocity profiles to estimate Vs_{avg} as well as the assumption that similar surficial geologic materials will have similar mechanical properties and therefore similar shear wave velocities. We first combine the surficial geologic map units into four groups based on their similar mechanical properties (Table 7.2). With these geologic groupings, we group the *Vs* profile stations to collect a set of profiles for each geologic grouping. Finally, we calculate the mean and median of Vs_{avg} of the profiles within the grouping. With these estimates of mean and median, we adjust the values to whole numbers in the Vs_{avg} estimate column to acknowledge the limited data on which we are basing the value (Table 7.3, Figure 7.17). Group 1 has a mean Vs_{avg} value of 238 m/s and a median value of 214 m/s. In Becker and others (2011), a relational table is developed which converts surficial geology units into seismic site classes. In this table, the Group 1 units are converted into site class E sediments (<180 m/s). We therefore use a conservative (lower than the mean and median values of the data) Vs_{avg} estimate of 180 m/s for this unit. Group 2 is composed of fine clay sediments and has a mean and median Vs_{avg} value of 160 m/s calculated from two stations located near each other in the Boston Basin. The Becker and others (2011) relational table converts some fine clay deposits to site class E sediments and some to site class D sediments. We therefore estimate Vs_{avg} in fine clays across the state higher than the estimates of the two profiles we have in Group 2 at 200 m/s. Group 3 has a mean Vs_{avg} value of 430 m/s and median value of 254 m/s. In Figure 7.17, the Vs_{avg} values in the grouping have one large outlier skewing the mean estimate. We therefore use a Vs_{avg} estimate of 250 m/s in the group, which is approximately the median. Group 4 is composed of denser till surficial geologies and has a mean Vs_{avg} value of 402 m/s and median value of 426 m/s. This is a balanced distribution, and we use a whole number estimate of 400 m/s for Vs_{avg} which is approximately the central tendency of the data. In Figure 7.18, we show the individual shear wave velocity profiles of each of the 4 groupings as well as the measured median Vs_{avg} value and the estimated Vs_{avg} value.

Table 7.2: Surficial geologic groupings of the Massachusetts units into 4 groups of similar mechanical properties

Group	Units
Group 1	Artificial fill; Cranberry bog deposits; Salt-marsh and estuarine deposits; Swamp deposits
Group 2	Glacial stratified deposits, fine; Glacial stratified deposits, glaciomarine fine
Group 3	Floodplain alluvium; Alluvial-fan deposits; Beach and dune deposits; Inland-dune deposits; Valley-floor fluvial deposits; Stream-terrace deposits; Marine regressive deposits; Glacial stratified deposits, coarse; Stagnant-ice deposits; Talus deposits
Group 4	Glacially-modified coastal plain hill deposits; End moraine deposits; Thrust-moraine deposits; Thick valley till and fine deposits; Thin till; Thick till
Bedrock	Bedrock outcrops

Table 7.3: Mean, median and estimated Vs_{avg} values for the four geologic groupings.

Group	# stations	Mean Vs_{avg} (m/s)	Median Vs_{avg} (m/s)	Estimated Vs_{avg} (m/s)
Group 1	13	238.24	213.98	180
Group 2	2	160.80	160.80	200
Group 3	7	430.33	254.76	250
Group 4	13	402.60	426.02	400

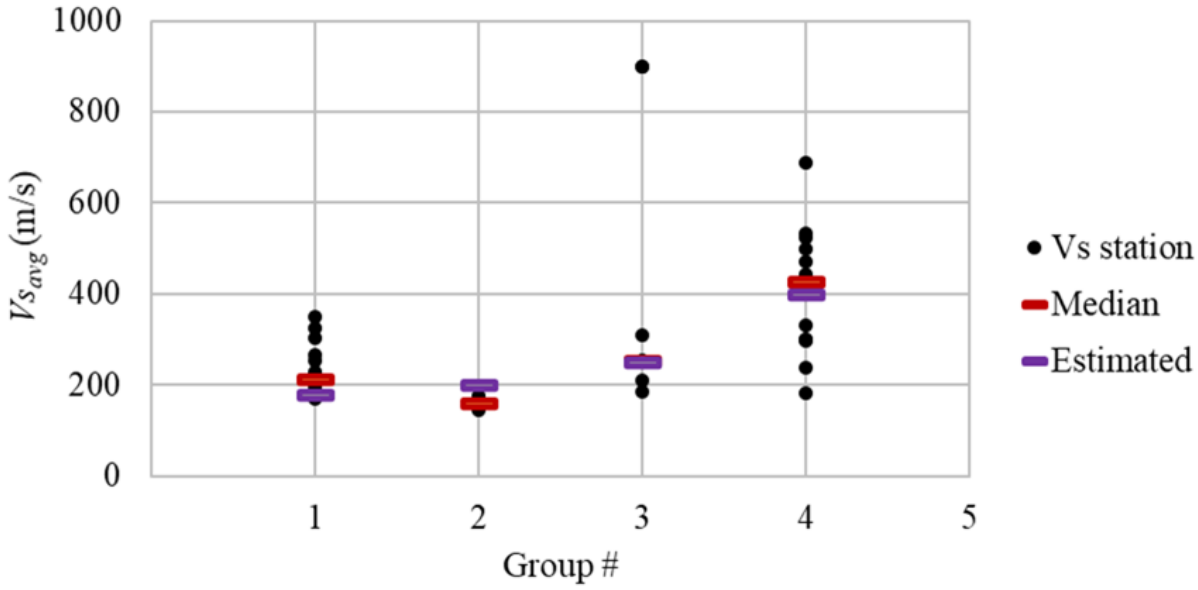

Figure 7.17: Vs_{avg} values of each station within each grouping with the median (red line) computed from the Vs_{avg} values and the assigned Vs_{avg} value used in the study (purple line) listed in Table 7.3

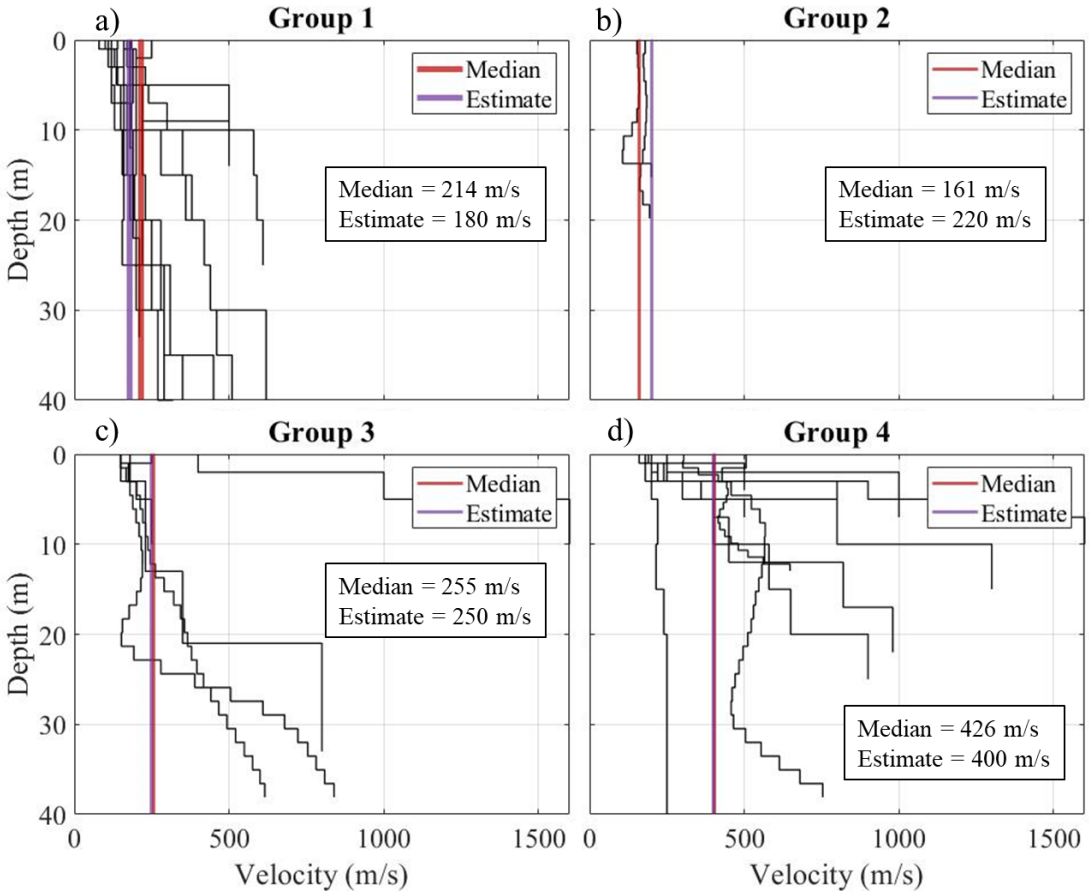

Figure 7.18: Raw shear wave velocity profiles for the four geologic groupings and each median and estimate value as a vertical line

Following the estimate of Vs_{avg} for each geologic grouping, we convert grouped geologic map units to the estimated Vs_{avg} values in Table 7.3.

Methods 3.3 – Computing *Vs30* from the depth to bedrock and Vs_{avg} maps

With a depth-to-bedrock map (Figure 7.15) and Vs_{avg}, we calculate *Vs30* by applying Equation 2 to both. We assume a bedrock velocity (V_R) of 2500 m/s, similar to the shear velocity used for bedrock in the Central and Eastern United States (Stewart and others, 2020; Goulet and others, 2017, 2018; Pacific Earthquake Engineering Research Center (PEER), 2015a, 2015b) and calculate d_R as $30 - d_s$.

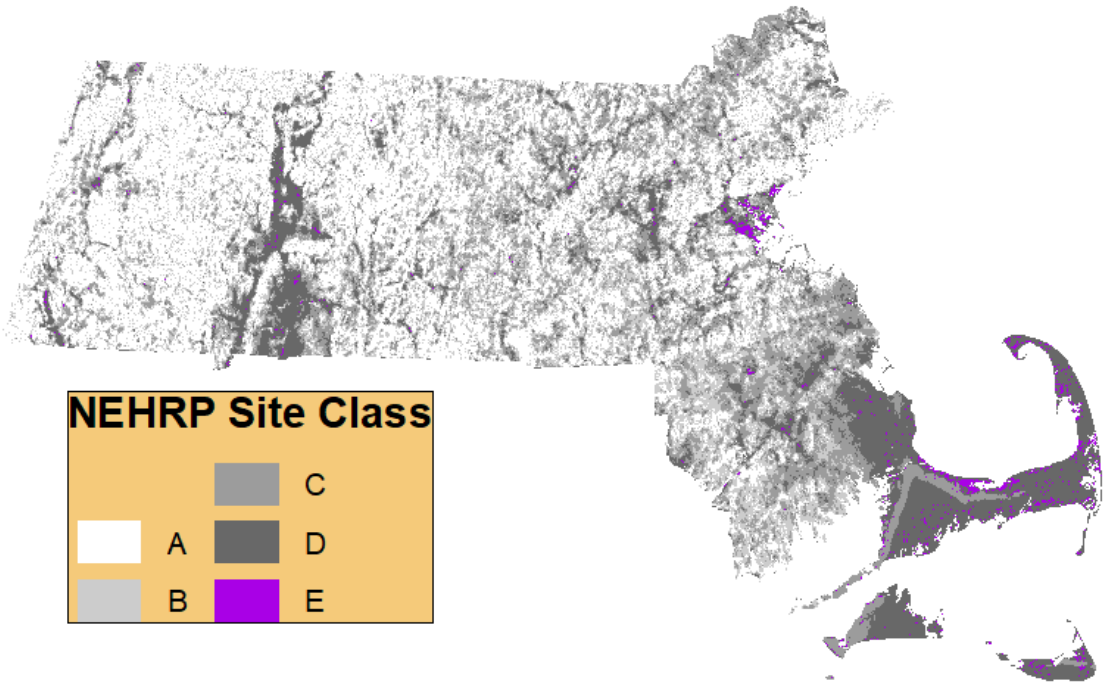

Figure 7.19: Final *Vs30*-based seismic site classification map using the *Vs30* groupings in Table 7.1

4.0 Results

The resulting *Vs30* -based seismic site class maps are shown in Figure 7.19. In the Connecticut River Valley and the Boston Basin, the bedrock depth decrease is clearly shown as one moves from the center of the basin to the edge. Site classes change from class D or E in the basin center to a band of class C along the basin margin, and ultimately to site classes B and A in the uplands where compact tills are the dominant materials and the depth to bedrock is shallow. In the Boston Basin, the large site class E deposit is artificial fill. On Cape, the bedrock depth is much greater than 30 m and thus *Vs30* values are calculated from the overburden Vs_{avg}. The overburden sediments on Cape Cod are mostly in Group 3 (Vs_{avg} = 250 m/s) and are site class D. Some are in Group 4 (Vs_{avg} = 400 m/s) and include the Sandwich Moraine and are site class C. On the northern shore of Cape Cod, there are sediment deposits in Group 1 (Vs_{avg} = 180 m/s) which at this depth are site class E. In this region the overburden is greater than 30 m, so $Vs30 = Vs_{avg}$. Thus, these site classes are laterally consistent.

5.0 Limitations

Our procedure uses a simple layer-over-halfspace model for the Commonwealth of Massachusetts and assigns a Vs_{avg} value based on the sediments exposed at the surface. In reality, the subsurface is more complex, likely with multiple layers and multiple velocities above the bedrock. Despite this limitation, estimating *Vs30* using the simple layer over

halfspace model produces useful, reproduceable and conservative results. Since most sediment profiles increase in velocity with depth, the actual Vs_{avg} through the sediment profile is likely higher than we estimated. Figure 7.20 shows 3 profiles with the same depth to bedrock (20 meters) and same basement velocity (2500 m/s): a) a layer-over-halfspace profile, b) a 3-layer profile with layer thicknesses equal to 5, 5, and 10 m, and layer velocities equal to 220, 250, and 400 m/s, respectively, and c) a linearly increasing velocity model with velocity = 220 + 4.38 * depth. The slope of the line is the slope calculated for the generic Boston Basin velocity model produced in Baise and others (2016). Each model has the same velocity at the free surface (220 m/s). We calculate *Vs30* for all three profiles; the layer over halfspace model has the lowest *Vs30*. Since we estimate Vs_{avg} using the surficial sediment type, our *Vs30* estimates will most likely be lower than the true *Vs30* value. In this way, our procedure is simple, repeatable, and conservative, although we advocate developing more complex 3-dimensional shear wave velocity models, which would increase the accuracy of the *Vs30* map.

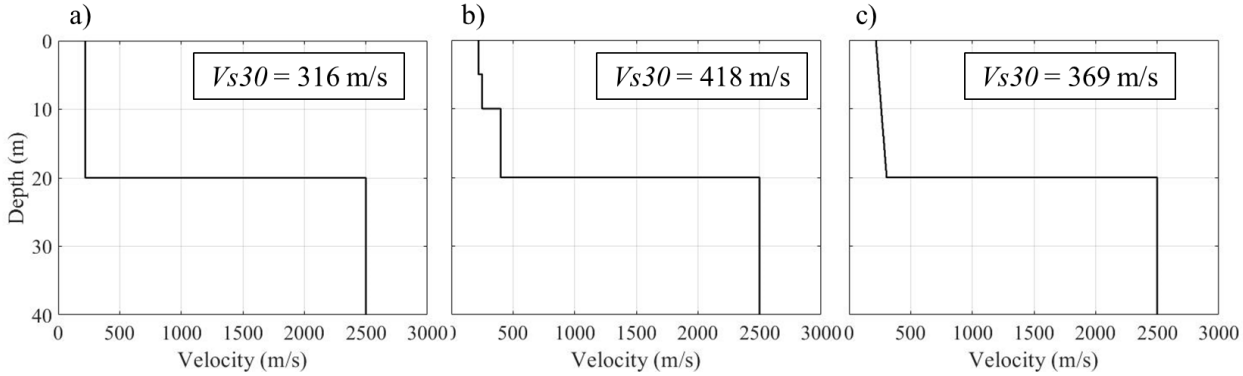

Figure 7.20: a) Layer over halfspace model with the overburden velocity = 220 m/s. b) Three-layer velocity model with layer thicknesses. c) Linearly increasing model

References

Baise, L. G., Kaklamanos, J., Berry, B.M., Thompson, E.M. (2016). Soil Amplification with a strong impedance contrast: Boston Massachusetts. Engineering Geology 202 (2016) 1-13.

Becker, L.R., Patriarco, S.P., Marvinney, R.G., Thomas, M.A., Mabee, S.B., and Fratto, E.S., 2012, Improving seismic hazard assessment in New England through the use of surficial geologic maps and expert analysis, in Cox, R.T., Tuttle, M.P., Boyd, O.S., and Locat, J., eds., Recent Advances in North American Paleoseismology and Neotectonics East of the Rockies: Geological Society of America Special Paper 493, p. 221-242, doi:10.1130/2012.2493(11).

Borcherdt, R.D. (1992). Simplified site classes and empirical amplification factors for site-dependent code provisions. NCEER, SEAOC, BSSC workshop on site response during earthquakes and seismic code provisions, Univ. Southern California, Los Angeles, California, Nov. 1992.

Borcherdt, R.D. (1994). Estimates of Site-Dependent Response Spectra for Design (Methodology and Justification). Earthquake Spectra, Vol 10, No. 4, 1994.

Goulet CA, Bozorgnia Y, Abrahamson NA, et al. (2018) Central and eastern North America ground—motion characterization—NGA-East final report. PEER report 2018/08. Berkeley, CA: Pacific Earthquake Engineering Research Center.

Goulet CA, Bozorgnia Y, Kuehn N, et al. (2017) NGA-East ground-motion models for the U.S. Geological Survey National Seismic Hazard Maps. PEER report no. 2017/03. Berkeley, CA: Pacific Earthquake Engineering Research Center.

Mabee, S.B., C.C. Duncan, and W.P. Clement, 2023, Massachusetts depth to bedrock. Massachusetts Geological Survey Open-File Report 23-01.

Mabee, S.B. and C.C. Duncan, 2017, Preliminary NEHRP soil classification map of Massachusetts – Appendix B Hager Geoscience Shear Wave Velocity Data and Analyses. Prepared for the Massachusetts Emergency Management Agency and Federal Emergency Management Agency, 232 p.

NEHRP (1994) NERPT Recommended Provisions for Seismic Regulations for New Buildings. Building Seismic Safety Council for the Federal Emergency Management Agency.

Pacific Earthquake Engineering Research Center (PEER) (2015a) NGA-East: Median ground-motion models for central and eastern North America. PEER report no. 2015/04. Berkeley, CA: PEER, University of California.

Pacific Earthquake Engineering Research Center (PEER) (2015b) NGA-East: Adjustments to median ground-motion models for central and eastern North America. PEER report 2015/08. Berkeley, CA: PEER, University of California.

Pontrelli, Marshall and Baise, Laurie G. and Ebel, John E., Site Characterization Maps of New England Based on Local Geophysical and Geologic Data. ENGEO-D-22-01263, Available at SSRN: https://ssrn.com/abstract=4214053 or **http://dx.doi.org/10.2139/ssrn.4214053**

Stewart JP, Parker GA, Atkinson GM, Boore DM, Hashash YMA, Silva WJ. Ergodic site amplification model for central and eastern North America. Earthquake Spectra. 2020;36(1):42-68. doi:10.1177/8755293019878185

Stone, J.R., Stone, B.D., DiGiacomo-Cohen, M.L., and Mabee, S.B., comps., 2018, Surficial materials of Massachusetts—A 1:24,000-scale geologic map database: U.S. Geological Survey Scientific Investigations Map 3402, 189 sheets, scale 1:24,000; index map, scale 1:250,000; 58-p. pamphlet; and geodatabase files, **https://doi.org/10.3133/sim3402**

Thompson, E.M., Carkin, B., Baise, L.G., Kayen R. E., 2014. Surface Wave Site Characterization at 27 Locations Near Boston, Massachusetts, Including 2 Strong-Motion Stations. U. S. Geological Survey OFR 2014-1232